THE UNIVERSITY
of EDINBURGH

Thermal energy storage for renewable integration: a techno-economic analysis in the Chilean energy context

Serguey Maximov

Doctor of Philosophy

The University of Edinburgh

2021

Abstract

Chile has set ambitious targets to reach 100% renewable generation in the electric system and supply 80% of its heating with sustainable sources by 2050. The fulfilment of these goals brings new challenges for balancing supply and demand and creates the need for providing the energy networks with operational flexibility from new sources. Thermal energy storage arises as an option that can provide part of this flexibility, decoupling supply and demand by time-shifting power delivery at a competitive cost and with fewer geographical limitations compared to other storage technologies. Although Chilean energy policy has recently turned its attention on these issues, there is still a lack of technical input for assessing the potential of thermal energy storage to support the deployment of renewables in the electric grid and for cleaning heating supply.

This thesis aims to bridge that gap and focuses on assessing how different thermal energy storage technologies can help to increase the share of intermittent renewables in the Chilean electric grid and in its residential heating sector. This is performed through techno-economic optimisation of the design and operation of specific thermal energy storage systems configurations.

In the case of the electric grid, a linear optimisation model of the Chilean network is developed. The long-term impact of pumped thermal energy storage on the total system's cost is assessed. Among the main findings, it is concluded that the integration of on-grid 8h capacity storage increases the solar photovoltaic fraction, which leads to reductions in operation and investment costs by 2050.

For the residential heating sector, a solar district heating network supported by borehole seasonal thermal storage is proposed as a clean alternative for heating in southern Chile. A simulation-based multi-objective optimisation of the system's design is performed, focusing on minimising cost and emissions. The results show that this system can be cost-competitive with some conventional heating technologies under specific circumstances. The presence of seasonal thermal storage helps drive down the total emissions by reducing the use of the auxiliary gas heater in winter.

Finally, the solar district heating network is combined with a heat pump, and the effect of the power-to-heat scheme supported by short and long-term storage is assessed. It is found that despite the positive impact on cost and emission of the heat pump integration under the proposed configuration, fast charging thermal storage technologies may be better suited to integrate the heat supplied by the heat pump than the slower charging borehole storage. Additionally, by combining the previously developed models, it is established that the flexibility

of the electric demand of a heat pump collocated with thermal storage decreases the strain on the electricity system expansion compared with inflexible demand. The findings reported in this thesis set the ground for further research, potentially using more detailed models and assessing other thermal storage technologies to highlight their value and encourage the use of thermal energy storage to assist the Chilean energy transition. Furthermore, these tools and analyses could be applied to other countries and areas following similar energy transition pathways.

Lay Summary

During the last 200 years, our society has relied on fossil fuels, such as coal, oil and natural gas, to satisfy our diverse energy requirements. The pressing need to control climate change has driven most countries to begin a shift towards using cleaner energy sources. As expected, modifying the technologies that run our world is complex and brings many challenges that need to be addressed. One of them is to overcome the intermittent nature of the most popular clean energy sources: solar and wind generation.

Technologies using sun and wind only produce energy when the sun is shining or the wind is blowing, but our energy requirements usually do not adapt to these natural patterns. This can lead to periods when energy is required but not available, such as a windless winter evening. Hence, if a general movement towards cleaner and affordable energy generation is to be undertaken, technologies that could bridge the time mismatch between energy availability and demand need to be developed.

This thesis proposes the use of thermal energy storage as an economical solution to bridge this timing mismatch. This kind of storage technology can store energy produced by solar or wind generation in moments of low energy needs in the form of heat and make it available when required. It can store energy from minutes to even months, be installed almost anywhere, and be designed to release energy as heat or electricity. In this thesis, the suitability of thermal storage for helping to increase the use of solar and wind energy in the electricity system and for house heating is investigated using Chile, a country that has set ambitious targets for renewable generation, as an example.

Firstly, using models of the Chilean electricity system, the best size, location and deployment timing of thermal energy storage were estimated. The impact of this storage on renewable generation and carbon emissions in the next 30 years were discussed. Next, the effect of thermal storage on a communal heating network using the sun as the main energy source was investigated. In this case, thermal storage systems with short (hourly to daily) and long (monthly to yearly) duration capacities were considered. The best design of different components of the hating system was evaluated to achieve low cost a well as emissions, which are competing targets. Finally, the benefits of combining the operation of the electricity system with heat networks were studied. For this, heat pumps that buy electricity to provide heat and their operation with thermal storage were analysed and their beneficial effects on the overall energy system estimated.

The discussion and results of this thesis can offer helpful information to the Government and other actors of the Chilean energy sector. The tools and methods developed in this thesis could be applied to other countries or areas looking for options to increase the use of intermittent renewable generation such as solar and wind.

Acknowledgements

I would like to start thanking my PhD supervisor, Dr Daniel Friedrich, for his support and advice through this process. I truly appreciate his approach to PhD supervision, managing to balance the freedom to pursue independent research with constant and thorough guidance. I enjoyed each of our interactions, either academic meetings or coffee breaks and other social events. The effort he puts into making all his students feel part of a group is very helpful in dealing with the ups and downs of research. Thank you, Daniel, for being an excellent academic role model, but especially a good and kind human being.

I would also like to thank my second supervisor, Prof Gareth Harrison, for his comments, especially in the last part of the PhD, and Dr Harry van der Weijde for his spot-on advice and suggestions during the annual reviews.

I would also like to extend my gratitude to all the people that at any point were parts of our research group, especially Renaldi, for his "old PhD student" wisdom and for helping me with his model; Jesus, for the squash matches and for setting a high academic bar for the rest of us to reach; Jafar, for his unique sense of humour; Abdullah, for all the sweets and treats; Sajid, for the challenging questions and interesting academic (and not so) discussions, Andrew and Lukas for being nice late additions to our virtual coffee meetings. Special thanks to Ruben, with whom we have shared many good conversations, academic discussions, and the complexities and enjoyment of balancing family life and research; thanks for your friendship.

Other than all the academic knowledge and skills I acquired during these years, I am grateful for the opportunity of sharing experiences with bright people from different cultural backgrounds. It has been very nice to share time with you and learn from you, Will, Ricardo, Rodrigo (and all the Mexican crew), Dan, Ilaria, Syahin, Winnie, Hawoi, Juan Pablo, Syahrul, Arturo, Jingjie, Haris, Francesco, Thanasios, Anna, Gerard, Gunel, Aldo, Thibaut, Eduardo, Hongye, Maja, Fabian, Halil, Kevin and Nadir. All of you have, at some point, made a difference in my daily life and made this process more enjoyable.

To my parents, thanks for giving me all the opportunities for developing myself and for your encouragement and support from afar during these years.

Finally, I would like to thank my partner Yenn, who helped me to decide to pursue a PhD and who, with her example and support, has helped me to overcome the last bit of this adventure. Thank you for your companionship all these years and especially during the most challenging months of lockdown. You have been the best office-mate I would have dreamed of.

This PhD was financed by the National Research and Development Agency (ANID) Scholarship Program, Doctorado Becas Chile 2017 — 72180200.

Declaration

I declare that this thesis was composed by myself, that the work contained herein is my own except where explicitly stated otherwise in the text, and that this work has not been submitted for any other degree or professional qualification except as specified.

Serguey Maximov

Contents

List of Figures

List of Tables

Nomenclature

Abbreviations

ACAES	Adiabatic compressed air energy storage
BTES	Borehole thermal energy storage
CAES	Compressed air energy storage
CCGT	Combined cycle gas generation plant
COP	Coefficient of Performance
CSP	Concentrated solar power
DH	District heating
DH+HP	District heating with heat pump integration
DHW	Domestic hot water
DLSC	Drake Landing solar community
DNI	Direct normal irradiance
GF	Ground floor
GHG	Greenhouse gas
GHI	Global horizontal irradiance
HDD	Heating degree days
HX	Heat exchanger
IHDS	Indoor heat delivery system
LCOE	Levelized cost of energy
LCOS	Levelised cost of storage
LMTD	Logarithmic mean temperature difference
LTS	Long term storage
NRMSD	Normalised root-mean square deviation
OCGT	Open cycle gas generation plant
PCM	Phase change materials
PDA	Air pollution management plan
PDSP	Percentage of hours of the year with different spot price values between two iterations
PELP	Energy planing process of the Chilean Ministry of Energy
PTES	Pumped thermal energy storage
PV	Photovoltaic
SE	Specific emission per unit of energy
SF	Solar field
SFr	Solar fraction

SIC	Central interconnected electricity system
SING	Northern interconnected electricity system
STS	Short term storage
UF	Upper floor
UTES	Underground thermal energy storage

Mathematical Symbols

ΔT	Temperature difference	[°C]
$\Delta T_{HX1_{STS}}$	Temperature difference between outlet and inlet on the cold side of the heat exchanger connecting the SF with the STS	[°C]
$\Delta T_{HX2_{DH}}$	Temperature difference between outlet and inlet on the cold side of the heat exchanger connecting the STS with the DH	[°C]
$\dot{Q}_{boiler}$	Thermal power delivered by the boiler	[kW]
$\dot{Q}_{fuel}$	Thermal power delivered by the fuel	[kW]
$\dot{Q}_{HX2}$	Thermal power through the heat exchanger connecting the STS with the DH	[kW]
$\dot{Q}_{LTS_{charge}}$	Thermal power discharged from the long term storage	[kW]
$\dot{Q}_{LTS_{disch}}$	Thermal power charged to the long term storage	[kW]
$\dot{Q}_{pumps}$	Electric power consumed by the pumps	[kW]
$\dot{Q}_{SF}$	Thermal power delivered by the SF	[kW]
η_{LTS}	Roundtrip efficiency of the LTS	[-]
η_{Ssys}	Efficiency of the system using the solar energy collected in the SF	[-]
θ	Optimal tilt angles	[°]
ACH/h	Air exchanges per hour	[1/h]
c_p	Specific heat capacity	[kJ/kgK]
c_v	Volumetric heat capacity	[kJ/m^{3}K]
C_{elec}	Electricity cost from running the pumps	[€/a]
C_{env}	Environmental cost associated to a carbon tax	[€]
C_{fix}	Fixed cost of operation of each technology	[€]
C_{fuel}	Fuel cost from running the boiler	[€/a]
C_{inv}	Investment cost	[€]
$C_{O\&M}$	Operation and maintenance cost	[€/a]
C_{var}	Variable cost of operating the technology	[€]
D_i	Demand in node i	[MW]
D_{pipe}	Pipe diameter	[m]
EF_{fuel}	Emission factor of the fuel	[kgCO_2/kWh]
EF_{grid}	Emission factor of the electric grid	[kgCO_2/kWh]
G	Global irradiance on the collector's surface	[kJ/h·m^2]

G_i	Generation in node i	[MW]
I_{pipe}	Pipe's heat transfer coefficient considering insulation	[kJ/h·m^2·K]
$LCOE$	Levelized cost of energy	[€/kWh]
LTS_{pump}	Mass flow rate per string of the LTS	[kg/s]
LTS_{vol}	Long term storage volume	[m^3]
P_{mut}	Mutation probability	[-]
Q_{load}	Total annual demand of the load connected to the district network	[kWh/a]
r	Discount rate	[-]
R_i	Energy retrieved from storage in the node	[MW]
S_i	Energy stored from storage in the node	[MW]
SE	Specific emission per unit of heating provided	[kgCO_2/kWh]
SF_A	Solar field area	[m^2]
SFr	Solar fraction	[-]
STS_{vol}	Short term storage volume	[m^3]
$T_{DH_{ret}}$	Return temperature of the district heating	[°C]
$T_{DH_{sup}}$	Supply temperature of the district heating	[°C]
T_{ext}	External/ambient temperature	[°C]
T_{ij}	Energy transmitted between nodes i and j	[MW]
$T_{LTS_{avg}}$	Average temperature across the LTS	[°C]
$T_{LTS_{ctr}}$	Temperature at the centre of the LTS	[°C]
$T_{SF_{in}}$	Inlet temperature to the solar collector	[°C]
$T_{SF_{out}}$	Outlet temperature from the solar collector	[°C]
$T_{STS_{btm}}$	Lowest temperature in the STS / temperature at the bottom of the cold tank	[°C]
$T_{STS_{top}}$	Highest temperature in the STS / temperature at the top of the hot tank	[°C]
v_{max}	Maximum flow velocity allowed in the pipe	[m/s]

Chapter 1

Introduction

During the last decades, the necessity for preventing the effects of extreme climate change has driven the world energy systems towards cleaner generation technologies. This has led towards reducing the dependency on fossil fuel and increasing the share of renewables, with some future scenarios suggesting the global share of intermittent renewable generation reaching close to 60% by 2050 (IRENA, 2019b). Furthermore, the increasing electrification of the final energy use (which is expected to rise from less than 20% by 2015 to more than 40% by 2050 (IRENA, 2019b)) raises new challenges for the design and operation of the energy grid. These challenges arise mostly from the growing complexity of balancing supply and demand in a scenario with high share of intermittent renewable generation. In conventional fossil fuel based systems, this balancing capability is provided mostly by thermal generation, which can adapt to the demand thanks to the readily available chemical energy stored within the fossil fuels. However, the decrease of their participation on the energy systems creates the need of providing alternative sources of flexibility to to allow for further increasing the share of the most cost-competitive renewable generation, such as solar photovoltaic (PV) and wind (Strbac *et al.*, 2016).

According to the IEA, flexibility is "the ability of a power system to reliably manage the variability and uncertainty of demand and supply across all relevant timescales, from ensuring instantaneous stability of the power system to supporting long-term security of supply" (IEA, 2018a). This broad definition is going to be assumed within this thesis. It considers, for instance, the short term frequency stability of the grid, which is the most common example of operational flexibility, but also encompasses the bulk storage of energy that allows for balancing intraday and longer periods of supply and demand mismatches. Some of the most commonly mentioned sources of flexibility for electric systems are enhancing and strengthening the grid, improving variable renewable generation forecasting, demand side management, integration of energy markets and systems, and energy storage (Gallo *et al.*, 2016). Among these options, energy storage is arguably the most effective, as it can decouple supply and demand by time shifting power delivery. Amidst energy storage technology options, thermal

energy storage (TES) has important advantages, as it tends to present low costs per unit of stored energy, can be independent of geographical or geological constraints, it has low cycling efficiency degradation and it can be designed to store energy for months (White *et al.*, 2013; IRENA, 2020).

Chile, having large potentials for solar and wind generation, has recently increased its targets to achieve 100% renewable generation of electricity by 2050 (Ministerio de Energia, 2021a), creating flexibility requirements above the world's average. This, exacerbated by the topological limitations of the energy network, has led to the energy policy to address flexibility requirements and generating the first national strategy for the electric system's flexibility in 2020 (Ministerio de Energia, 2020b). However, so far, this strategy has focused on setting the background and defining pathways to promote flexibility in general, but more in depth technical analysis of specific technologies is required to promote concrete technically and economically optimal solutions.

In addition to the electricity sector, Chile requires to transition its heating sector, which represents 53% of the final energy use in households and it is supplied in a 35% by fossil fuels, 2% by electricity and close to 63% by biomass (Yáñez *et al.*, 2019). It is worth mentioning that this biomass is mostly high humidity firewood burned in low efficiency stoves, and it is responsible for close to 85% of the particulate matter pollution (Ministerio de Energia, 2020d) that is the main cause of acute air pollution crisis in cities and towns of southern Chile during the winter season (Ministerio del Medio Ambiente, 2018). In response to this situation, the Chilean Government has launched in 2020 its Strategy for Residential Energy Transition (Ministerio de Energia, 2020d) and in 2021 the National Strategy for Heat and Cold (Ministerio de Energia, 2021c), which set the goal to reach 80% sustainable energy for heating by 2050. This strategy, for the first time in Chile's energy policy history, sets a framework to specifically focus on heat decarbonisation. Although at this stage, it does not provide specific pathways to achieve its goals, it mentions district heating (DH) as one of the technologies that would enable the sector's transition.

The specific mention of DH as one of the technological options is based on its inherent operational flexibility, as this technology can easily be combined with TES to balance fluctuations in demand and can enable the use of various energy sources including industrial excess heat, geothermal, sustainable and clean biomass and solar energy (International Energy Agency, 2019a). Moreover, thanks to its natural thermal inertia and access to cheap energy storage, DH are especially well suited to facilitate the integration of the electricity and heating sectors, promoting additional flexibility to both, electricity and heating systems through the integration of their demands and their energy generation sources (IRENA, 2020). Although recent studies

have identified the potential for wide DH implementation in Chile (Paardekooper *et al.*, 2020), there is a lack of studies that assess the behaviour of specific DH configurations under Chilean conditions. Especially, there is no assessment of how solar thermal energy would operate integrated to DH networks in the cool but sunny conditions of southern Chile.

Therefore, this thesis applies techno-economic optimisation models to assess the potential for TES to support the Chilean energy transition. It investigates the capability of TES to provide additional flexibility to the electricity grid, to support the use of clean energy sources in the heating provision and to facilitate the integration of heating and electricity systems, increasing their flexibility and efficiency of operation.

1.1 Research question

As can e summarised from the previous section, the motivation of this thesis is to study the capacity of thermal energy storage to support the deployment of technologies that would advance the clean energy transition. This motivation opens a general research question addressed in this thesis, which is **how can thermal energy storage support the transition towards a cleaner energy matrix?**. Given the many possible perspectives to approach this question, in the context of this thesis, it is addressed by focusing on the following particular questions:

1. Can thermal energy storage at grid level increase the penetration of renewable generation in the electricity grid?
2. What are the optimal locations and sizes for on-grid pumped thermal energy storage to minimise the cost of the future energy system?
3. How can thermal energy storage support the use of variable renewable energies in residential heating applications?
4. How can thermal energy storage increase the flexibility of thermal demand and facilitate its integration with the electric grid for the provision of clean heating?

Although these questions are addressed in the Chilean context the analysis and conclusions can be applied to other countries and territories, especially to those with similar geographical and climatic characteristics.

1.2 Contribution to knowledge

The work presented in this thesis relies on mathematical modelling, simulations and different optimisation techniques to evaluate the technical and economic merits of TES in the Chilean energy context. Nevertheless, the methodologies presented could be applied to other locations and different energy system designs.

The following list of methods developed specifically to tackle the aforementioned research questions can be considered novel, as they are developed specifically for this research:

- A machine learning method based on a multiple linear regression was developed to predict the temperature of the borehole long term storage after an initial 6-year charging phase. This allows for skipping the simulation of those initial years and reducing the total optimisation time. This tool is applied through Chapters 4 and 5 and explained in detail in Appendix B.
- A novel method to improve the convergence of the genetic algorithm used for the multi-objective optimisation was proposed and implemented. The implementation of this method is presented in Appendix E and used for the optimisation process in Chapters 4 and 5.
- An iterative method of evaluating the new electricity market equilibrium spot prices is proposed and applied in Chapter 5.

The following is a list of the results that can be considered original, either because of the particular problem being addressed, the methods used for the analysis or their specific results in the context of the Chilean energy system:

- **The assessment of the long term role of on-grid TES on the deployment of intermittent renewable generation in the Chilean electricity system.** Thermal storage for electricity, such as pumped thermal energy storage (PTES), has specific characteristics and advantages when compared to other technologies for electricity storage such as lithium-ion batteries or pumped hydro. These special characteristics were included in a dispatch and expansion optimisation model of the Chilean electricity system, and the economic benefit of the availability of this technology was evaluated.
- **The techno-economic analysis of the suitability of solar thermal district network with seasonal thermal storage for the special sunny and cool conditions of southern Chile.** A framework for a multi-objective simulation-based optimisation was developed to optimise the design of the system under specific constructive and climatic conditions of southern Chile. Methodologies for decreasing the simulation time of high thermal inertia energy storage and for increasing the multi-objective optimisation Pareto front development were proposed. Several design features were optimised using a de-

tailed representation of the system and the resulting optimal system's techno-economic performance was compared with conventional heating alternatives. The effect of the presence of seasonal storage on the optimal tilt angle of solar collectors was investigated.

- **The evaluation of the added techno-economic value of integrating a power-to-heat scheme with a solar thermal network with seasonal thermal storage operating under future variable electricity spot prices.** A model of a heat pump was added to the simulation and future local spot prices were projected to simulate the power-to-heat system's operational logic. The system was re-optimised and its techno-economic performance was compared to systems optimised without the power-to-heat addition.
- **The proposal and implementation of a method to assess the value of the flexibility of power-to-heat schemes with thermal storage in comparison with non-flexible demands.** The dispatch and expansion optimisation model of the Chilean electricity grid was integrated with the simulation-based optimisation model of the solar district network with power-to-heat integration. The proposed method was run to determine the modified spot prices when a large scale deployment of flexible power-to-heat schemes operate in the electric market. The impact on the electric grid expansion and on the spot price was assessed and contrasted with the effects of inflexible demand.

The methods and results of this thesis could be of interest to researchers, engineers and policy planners involved in the areas of energy system integration, the flexibility of energy systems and sustainable heating technologies.

1.3 Thesis structure

This document consists of 6 chapters. The content of each of them is summarised in the following list, and a schematic representation of how they interact is presented in Figure 1.1.

- **Chapter 2** presents background on some of the most common methods used for energy system analysis and reviews previous energy modelling methods applied to assess the Chilean energy system. It sets the stage for the Chilean energy policy evolution in recent years, with a special focus on the requirements of flexibility and the incorporation of heat in the energy agenda. Finally, it presents a summary of the different TES technologies, some of which are used in the models developed in the next chapters.
- **Chapter 3** adapts and applies a linear optimisation framework developed in Python to generate a model of the Chilean electricity grid. It analyses the long term expansion of the grid and assesses the effect of PTES on the future investments and operation of the system. Optimal quantities and locations of future generation and storage expansion are presented and analysed.

- **Chapter 4** develops a framework for optimising the design of a solar district heating network with seasonal energy storage, integrating a TRNSYS based simulation with a genetic algorithm optimisation coded in Python. It modifies an existing simulation model, generating parametric expressions for the piping design, head losses and pump sizing, adapting the simulation to different initial design conditions. Results of optimal sub-system sizing and optimal operational values are presented and the effects of their optimisation are discussed.
- **Chapter 5** performs a re-optimisation of the model developed in Chapter 4 considering the addition of power-to-heat technologies in the form of resistance heaters and heat pumps. A technique to construct an annual spot price based on representative days is proposed and applied to simulate the operation of the electric heaters purchasing energy based on spot price variation. The optimal configurations techno-economic performance are compared with the system without power-to-heat integration. Finally, it integrates the results of the simulation-based optimisation model with the model developed in Chapter 3. The effects on the electric grid's operation and expansion caused by the additional flexible demand of large scale penetration of district networks with power-to-heat integration are assessed and compared against the effects of inflexible alternatives.
- **Chapter 6** summarises the conclusions of the previous three chapters and draws new conclusions integrating the previous chapters' analyses. Additionally, it proposes further research that could build on the methods and results presented in this thesis.

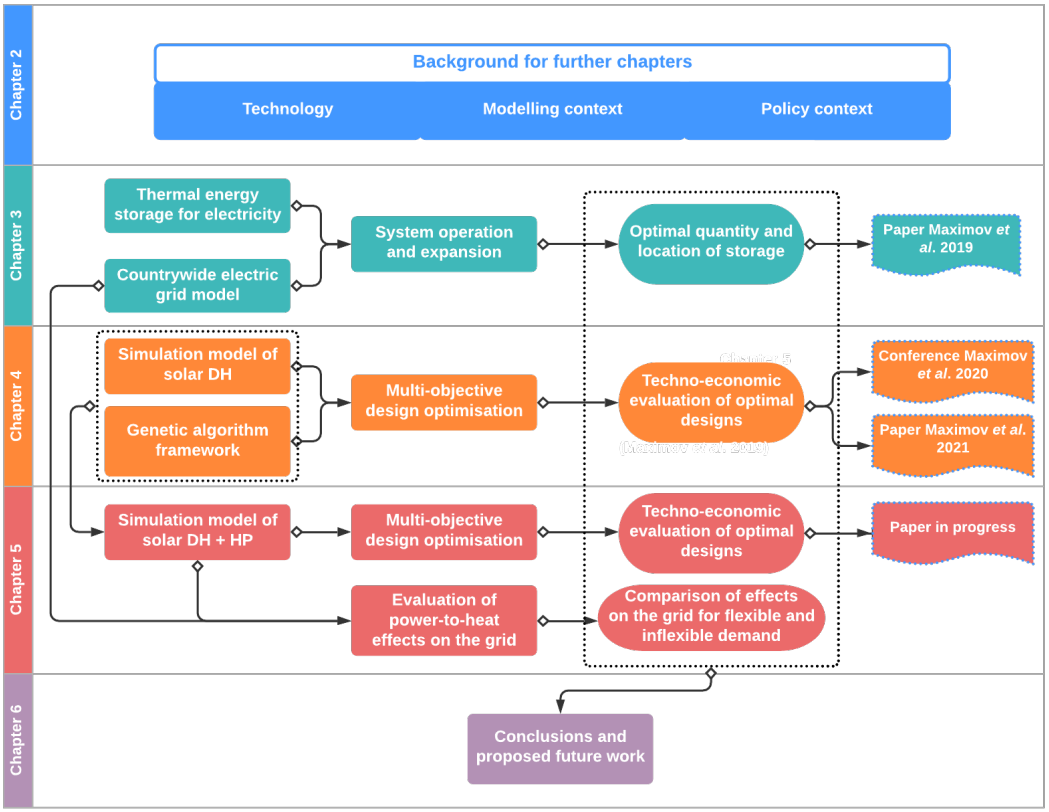

Figure 1.1: Scheme of the thesis structure and the relation of the models developed during the thesis

Chapter 2

Background

This chapter provides a background on the structure and main characteristics of the Chilean energy system. Following, it presents a review of the modelling efforts to represent and optimise the design and operation of this system with the aim to identify gaps in knowledge that are worth addressing. It also presents a summary of the changes and advances of the last years' Chilean energy policy around energy storage, grid flexibility and clean heating pathways with the objective to put this research in context and highlight its relevance in the current scenario. Finally, it presents a background on the main technologies analysed in this thesis with the aim to consider their advantages and drawbacks.

2.1 Chilean energy system structure and characteristics

Chile is 4,300 km long and, on average, 175 km wide. Most of its territory is land-marked by mountains, with the Andes dominating the eastern border and several smaller mountain ranges crisscrossing north to south and east to west. This gives the country an average altitude of 1,800 m and defines and constrains the energy infrastructure potential.

Chile's climate area can be roughly broken into four quarters. The northernmost area of the country is dominated by the arid Andes highlands and the Atacama desert. This transitions towards a mediterranean climate in the centre of the country. The southern area corresponds to an oceanic climate which transitions onto a sub-polar climate in the far south.

The conditions defined by topography and climate define that close to 80% of the population resides in the central and central-south areas, and determines the availability of renewable resources along the country.

For its supply of energy, Chile largely depends on imports, as its domestic energy production covers only about one-third of its close to 32 Mtoe (tons oil equivalent) total primary energy supply. Oil is the largest primary energy source, followed by biofuels (mainly firewood for house heating) and coal. This is better appreciated in Figure 2.1, where it can be noticed that fossil fuel accounts for 70-85% of the total energy supply (Ministerio de Energia, 2017c). In this figure, it is clear that transport and the industrial sector (which includes the large copper mining

operations in the north of the country) represent each slightly above one-third of the total final energy demand. The remaining 25% is used by the public commercial and residential sectors, which are often grouped under the "building sector" label, as most of its energy demand arises from building thermal conditioning and people's energy use within buildings. From a purely electric demand perspective, 60% of the total demand is required by the industry, with mining representing almost half of it. The remaining 40% is used by the building sector with transport having yet a negligible participation in the electricity demand.

Most of the primary fossil fuel supply has to be imported, as Chile has very low fossil fuel production, and 100% of the oil, 95% of coal and 80% of natural gas are shipped from abroad. Only a small amount of natural gas is produced in the far south of the country, where it is used locally for heating, electricity generation and methanol production.

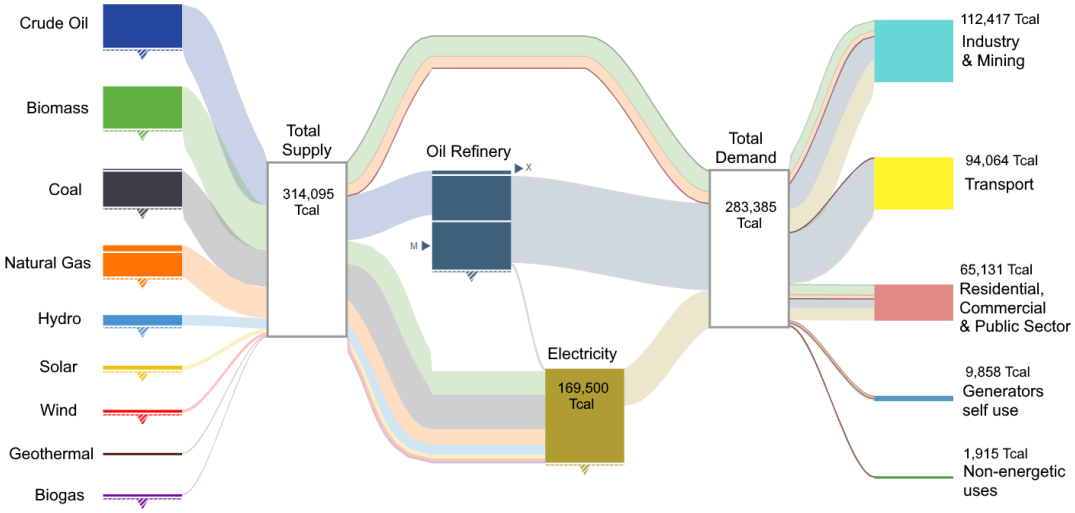

Figure 2.1: Sankey diagram of the energy supply and demand in Chile

With respect to renewable resources, solar is the most abundant, with an estimated potential above 1,500 GW. As can be appreciated in Figures 2.2(b) and 2.3(a), this extraordinary resource is concentrated in the northern part of the country. This is a sparsely populated area with an important electricity demand (as can be seen in Figure 2.3(b)), mostly from the mining industry. The on-shore wind potential has been estimated at around 40 GW in the areas covered by the national interconnected system (shown in Figure 2.2(a)). It is more evenly distributed along the country than the solar resource, but it tends to concentrate in the north and south of the country. There is important wind potential in the far south area of the country, but the distance from the main demand makes its current development unfeasible. The potential for off-shore wind has been estimated at around 1 GW. This relatively low potential is hindered by the rough waters of the Pacific Ocean and the high depth of the coastal waters, which forces the use of floating technology to develop close to 90% of said potential (World Bank, 2020). Hydroelectricity is the most developed renewable generation technology,

with close to 7 GW installed capacity, mostly in the south of the country. There is a remaining 5 GW potential to be developed, but most of it is far from the demand centres and the remaining confronts important resistance from the population due to the local environmental impacts (Bardeen, 2018).

The electricity system consists of a main national electricity network, shown in Figure 2.2(a). This system covers 95% of the population and concentrates 99% of the 27 GW of installed capacity in 2021 (21 GW in 2016). The remaining systems cover cities located in the southernmost area and isolated and insular localities. As it is clear from the figure, the system is practically linear and it is not interconnected with neighbouring countries, which limits the possibility of balancing the system by importing or exporting energy.

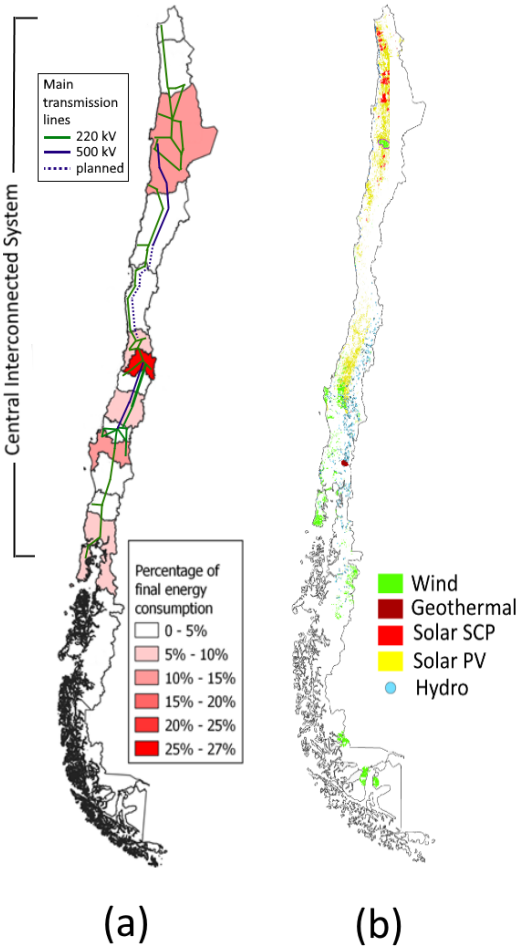

Figure 2.2: (a) Simplified diagram of the interconnected electricity system superposed to the total energy demand distribution by regions. (b) Areas where the renewable potential can technically and economically be developed. (Adapted from Ministerio de Energia (2019a) and Ministerio de Energia (2021d))

Figure 2.3 shows the geographical distribution of the renewable potential in the areas of the country covered by the main electric system and contrasts it with the main demand zones. As it can be noticed, the main demand concentrates in the centre of the country, where there is no abundance of renewable potential. This creates the requirement of transporting electricity for several hundreds of kilometres, generating an additional burden on the system. The northern area of high demand corresponds to the mining industry. This demand coincides with the area of the highest solar potential. However, the continuous operation pattern of mining facilities creates the requirement of balancing technologies, such as energy storage or conventional generation, to allow for the operation at night time.

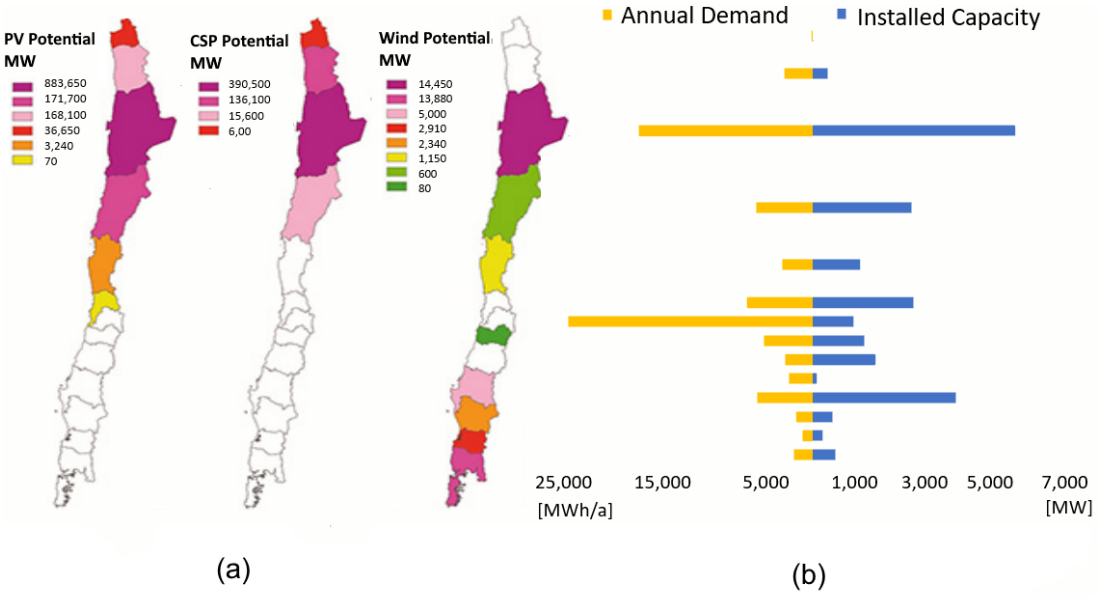

Figure 2.3: (a) Geographical distribution of renewable potential by region in the interconnected electricity system. (Adapted from Santana *et al.* (2014)) (b) Current installed capacity of electricity generation and annual electricity demand.

Based on the local temperature along the year, the country is divided into seven thermal zones that can be appreciated in Figure 2.4. These zones, as can be expected, are organized from north to south, with a local effect of altitude on the east of the country due to the Andes mountains. As it can be seen in the figure, the preferred fuel for heating in the coldest areas is firewood, due to its abundance and low cost. An anomaly can be noticed in zone 7, which demand is dominated by the sub-polar city of Punta Arenas, where firewood is scarce but there is supply of cheap locally produced natural gas. In the warmer areas, on the other hand, the preferred energy sources for heating are electricity and gas (natural and LPG) as in those zones there is no easy access to cheap biomass. The use of firewood creates an acute local pollution problem in many towns and cities of southern Chile which require immediate action to address in an effective manner (Molina *et al.*, 2017).

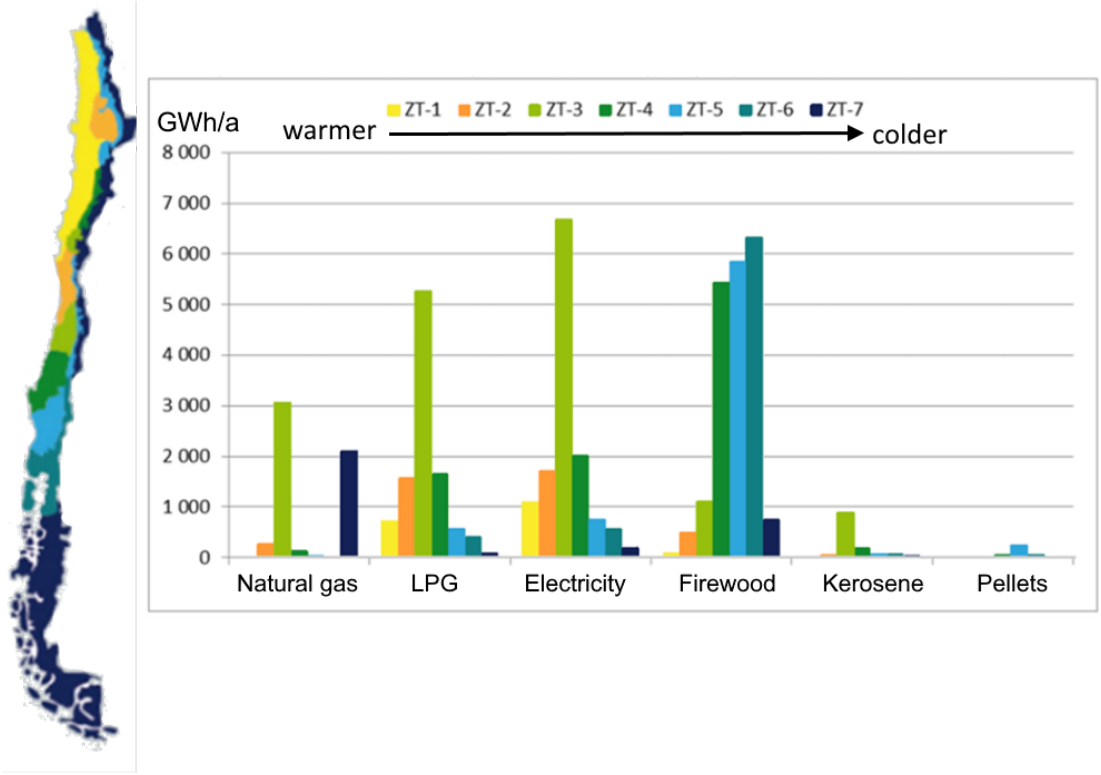

Figure 2.4: Thermal zones in Chile and energy consumption for heating in each zone by type of fuel. (Adapted from Ministerio de Energia (2019a))

2.2 Role of flexibility in the Chilean energy system transition

There is a consensus on the need to increase renewable energy participation in the energy matrix to limit global warming below the 2°C average temperature rise. According to IRENA, 85% of the global electricity and 60% of the total energy need to come from zero-emission technologies by 2050 to reach this goal (IRENA, 2019b). The cheapest and most developed of these technologies are currently solar photovoltaics (PV) and wind generation, which are unfortunately variable and intermittent. This future energy system's configuration with high participation of inflexible renewable generation would require the addition of further flexibility sources to overcome the challenges of balancing supply and demand.

The Chilean electricity system is not alien to these new requirements. In 2018, in a report focusing on the country, the IEA suggested that large shares of non-dispatchable renewable generation requiring higher flexibility provision will force baseload-designed coal power plants to operate more as cycling mid-merit and peaking generators (IEA, 2018b). Since the publication of this report, the Chilean Government has announced the total coal phase-out by 2040 (Ministerio de Energia, 2020f), has increased its renewable generation goals from 70% to

100% by 2050, and has announced that the backbone for a whole system decarbonisation will be electrification, with the aim of achieving carbon neutrality by 2050 (Ministerio de Energia, 2021a). This puts a much more intense strain on the electricity system than IEA's prevision in 2018 and highlights the need for different sources of flexibility.

The need for systemic flexibility has led the Chilean energy policymakers to produce the first version of a strategy to increase the flexibility of the electric system (Ministerio de Energia, 2020b). However, at this stage, this strategy is limited to defining reforms to the electricity market to promote flexibility and reliability of the system, focusing mostly on generation and storage, without analysing the possible contribution of specific technological alternatives. This stresses the importance of making available information on the value of different demand flexibility measures, as there is no unique solution and combinations of various flexibility options would be required to manage the systems of the future (Lund *et al.*, 2015), with improvement in transmission and distribution infrastructure, deployment of various energy storage technologies, more flexible demand and integration of multi-vector energy systems playing all an important role in this flexibility solutions mix (IRENA, 2018).

The following sections of this chapter summarise energy system modelling options that can be used for analysing the role of flexibility providing technologies and review some applications to the Chilean energy system context.

2.3 Energy system models

Energy system models are representations of the operation of a given energy system. Their main purpose is to support the design, planning, implementation and operation of energy systems. Most of them can be classified as optimisation or simulation models. A simulation may be defined as a representation that replicates the operation of a system under defined conditions. In other words, it mimics the behaviour of a system for one specific configuration and set of assumptions. Optimisation, on the other hand, is the mathematical modelling of the system that allows finding the values of a number of decision variables that minimise or maximise one or more objectives. These decision variables are usually design or operational characteristics of the system, and the objectives are often cost or a performance indicator of the system (Lund *et al.*, 2017). It focuses on mathematically formulating the objective function and sets a number of constraints that represent the physical characteristics of the system.

A simulation model, in general, tends to represent the different parts of the system with more complex models, which may include solving differential equations or using finite element modelling. This makes simulation often a closer representation of the operation of the real system but adds a toll on the computing time. Optimisation typically needs to evaluate the objective function many times. Hence, it often employs reduced-order representations to

decrease the computational time of each evaluation. These differences have to be taken into account when analysing the results of any study including these methods (Renaldi, 2018). It has to be noticed that these two kinds of models are not necessarily mutually exclusive, as simulation can be used for optimising certain variables and optimisation can be used to predict the behaviour of a system. Furthermore, simulation-based optimisation combines both techniques by using an optimisation algorithm that runs a simulation to evaluate the objective function instead of evaluating a simplified mathematical formulation.

A general optimisation problem can be expressed as:

$$\begin{aligned} min \quad & f(x) \\ s.t. \quad & h(x) = 0 \\ & g(x) \leq 0 \end{aligned} \tag{2.1}$$

where x is the set of decision variables to be optimised, f is the objective function and h and g are the constraints.

Depending on the nature of the variables being optimised, the problem can be classified as an operational optimisation, a design and operational optimisation, or a synthesis, design and operational optimisation. Operational variables can be mass flow rates, temperature setpoints or any setting that could be modified during the operation. Design variables can be the size or rating of the equipment included in the system, and synthesis variables correspond to decisions on whether to include or not pieces of equipment or connections between them (Renaldi, 2018).

Depending on the linearity of f, h and g, and the kind of variable x in the equation 2.1, an optimisation problem is classified into different categories:

- Linear programming (LP), when f, g and h are linear and all variables are continuous.
- Non linear programming (NLP), when f, g or h are non-linear and all variables are continuous.
- Mixed integer linear programming (MILP), when f, g and h are linear and some variables are discrete.
- Mixed integer non-linear programming (MINLP), when f, g or h are non-linear and some variables are discrete.

Depending on these categories, there are different methods or algorithms to find the optimal solution. Deterministic algorithms require complete mathematical knowledge of the problem's formulation and perform predefined search patterns to find a solution. LP problems are the simplest to solve using deterministic approaches, but they usually involve a trade-off inaccuracy, as many physical phenomena are non-linear, and a linear approximation (linearisation) is required to model them as an LP. The *simplex* and *interior point* algorithms are a couple of commonly used methods for LP optimisation. MILP problems keep the linear approximation,

but the presence of discrete variables allows for modelling *on-off* processes that are very common in energy systems. They are slower to solve, as to tackle MILP problems it is required to solve several linear sub-problems (relaxations) (Renaldi, 2018). The most common algorithm for solving MILP problems is *branch and cut*, which solves the linear relaxations of the original problem and then adds further linear constraints to drive the solutions towards an integer value (Kumar and Mageshvaran, 2020). Algorithms for NLP usually employ derivatives of the objective function to search for optimal solutions within the feasible region, but at the current state of development they can get stuck on a local optimum, thus a global optimal solution is not guaranteed. MINLP problems are the most difficult to solve, as they combine the branching methods for solving mixed integer problems with algorithms to approximate the optimal solution in non-linear formulations (Kumar and Mageshvaran, 2020). Furthermore, the computational time required to solve a MINLP problem is usually several orders of magnitude higher than of a MILP (Voll, 2013).

An alternative to deterministic algorithms is meta-heuristic algorithms. These algorithms use randomised patterns to explore the solution space and look for the most optimal solution. In order to perform this exploration, meta-heuristic algorithms need to be able to evaluate the objective function at any point of the space, but they do not require to analyse the mathematical structure of the objective function or the constraints. Therefore, they can be applied to problems where the mathematical formulation is not known (black-box models) or where deterministic methods fail due to the complexity of the objective function (Voll, 2013). However, due to its randomised search pattern and lack of knowledge of the objective function's properties, meta-heuristic algorithms are usually slow to converge and cannot guarantee a global optimum solution for every problem.

A particular example of a meta-heuristic approach to optimisation is the genetic algorithm (GA), an evolutionary algorithm inspired by the theory of evolution and survival of the fittest. The algorithm starts with a (usually) random initialisation, where a population (set of individuals) is created. Each of the individuals can be represented as a vector of values for each of the variables (genes). The objective function is evaluated for every individual, defining their fitness. Next, the algorithm selects individuals based on their fitness and additional criteria depending on the specific algorithm and its initial configuration. Non-selected individuals are eliminated and surviving individuals are stored as optimal candidates. Besides, selected individuals become parents of a new generation by randomly allocating pairs of selected individuals and exchanging their genes (mating). With the objective of diversifying the genetic pool, the offspring individual, containing a random mix of its parents' genes, also undergoes a process where some of its genes may randomly change (mutation). The process of creation of a new generation is controlled by mating and mutation operators which are defined at the beginning of the optimisation process or may adapt along with the evolution of the population. The newly created offspring are evaluated and the fitness-based selection process is repeated until a

certain stopping criterion is met. The optimal solution (or closest to optimal, as optimality is not guaranteed) is constructed by selecting all the non dominated solutions, which means that every member of the solution performs better in at least one objective function to every other individual evaluated during the optimisation. Figure 2.5 presents a schematic representation of a GA optimisation process.

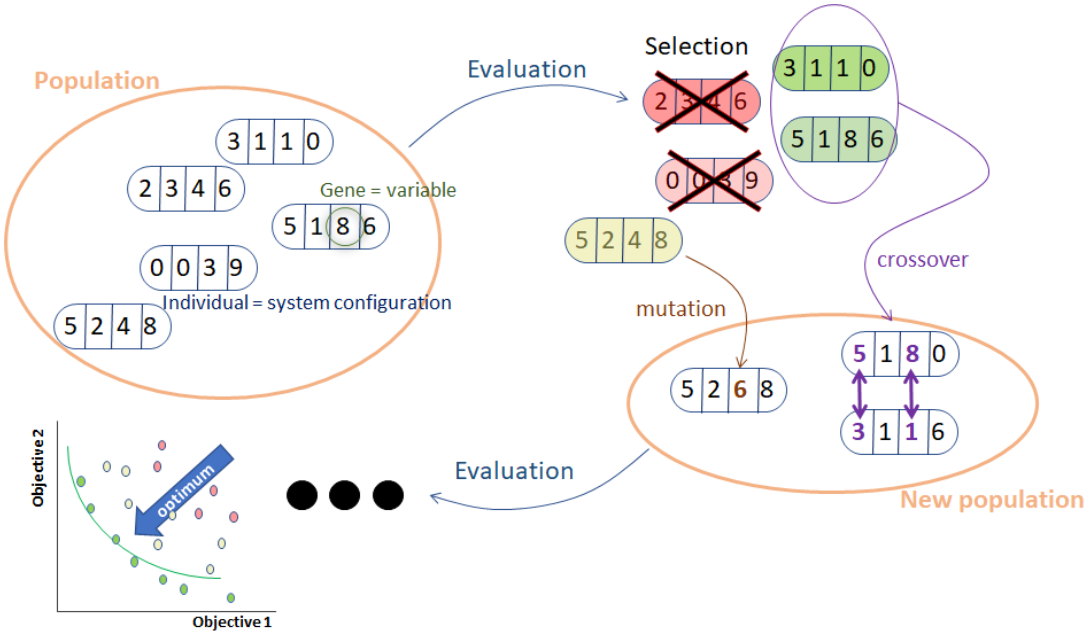

Figure 2.5: Schematic representation of a genetic algorithm with four optimisation variables and two objectives

Meta-heuristic algorithms in general, and GA in particular, are especially well suited to operate in simulation-based optimisation, as they do not require to "understand" all the calculations and assumptions behind the simulation, but suffice with the value of the objective function given as an output of the simulation. Another advantage of GA is that they can be applied straightforward on multi-objective optimisation problems, as they treat multiple objective functions independently and only combine them to select the best individuals. The main drawback is that each evaluation of an individual requires running an entire simulation, which may range from a few seconds to several minutes (or even more).

In the next section, the application of some of these models to assess energy systems in the Chilean context is discussed with the objective to detect gaps yet to be covered.

2.4 Energy models for the Chilean energy system

Traditionally, the Chilean energy policy has focused predominantly (if not exclusively) on the electricity system. Even though, as it will be discussed in Section 2.5, this has begun to change in the last years, by far the main stock of energy models and studies are focused on modelling the electricity grid and few cover thermal uses. This section aims to present a summary of models and studies applied to Chile that cover optimisation and simulation of energy systems, focusing especially on those that include TES and alternative heating technologies in their analysis.

The most common models found in the literature are mathematical programming approaches that analyse the operation and expansion of the electric system. Haas *et al.* (2019) developed a four nodes linear programming model of the Chilean electric grid based on LEELO (Haas, 2018). They used this model to perform a multi-objective optimisation of the system's expansion, minimising the cost of the system, the need for new transmission lines and hydropeaking (fluctuation in flow releases from hydropower reservoir that provides flexibility response to the grid but that deteriorates the downstream river ecology). This study was the first that tried to include the socio-political criteria (public opposition to transmission lines) and ecological criteria (degradation of river basins). It also showed that relatively coarse representations of the Chilean electric grid (four nodes, in this case) may be used for analysing long term expansion planning.

Mena *et al.* (2019) developed a linear optimisation model of the Chilean electricity grid with the objective to analyse the effect of CSP systems with TES based on the SWITCH platform (Fripp, 2012). Verastegui *et al.* (2021) built on Mena's research and developed a power system expansion planning model that incorporates a linear relaxation of the unit commitment problem with a more detailed representation of the transmission and hydro networks and inclusion of battery storage. Based on representative days, they analysed three different decarbonisation pathways with distinct coal phase-out horizons with the aim of getting insight into the flexibility requirements in a high renewable penetration future. Verastegui *et al.* (2020) also used the same approach but focused on evaluating the effects of the electrification of firewood domestic heating. In this study, the heating supplied by firewood was estimated at a regional level and fractions of it were added as an electricity demand according to various electrification scenarios. They did not explicitly include flexibility options on new heating electricity demand, but they emulated flexible consumption by creating sensitivity analysis scenarios with different degrees of smoothing of the heat demand curve while keeping the total thermal consumption constant. Their main findings were that, as it can be expected, large amounts of flexibility in the way of electricity storage (modelled as batteries in this study) are required to cope with high degrees of electrification. These requirements are reduced in the cases where the extra demand is smoother, decreasing the total cost of the system. This means that there is a clear

value in making future heat demand more flexible. However, a more explicit representation of the flexible capabilities of different technologies, such as TES coupled with large heat pumps (HP) or the use of solar thermal heat, is still to be implemented and assessed in this kind of model.

Osorio-Aravena *et al.* (2021) also developed a linear programming model of the Chilean energy system with six nodes based on LUT Energy System Transition model (Prina *et al.*, 2020). It is the first study using an optimisation approach considering the coupling of several sectors: electricity, heat and transport. Four scenarios, reflecting different policy pathways were assessed, and the energy system's development projected until 2050 considering the interactions between the different systems. So far, this is the most complete effort for investigating the effects of different energy systems coupling. However, these couplings seem to rely on instantaneous energy transformations, and the effects of technologies such as TES and the flexibility that they can provide are not explicitly accounted for.

Other linear programming and mixed linear programming approaches to the Chilean electric grid have been developed by Babonneau *et al.* (2021) based on ETEP (Babonneau and Haurie, 2015), Gaete-Morales *et al.* (2019), using PowerGAMA (Svendsen, 2021) and Munoz *et al.* (2017) using AIMMS (AIMMS, 2021).

The only study found that generates a specific model for the heating sector is Paardekooper *et al.* (2020), which applied the Heat Roadmap methodology (Heat Roadmap Europe, 2020) and developed a scenario based simulation model on EnergiPLAN (Aalborg University, 2021) for a countrywide assessment of the potential of district heating using a set of different energy sources, such as combined heat and power, heat pumps, solar and geothermal heat, biomass and gas boilers. This study is, at this date, the only known publication aiming to assess heating at a systemic level and commenting on its potential integration with the electricity sector. This study is based on Paardekooper *et al.* (2019), a previous report that presents more details on the modelling, based on the recently developed Chile' heat demand map (EBP Chile, 2019). This study proposes to use the integration of heat and power to balance the fluctuating nature of wind and solar PV with electricity from CHP generators that provide heat to DH. When renewable electricity is abundant, the CHP generation is reduced and the required heat is supplied by large heat pumps that consume the renewable electricity. They showed that by implementing DH and the previously mentioned heat and power integration, there are important increase in wind penetration and a decrease in particulate matter emissions, without increasing the total cost of the system. Interestingly up to 40-50% of the total heating demand can be shifted to DH networks without incurring extra costs and still producing the previously mentioned positive impacts.

With regards to studies focusing on modelling TES technologies, they are mostly constrained to building level simulations. For instance, an EnergyPlus (NREL, 2021) based model of a single multi-storey building located in Santiago was developed by Venegas-Troncoso *et al.* (2019) to analyse the technical feasibility of an ice energy storage. Important reductions in cooling energy are noted. However, no economic analysis nor broader systemic implications of the technology are reported. A similar analysis was performed by Bohórquez-Órdenes *et al.* (2021) for a single house using wall-embedded PCM materials. The only reference related to long term TES technologies was found in Roth *et al.* (2004). In this study, a one borehole heat exchanger was tested in the city of Valparaiso (central Chile) with the objective to obtain local ground heat conductivity. Several tests were performed and a conductivity of 1.8 W/mK was obtained. No follow up or further mention of the BTES technology has been found.

This short review of existing models shows that there is an opportunity to develop models that investigate the use of TES in the electricity system and integrate the electric system with heating applications, studying in detail the effects of this integration on the flexibility and efficiency of both systems. The following section provides a context for the need for these kinds of studies from the perspective of the current state of the Chilean energy policy.

2.5 Chilean energy policy in the recent years

This section does not aim to perform a complete review of the Chilean energy policy but to present a quick summary of its evolution to establish a temporal context for the current situation and highlight how the research presented in this thesis fits this setting. A more extensive review of the last ten years development in Chilean energy policy can be found in Simsek *et al.* (2019) and IEA (2018b).

As it was pointed out previously, during most of the past years, Chilean energy policy has focused almost exclusively on the electricity sector. Moreover, it can be argued that since the liberalisation of the electricity sector in the early 1980s, Chile's energy policy actions were concentrated only on promoting competitiveness in the electricity market and regulating safety and technical procedures of the fuel and electricity system operations (Madariaga and Gladina, 2018; Borquez, 2020). This state of affairs began to change in the early 2000s when a prolonged drought limited the hydro generation and the gas supply from Argentina was cut due to internal problems, forcing the Government to take a more active role in defining pathways for the development of the energy sector. This led to the enactment of laws to increase the market competitiveness of non-conventional renewable energy (2004-2005), the creation of new public bodies, such as the National Programme for Energy Efficiency (2005) and the Ministry of Energy (2010), and the publication of the first attempt of a coordinated energy policy (CNE, 2008). The first step was provided by the "Short Law I" (2004), which decreed reduction in transmission charges of energy for renewable generation below 20

MW and exemption for those generators below 9 MW. It was followed by the "Short Law II" (2005), which imposed that by 2010, 5% of the total energy supplied by the distributors must come from non conventional renewable sources (explicitly excluding hydro above 20 MW) (Madariaga and Gladina, 2018).

In the last decade, the energy policy has evolved, considering participatory approaches to cope with the much more frequent socio-environmental conflicts related to energy projects (Bohórquez-Órdenes *et al.*, 2021), including climate change goals expressed in the Intended Nationally Determined Contributions (Gobierno de Chile, 2015) and decreasing the concentration of the energy generation sector. This heralded a change in the paradigm towards a much more active role of the State in the definition of the energy system of the future, consolidated in a document called "Energy 2050 - Chilean Energy policy" (Ministerio de Energia, 2015), a long scope energy policy which defined the official vision of the State about energy sector. This vision materialised through the definition of four pillars to develop the Chilean energy system: (1) Quality and Security of supply; (2) Energy as driver of economic development; (3) Energy in harmony with the environment; and (4) Energy education and efficiency. This version of the energy policy still focused mainly on the electric sector but incorporated concepts like promotion of "cleaner heating" and "collective heating" in zones with higher pollution levels, "affordable heating" to reach thermal comfort in households, and policies for sustainable and efficient use of firewood. Furthermore, it was drafted following a participatory process including experts of academia, industrial stakeholders and environmentalists, which provided the document with a higher public opinion validation and diffusion. Following this new policy and its inclusion of concern for clean and affordable heating services, a series of documents supporting this new scope has been developed. Some notable examples are the guidebook for district heating project development (Morales *et al.*, 2018); the first attempt to spatially represent heat demands through heat maps in four cities of southern Chile (EBP Chile, 2019); a strategy for energy transition in the residential sector (Ministerio de Energia, 2020d), which sets one of its objectives on providing alternatives to the use of firewood at accessible costs; and the Strategy for Heating and Cooling (Ministerio de Energia, 2021c). This last document acknowledges the low relevance that cooling, and particularly heating, have been given in the energy planning process, and aims to combine all the previously disperse heating and cooling related initiatives into a coherent policy. It identifies barriers and challenges towards achieving a clean, affordable and reliable heating supply for the population, and defines an action plan to tackle some of these barriers in the short and medium term.

Additionally and in line with the last obligations included in the National Determined Contributions (Gobierno de Chile, 2020), the Chilean Government has announced the phase-out of coal generation by 2040 (Ministerio de Energia, 2020f). This, together with the announcement of a new goal of 80% renewable generation by 2030 and 100% by 2050, anticipates a strain on the electricity system and had prompted to create a strategy to increase the flexibility

of the electricity grid (Ministerio de Energia, 2020b). At this stage, said strategy focuses on identifying normative and market barriers for implementing flexibility measures and proposes some general actions to tackle them, but from an electric-only system perspective. In particular, there is no mention of the integration of energy systems and how TES could increase the overall flexibility. So far, the only proposal for TES use as a flexibility provider in the electric system is the use of molten salts TES as an alternative to totally decommissioning coal generation plants, and transforming them into storage facilities (Ministerio de Energia, 2020c).

The scenario just described reinforces the idea that it is now an ideal moment to research technologies that provide flexibility and facilitate energy systems integration in Chile. Especially, with the aim to promote a whole system approach in the development of the new Chilean energy policy and support the decision making process of the next years. This includes, but is not limited to the study of the capability of TES to provide direct flexibility to the electricity system; investigating the ability of TES to support the deployment of more efficient, cleaner and affordable solutions for residential heating, such as district heating networks and solar heating; and researching the role of TES in fostering the integration of the electricity and thermal systems, enhancing their operational efficiency and reliability.

2.6 Thermal energy storage technologies

As it was pointed out in Chapter 1, energy storage, as one of the sources of flexibility, is necessary for modern systems that have to deal with a high share of intermittent technologies. One of the alternatives for this is using thermal energy storage that has some special characteristics and advantages. The most important is that it usually requires very cheap and abundant storing media, which makes its cost per unit of stored energy low, compared to other technologies such as Li-ion batteries, making it a good candidate for medium to long term storage. It is also generally less constrained by geological and geographical conditions. In addition, it is especially well suited for providing flexibility to thermal energy systems, such as domestic heating and industrial heat, as it does not require energy transformation to store and release heat, reducing the need for additional equipment. Furthermore, TES has a high potential of integrating intermittent renewable sources such as wind and solar into the heating or cooling sector via power-to-heat schemes, increasing the flexibility of both electricity and thermal systems, helping to reduce renewables curtailment (IRENA, 2020).

Figure 2.6 presents the main applications that have been identified for TES, with most of them being directly or indirectly addressed in the course of the work presented in this thesis.

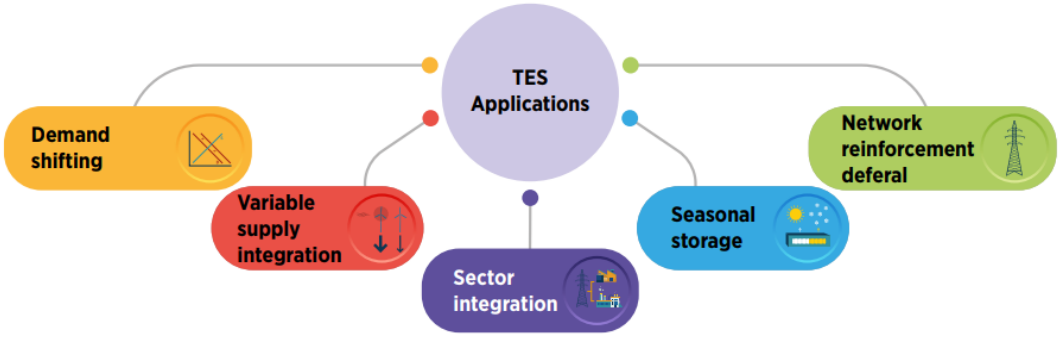

Figure 2.6: Main application of thermal energy storage in energy systems (IRENA, 2020)

There are different ways to classify thermal energy storage technologies. The most common classification is based on the energy retaining mechanism being used as sensible, latent and thermochemical. An alternative classification is by the temperature of the storage, which are usually classified in sub-zero (below 0°C), low grade (0-100°C), median (100-500°C) and high (above 500°C). The last usual classification is by the duration of the storage capacity by time, where short term (seconds to few hours), medium (several hours to few days) and long term (months) are identified (IRENA, 2020). Figure 2.7 presents a summary of the different TES classifications and some technological examples.

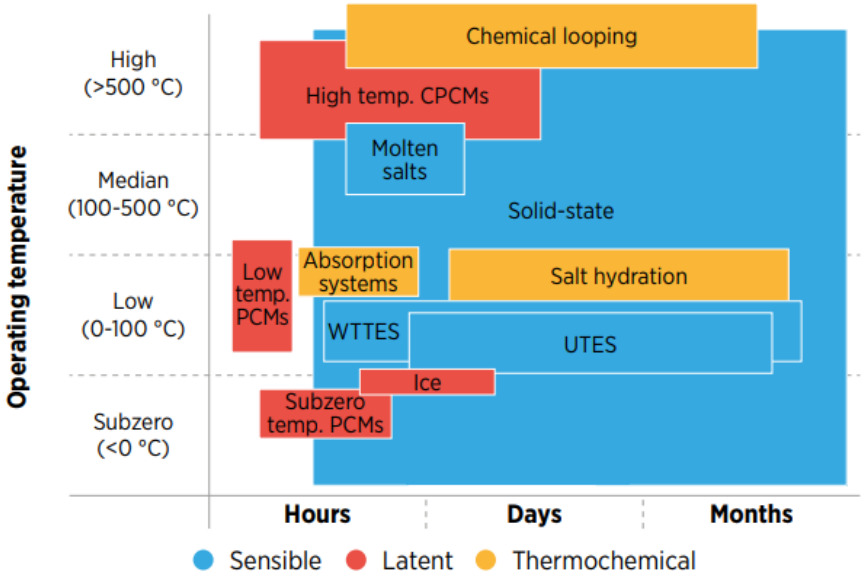

Figure 2.7: Classification of some TES technologies according to IRENA (2020). PCM: phase changing material, CPCM: composite phase changing material, WTTES: water tank thermal energy storage, UTES: underground thermal energy storage

2.6.1 Sensible energy storage

In sensible heat storage, the energy stored is proportional to the temperature variation of the storing media without phase change or any chemical reaction taking place. The stored energy can be expressed according to equation 2.2.

$$Q = m \cdot c_p \cdot \Delta T \tag{2.2}$$

Where m is the mass of the storing material, c_p is the specific heat capacity and ΔT is the temperature difference between the charged and discharged states.

From the equation,2.2 it is clear that a material with higher c_p allows for higher density heat storage, therefore smaller relative storage mass. However, as space availability is often a constraint for the location of these systems, the storing media density is also relevant for sensible heat applications, therefore, volumetric heat capacity (c_v) is usually used when selecting the storing media.

The storing media used for sensible heat storage applications can be subdivided into solid and liquid. Liquid storage media have the advantage that the same medium can be used for heat transport and storage. This removes the need for a heat exchanger on the storage side. In addition, the density difference created by hot and cold fluid creates a thermal gradient across the storage system called thermal stratification, which decreases the convection and improves the efficiency of the storage (Reddy Prasad *et al.*, 2019) and increases the available exergy in the storage (Lizana *et al.*, 2018b). One of the limitations of liquid storage media is that the temperature operation range of the system is usually narrow, limited by the phase-change temperatures of the liquid. The most common liquid storage media are water (20-95°C), mineral oils (200-400°C), and molten salts (300-600°C). Solid storage media, on the other hand, have usually very broad operational temperature ranges. However, the capacity of charging and discharging solid media is limited by the heat transfer between the heat transport fluid and the solid. Therefore, higher heat exchange areas or higher fluid flow rates might be required for increasing the charging rate capacity, which usually means increases in investment and operational costs. This problem also arises in the discharging phase, as the outlet temperature gradually starts decreasing with time, leading to decreases in round trip efficiency (Alva *et al.*, 2018). Some of the most common solid heat storing media are rocks, soil and concrete.

The main features of sensible energy storage are its low cost and use of widely available non-hazardous materials. However, compared with other alternatives, it has low heat density, requires extensive insulation, especially for high temperature applications, and presents non-isothermal behaviour in charging and discharging (Avghad *et al.*, 2016).

2.6.2 Latent energy storage

In latent heat storage, the energy is stored in the latent heat of phase change of the media, also known as phase change material (PCM). Although solid-solid and liquid-gas PCM materials exist, solid-liquid are the most commonly used PCM, as they have lower volume variation and relatively high latent heat (Sarbu and Sebarchievici, 2018; Alva *et al.*, 2018). They absorb energy from the surroundings to sustain a fusion process and release energy to the surroundings during the reverse transformation. This process is isothermal, therefore, there are no changes in temperature during the phase change. The heat stored or released by the media is proportional to its latent heat of phase change, as shown in equation 2.3.

$$Q = m \cdot \Delta q \tag{2.3}$$

Where m is the mass of the PCM medium and Δq is the latent heat of fusion.

PCM can be categorised in organic, inorganic and eutectic mixtures, depending on their chemical composition. Some examples of organic PCM are paraffins and polyalcohols, while examples of inorganic PCM are water (used to form ice), salt hydrates and metal alloys (Reddy Prasad *et al.*, 2019).

PCM materials have usually higher energy density than sensible media, therefore, these technologies are well suited for applications where space is constrained, such as building walls or roof integration (Mousavi *et al.*, 2021). Additionally, their isothermal behaviour allows for a more stable heat transfer and a more controlled charge and discharge process for accurate temperature regulation (Wang and Baldea, 2013).

One of the drawbacks of PCM is their low conductivity which makes them less suitable for systems where fast heat extraction is required (Alva *et al.*, 2018). Also, there is still a lack of commercially available PCM that could meet all the required characteristics for a competitive latent energy storage system (Jouhara *et al.*, 2020). This means that their current use is mostly focused on niche applications, such as the aforementioned space constraint built environment.

2.6.3 Thermochemical energy storage

Thermochemical storage uses reversible chemical reactions often involving the breaking and formation of bonds to store energy. The storing media absorbs heat from the environment in an endothermic chemical reaction and releases heat in an exothermic reaction, in a process also referred as chemical looping. Good thermochemical storage media allow for fully reversible reactions, keeping high cycling storage efficiencies. Alternatively, thermochemical energy storage can be achieved by sorption processes, where a gas or a vapour is captured by a sorbent in a condensed state by means of less intense physical interactions (Lizana *et al.*, 2017).

Some advantages of thermochemical heat storage are isothermal discharge temperature, the highest energy density among TES, and the ability to store heat with high efficiency for as long as the chemical reaction is not reversed or the storing material is not degraded (Reddy Prasad *et al.*, 2019), which makes this technology a good candidate for seasonal storage. However, this technology is mainly at a R&D stage which translates into a high cost and creates uncertainty with regards to reliability and toxicity (BEIS, 2016b).

With the aim to supplement the quick summary of the different TES technologies, Figure 2.8 shows the maturity level of some selected TES technologies for heating and electricity generation.

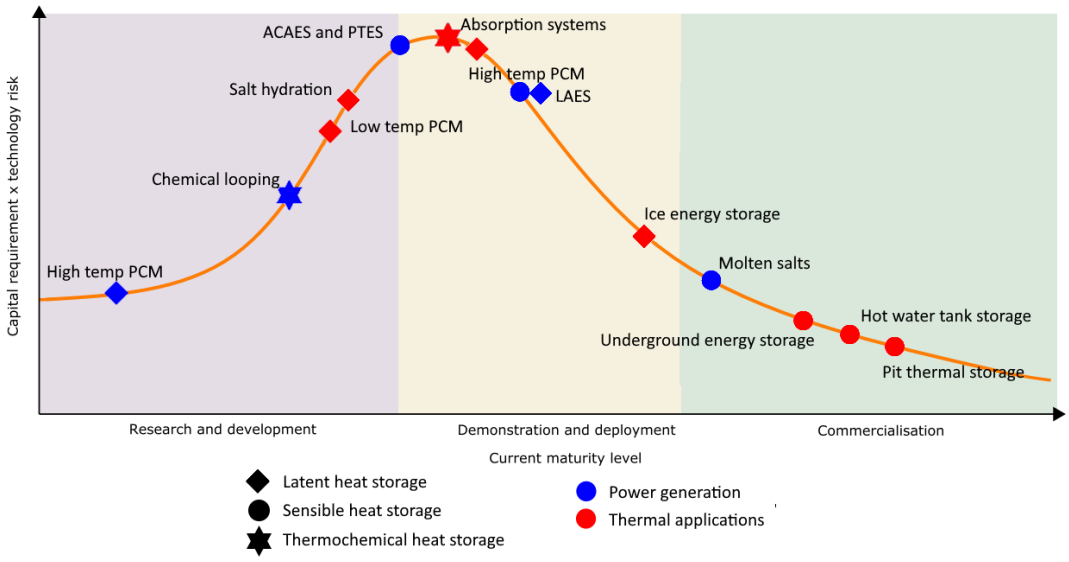

Figure 2.8: Maturity level of some TES technologies. (Adapted from International Energy Agency (2014b) and updated according to IRENA (2020))

As mentioned in Chapter 1, this thesis focuses on TES technologies for supporting the deployment of renewables in the Chilean energy system. Therefore, a review of specific TES alternatives that could be applied in the Chilean context in the residential solar heating and wind and solar PV integration in the electricity systems is presented in the following sections.

2.6.4 Thermal energy storage for heating applications

Domestic heating applications comprise the energy needed to keep the internal temperature around 20-21°C and to supply domestic hot water at 40-50°C. In systems where hot water is used as the heat carrier, these temperatures have been normally achieved by circulating hot water at temperatures above 80°C. New fourth generation district networks supplying temperatures between 30 and 70°C improve systems' overall efficiency and have easier

integration of low grade heat sources such as waste heat and solar thermal (Lund *et al.*, 2014). Considering this and in order to align with the thesis objectives, this review focuses on TES technologies that operate in this temperature range and could support the integration of low grade solar thermal energy.

Hot water tank storage

Hot water tanks are the simplest and most commonly found TES technology, and consist of a tank (usually stainless steel, hard polymer or concrete) containing hot water. It usually also incorporates auxiliary heating components, such as heat exchanger coils or resistance heating elements, and stratification enhancement devices. The latter is important for maintaining thermal stratification within the tank, which substantially improves storage efficiency and the overall operation of the system (Furbo, 2015). It is the most mature and affordable TES technology, therefore, most of the current research in this area is related to its operation and integration with other systems (Banister and Collins, 2015; Renaldi *et al.*, 2017).

By far, the most common application of steel hot water tanks are in individual residential heating and hot water systems, with tanks' storage capacities ranging from hours to a few days. They are widely used for domestic hot water, both supporting solar collectors or with electric heaters at household level. Larger hot water tanks are also used to regulate intra-day variations (BEIS, 2016b). However, for seasonal storage capacities, such as those required to support the operation of district heating networks with solar heat, steel tanks become expensive and concrete that could be above or underground is favoured. Moreover, for these applications, also referred in this thesis as long term storage (LTS), large tanks tend to be more expensive than the alternative underground thermal energy storage (UTES) technologies. This can be appreciated clearly in Figure 2.9. where costs per cubic meter of water-equivalent storage are presented as a function of the total storage volume.

Pit thermal storage

An underground pit is basically a large pool excavated in the ground lined with an impermeable material and filled with water or a mix of water and gravel. The gravel is used to facilitate the stratification in the water, however, as it has lower heat capacity, it reduces the volumetric storage capacity of the pit by around 30-50%. Another reason for using gravel is to facilitate the supporting of the pit's roof allowing to use the surface of the roof (Mangold and Deschaintre, 2015). The top of the pit is insulated, but on the bottom and sides is usually the soil surrounding the pit which acts as a natural insulator. Its operational characteristics are similar to the tank storage, but the costs of construction are lower for the same storage capacities (as shown in Figure 2.9), mainly because it does not require the structure of the tank. Similarly to a stratified tank, the injection and extraction of hot water occurs at the top of the storage and that of the cold water happens at the bottom of the storage.

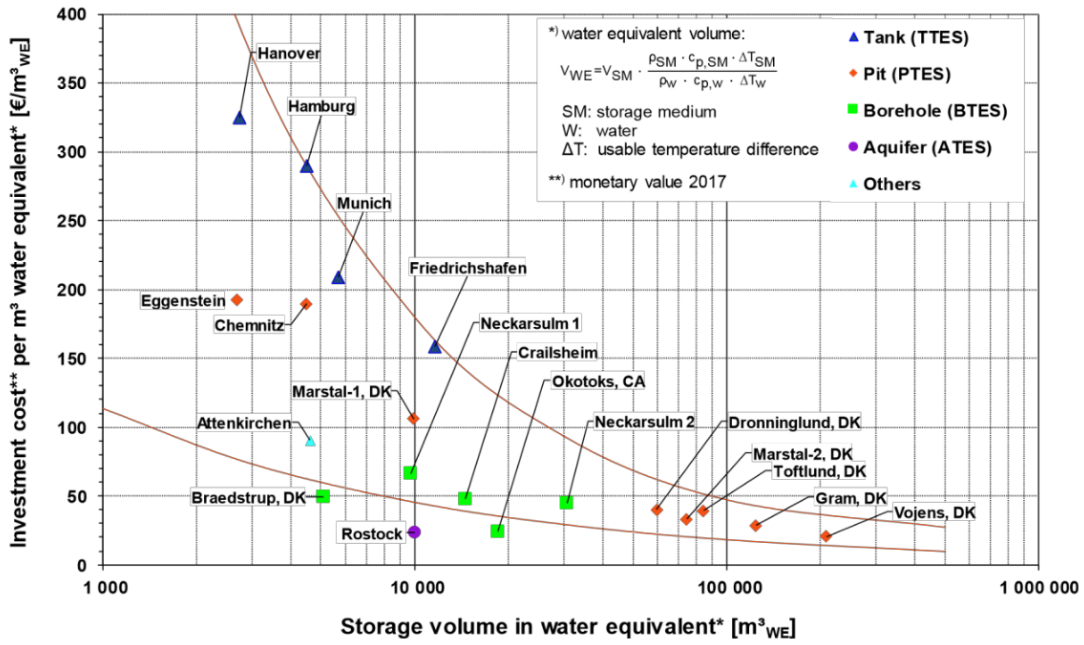

Figure 2.9: Investment cost in €/m^3 of water-equivalent storage capacity for different seasonal TES systems (Planenergi, 2019). Water-equivalent is the corresponding water volume to store the same amount of thermal energy and is calculated according to the equation shown at the top of the figure

A schematic representation of the pit storage and other long term TES technologies is presented in Figure 2.10.

Borehole thermal storage

In borehole thermal energy storage (BTES) heat is directly stored in the ground. In order to allow for heat exchange between the heat carrying fluid (hot water) and the ground, vertical boreholes are drilled into the ground in a hexagonal or cylindrical array and U-shaped pipes are inserted into them. These U-pipes are connected in series in the radial direction, forming a string. Several strings are connected in parallel to cover all the boreholes. A scheme of this design is presented in Figure 2.11

During the thermal charging, the water is circulated from the boreholes at the centre towards the periphery. This makes the boreholes at the centre hotter and boreholes at the periphery colder, which creates a radial thermal stratification that decreases the heat losses by reducing the temperature difference with the surrounding soil. For discharging, the water flow direction is reversed so the cold water is preheated in the periphery and heated at the maximum temperature in the centre. This helps keeping the radial thermal stratification in the soil while achieving a counter-flow heat exchanger like effect on the water.

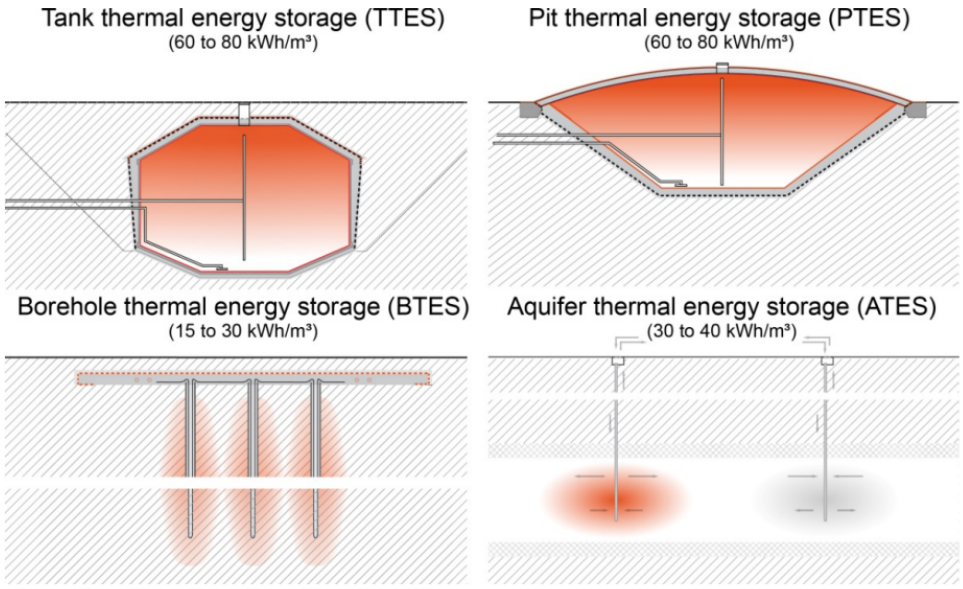

Figure 2.10: Diagrams of the main seasonal TES technologies (Mangold and Deschaintre, 2015). The heat stratification can be appreciated as the darker orange colour represents higher temperature. Values of approximate energy densities for these storage are also presented

Borehole TES systems are best suitable for places that have soil that is easy to drill, with high specific heat and thermal conductivity and a very low hydraulic conductivity (Alva *et al.*, 2018; Yang *et al.*, 2021). The presence of groundwater is desirable as it increases the soil's specific heat, but the water flow is not desirable, as it may cause the water to carry the heat away from the pipes (Catolico *et al.*, 2016). It is interesting to note that the soil conductivity has two competing effects, as a low conductivity soil creates better natural insulation, therefore decreasing the thermal losses. On the other hand, low conductivity decreases the capacity of the system to be charged by increasing local heat stratification around each borehole and decreasing heat transmission from the water to the soil. This can be seen in Figure 2.12, where a single two borehole string is analysed by Catolico *et al.* (2016) with a detailed numerical model for a high and low thermal conductivity (λ=0.5 W/mK and λ=3.0 W/mK).

In this image it is clear that a higher conductivity allows for more heat to move away from the boreholes, which decreases the rate of heat recovery from the system, decreasing the storage's efficiency. Catolico *et al.* (2016) argues that heat extraction efficiency increases with decreasing soil thermal conductivity. This is corroborated by a study by Welsch *et al.* (2016). However, Welsch also concludes that a higher conductivity favours the heat delivery into the storage media, allowing for larger amounts of energy to be stored in the system, and therefore more energy to be recovered in winter, even if lower overall storage efficiency is achieved. Their results are shown in Figure 2.13, which for the same energy supply and demand, presents the total annual stored and extracted energy from a BTES for different soil

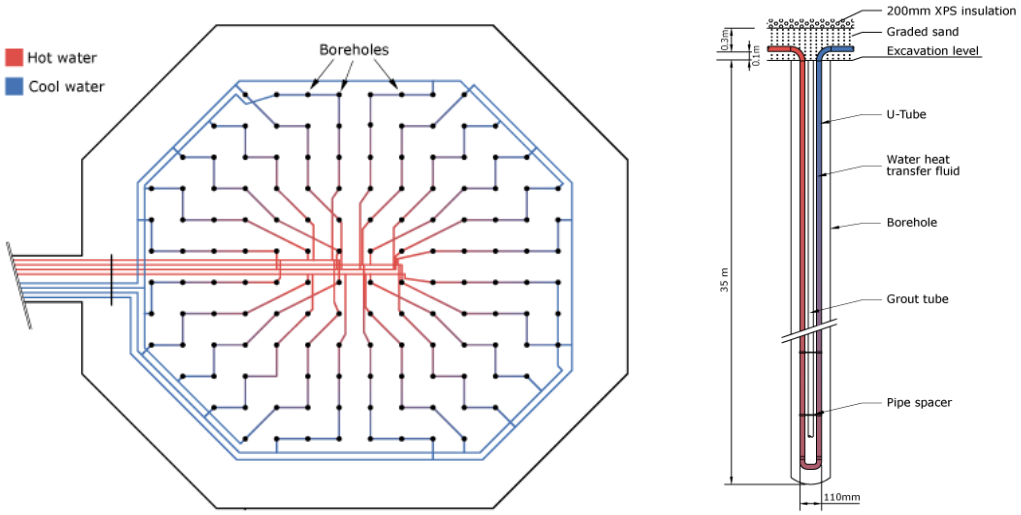

Figure 2.11: Schematic representation of the borehole distribution and location on a plan view (left) and of a U-pipe inside a borehole on an elevation view (right) (DLSC, 2019)

conductivity. The lower thermal energy stored with smaller soil conductivity can also be seen in Figure 2.12, where after the charging phase it is clear that part of the soil between the boreholes has barely increased its temperature for λ=0.5 W/mK. In contrast, for λ=3.0, the volume between the boreholes is hotter, thus storing more energy in total.

Aquifer thermal storage

An aquifer is a layer of permeable rock saturated with water. Due to its permeability, water can be extracted and stored in this rock formation. Although the main applications of aquifer tend to be cool water extraction for summer cooling, they can also be used for storing heat (BEIS, 2016b). An aquifer thermal energy storage (ATES) used for heating, typically consists of two or more separated wells, with some used for injecting hot water and the others for water extraction. However, mono-well systems that use internal thermal stratification similar to a thermocline water tank are also possible (Mahon *et al.*, 2022). Regardless of the configuration, water is used as heat carrying medium, while the storing media consist of the water itself and of the rocks forming the geological formation of the aquifer (Yang *et al.*, 2021).

Geological formations with good properties of ATES system are limited as they require to meet several characteristics, such as high hydraulic conductivity, top and bottom confining layers with low hydraulic conductivity, low natural groundwater flow, and suitable water chemistry at high temperatures (Yang *et al.*, 2021). However, when these requirements are met ATES are an attractive alternative owing to their usually large storage capacity, relatively low

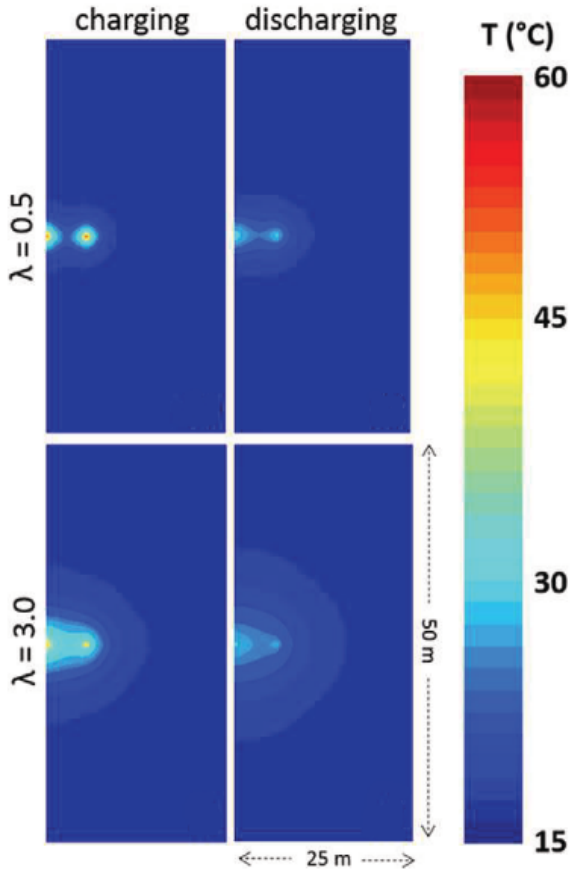

Figure 2.12: Effect of the soil's thermal conductivity in the temperature field development around boreholes after charging and discharging seasons (Catolico *et al.*, 2016)

environmental impact, and good economic viability due to the little required infrastructure and limited drilling (Mahon *et al.*, 2022). Currently, this technology is relatively mature, with close to 3,000 systems around the world and more than 80% of them located in the Netherlands (Fleuchaus *et al.*, 2018).

2.6.5 Thermal energy storage for electrical applications

Thermal energy is one of the oldest ways of industrial level electricity generation. The most common way to implement thermal generation is by increasing the enthalpy of a gas and later expanding it through a turbine in a Rankine cycle (steam turbine) or a Brayton cycle (gas turbine). In both cases, heat addition is required to increase the enthalpy of the gas. Thus, TES seems to be a candidate to store heat and deliver it when necessary to operate the turbine and generate electricity. However, in order to operate traditional thermal cycle generation efficiently, high temperatures (above 250°C for steam cycles, above 150°C for organic cycles and above 500°C for gas turbine cycles) are usually required unless a low temperature energy sink is available. This limits the possibility of storing the heat for elec-

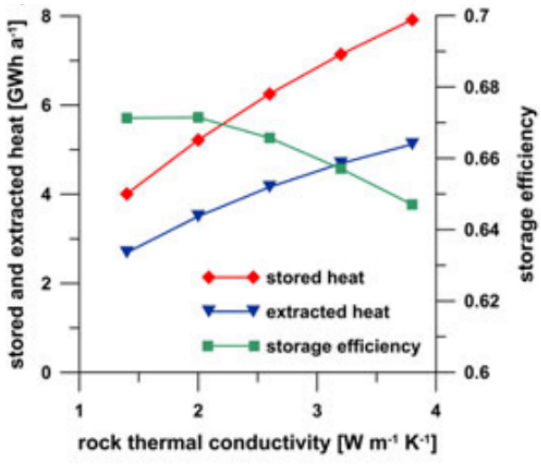

Figure 2.13: Effect of the soil's thermal conductivity on the stored heat and the storage efficiency (Welsch *et al.*, 2016)

tricity generation for long periods, due to increased thermal losses. An option to circumvent this problem is to use thermochemical storage such as calcium looping Bravo *et al.* (2020). However, these technologies are still in an early development stage and they require further research. Considering this, the next paragraphs will describe some of the TES technologies for electricity generation operating with sensible heat media.

Molten salt energy storage

Molten salt technologies are the most mature TES technology for electricity generation. They are widely used in commercial concentrated solar plants (CSP) with 21 GWh_{el} installed by 2019 (Bauer *et al.*, 2021). They usually consist of two large insulated tanks that store a eutectic mix of $NaNO_3$ and KNO_3. The salt mix has a melting point of around 240°C and a maximum stable operational point around 570°C, although other salts mixes, for example, with the addition of $LiNO_3$, have been investigated showing improvements in melting and maximum operational point temperatures (Fernández *et al.*, 2019). During the charging phase, the salt is heated and stored in the hot tank. For discharging, the salts are pumped towards the cold tank and reject heat through a heat exchanger. The heat rejected by the salts can be used to produce high-pressure steam and generate electricity in a steam turbine. In typical molten salt storage in CSP plants, the molten salts are kept at around 290°C in the cold tank and 560°C in the hot tank, with the molten salt operating as storage media and working fluid. Chile has recently installed the first of these systems at commercial level in Cerro Dominador CSP power plant, with 110 MW generation capacity and 17.5 hours of storage capacity in molten salts storage (Cerro Dominador, 2020). In addition, it has been proposed to use this technology to reconvert existing coal power plants into storage units with the molten salt technology charged with grid electricity through a resistance heater, while keeping the original steam cycle of the coal power plant to generate electricity (Ministerio de Energia, 2020c). Although

the configuration of the storage system is the same of that of a CSP plant, these systems are considered "Carnot batteries", as they are charged with electricity rather than with direct heat, but not pumped thermal energy storage, as the charging is performed with a resistive heater rather than a heat pump.

Adiabatic compressed air storage

Adiabatic compressed air storage (ACAES) systems, store energy in high pressure compressed air, in a similar way as a traditional CAES system. However, during the compression process, they store the heat removed from the air in a TES rather than dumping it into the environment like traditional CAES systems. This allows to use the stored heat to increase the air's temperature during the discharge expansion process avoiding the use of fossil fuels (IRENA, 2020), hence, ACAES can be included in the TES category. Figure 2.14 presents a diagram of the configuration of an ACAES system.

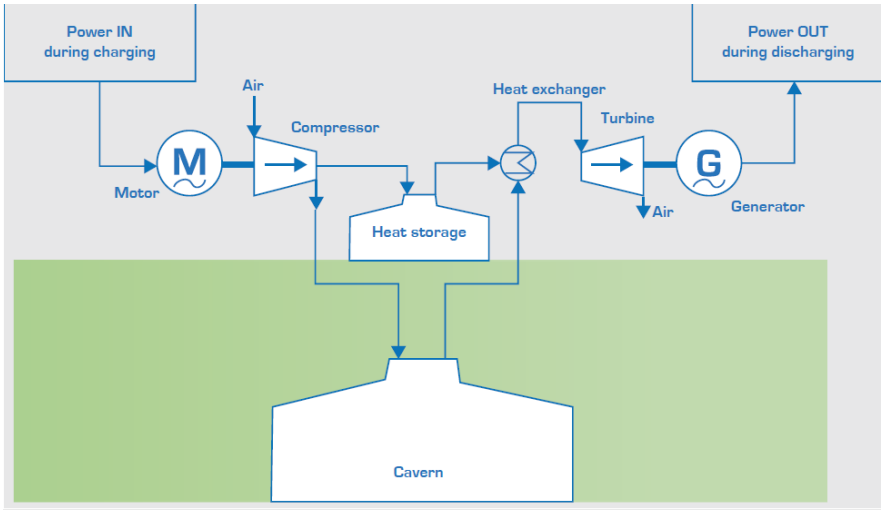

Figure 2.14: Scheme of operation of a typical ACAES system (EASE, 2016a)

This technology has similar geographical limitations than CAES, as the compressed air requires a large high-pressure reservoir, which usually can be achieved at a reasonable cost by using large underground caves or salt deposits. As stated by Barbour *et al.* (2021), although some demonstration plants have been built, the low efficiency achieved by these projects shows that this technology requires more development to be commercially viable. One of the challenges yet to be solved is that constant volume air storage systems cause transient pressures during discharge, which produce inefficiencies in the turbo-machinery. Alternative isobaric storage has been proposed. The earlier proposals were variable volume systems, including underwater flexible bags (Pimm *et al.*, 2014; Garvey, 2012) or water filling reservoirs (Nielsen and Leithner, 2009; Mazloum *et al.*, 2017). Recently, variable volume storages with pistons operated by the condensation-evaporation of volatile fluids have also been proposed (Chen *et al.*, 2018).

With regards to the thermal storage itself, most of the proposed systems correspond to de-coupled TES with different liquid storage media. As several compression stages with inter-cooling are required, Barbour *et al.* (2015) proposes to investigate the use of coupled packed bed TES for the lower pressure compression stages, which reduces the need for heat exchangers and pumping equipment and would reduce the exergy loss caused by thermal mixing in the TES without requiring high-pressure tanks.

Liquid air energy storage

Liquid air energy storage (LAES) is a cryogenic TES technology. Like ACAES, it stores compressed air to later drive a turbine and generate electricity. However, in LAES systems the air is cooled and compressed until it liquefies, which means that the storage volume has to be much smaller and can be at atmospheric pressure, allowing even to move the liquid air and use it in other applications, such as cold chains (IRENA, 2020).

Different cycles have been proposed for the air liquefaction process, most of them considering several gas compression, heat removal and gas expansion stages, while the discharging process is usually performed by a Rankine cycle (Hamdy *et al.*, 2019; Vecchi *et al.*, 2021). In general, during charging, electricity is used to compress the air to high pressure (> 60 bar), and the heat produced during compression is stored in a heat storage system (> 300°C). The compressed air is cooled (-145°C) by the cold storage and liquid air (-196°C) is obtained by expanding back to ambient pressure. For discharging, liquid air is returned to gas through evaporation and part of the "waste" cold is stored and used in the liquefaction stage. The air is further heated by the previously stored heat and is used to drive a turbine to generate electricity (Ding *et al.*, 2016; IRENA, 2020). Figure 2.15 presents a diagram of the configuration of a LAES system.

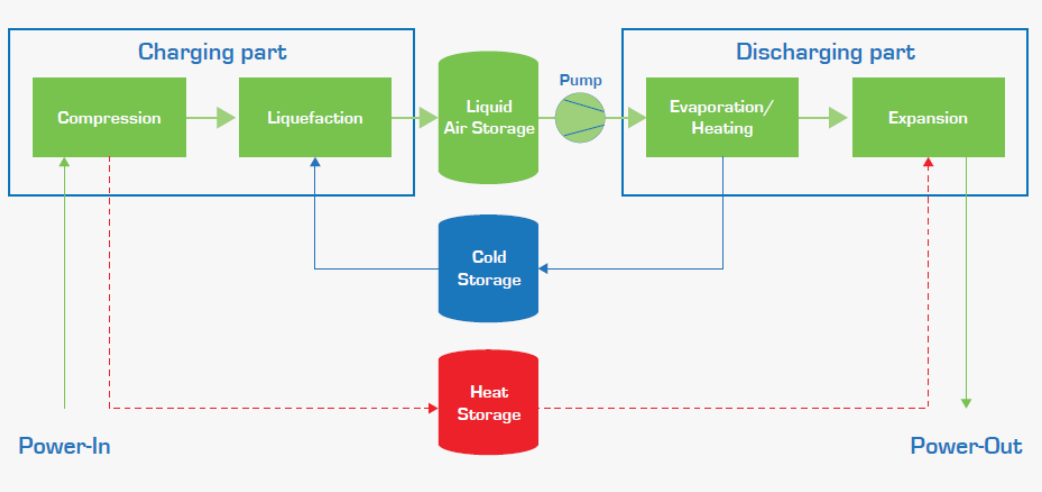

Figure 2.15: Scheme of operation of a typical LAES system (EASE, 2016b)

LAES is currently a more developed technology than ACAES and PTES, with several demonstration plants in operation (Barbour and Pottie, 2021). It has higher energy densities than other TES alternatives, thus can store energy in smaller containers, which removes the geographical/geological constraint imposed on (A)CAES. Another interesting characteristic of this technology is that it is well suited for integrating with other energy processes, such as waste heat recovery, liquefied natural gas re-gasification facilities and even PTES storage systems. A thorough review of different hybrid LAES configurations is presented by Vecchi *et al.* (2021).

Pumped thermal energy storage

Pumped thermal energy storage (PTES) is based on a high-temperature heat pump (HP), which converts electricity into heat and stores it in thermally isolated tanks. On discharge, a thermal engine cycle is used to convert the stored thermal energy back into electricity. The working fluid is a gas, while the storing media can be any material, although cheap sensible solid materials are more common in the different proposed concepts (Benato and Stoppato, 2018). This technology has also been called "Carnot battery", although, it can be argued that Carnot battery is a more general concept that encompasses every technology able to store electricity as heat and convert it back to electricity using a heat cycle, meanwhile PTES requires the heat to be pumped from a cold to a hot reservoir using a HP, using the reverse cycle to generate electricity. This technology is still under development and has a low technology readiness level compared to other grid electricity technologies (Dumont *et al.*, 2020).

The main classification within PTES systems is by the interactions between the working fluid and the storage media. Systems where the working fluid enters the storage tanks and has direct contact heat exchange with the storage materials are called *coupled* systems, whereas systems where the working fluid delivers heat to the storage medium through a heat exchanger are called *de-coupled* systems.

Coupled systems usually are designed with a solid storage material that fills the storage tank in a packed bed with high surface to volume ratio (pebbles) to maximise heat exchange. The main advantage of this configuration is that it does not require extra heat exchangers and that the storage media are cheap rock type materials (like quartz) that is stored in two thermally stratified tanks. However some of the drawbacks are that the storage tank has to be built to sustain the high pressure of the hot gas, as it has to be in direct contact with the storing material. Also, if not designed appropriately, the gas may suffer high-pressure losses while passing through the packed bed, and the packed bed material can become brittle due to thermal stresses caused by the cyclic operation (Dumont *et al.*, 2020).

De-coupled systems require a fluid in the secondary circuit, therefore, they can use the same fluid as a storage media. As heat exchangers are required to heat the storing media, the proposed designs for de-coupled systems use four storage tanks, two for the cold storage and two for the hot storage (Davenne and Peters, 2020). The main advantage of de-coupling the working circuit from the storage circuit is that storage can operate at near atmospheric pressures, which means storage tanks are cheaper and larger storage capacities can be achieved. The use of four tanks can be circumvented by using solid storage and a gaseous heat carrier in the storage circuit, as proposed by Davenne and Peters (2020).

Regardless of the coupling or not, the thermodynamics of the working fluid circuit remains the same. A schematic representation of a coupled PTES proposed by McTigue *et al.* (2015) using a Brayton cycle alongside a temperature-entropy (T-S) diagram is presented in Figure 2.16.

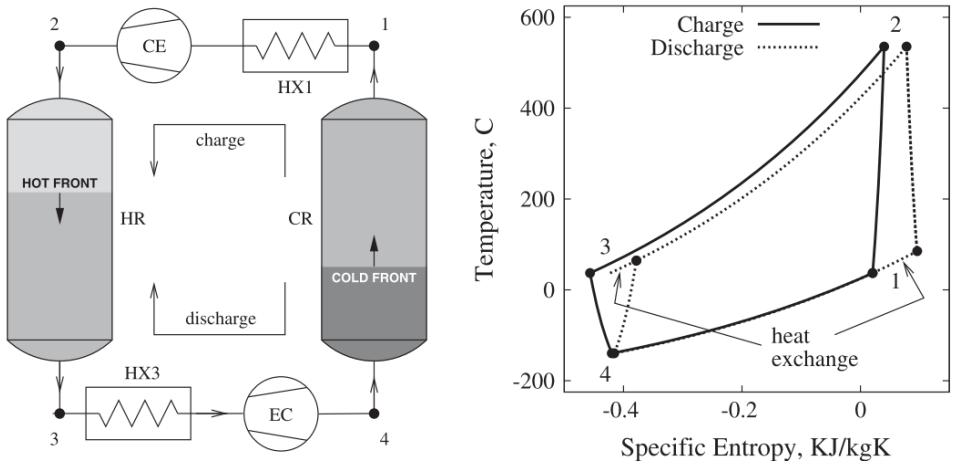

Figure 2.16: Example of a coupled PTES system operation scheme (left) and the corresponding T-S diagram (right). CE/EC correspond to compressors and expanders (turbo-machinery or piston equipment) and HX1/HX3 to heat exchangers to counter for the irreversibilities of the compression and expansion processes and keep the inlet turbomachine temperatures at their nominal value (adapted from McTigue *et al.* (2015))

In charge mode, the working fluid is compressed by using electricity from the grid and its temperature increases (1-2), the heat is transferred from the working fluid to the hot storage (2-3), the working fluid is expanded and its temperature decreases (3-4), the working fluid cools down the cold store (4-1). The work absorbed by the system and stored corresponds to the area within the anti-clockwise discharge cycle on the T-S diagram. While discharging, the working fluid flow is reversed and it is cooled inside the cold store (1-4) and later compressed reaching near ambient temperature (4-3). The working fluid is then heated inside the hot storage tank (3-2) and then expanded generating useful work (2-1), which corresponds to the

area inside the clockwise cycle (dotted line in Figure 2.16). Figure 2.17 presents a scheme proposed by Google founded star-up Malta X project, which uses a de-coupled system with air as working fluid and molten salts as hot storage and a coolant fluid in the cold storage tanks.

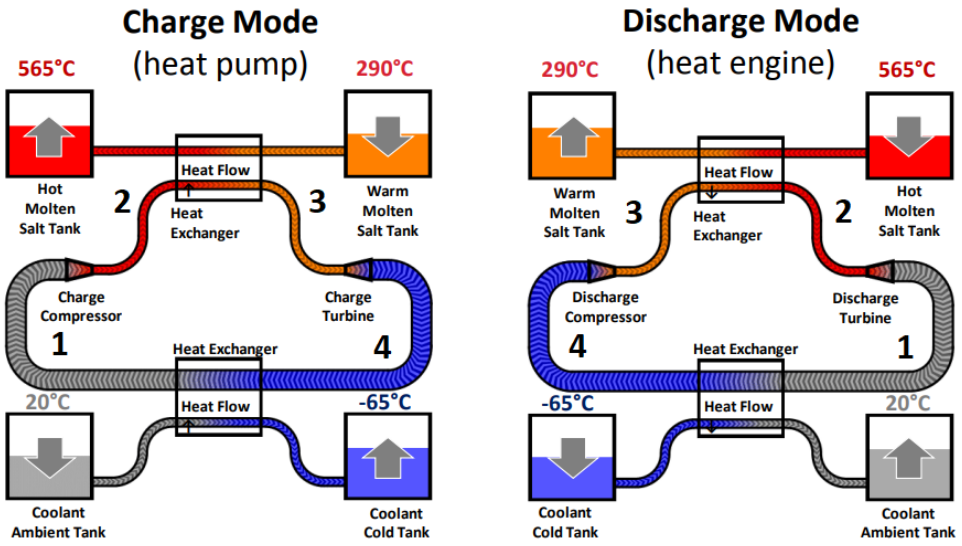

Figure 2.17: Example of a de-coupled PTES system operation scheme proposed by Malta X (adapted from Freund (2019))

Other notable PTES system designs and configurations are the use of the transcritical CO_2 cycle with de-coupled water/ice storage (Morandin *et al.*, 2012) and the compressed heat energy storage (CHEST) concept proposed by Steinmann (2014); Steinmann *et al.* (2019) which uses a Rankine cycle with water as working fluid and a combination of coupled and de-coupled sensible and latent heat storages, and a heat exchanger at environment temperature instead of a cold storage. Steinmann *et al.* (2019) and Frate *et al.* (2020) also propose the use of an Organic Rankine Cycle instead of a steam cycle, which would allow to operate at lower temperatures and use low-grade heat sources, such as geothermal, flat plate solar thermal heat or industrial waste heat, to charge the system and integrate the PTES with district heating networks and seasonal TES.

2.7 Methods for techno-economic assessment

Historically, the drive for maximising profits has made economic analysis the most common practice for new projects' decision making. This has been also the case for energy projects, which led to high reliance on fossil fuels, disregarding their impact on global warming and local pollution. However, during the last decades, social and environmental sustainability of projects has taken a key role. This brings the challenge of confronting the inherent trade-offs of multiple objectives. Furthermore, these objectives are generally non-commensurate, which complicates their comparison and eventual aggregation into a single indicator.

This section introduces two analysis tools that are used consistently in this thesis to evaluate projects from purely economical and multi-objective perspectives.

2.7.1 Levelised cost of energy

The Levelised Cost of Energy (LCOE) is the classic techno-economic metric for assessing energy related projects and technologies. It represents the present value of the total life cycle costs involved in the generation of each unit of energy during the lifetime of any technology that produces or saves energy, and it is defined by equation 2.4 (Short *et al.*, 1995).

$$LCOE = \frac{\sum_{i=1}^{n} \frac{I_i+F_i+V_i}{(1+r)^i}}{\sum_{i=1}^{n} \frac{E_i}{(1+r)^i}} \tag{2.4}$$

I_i is the investment in year i, F_i are the fixed costs of operation in year i, F_i are the variable costs of operation in year i (which may include the purchase of fuel and any other supply for the operation) and E_i corresponds to the energy delivered in year i. n is the assumed lifetime of the project, and r is the discount rate used for the evaluation.

It provides a simple and straightforward way of consistently comparing the costs of different energy producing technologies with different characteristics considering the value of money and a commodity (energy in this case) in time.

Its main limitations, however, are that it does not account for time effects associated with matching energy production to demand. Therefore, it underestimates the value of flexibility. Furthermore, as it only considers only money transfers for assessing the technology, it relies on market and policy signals to transform any non-monetary externality of the technology into a pecuniary metric, for instance, carbon markets or taxes.

However, generally, there is an absence of mechanisms to economically account for the externalities. Moreover, even if they are in place, their effectiveness to represent accurately the relevance of the impacts of the technology on other domains such as the environment or human activities is questionable (Benes and Augustin, 2016). This leads to the need to explicitly incorporate other metrics in the analysis.

2.7.2 Pareto front analysis

When performing energy system optimisation with one objective, it is expected that one optimal solution can be achieved. When different criteria are considered and set as objectives of a techno-economic assessment, different compromises and trades off arise and a unique solution is often not possible to achieve without the existence of a metric to commensurate the different criteria.

One common approach used to deal with these situations is the Pareto optimality analysis. Pareto optimal solutions are defined as a set of "non-dominated" solutions in the objective space, defining a boundary beyond which none of the objectives can be improved without sacrificing at least one of the other objectives. From the mathematical point of view, the definition of the dominance between two solutions in a minimisation example can be expressed as a solution x_1 dominates a solution x_2 if they comply with equation 2.5

$$f_i(x_1) \leq f_i(x_2)\ \forall i \in \{1,...,m\} \quad \& \quad \exists j \in \{1,...,m\} \mid f_j(x_1) < f_j(x_2) \tag{2.5}$$

f_i and f_j are different objectives and m is the total number of objectives.

Therefore, a solution x^* is said to be non-dominated or Pareto optimal if no other feasible solution dominates it. The set of all non-dominated solutions forms the Pareto front, representing the optimal trade-off between all objectives. This can be graphically visualized for two objectives in Figure 2.18, where x^* dominates x_2 but does not dominate X_1.

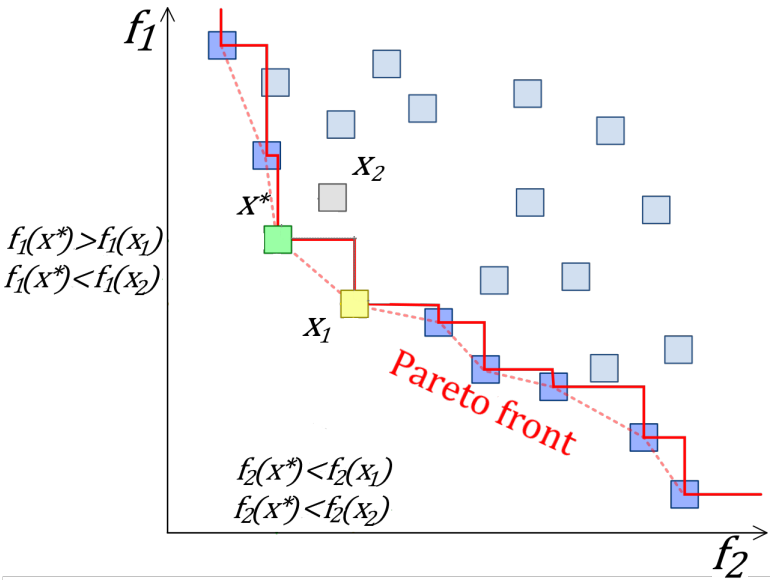

Figure 2.18: Graphical representation of a Pareto front and domination conditions

The solutions in the Pareto front are equal from the point of view of the problem's optimality, and a further criterion is to be imposed in order to decide on unique solutions.

2.8 Background summary

Based on the information presented in this chapter it is possible to draw the following summarising points that lead to the analysis performed in this thesis.

- The Chilean energy policy has evolved and it is starting to consider thermal uses and particularly domestic heating in its planning scenarios.
- In most of the planning scenarios the electrification of heating is assumed as the main mean of decarbonisation.
- It is important that the heat electrification process includes flexibility considerations to minimise the extra strain on the electric grid.
- Thermal storage technologies can be a source of said flexibility. Several technologies in different maturity stages can provide various services at an electric grid level and in heating applications.
- Different techniques have been identified to model and assess the impact that these technologies may have on the Chilean energy system.
- Linear optimisation has been identified as a modelling approach of the Chilean electric grid that allows assessing multiple long-running scenarios with sufficient detail while keeping the main features of spacial demand and resource distribution.
- Due to more complex dynamics, long term underground heating requires a more detailed simulation approach. However, meta-heuristic algorithms can be used to optimise the design and operation of the simulated systems.

Chapter 3

Thermal storage in the Chilean electric grid

The work presented in this chapter has been published in the article "Long term impact of grid level energy storage on renewable energy penetration and emissions in the Chilean electric system" published in *Energies* (Maximov *et al.*, 2019).

3.1 Introduction

Chile has significant potential for renewable energy, but its long and narrow shape poses a challenge for integrating renewable energy into the electricity system. In particular, the values of annual global horizontal irradiance (GHI) and direct normal irradiance (DNI) reach up to 2,700 kWh/m^2·a and up to 3,700 kWh/m^2·a respectively in the northern area. However, in 2012 the System Operator warned that 450 MW was the maximum capacity of intermittent generation which could be deployed in the northern system due to grid restrictions (CDEC-SING, 2012). In the last years, this limit has increased, mostly due to improvements in the transmission capacity, especially with the interconnection of the Northern Interconnected System (SING) and the Central Interconnected System (SIC).

In 2018, there were 2,250 MW of photovoltaic (PV) and 1,520 MW of wind generation in operation according to data from the National Energy Commission (Comision Nacional de Energia, 2018), which represents around 16% of the total installed capacity. Nevertheless, in order to sustain the continued deployment of these technologies, further grid improvements are required. Moreover, according to the Energy Roadmap for 2050, under the electric grid structure exiting in 2014, it was only possible to generate up to 41% of energy from intermittent renewables (Comité Consultivo de Energía 2050, 2015). Therefore, wit ith the aim of reaching the goal of 70% of electricity from renewables by 2050 (Comité Consultivo de Energía 2050, 2015), it would be necessary to increase the operational flexibility of the grid, with energy

storage being one of the most interesting alternatives (IEA, 2018b). It is important to note that by the time of developing the study included in this chapter, the official goal of renewable generation penetration was 70% by 2050, therefore is the one considered for the analyses, even though the current goal has been increased to 100% (Ministerio de Energia, 2021a).

Munoz *et al.* (2017) showed that from a market perspective achieving 70% renewables was possible even without additional policies such as promotion of energy storage. However, there are some technical constraints that could hinder achieving this target and a more detailed analysis is required. Due to the local geography, the Chilean electricity network has a radial topology. This characteristic increases the probability of bottlenecks and constrains the ability of transmitting large amounts of energy along the country. Furthermore, until 2017 the two main electric systems (SIC and SING) were not connected, hindering the possibility of supplying the cities and industries in the central area of Chile (around the cities of Santiago and Concepcion) with electricity produced with clean solar technology in the North. This changed in late 2017 after the interconnection of the two main electricity systems, as now over 99% of the installed capacity is connected and coordinated by an independent centralised authority.

The 400 km, 500 kV SIC-SING interconnection allows to transfer of energy between the northern part of the system, abundant in solar resources and the rest of the country, where more than 90% of the population resides. However, there are still many barriers to higher integration of intermittent renewable generation into the grid. In this sense, Haas *et al.* (2018) analysed the different economic, regulatory and technical barriers that prevent higher penetration of solar energy in Chile. Two of the main technical barriers are the constraints in transmission capacities, also highlighted by Nasirov *et al.* (2015), and the lack of flexible backup. Energy storage technologies such as batteries, pumped hydro, molten salts and hydrogen could provide this flexibility and should be assessed in the context of increased non-dispatchable renewable generation. However, to achieve the large scale integration of intermittent renewables and energy storage it is important to reform the market and regulatory framework which was designed for conventional and dispatchable electricity generation (Hu *et al.*, 2018; Forrester *et al.*, 2017). For example, energy storage systems can provide a number of services and roles, such as frequency response service and short term operating reserve but most markets have limited mechanisms to enable this stacking of services (Forrester *et al.*, 2017).

A number of researchers have assessed the impact of energy storage in Chile's electric system. For instance, Moreno *et al.* (2017) studied the effects of pumped hydro on the integration of renewables and assessed the value of adding storage in the Chilean system. In particular, they evaluated the conversion of conventional hydropower generators to pumped hydro storage plants. Interestingly, they showed that this transformation has better synergies with solar PV than with wind generation due to wind production being more distributed during the day if compared with solar. Suazo-Martinez *et al.* (2014) presented a framework for the optimisation of energy storage sizing. They applied the methodology to optimally size pumped

hydro-like energy storage in the former SING system to provide secondary reserve and energy arbitrage services for the period between 2020 and 2030. They showed that the optimal installed capacity of storage in the northern system depended strongly on the investment costs, but for pumped hydro with costs of 400–900 €/kW and 17 €/kWh, the optimal power capacity was between 100 and 200 MW with energy capacities between 5 to 10 h.

Within the multiple options for electricity storage, thermal energy storage (TES) for electricity production presents some relative advantages with respect to other energy storage technologies. Probably the most important is that, excluding adiabatic compressed air storage (ACAES), it has no geographical or geological constraints, such as those presented by pumped hydro or compressed air energy storage (CAES). In addition, it uses only relatively common and non-hazardous materials in comparison with chemical storage, and it is potentially cheaper than the different available battery storage technologies (White *et al.*, 2013; Lund *et al.*, 2016). The first point is particularly important in the Chilean case because all the existent hydroelectric dams that could potentially be converted to pumped storage are located in the South, while the solar resource is located in the North and the main demand is in the middle. Alternatively, pumped hydro storage located in the North using seawater has been assessed, but building a 300 MW project has been delayed due to a lack of finance (Peña, 2021).

Pumped thermal energy storage (PTES) is a thermo-mechanical energy storage technology that uses electrically-driven heat pumps to create a temperature difference between two thermal reservoirs. When electricity is needed, the system operates backwards and uses the temperature difference to drive a thermal cycle to generate electricity (Steinmann, 2017). PTES is expected to achieve efficiencies up to 70% (McTigue *et al.*, 2015) and under a levelised cost of storage analysis (LCOS), it could be competitive with other more developed large-scale energy storage technologies, such as CAES and even pumped hydro (Smallbone *et al.*, 2017). Taking this and the characteristics of TES technologies for electricity generation presented in Chapter 2 into account, and considering the availability of projected cost and efficiency data for PTES published by Smallbone *et al.* (2017), this technology was chosen for the analyses presented in this chapter. Notwithstanding, the methods applied can be applied to any other TES technology for electricity storage, given that there are available cost and efficiency projections.

By 2018, there were only 54 MW of electricity storage in form of lithium-ion batteries connected at grid level in Chile (Revista de Electricidad, 2018). While it is clear that more energy storage is required to achieve the goal of 70% of electricity from renewables, it is not clear how much and where the energy storage should be deployed to enable the large scale deployment of renewable generation. Integrated simulation and optimisation methods of the complete electricity system are required due to the complex interplay between generation, transmission and energy storage.

This chapter presents a quantitative analysis of the long-term impact of on-grid storage on the deployment of intermittent generation technologies in the recently connected Chilean national electric grid. As part of this analysis, it assesses the use of a new storage technology (PTES), considering its efficiency, projected investment and operational costs. A linear optimisation approach is used to model the Chilean electricity system and to assess a number of scenarios with variable on-grid electricity storage. The use of a linear optimisation model to address this analysis is required as it allows for a manageable time to perform the optimisation for multiple future scenarios, determining optimal design and operational features of the system. As will be explained in the next section, the climatic, geographic and demographic characteristics of Chile allow for its representation in few nodes, while keeping the main features of demand and generation. This follows the pattern of previous studies covering and optimising different features of the Chilean electricity system under various conditions, further discussed in Section 2.4. The trade offs and limitations of this modelling approach are further discussed in Section 3.2.11

3.2 Method

This section presents the general method used for performing the analysis carried out in this chapter and presents details of the modelling assumptions and scenarios defined for the study.

3.2.1 Optimisation model

The model of the Chilean energy system used in this chapter is a linear programming optimisation model based on Urbs (Dorfner, 2018) with additions and modifications to account for the water storage capacity of hydroelectric dams and the thermal storage of concentrated solar power (CSP) plants. Urbs is a model written in Python 3 (Van-Rossum, 1995), which relies on Pyomo (Hart *et al.*, 2017) for optimisation set-up and on Gurobi (Gurobi Optimization Inc, 2010) as solver. It minimises the cost of the system's expansion and dispatch operation expressed as a function of annualised costs. In its most general form, this cost is calculated according to equation 3.1.

$$C = C_{inv} + C_{fix} + C_{var} + C_{fuel} + C_{env} \tag{3.1}$$

Where C_{inv} is the annualised cost of investment at the beginning of the analysed period C_{fix} is the fixed cost of operation of the system during that period, C_{var} is the variable cost of operating the system in that period, C_{fuel} is the cost of the fuel used to operate the system and C_{env} is an environmental cost associated to a carbon tax. These costs are calculated for generation, transmission and storage technologies and a discount rate (r) of 7% is used

to spread the investment cost over the lifetime of the technology. The minimisation model is solved for one year using a one-hour time step. For each time step, the model defines the unit commitment of each available technology, the energy transmitted between nodes and the energy stored and retrieved. It also calculates whether it is economically convenient to invest in more installed capacity of a given generation technology, transmission or storage at the beginning of that year.

The main constraint of supplying the electricity demands in each node in each time step is given by equation 3.2.

$$D_i \leq G_i + \sum_j T_{ij} - S_i + R_i \tag{3.2}$$

Where D_i and G_i represent the demand and generation in Node i, T_{ij} represent the energy transmitted between Nodes i and j and S_i and R_i are the energy stored and retrieved from storage in the node.

Electricity generation is calculated in each node i and time step t according to equation 3.3

$$G_{i,t} = \sum_k Pd_{i,k} \cdot \tau_{i,k,t} \cdot \Delta t + Pnd_k \cdot S_{p,t} \cdot \Delta t \tag{3.3}$$

Where Pd is the installed capacity of each dispatchable technology k, τ is the variable representing the instantaneous load factor of each dispatchable technology (going from 0 to 1), Pnd is the installed capacity of non-dispatchable technology and S is the relative value of the intermittent resource p in each time step (between 0 and 1).

As some technologies have a limited capacity of ramp-up or down its generation in each time step and there are minimum generation capacities, $\tau_{i,k,t}$ is constrained according to equations 3.4 and 3.5

$$\tau_{k,t} \geq \underline{Pd_k} \tag{3.4}$$

$$|\tau_{k,t} - \tau_{k(t-1)}| \leq \overline{PdR_k} \tag{3.5}$$

Where $\underline{P_k}$ is the normalised, minimal operational state of the technology and $\overline{PdR_k}$ the normalised, maximal gradient of ramping of the technology per time step.

For generating electricity from fuels, commodities c have to be available and transformed in the generation process. This transformation is defined by equation 3.6, constrained by the maximum annual stock of such commodity in node i 3.7.

$$\frac{Pd_{i,k} \cdot \tau_{i,k,t}}{\eta_{k,c}} = F_{i,c,t} \tag{3.6}$$

$$\sum_t F_{i,c,t} \leq \overline{F}_{i,c} \tag{3.7}$$

Where $\eta_{k,c}$ is the efficiency of transforming commodity c in electricity by the use of technology k, F is the amount of commodity used and $\overline{F}_{i,c}$ the stock of commodity available for each year of operation.

The transmission is modelled as DC lines with an efficiency that dissipates a constant fraction of the power that flows through the cables, according to equation 3.8.

$$\begin{aligned} T_{ij,t} &= T^j_{i,t} \cdot \eta_{ij} \\ T_{ij,t} &\leq Tc_{i,j} \end{aligned} \tag{3.8}$$

Where $T_{ij,t}$ is the energy imported to node j from node i and $T^j_{i,t}$ is the energy exported from node i to node j, with η_{ij} representing the constant fraction of the power losses and $Tc_{i,j}$ the maximum capacity of the line.

The stored energy retrieved from the storage is modelled according to equation 3.9. While the storage itself is modelled with an efficiency for charging, another for discharging and a time depending discharge rate, according to equation 3.10.

$$\begin{aligned} S_{i,t} &= \sum_s \varepsilon^{\text{out}}_{i,s,t} \\ \varepsilon^{\text{out}}_{i,s,t} &\leq \min(Sp_{i,s} \cdot \Delta t, \varepsilon_{i,s,t-1}) \end{aligned} \tag{3.9}$$

Where $\varepsilon^{\text{out}}_{i,s,t}$ is the energy that is retrieved from the storage, $Sp_{i,s}$ is the power capacity of the storage and $\varepsilon_{i,s,t-1}$ is the energy stored in the previous time step. The same equation and restriction as those presented in 3.9 apply to the charging process of the storage.

$$\varepsilon_{i,s,t} = \varepsilon_{i,s,t-1} \cdot (1-d_s)^{\Delta t} + e^{\text{in}}_{i,s} \cdot \varepsilon^{\text{in}}_{i,s,t} - \frac{\varepsilon^{\text{out}}_{i,s,t}}{e^{\text{out}}_{i,s}} \tag{3.10}$$

Where $\varepsilon_{i,s,t}$ is the instantaneous energy content inside the storage, $e^{\text{in}}_{i,s}$ and $e^{\text{out}}_{i,s}$ are the efficiencies of charging and discharging the storage and d_s are the time depending self discharge losses, expressed as a percentage of the energy stored.

The equations and constraints presented above constitute the formulation for a minimum working model. The detailed mathematical formulation spans several sections and can be checked in Dorfner (2018), Section 3.2.

Additional equations to model specific characteristics of CSP generation were added. In this case, heat was added as an intermediate energy vector. The collection of solar energy and its transformation in heat was modelled with a fixed time series, like every other intermittent generation (second term in equation 3.3). The storage was modelled to store heat rather than electricity and the turbine was modelled to convert heat into electricity. For the new CSP capacity being installed, the relation between the capacity of the solar field to generate heat (at maximum irradiance) and the power capacity of the turbine was fixed at 2.5, while the storage was fixed at 17.5 hours. Therefore, for each new MW of installed CSP electricity generation capacity, the model automatically installs 2.5 MW_{th} of heat generation and 17.5/0.37 = 47.3 MWh_{th} of thermal storage (with an assumed turbine efficiency of 0.37). This is further explained in Section 3.2.9

In order to assess the long-term behaviour of the system, the model is run from 2020 to 2050 every five years, considering the installed capacity output of the year x as input for the year x+5, as well as the evolution in demand and change in costs of investment and operation of the technologies, detailed in Sections 3.2.4 and 3.2.5.

The Chilean electricity system was modelled with four nodes numbered from north to south, as shown in Figure 3.1. This number of nodes was chosen as an approximation of the real system that would allow to capture the main specific characteristics in energy resources availability and electrical consumption of the different areas of Chile, while keeping the computational complexity manageable. Some of these main characteristics for each node are:

- Node 1: It represents the former SING system, which was not connected to the rest of the country until 2017, meaning it was self-sufficient. It accounts for 25% of the total demand with a relatively flat daily consumption profile due to high share of 24/7 operating mining industry. It has the highest potential for solar energy but its current installed capacity is mostly coal, combined cycle gas (CCGT) and open cycle gas (OCGT) plants.
- Node 2: It represents the northern part of the former SIC system and accounts for only 15% of the demand and presents a high solar potential. Currently, it has a combination of wind, solar and fossil fuel (coal, gas and diesel) generation.
- Node 3: It represents the central part of the former SIC system, home to more than 60% of the population and accounts for around 43% of the total demand. Its installed capacity is a mixture of hydropower, CCGT and coal power plants. It does not have especially good renewable resources and it is historically a net importer of energy.
- Node 4: It represents the southern part of the former SIC system with only 15% of the demand but high installed capacity of hydropower and good wind potential. It has been historically a net exporter of electricity.

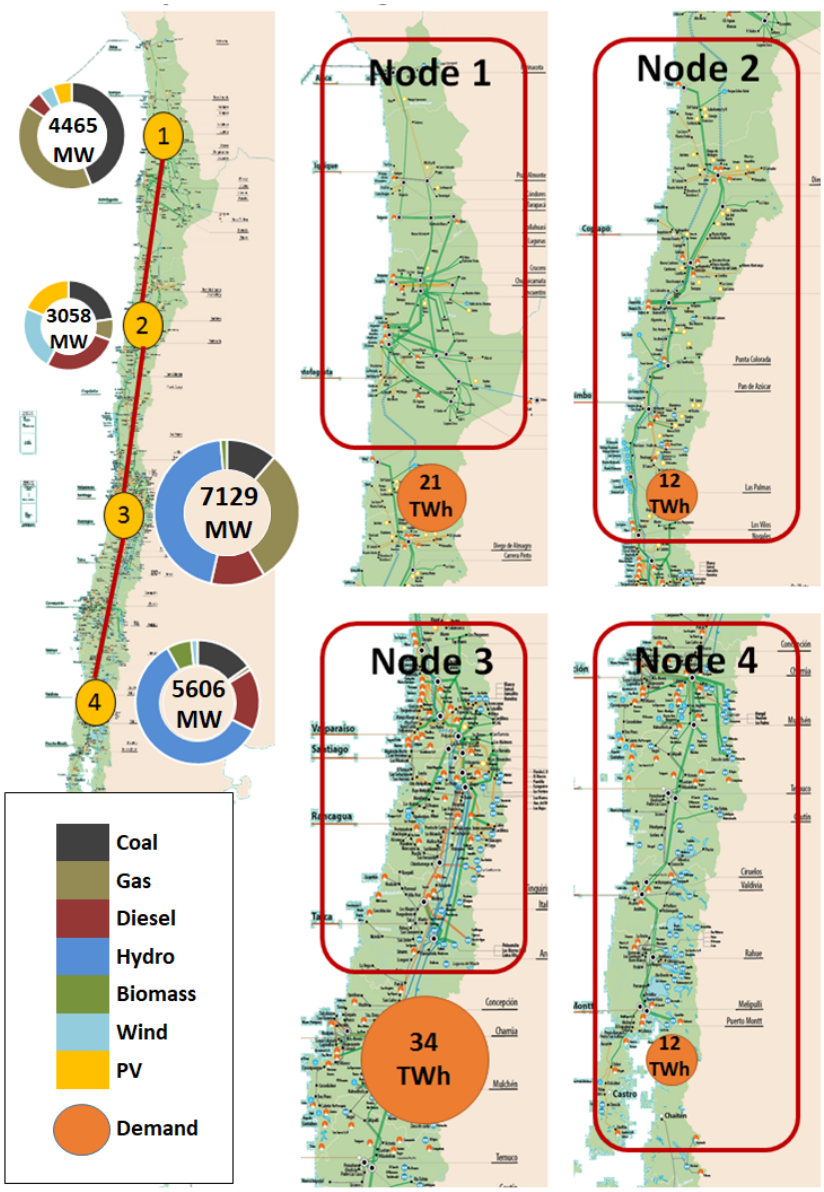

Figure 3.1: Nodes considered in the model with installed generation capacities and demands in 2016 according to Coordinador Eléctrico Nacional (2017)

3.2.2 Installed Capacity

The system was modelled according to the 2016 configuration, prior to the connection of SIC and SING. The data for the installed capacity per technology (shown in Table 3.1) were obtained from the National Electric Coordinator. For the year 2020, projects in the pipeline of the Chilean National Expansion Plan are added (Ministerio de Energia, 2017a). These include Cerro Dominador project (110 MW), the first CSP project in South America that considers molten salt storage tanks with a capacity of 17.5 h of operation. Slack power plants are included in each node with infinite capacity and high operational cost, ensuring that the condition in equation 3.2 is always met. The cost of operation of these slack power plants is equal to short duration unmet load in the system, according to Lima *et al.* (2012).

Generation Technology	Node 1	Node 2	Node 3	Node 4	Total
Coal	1959	694	805	850	4308
OCGT	53	237	262	60	612
CCGT	1745	0	1883	0	3628
Diesel	232	840	860	912	2844
Hydro reservoir	0	0	1645	1775	3420
Hydro streaming	0	0	1559	1554	3113
Biomass	0	0	101	362	463
Geothermal	17	0	0	0	17
Wind	200	709	18	93	1020
Photovoltaic	259	578	46	0	883
CSP	0	0	0	0	0
Total	4465	3058	7179	5606	20,308

Table 3.1: Installed capacity per node for 2016 in MW

It is important to notice that the units of the same technology located in a same node are treated as an aggregated power plant with an equivalent capacity.

3.2.3 Transmission

Transmission between nodes was approximated by the capacity of the main lines that connect the principal areas of the system according to Table 3.2. The presented efficiencies represent losses of 2.3% of the total generation in the transmission lines. The line capacity was increased every 10 years, following the increase in total demand. It was assumed that the transmission between Nodes 2 and 3 would increase 60% faster to allow the transmission of the solar generation to the point of higher consumption.

Transmission line	Efficiency	Capacity [MW]			
		2020	2030	2040	2050
Node 1–Node 2	0.85	1500	1756	2012	2269
Node 2–Node 3	0.9	1500	1910	2320	2730
Node 3–Node 4	0.9	2000	2342	2683	3025

Table 3.2: Transmission line capacities and efficiencies for Scenarios 0 to 4 (defined in Section 3.2.7)

3.2.4 Investment and Operational Costs

Costs for investment, operation and fuel were obtained from the average scenario in Chile's Long Term Energy Plan (Ministerio de Energia, 2018). Table 3.3 shows the investment costs of renewable energy and the projected cost of fuels used in the model. The lifespans assumed for the annualisation of the investment cost are 30 for CCGT, OCGT and CSP, 25 for diesel engines, wind, PV and biomass (Ministerio de Energia, 2019b) and 20 for PTES (Smallbone *et al.*, 2017).

		2020	2025	2030	2035	2040	2045	2050
PV *	[€/kW]	923	799	717	668	616	561	504
CSP		6315	5626	4937	4592	4248	4133	4018
Wind		1490	1408	1326	1245	1163	1082	1000
Biomass		2611	2565	2520	2474	2429	2394	2360
Geothermal		5429	5293	5157	5021	4884	4748	4721
Diesel	[€/MWh] **	56.3	63.5	68.7	73.4	77.9	79.6	82.6
Natural Gas		32.4	32.4	34.3	34.6	34.6	35.9	37.4
Coal		9.6	9.7	9.7	9.8	10	10	10
Biomass		9.7	9.7	9.7	9.7	9.7	9.7	9.7

* For Nodes 3 and 4 the cost is considered to be 35% higher due to the high presence of rooftop generation.

** Corresponds to the thermal energy of the fuel.

Table 3.3: Projected investment costs of renewable generation and fuels

3.2.5 Hourly Demand

Hourly electricity demand was obtained from the National Electric Coordinator (Coordinador eléctrico nacional, 2018) for 2016 for SING (Node 1) and SIC (Nodes 2, 3 and 4). The regional National Energy Balance 2016 (Ministerio de Energia, 2017c) is used to spread SIC's total demand between the Nodes 2 to 4. For projecting the demand until 2050, a linear model,

which is fitted with the demand for 2016 and the projected demand for 2046 from Ministerio de Energia (2018) is used for the entire country. This growth is spread between the four nodes according to the expected growth trends of total energy consumption presented in Ministerio de Energia (2018). Figure 3.2 presents the total annual projected demand for the four nodes.

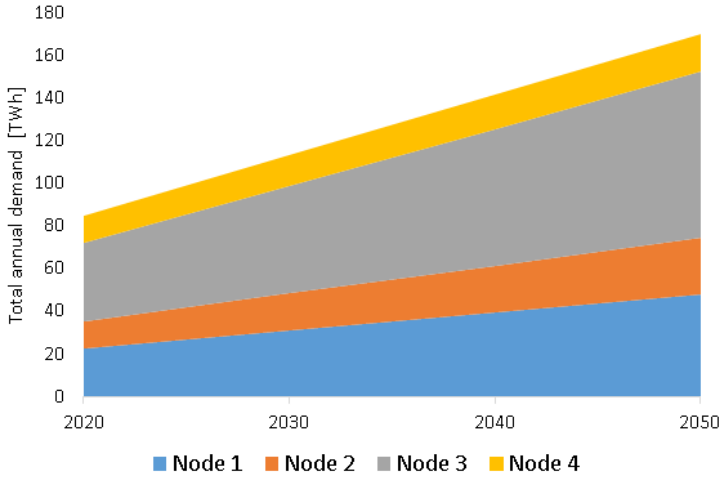

Figure 3.2: Projected annual demand per node

Figure 3.3 presents the hourly demand during one week, which allows to compare the demand behaviour of Node 1 against Nodes 2, 3 and 4. Node 1 presents a much flatter and noisier demand, as it is dominated by mining industry consumption which operates 24/7 and which large equipment's start and stop is more noticeable.

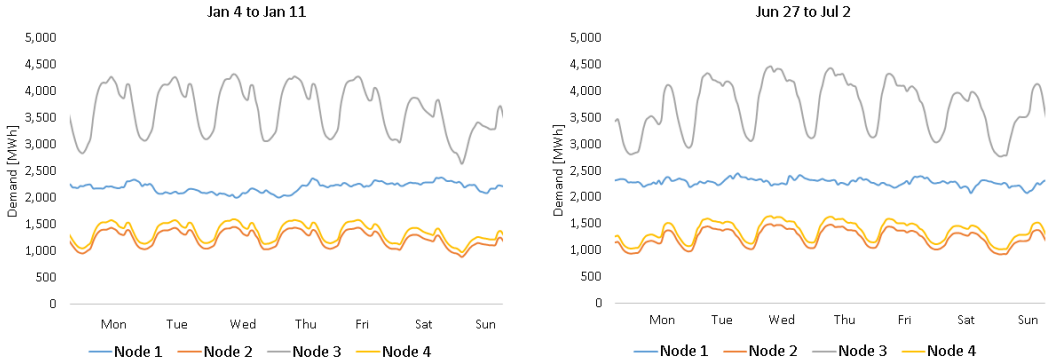

Figure 3.3: Hourly demand in summer (left) and winter (right) weeks per each node in the year 2016

Like any projection, the demand forecast from Chile's Ministry of Energy is based on a large number of assumptions such as projections of population growth, energy productivity, sustainable behaviour as well as an increasing share of electric vehicles and electric heating. However, the specific intra-daily effects of these changes are not explicitly presented by the sources used to create the energy projection. Therefore, the shape of the daily demand is increased proportionally for each hour of the year.

3.2.6 Renewable Resource

The Urbs framework handles renewable resources as deterministic capacity factors time series, which means that the resource time series had to be pre-processed into values between 0 and 1, where 1 represent the maximum power output of the system.

The hourly data for solar PV and wind resources were obtained from Pfenninger and Staffell (2017) directly as capacity factors. These data are based on the MERRA-2 reanalysis database, which is built with satellite data corrected with local observations (Molod *et al.*, 2015). In the case of solar PV, the capacity factor corresponds to an optimally tilted fixed array (maximising annual generation based on latitude). In the case of wind, it considers a conventional turbine with 50 m hub height. As Pfenninger and Staffell (2017) does not include data for CSP generation, typical meteorological year DNI was obtained from Ministerio de Energia (2017b). This serie of DNI values was transformed into capacity factors normalising by the maximum annual DNI.

In order to get a better representation of the existing renewable projects, the geographical data points were chosen to match the location of existing clusters of plants, as shown in Table 3.4. In the case of solar for Nodes 3 and 4, considering the comparatively lower solar resource, the main cities were chosen to account for mostly rooftop systems which are expected to be installed in these areas.

Solar and wind resources are considered to be constant during the analysed period. However, a location with a higher capacity factor is chosen for Node 4 after 2025 because it is expected that in the near future, locations with better wind resources that are currently far from the main transmission lines are going to be developed due to the expansion of the transmission system. For the hydroelectric generation, the average hourly capacity factor of the existing off-the-river hydroelectric power stations was used. These capacity factors were decreased by 0.386%/a from 2025 to 2040 and by 0.737%/a from 2040 to 2050 in order to account for the impact of climate change in the main Chilean basins, in accordance to Vargas *et al.* (2012), which predicts a reduction in annual rainfall. The maximum potential of renewable generation at each node was defined according to the limits set by Santana *et al.* (2014)

		Name of Location	Latitude	Longitude	Average Capacity Factor
Node 1	Solar	María Elena	-22.34	-69.66	0.249
	Wind	Valle de los Vientos	-22.48	-68.82	0.191
Node 2	Solar	Diego de Almagro	-26.39	-70.04	0.237
	Wind	Los Cururos	-31.05	-71.63	0.206
Node 3	Solar	Santiago	-33.44	-70.65	0.213
	Wind	Ucuquer	-34.04	-71.63	0.143
Node 4	Solar	Temuco	-38.73	-72.58	0.181
	Wind (existent)	Renaico	-37.72	-72.59	0.194
	Wind (after 2025)	Osorno costa	-41.00	-73.84	0.295

Table 3.4: Locations used for solar and wind data for each node

and are presented in Table 3.5. The maximum capacity for conventional generation was left unconstrained but it was considered that no coal power plants were to be constructed after 2025, taking into account the agreement between the Ministry of Energy and the Electricity Generator's Association (Energy Live, 2018).

	Node 1	Node 2	Node 3	Node 4
Wind	11,000	1,152	150	24,000
Photovoltaic	700,000	140,000	7,500	7,500
CSP	380,000	29,000	0	0
Geothermal	1,000	0	500	100
Biomass	0	0	200	1,000

Table 3.5: Maximum capacity of renewable generation to be installed in each node [MW]

3.2.7 Scenarios

To assess the impact that on-grid storage can have on the Chilean electricity system in the long term, six scenarios with different energy storage and transmission expansions are analysed. The details of the storage for Scenarios 0 to 3 are shown in Table 3.6, while the results of storage optimisation for Scenarios 4 and 5 are presented in Section 3.3.2. The first scenario (Scenario 0) can be considered "business as usual" and it does not consider any on-grid electricity storage. Three exploratory scenarios with different amounts of on-grid storage were considered (Scenario 1, Scenario 2 and Scenario 3). These scenarios consider a predefined amount of storage power and duration capacity deployed on the grid. The storage power capacity is assumed to increase linearly over time, while the energy storage capacity changes accordingly to keep a constant time capacity in hours.

Scenario 1 was constructed by installing 50% of the storage power capacity obtained by running the model under very favourable conditions for storage deployment: demand and prices for 2050 but considering an initial generation installed capacity as for 2020 and a low price for storage (350,000 €/MW and 50 €/MWh). It considers a fixed storage duration capacity of 8 h. Scenario 2 considers an increase in energy storage duration capacity to 30 h without modifying the installed storage power capacity, while Scenario 3 considers an increase of 30% of the installed storage power capacity, keeping the 8 h of storage from Scenario 1.

A more realistic scenario (Scenario 4) considered the availability of pumped thermal energy storage (PTES) at a cost according to Table 3.7. As all previous scenarios assumed a fixed increase in the transmission, Scenario 5 is an exploratory scenario to assess the transmission system upgrade under the option of higher storage penetration in the grid. Scenario 5 considers the same cost of storage as Scenario 4 but instead of assuming a transmission expansion according to Table 3.2, it assumes a cost for expanding the transmission capacity and includes that decision in the optimisation model. In order to analyse the influence of the cost of expansion, two versions of Scenario 5 are created: Scenario 5a with costs of 400,000 €/MW (approximately equivalent to 900.000 €/km) and Scenario 5b with an expansion cost of 250,000 €/MW (approximately equivalent to 550,000 €/km). These values are based on real investment cost of transmission lines from Comision Nacional de Energia (2015). An average distance of 650 km between each node and a double circuit of 500 kV, with 1500 MW of capacity was assumed.

A summary with the differences between the scenarios is presented in Table 3.8

		Node 1	Node 2	Node 3	Node 4	Total
Scenario 0	Storage power by 2050 [MW]	0	0	0	0	0
	Storage energy by 2050 [h]	0	0	0	0	0
Scenario 1	Storage power by 2050 [MW]	2,806	3,252	606	606	7,270
	Storage energy by 2050 [h]	8	8	8	8	8
Scenario 2	Storage power by 2050 [MW]	2,806	3,252	606	606	7,270
	Storage energy by 2050 [h]	30	30	30	30	30
Scenario 3	Storage power by 2050 [MW]	3,648	4,228	788	788	9,451
	Storage energy by 2050 [h]	8	8	8	8	8

Table 3.6: Installed capacity of storage for Scenarios 1, 2 and 3 in the year 2050

3.2.8 Pumped Thermal Energy Storage Modelling

The PTES model is based on the work of Smallbone *et al.* (2017). The roundtrip efficiency was set at 67%, according to the target system, while the self-discharge rate was set to 1%/day. The efficiency of 67% was included in the model by considering a COP of 1.5 during charging and an efficiency of 0.45 during discharging, this increased the self-discharge, as more energy was inside the storage at any given time.

The investment costs were set at Smallbone's most conservative estimate for 2020 and shifted linearly towards the technical potential by 2050, in accordance to Table 3.7. For this kind of technology, the addition of extra energy capacity is straightforward, as it depends mostly on the size of the tanks, which is independent of the power capacity. Thus, both costs can be added without incurring in double counting, as the power investment cost depends primarily on the cost of the compression/expansion equipment, while energy investment costs depend on the size of the tanks and the quantity of the energy storing media.

	2020	**2025**	**2030**	**2035**	**2040**	**2045**	**2050**
Power investment cost [€/kW]	800	725	650	575	500	425	350
Energy investment cost [€/kWh]	20	18.83	17.67	16.5	15.3	14.17	13

Table 3.7: Projected investment cost for pumped thermal energy storage (PTES)

3.2.9 CSP and Hydroelectric Reservoir Modelling

The underlying model (Urbs) allows to generate, consume, transfer and store different resources. However, it does not include the possibility of directly storing intermittent renewable energies, as these are provided as a capacity factor from 0 to 1 and not as an energy flow. Thus, an intermediate commodity had to be used to allow for storing energy before its conversion to electricity. Figure 3.4 shows this logic for CSP and hydroelectric power plants with reservoirs.

In the case of CSP, the DNI is expressed as a capacity factor and transformed into heat by the solar field. The heat can be transformed into electricity by the power block or stored in the thermal storage, from where it can be retrieved to generate electricity later. In the case of the hydroelectric dams, the river water influx expressed as a capacity factor of an equivalent off-the-river power station is transformed into energy-equivalent dammed water, which can be used to generate electricity in the turbine or stored for later use. In this case, it was assumed that the turbine has an additional operational cost of 30 €/MWh to simulate the opportunity cost of using the stored water to generate electricity instead of storing it for future uses. While CSP power plants may have different combinations of solar field, storage and power block sizes, the Cerro Dominador power plant (Cerro Dominador, 2020) was used as a model for the new added capacity. This means that all the new CSP capacity added to the system had a

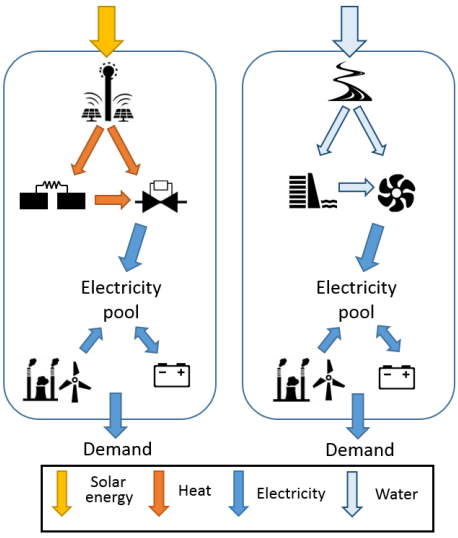

Figure 3.4: Scheme of the modelling of CSP (left) and hydroelectric power stations (right) with storage

solar multiple of 2.5, meaning that its solar field has a nominal capacity 2.5 times larger than the nominal capacity of the power block. Also, it was assumed an efficiency of 37% for the power block, and 17.5 h of thermal storage capacity, which means that the plant could operate up to 17.5 hours at its nominal capacity in periods without sunshine. These values also agree with the optimal values found by Bravo and Friedrich (2018).

3.2.10 Other Important Assumptions

Other important assumptions used to develop the model are:

- It was assumed that there is no expansion of coal generation from 2025. This was based on the agreement signed in early 2018 between the Government and the generation sector that no new coal fired power plants are developed unless they are equipped with carbon capture and storage (Energy Live, 2018).
- The obsolescence of the existing power stations was considered and the installed capacity was decreased in each period taking into account their initial year of operation and expected lifespans. While new plants are usually designed for a lifespan of 15 and 25 years for diesel and gas/coal, respectively, most plants have their lifespan extended by 5 to 15 years (Foy *et al.*, 2014; BEIS, 2016a). Here, lifespans of 25 years for diesel engines, 30 years for OCGT and CCGT and 40 years for coal power plants were assumed. The same lifespans were assumed for the newly installed capacity.

- Another important assumption was that there is no new development of large hydropower projects. This strong assumption was based on the public opposition that these projects have had in recent years (Agostini *et al.*, 2017; Bardeen, 2018) and aimed to show that a high percentage of electricity from renewables is achievable even without the construction of large hydroelectric projects.
- It was considered that there is no limitation on the availability of fuels for the operation of the conventional power plants (coal, natural gas and diesel) and biomass power plants, and that there is no limitation on maximum installed capacities of conventional generation technologies (other than coal).
- Chile was the first country in South America to introduce a carbon tax of 5 US$/t$CO_2$ in 2017 (Ramstein *et al.*, 2018). Using the conversion of 1$ = 1 €, a 5 €/tCO_2 fixed carbon tax was considered for all the modelled scenarios. This low carbon tax will have a limited impact on the decarbonisation of the power sector (Diaz *et al.*, 2020) and was introduced with the aim of implementing the regulatory framework, infrastructure and social acceptability (Pizarro *et al.*, 2019).

3.2.11 Limitations of the modelling approach

A fast solving optimisation model has been proposed to allow to perform analysis of multiple scenarios and several years in the future. However, this speed of convergence generates several trade offs and limitations that are summarised following.

As discussed in Section 2.4, a four node model represents relatively accurately the broad location of different technology generation and demand. However, it does not allow to consider local transmission constraints in areas rich in renewable potential that are further away from the main transmission system. In the current model, any generator located in each node automatically delivers power in the node and the only transmission constraints arise when providing energy to a neighbouring node.

The aggregation of generation of the same technology in each node decreases the granularity of the generation units. This produces the loss of detail of each unit's individual characteristics, such as minimum operational capacity and ramp-ups.

From the transmission perspective, the linear representation of electricity networks assumed direct current (DC) transmission, neglecting the effect of reactive power and the requirements of balancing frequency. This tends to favour non synchronous generation such as solar PV. In addition, the model assumed a fixed rate of transmission loss. This fixed rate was set to approximate the average annual losses of the transmission network and does not account for variation due to congestion in local lines. Furthermore, the distribution network, which is responsible for an important fraction of the total losses in the network has not been modelled, amplifying the possible discrepancies of losses between the model and the real system.

While the model assumes trends that vary the investment cost of specific technologies in the future, it does not account for local learning rates. This means that the cost of installing and operating a specific technology in the country does not change if more for said technology has been installed in the past.

The discount rate considered in the model represents the social discount rate currently in use for infrastructure projects in Chile. It is lower than the discount rates used by private investors, and it is meant to represent the interest of the Government as a representative of the whole society. However, it may fail to represent the real will to invest of private generation companies. Moreover, this interest rate has been fixed throughout the period. This assumption does not consider changes in the economic situation of the country and might overestimate the future level of the interest rate, as this tends to decrease when countries increase their economical development.

The carbon tax considered in the model has been modelled as an extra cost directly paid by each conventional generator and has been assumed fixed. However, it is expected (and even proposed in the official energy policy (Ministerio de Energia, 2021d)) that it should increase in time. The assumption of higher carbon tax levels could lead to higher penetration of renewable generation and higher requirement of storage. Nevertheless, as proposed by Diaz *et al.* (2020), the current implementation of the Chilean carbon tax in the electricity market is more complex than a simple charge to each generator and some authors have argued that it does not affect investment decisions, as it is automatically transferred to the final clients. Therefore, the real effect of the Chilean carbon tax exceeds the capabilities of this model and would require a more detailed representation of the market to be explored.

3.3 Results and Discussions

First, the results and discussion of the scenarios with fixed energy storage (Scenario 1, 2 and 3) and subsequently the results of the scenarios with optimised storage (Scenarios 4 and 5) and transmission expansion (Scenario 5) are presented. In all the cases Scenario 0 is used as a reference. Table 3.8 presents a summary of the differences of all the considered scenarios. The main differences between the scenarios is while the first three use predefined storage deployment rates, Scenarios 4 and 5 allow the model to optimally determine the deployment of storage. In addition, Scenario 5 allow the model to optimally define the transmission, while the other scenarios assume a predefined (exogenous to the model) expansion. For more specifics on the assumptions of each scenario refer to Section 3.2.7.

	Transmission	Storage deployment	Storage capacity per unit (hours)
Scenario 0	Base case with no storage and fixed transmission expansion		
Scenario 1	Fixed expansion	Low fixed rate deployment	Low capacity (8 h)
Scenario 2	Fixed expansion	Low fixed rate deployment	High capacity (30 h)
Scenario 3	Fixed expansion	High fixed rate deployment	Low capacity (8 h)
Scenario 4	Fixed expansion	Optimised deployment	Optimised sizing
Scenario 5a	Optimised expansion at higher cost	Optimised deployment	Optimised sizing
Scenario 5b	Optimised expansion at lower cost	Optimised deployment	Optimised sizing

Table 3.8: Summary of main differences between the considered scenarios

3.3.1 Scenarios 1, 2 and 3

As shown in Table 3.6, Scenarios 1, 2 and 3 do not include energy storage in the optimisation formulation, meaning that its addition is an exogenous process and is seen as "free" from the system's perspective. After running the model for the different scenarios, it is evident that storage has an impact on the amount of non-dispatchable renewable capacity that is installed in the system, as is shown in Figure 3.5.

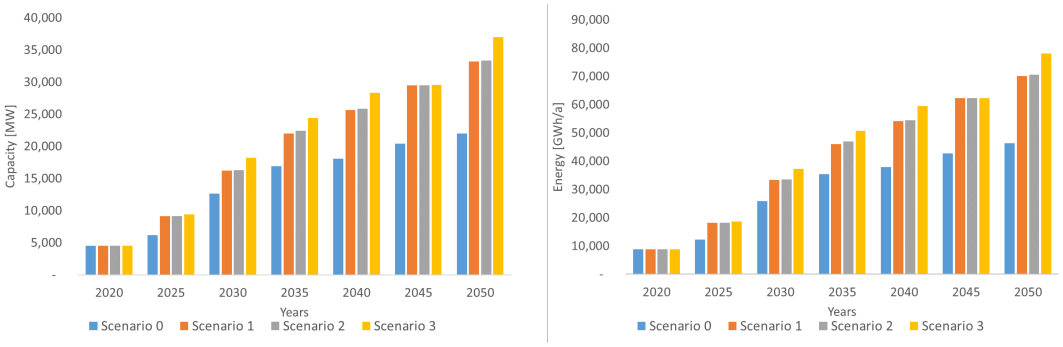

(a) **(b)**

Figure 3.5: Evolution of (a) the installed capacity and (b) the energy generation of combined PV and wind generation under Scenarios 1, 2 and 3

Figure 3.5a shows that, in the long-term in Scenario 0 (no storage), there is already a significant increase in the installed capacity of non-dispatchable renewables. This increase is mostly due to PV, which is cheaper than wind. In addition, northern Chile has a very good solar resource, which together with the daily solar cycle, leads to strong synergy with energy storage systems with a capacity for around half a day. However, it is worth mentioning that

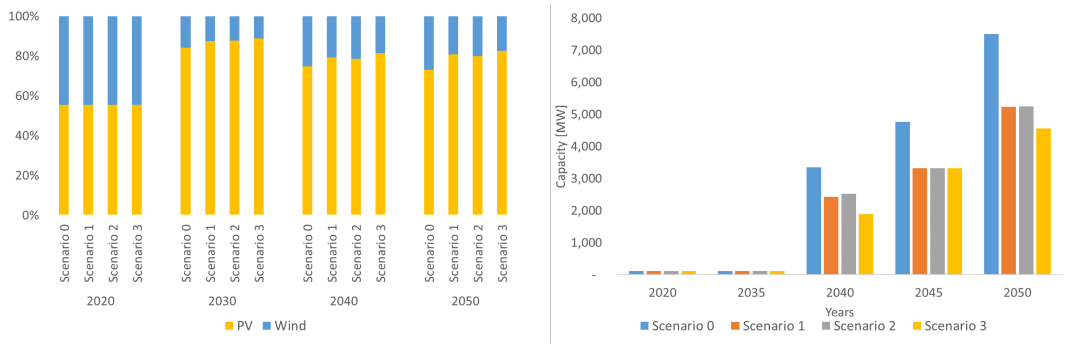

(a) **(b)**

Figure 3.6: Relative evolution of (a) PV and wind installed capacity per scenario and (b) the evolution of the installed capacity of CSP

the relative increase in wind generation capacity is higher in the scenario with no storage, as shown in Figure 3.6a. This is probably due to wind being on average more evenly distributed during the day. This agrees with Moreno *et al.* (2017), who showed that the development of solar PV increases the value of pumped hydro projects more than wind energy. However, energy storage systems with a capacity for more than a day (Scenario 2) lead to a relative increase in wind generation capacity due to the less regular wind resource profile.

Figure 3.7a shows that the emission factor of the system decreases drastically even in the scenario with no storage, reaching 22% of the value at 2020 by 2050. This is mainly due to the assumed decommissioning of 3,010 MW of coal generation during this period, representing 58% of 2020's coal installed capacity. This also explains the large decrease of the emission factor in 2040, when 1,300 MW of coal are decommissioned. This result underlines the importance of a planned decommissioning of the ageing coal power generators. The main difference in emission factor comes from the more important role of natural gas in Scenario 0, with more than 4 GW of CCGT generation installed between 2020 and 2050, which contrasts with the close to 1.5 GW installed by the other three scenarios in the same period. However, as by 2050 natural gas represents less than 8% of the total generation in Scenario 0, the absolute difference in emission factors between the scenarios is small compared to the overall decrease. The reason for this relatively small difference in emissions, even though in Scenarios 1, 2 and 3 there are substantially larger capacities of wind + PV, is that in absence of electricity storage, in Scenario 0 there is a rise in the installed capacity of dispatchable CSP, as shown in Figure 3.6b, as its storage capacity provides the required flexibility. This, however, has an impact on the investment costs of the system (Figure 3.8b), as CSP is a much more capital intensive technology than PV. Figure 3.7b presents the variation of each scenario with respect to Scenario 0, which is considered here as a reference. From it, is clear that the change of the emissions is not monotonic, as the problem represents a system with many different interacting constraints that lead to complex and unexpected behaviour. For example,

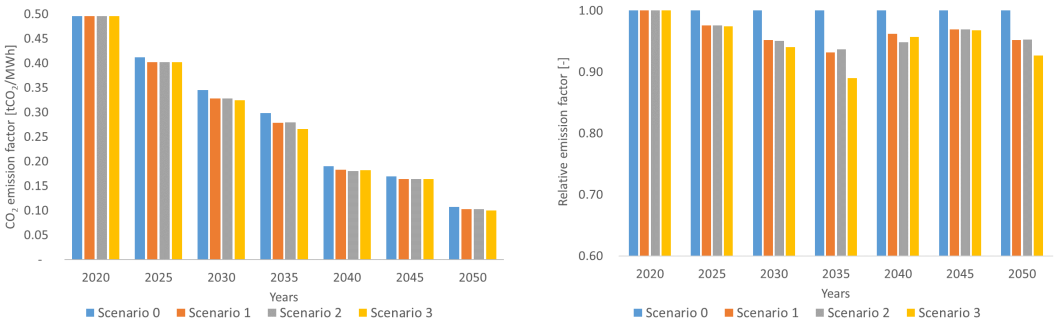

(a) **(b)**

Figure 3.7: Evolution of (a) the absolute emission factor and (b) the relative emission factor for Scenarios 1, 2 and 3 with respect to Scenario 0

for 2035, Scenario 2 presents a higher emission factor than Scenario 1, despite having more energy storage and PV generation capacity. The explanation for this particular case, is that the higher energy storage capacity is not enough to balance the extra PV generation by its own and the economically most efficient alternative is to run CCGT generation for more hours to balance the extra PV.

Figure 3.8a presents the costs of operating the system for one year, including fuel and other fixed and variable costs, whereas Figure 3.8b shows the annualised costs of investments at the beginning of every five years period. It must be noted that these costs are cumulative, because the annualised cost of an investment is applied until the end of its life, which explains the general increasing trend. Figure 3.8a, on the other hand, presents a decreasing trend, which is explained mostly by the decrease in fuel consumption due to the increase in renewable generation penetration. Figure 3.8b shows that after 2040, the scenarios with storage have lower investment costs than Scenario 0. This is due to the possibility to include cheap renewable generation (as PV) backed by the existent storage. Scenario 0, on the other hand, must install more expensive renewable technologies, such as CSP, as it has not enough storage to back the operation of non-dispatchable renewable generation.

From the results, it is evident that Scenario 2 (30 h of storage) achieves only a small improvement compared with Scenario 1 (8 h of storage), despite having almost 4 times more storage capacity. This agrees with the results presented in Section 3.3.2, which shows that the optimal energy storage size is around 9 h. Scenario 3 is the one that achieves the highest cost reduction with respect to Scenario 0, reaching an 18% decrease in operational cost and a 19% in accumulated investment by 2050.

As Scenarios 1, 2 and 3 consider storage to be given, the difference in costs with Scenario 0 represents the maximum cost that energy storage can have in order to make the system at least as cheap as the case without storage. Scenario 1 is analysed to find this maximum cost of storage, assuming an energy storage system cost per MWh of capacity (no additional cost

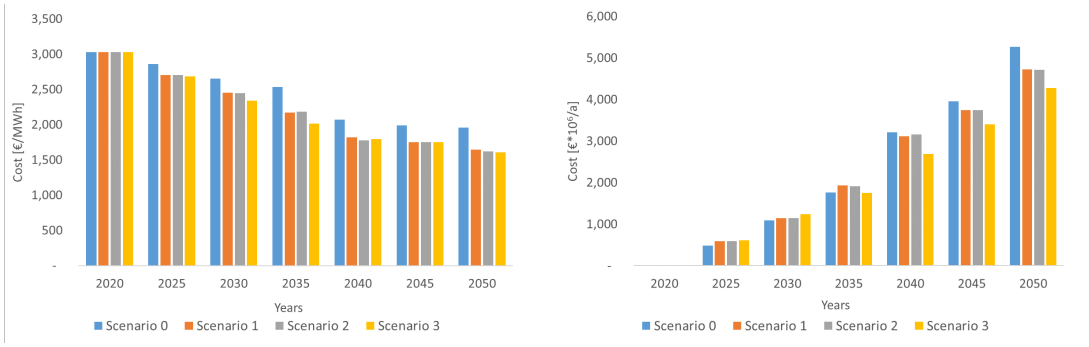

(a) **(b)**

Figure 3.8: Evolution of (a) the operational cost and (b) the annualised investment cost for Scenarios 1, 2 and 3

per power capacity) and another with cost per MW (zero cost of additional energy capacity). Table 3.9 presents the maximum investment costs of storage for these two cases on an annual basis. It shows that to be economically attractive to install in 2025 the amount of storage given in Scenario 1, it has to cost less than 43 €/kWh, which is well below the predictions of long term utility battery storage for 2025 (350 €/kWh (Hayward and Graham, 2017); 530 €/kWh (Schmidt *et al.*, 2017)). Although this cost could be achieved with pumped hydro (IRENA, 2017), the availability of the cheapest hydro resource is located in the south, while the main requirement of storage is in the north, where current cost estimates for pumped hydro using sea water are around 1400 €/kW (although on an energy basis, estimates are around 10 €/kWh) (Valhalla Energy, 2017). Costs for storage added after 2035 are probably achievable, however, the benefits calculated for this period consider that cheaper storage was installed in the previous years.

	2025	**2030**	**2035**	**2040**	**2045**	**2050**
Maximum investment cost [€/kWh]	43	144	139	166	158	542
Maximum investment cost [€/kW]	340	1155	1110	1370	1230	4330

Table 3.9: Maximum annualised investment costs of storage based on energy and power capacity, respectively

This analysis shows that it is not realistic to achieve the rates of storage deployment presented in these scenarios. A more realistic approach, with actual projected storage technologies' costs included in the optimisation, must be analysed.

3.3.2 Scenarios 4 and 5

In contrast with Scenarios 1, 2 and 3, Scenarios 4 and 5 include the energy storage as well as the transmission capacity (only Scenario 5) in the optimisation problem. The results show that for these scenarios, storage deployment starts after 2040, when PTES investment costs are expected to reach 500 €/kW according to Table 3.7. The optimal amount of storage in each node for in 2050 is presented in Table 3.10. This table confirms that energy storage presents higher value in supporting solar generation (PV) rather than wind, as the storage capacity concentrates in the sunniest northern nodes (Node 1 and 2) and no storage is installed in Node 4, the node with the lowest solar and highest wind resources. Also, it shows that the optimal energy capacity for storage is around 9 h, but shows a difference between the optimal energy storage capacity of Node 1 and Nodes 2 and 3. This difference is most likely due to the different energy demand profiles. The demand in Nodes 2 and 3 are dominated by residential consumers and usually peaks around 21:00 to 23:00 and decreases sharply during the night (01:00 to 06:00). This means, that in Nodes 2 and 3, a 7 to 8 h storage capacity is enough to shift the solar energy production peak from 14:00 to the late evening peak. In Node 1, on the other hand, demand is dominated by the mining industry and is comparatively flatter and does not have the sudden decrease at night, which means that the energy stored during the day has to be retrieved over a longer period.

		Node 1	Node 2	Node 3	Node 4	Total
Scenario 4	Storage power by 2050 [MW]	1377	1508	761	0	3646
	Storage energy by 2050 [h]	12	7.5	7	0	9.1
Scenario 5a	Storage power by 2050 [MW]	1535	1605	593	0	3734
	Storage energy by 2050 [h]	11.3	7.3	6.8	0	8.9
Scenario 5b	Storage power by 2050 [MW]	1500	1682	557	0	3740
	Storage energy by 2050 [h]	11.7	7.4	7.4	0	9.1

Table 3.10: Installed capacity of storage in the year 2050 for Scenarios 4 and 5 after running the model

Scenario 5 also includes transmission expansion in the optimisation. The result of this transmission expansion optimisation is presented in Table 3.11. As expected, a cheaper cost of transmission investment tends to increase the expansion of the transmission system. However, this expansion takes effect only after 2045 and concentrates in the line connecting Nodes 2 and 3, which is used mainly to transfer cheap solar PV from the northern part of the former

SIC to the main consumption point in central Chile and under a cost of 550,000 €/km should more than double. According to the results, the connection between Nodes 1 and 2, is not expected to increase, as Node 2 has enough PV potential to supply Node 3 and there is no need to send energy from Node 1 to Node 3.

	Transmission Line	Transmission Capacity [MW]				
		2020	2030	2040	2045	2050
Scenario 5a	Node 1–Node 2	1500	1500	1500	1500	1500
	Node 2–Node 3	1500	1500	1500	1783	2898
	Node 3–Node 4	2000	2000	2000	2000	2000
Scenario 5b	Node 1–Node 2	1500	1500	1500	1500	1500
	Node 2–Node 3	1500	1500	1500	2200	3543
	Node 3–Node 4	2000	2000	2000	2054	2287

Table 3.11: Transmission capacity for Scenario 5

Figure 3.9a presents the evolution of the installed capacity of PV and wind generation, while Figure 3.9b presents the trend of the energy generated by these technologies for Scenarios 4, 5a and 5b, with Scenario 0 as reference. If comparing Figure 3.9a with the results for the first three scenarios presented in Figure 3.5, it is clear that the installed capacity of PV and wind increases less. It is interesting to note that the installed capacity of non-dispatchable renewables in Scenarios 4 and 5 in 2050 is similar to the installed capacity in Scenarios 1, 2 and 3 in 2035. This reinforces the idea that the ability to integrate PV and wind generation in the energy system is related to the amount of energy storage.

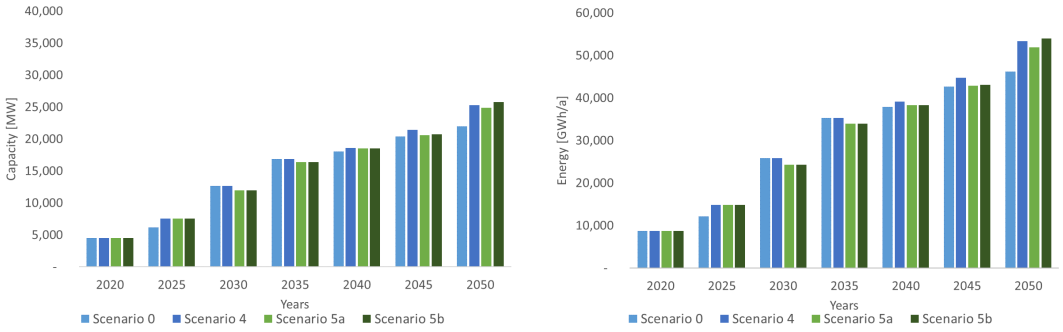

(a) **(b)**

Figure 3.9: Evolution of (a) the installed capacity and (b) energy generation of combined PV and wind for Scenarios 4 and 5

Figure 3.10a presents the absolute emission factor of the system for the different scenarios, while Figure 3.10b presents their evolution relative to Scenario 0. Similarly to Figure 3.7, it is evident that the general decreasing trend is driven by the decommissioning of ageing coal generation. In contrast to Scenarios 1 to 3, this figure shows that Scenarios 4 and 5 have

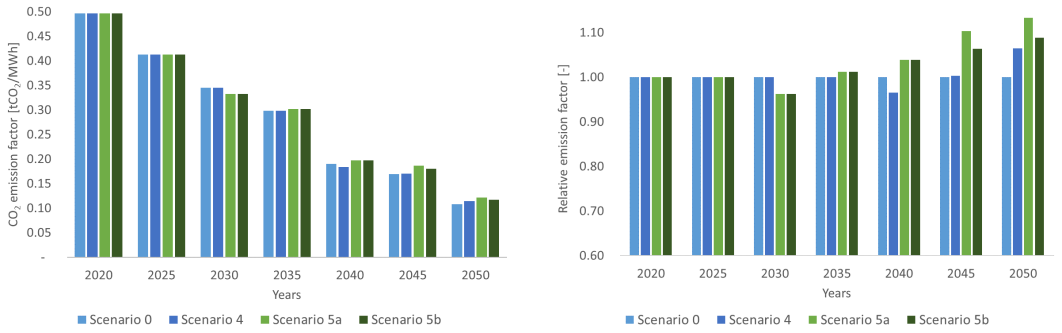

(a) **(b)**

Figure 3.10: Evolution of (a) the absolute emission factor and (b) the relative emission factor with respect to Scenario 0 for Scenarios 4 and 5

relatively higher emissions than Scenario 0. This is counter-intuitive, especially for Scenario 4, as it has the same transmission expansion as Scenario 0 but also has the option of installing energy storage, which allows an increase in the installed capacity of PV and wind. However, as the solar resource is particularly good in northern Chile, CSP with thermal storage becomes competitive with conventional options and is installed instead. Again, it can be seen that the change of the emissions is not monotonic, due to the many different interacting constraints. For example, in 2040 Scenario's 4 emission factor decreases with respect to Scenario 0 but in 2050 it increases. The decrease of the emission factor in 2040 comes from the fact that in Scenario 0, the absence of storage in Node 2 causes 600 MW more CCGT to be installed in Node 3, in contrast to Scenario 4, where PV plus energy storage in Node 3 is installed. In 2050, on the other hand, it is cheaper for the system in Scenario 4 to operate with PV with storage and coal than with extra CSP, so there are more emissions that in Scenario 0 are avoided by installing a higher amount of more expensive CSP.

Figure 3.11a presents the costs of operating the system for one year, including fuel and other fixed and variable costs, whereas 3.11b shows the accumulated annualised costs of investments in every year. The trends of both figures are similar to those in Figure 3.8. However, if compared with Scenarios 1, 2 and 3, the cost reductions in Scenarios 4 and 5 are lower. This is especially evident in the investment costs, as in this case there is a cost for installing energy storage and for expanding the transmission system (Scenario 5). In the case of the operational cost, the decrease is comparatively lower as the amount of total installed energy storage power capacity is lower, meaning that more fuel has to be burned to meet the demand. However, there is still an important cost reduction with respect to Scenario 0. In particular, the most realistic of the scenarios (Scenario 5b) reaches a 6% decrease of the annual system operation cost and accumulated investment cost by 2050 compared to Scenario 0.

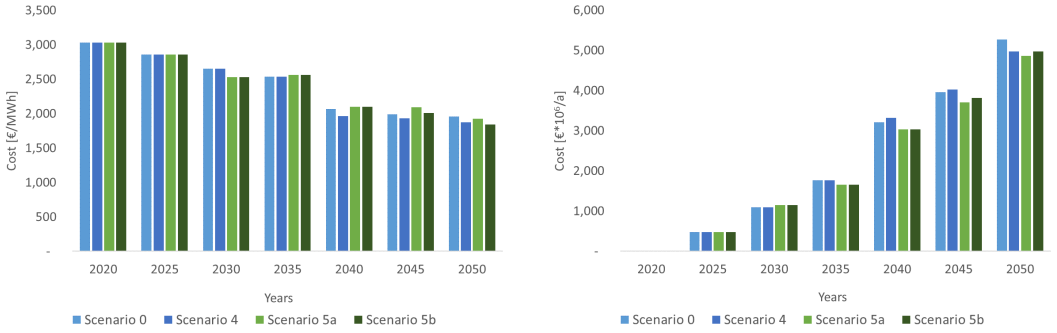

(a) **(b)**

Figure 3.11: Evolution of (a) the operational cost and (b) the annualised investment cost for Scenarios 4 and 5

The previous results and analyses have mainly assessed the achievable scenarios of non-dispatchable renewable generation and emissions at a country level. Figure 3.12 complements that analysis by presenting the geographical distribution of the energy generation of the different technologies for four of the analysed scenarios by 2050. Although in all scenarios the total annual generated solar energy represents around 50% of the total energy generated in that year, the most obvious difference between the scenarios is the relative participation of PV and CSP generation. As mentioned previously, a higher amount of energy storage in the grid shifts the solar installed capacity from CSP to PV, as a combination of PV plus a PTES-like storage systems results cheaper than CSP with molten salt storage.

According to the model, for all the analysed scenarios, the 70% renewable generation by 2050 goal set by the policy in 2015 is reached. Even more, 70% is reached in most of the scenarios without considering hydroelectric energy, as shown in Table 3.12. Despite being in accordance with results found by Munoz *et al.* (2017), this result is probably a slight overestimation of the total amount of non-dispatchable renewable generation achievable under these scenarios.

	Scenarios						
	0	**1**	**2**	**3**	**4**	**5a**	**5b**
Ren. Generation w/o hydro [%]	71.1	73.8	74.2	74.6	70.7	68.8	70.1
Ren. Generation with hydro [%]	84.3	86.7	87.1	87.4	83.7	81.8	83.1

Table 3.12: Percentage of energy coming from renewable generation including and excluding hydro power stations in the year 2050 for all the scenarios

The main source of possible overestimation of renewable generation integration in the current linear optimisation model is the lack of a binary variable to define the minimum operational output of conventional generation such as coal and CCGT, which overestimates the capacity of these technologies to back changes in non-dispatchable renewable generation. Also, the

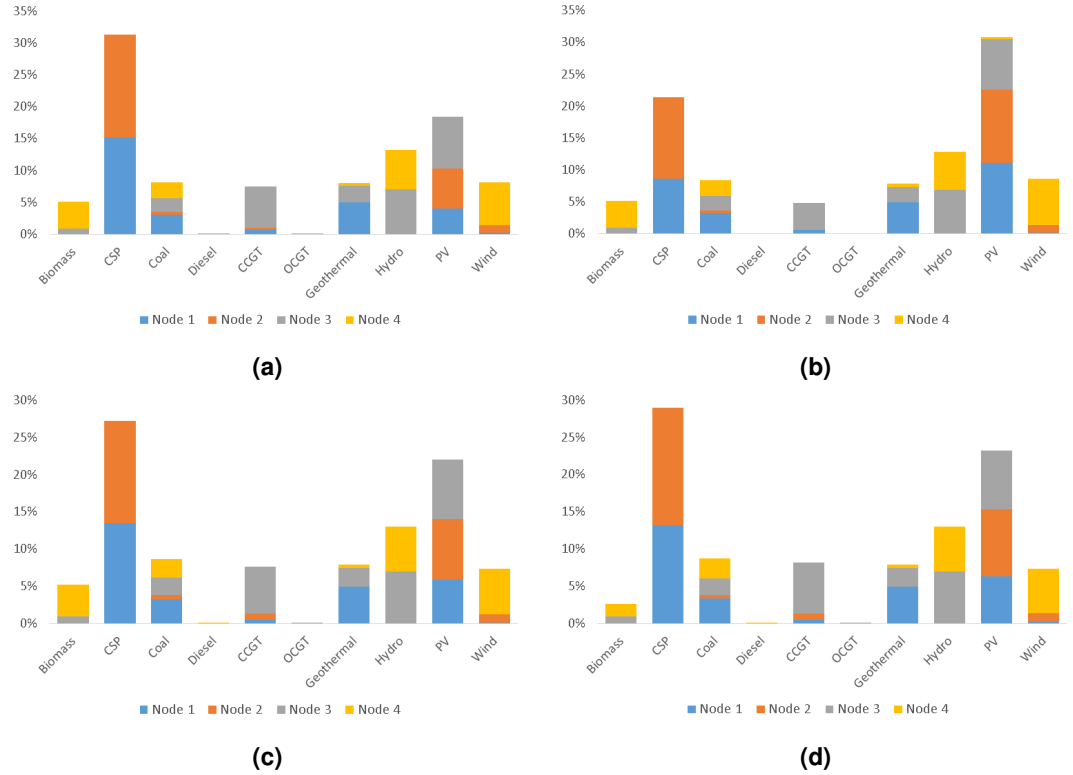

Figure 3.12: Distribution of energy generation by technology in each node for year 2050, (a) Scenario 0 , (b) Scenario 1 , (c) Scenario 4 and (d) Scenario 5b

current nodal resolution of the model does not allow to assess possible local constraints that could lead to transmission bottlenecks in renewable-resource rich clusters located at a certain distance from the main transmission lines. In any case, although it is expected that the inclusion of these missing features would decrease the total amount of renewables for a given scenario, it also is expected to increase the value of storage in the grid. Another feature that determines the results of this model is that as every period is run independently, the system is agnostic of the demand and prices variation in the future. This assumption usually leads to less economically optimal system configurations but is probably more realistic due to the uncertainty in long-term fuel price and technology cost predictions. Finally, the fact that transmission can be expanded in a continuous way, instead of in large discrete steps, promotes earlier transmission expansion. This also could lead to an overestimation of non-dispatchable renewable generation, because as shown in Figure 3.9, a delay in the transmission expansion causes a decrease in PV and wind penetration.

3.4 Conclusions

This chapter assessed the impact of grid-level energy storage on the decarbonisation of the Chilean electricity system. Efficient optimisation methods are required to find the optimal design and operation of the electric system due to the large size of the problem and the complex interplay between generation, transmission and energy storage. In this analysis, a linear programming model optimising the design and operation of the Chilean electricity system has been developed.

The linear optimisation model uses the Urbs framework, which was expanded with the ability to handle reservoir hydro generation and CSP plants with thermal storage. The Chilean electric system was modelled with four nodes representing the main parts of the system. Six scenarios were run for renewable generation, energy storage and transmission expansion between 2020 and 2050. These scenarios started with the current configuration of the electric system (installed capacity in 2016 and planned expansion to 2020) and evaluated different energy storage and transmission expansions. The problem was separated into independent expansion and annual operation problems, linked by the installed capacity of transmission, energy generation and storage technology.

The analysis showed that the main source of the grid emission factor decrease is the decommissioning of coal based generation and its replacement by a mix of solar generation and CCGT. The differences of emission factor between any scenario in 2050 were small in comparison with the decrease due to coal decommissioning (less than 5% of the emission factor in 2020 and less than 0.025 tCO_2/MWh in absolute terms). This means that in order to achieve a 78% decrease in emission factor by 2050, it is necessary to ensure a policy that would internalise coal based generation's externalities and encourage the decommissioning of the ageing units.

It is found that the addition of storage decreases the operational cost of the system by enabling the increased deployment of relatively cheaper non-dispatchable renewable technologies. For the Chilean system, the integration of energy storage leads to higher deployment of solar PV systems compared to wind turbines due to the very good solar resource and the strong synergy of the daily solar cycle with energy storage capacities of around half a day.

For the scenarios that include the storage costs projected for Pumped Thermal Energy Storage (PTES), the addition of storage could save 6% in annual system operation costs and in the total investment cost in generation from 2020 to 2050. As it shows high synergies with solar PV, this storage is most optimally located in the northern part of the country. Because in that area of the country there is no possibility of installing cheap pumped hydro energy storage, the option of installing a PTES-like storage appears especially attractive. The optimal storage capacities show good agreement with the demand profiles of the different nodes. The optimal storage capacity for the northern node is around 12 h due to the flatter demand

profile which is dominated by the continuously operating mining industry. On the other hand, the two central nodes are dominated by residential customers which have a lower night time demand and consequently, the optimal storage capacity decreases to around 7 h, as the main requirement is to supply the peak demand in the evening. In further works, it would be interesting to perform a comparative analysis between installing PTES-like storage in the northern area of Chile against locating potentially cheaper pumped hydro storage in the south (using natural lakes and reconverting existing hydro generators) or against more expensive pumped hydro in the north (purpose built seawater reservoirs).

It is interesting to note that the approximately 3.5 GW of installed storage capacity predicted by scenarios 4 and 5 in 2050, is close to the 3 GW predicted by scenario C with medium hydrology by the energy planning process 2020 (Ministerio de Energia, 2020g). Also, the 7.3 GW and 9.5 GW of 2050 storage capacity assumed for Scenarios 1, 2 and 3, coincides with the 7 to 9 GW predicted by the "Accelerated Transition" scenario of the last iteration of the energy planning process (currently still under development) (Ministerio de Energia, 2021d). These results, achieved with a more detailed representation of the Chilean electricity grid (further discussed in Chapter 5, Section 5.2.1), tend to validate the assumption considered in the model developed in this chapter, and confirms the relevance of considering PTES in the future electricity storage mix. This marks the achievement of the objective of introducing a TES technology for electricity in the Chilean context. Therefore, the next chapter will shift the focus of the analysis towards introducing and assessing the use of TES technologies for heating applications.

Since the writing of this chapter, a pathway for accelerated decommissioning of coal generation infrastructure has been agreed between the government and the generators. This pathway considers a scheduled retirement of 1,700 MW by 2024 and the agreement to retire the remaining 2,600 MW before 2040 (Ministerio de Energia, 2020e). Furthermore, there have been signals pointing that this target might be reached sooner, as in 2021 it was announced the conversion of a further 750 MW to biomass and natural gas by 2025 (Ministerio del Medio Ambiente, 2021). In addition, there have been studies analysing their possible re-conversion to green hydrogen and molten salt thermal storage (Ministerio de Energia, 2021b, 2020c). All these new developments should be taken into account in any future studies, as the early retirement of coal generation would decrease the flexibility provided by fossil fuel generation and would increase the requirement for new flexibility, therefore increasing the potential of on-grid energy storage.

Chapter 4

The value of seasonal thermal energy storage in solar district heating networks

The work presented in this chapter has been published in the article "Multi-objective optimisation of a solar district heating network with seasonal storage for conditions in cities of southern Chile" published in *Sustainable Cities and Society* (Maximov *et al.*, 2021).

4.1 Introduction

Most households in central and southern Chile do not reach thermal comfort during wintertime, with indoor temperatures often around 15°C (Urquiza *et al.*, 2017; Porras-Salazar *et al.*, 2020). Moreover, at a national level, the heating requirements are met mostly by burning firewood in stoves (47%) or in individual ventless gas heaters (31%) (Tolvett, 2015). The use of low quality firewood increases in southern Chile and creates a scenario of high levels of pollution indoors (Cortés and Ridley, 2014) and especially outdoors (Molina *et al.*, 2017), with the city of Coyhaique presenting average concentrations of PM2.5 close to 60 μg/m^3 and Temuco exceeding 45 μg/m^3, while the standard sets a maximum of 20 μg/m^3 (Ministerio del Medio Ambiente, 2018). An answer to this situation has come in the form of Air Pollution Management Plans (called PDA in Spanish) that provide families with programs and subsidies aimed at improving firewood quality and encouraging household retrofits. However, these plans have been criticised, as they also limit firewood use and focus on replacing it without considering the socioeconomic dimension (Reyes *et al.*, 2019). This situation creates the need for researching and proposing new sources and technologies for clean and affordable heating.

Ample international literature coincided in that district heating networks in urban areas can be part of the lowest cost decarbonisation pathway and can significantly reduce local emissions (International Energy Agency, 2019b; Hast *et al.*, 2018; Soltero *et al.*, 2016). This is mainly due to the possibility of taking advantage of economies of scale that allow using more efficient

technologies, getting better control of local emissions and integrating cheaper large scale storage to maximise the use of renewable resources. The Chilean Government has recognised the potential benefit of this technology and has mentioned it as an enabler for clean energy transition for heat in the National Strategy for Heat and Cold (Ministerio de Energia, 2021c) and has issued a Roadmap for District Heating Development to foster the development of this technology (Ernst Basler + Partner, 2016).

Chile presents medium to high solar resource along moss of the country, with global horizontal irradiance ranging between 1,400 and 2,600 kWh/m^2·a (Castillejo-Cuberos and Escobar, 2020; Molina *et al.*, 2017). The cities of Temuco and Coyhaique, in particular, have a good relation between annual heat requirements and the availability of solar resources. This is expressed in Table 4.1, where the heating degree days (HDD) and annual global horizontal irradiance (GHI) are compared. From Table 4.1 it can be noted that these Chilean cities are located in lower latitudes than cities with similar heating demands in Europe. This results in higher solar resource availability for a given heating requirement. This scenario suggests that solar thermal networks with seasonal thermal storage should be considered as an alternative for reducing GHG emissions and local pollution at affordable costs.

	Temuco	Paris	**Coyhaique**	Stockholm	Unit
Latitude	**-38.7**	48.8	**-45.6**	59.3	[°]
Annual HDD (base 15.5°C)	**1,748**	1,743	**2,901**	3,047	[HDD]
Annual GHI	**1,676**	1,405	**1,461**	1,154	[kWh/m^2·a]

Table 4.1: Comparison of conditions of the analysed locations and cities with similar heating requirements in Europe

The annual behaviour of the ambient temperature and the annual variation of the GHI for the cities under analysis are presented in Figure 4.1. It shows that the lowest temperature, hence, the highest heating demands are concurrent with the lowest solar energy availability. This means that to be able to supply a high fraction of the thermal demand from solar energy in winter the solar system would certainly be oversized for the rest of the year, which is economically sub-optimal. An alternative to this scenario is the option of storing part of the surplus energy available in summer in order to be used in winter by means of seasonal thermal energy storage.

Seasonal thermal energy storage has the capacity of storing solar energy captured in summer to supply winter heating demand, increasing the fraction of the annual heating demand supplied by solar energy, also known as solar fraction (SFr). As presented in Chapter 2, in order to achieve high storage capacities at an affordable cost, these systems store energy in inexpensive materials, such as water, soil or both. In borehole thermal energy storage (BTES) the soil is used as the storing media as well as insulating material: heat dissipates slowly due

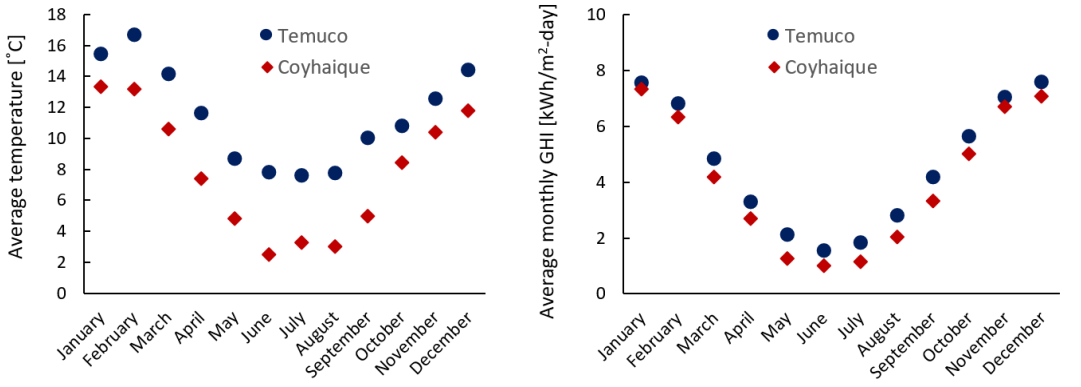

Figure 4.1: Average temperature each month (left). Average daily global horizontal irradiance (GHI) each month (right)

to the low soil thermal conductivity, and a radial horizontal thermal gradient is generated. In order to deliver and retrieve the heat from the soil, vertical holes between 20-100 m deep are drilled in the ground and water carrying U-shaped pipes are inserted in the holes. The hot water supply is connected at the centre of the storage and several holes are connected radially in series forming a string. Several strings are connected in parallel, covering the entire volume of the BTES. During the charging of the storage, hot water flows from the centre to the perimeter and the flow is reversed during the discharging to keep the horizontal stratification. For further information and schematics on BTES, please refer to Chapter 2, Section 2.6.4.

District heating networks and, particularly, the integration of seasonal thermal energy storage require sophisticated design and optimisation tools. This is because its state of charge creates a time coupling that requires to model longer periods of time, which is added on top of the complexity of modelling thermal transients in multiple equipment and subsystems. Many optimisation approaches to thermal networks have focused on exploring mathematical optimisation applied to the design of the network with a single objective function, such as Krug *et al.* (2020), who performed a non-linear optimisation approach, Blackburn *et al.* (2019), who presented a very fast to solve dynamic optimisation, or Romanchenko *et al.* (2021), who performed a mixed-integer unit commitment approach to assess the interactions of thermal energy storage and demand side response in a district heating network's operation. However, these approaches cannot be used in scenarios when more than one objective function needs to be considered, such as when assessing decarbonisation options at affordable costs, which are essential so that the district heating systems with seasonal thermal energy storage provide both environmental and economic benefits.

In previous research assessing the performance of solar systems with seasonal storage, Renaldi and Friedrich (2019) developed a simulation model based on the Drake Landing Solar Community project built in Canada (Natural Resources Canada, 2020). In their work, they analysed the performance of the system operating under British conditions and performed a

sensitivity analysis on some of the main variables. However, no optimisation of the system's configuration was performed. Rehman *et al.* (2018) compared the performance of different designs performing optimisation analysis on centralised and decentralised heating networks. However, the analysis was performed for cold Finish conditions, which differ from the sunny and cool conditions previously described for Chile. Lizana *et al.* (2017) performed a techno-economic analysis for solar heating networks operating in Mediterranean climates, which are similar in solar availability to the Chilean case, but in general, present lower heating demands. Shah *et al.* (2020) performed the optimisation of a similar system in various cold climate locations in the northern hemisphere. In their work, they carried out a multi-objective optimisation for two design variables of the system and compared their results with several single-objective optimisations. All these studies concluded that low emission solar district networks could be cost-competitive with conventional technologies under certain conditions.

However, no literature has been found on the assessment of the design and operation of these systems in the southern hemisphere, and particularly under the sunny but cool conditions of central and southern Chile. In addition, many of the available optimisation studies for seasonal thermal energy storage systems present only the optimisation results and do not go into detail about the corresponding system configurations. Furthermore, many studies consider only the sizing of the system but not the operational parameters. For example, no study has been found that investigated the optimal solar collector angle in relation to the design of a district heating system with long term storage. However, this information may be relevant in enabling further improvements and uptake of these systems.

In this Chapter, it is assessed the use of solar energy to provide domestic heating for social housing in Chile through a solar-driven heat network with seasonal thermal energy storage. For this, a detailed and fully parametrised TRNSYS simulation model was developed and linked through a custom Python interface to a multi-objective optimisation tool. This framework is used to perform a simulation-based multi-objective optimisation of the system's design with total costs and GHG emissions as objectives for the cities of Temuco and Coyhaique. Hourly heating loads were estimated for social housing blocks. The variability of internal gains, standard materials, geometry and typical families' occupancy rates were considered. The results of the optimisation present a range of system configurations that minimise the total cost and the GHG emissions. These objective functions are mutually competing; thus, each optimal system configuration presents a trade-off between emissions and cost. Consequently, the main parameters that define the system configuration and their interaction with these trade-offs were analysed, and effects of location, climate conditions and system size influence in the optimal solutions and in the competitiveness of the system with conventional heating options

were explored. An in-depth analysis of the optimal operational temperatures of the district network operating in Chile was included, and a novel analysis on the effects of optimising the collector tilt angle, considering the interaction of the local weather conditions, the shape of the thermal demand and the effects of the long term storage was performed.

4.2 Methods

In the context of the issues around domestic heating and the solar resource described in the previous section, this chapter develops a techno-economic analysis of the use of solar energy to provide domestic heating for two cities in southern Chile.

The general framework of the analysis is a multi-objective simulation-based optimisation with the system's cost and GHG emissions as optimisation objectives. This general framework consists of three main blocks and is presented in Figure 4.2:

1. Estimation of the heat load during a year for a specific building configuration and location.
2. Simulation of the performance of the system during one or more operational years.
3. Long term operation optimisation of the system configuration for a given heating load and location.

In broad terms, to lower the total system's emissions higher investments in solar collectors and storage are required, but the operational costs reduce due to the decline in the use of fuel. This means that if the saving from fuel use weighs in more than the cost of extra investment, the cost objective and emission investment align. In that case, the optimisation should result in a unique solution. However, as is usually the case with technologies in a relatively early stage of development, the investment costs can out-weight the savings. In this case, the objectives are opposing (as a "cleaner" system results in a higher total cost) and the optimisation results in a wide range of Pareto optimal solutions that provide a compromise between cost and emission levels (see Section 2.7.2 for further details).

4.2.1 Heating demand estimation

The heating load was calculated for social housing blocks in the cities of Temuco and Coyhaique. As shown in the first block of Figure 4.2, the calculation was performed on a multi-zone TRNBuild v3.0 model, which allows the simulation of the independent behaviour of rooms and areas of the flats. The geometry of a standard eight duplex flats block was drawn and imported from SketchUp, as shown in Figure 4.3. This geometry was based on a block of 8 duplex flats of 51 m^2 each, which emulates social housing designs at the current Chilean thermal

standard. Each flat was modelled with six thermal zones. The lower floor was defined with three zones: hall, kitchen and toilet; while the upper floor was approached as two zones: main bedroom and secondary bedrooms. The staircase was designed as a sixth zone, thermally connecting both floors.

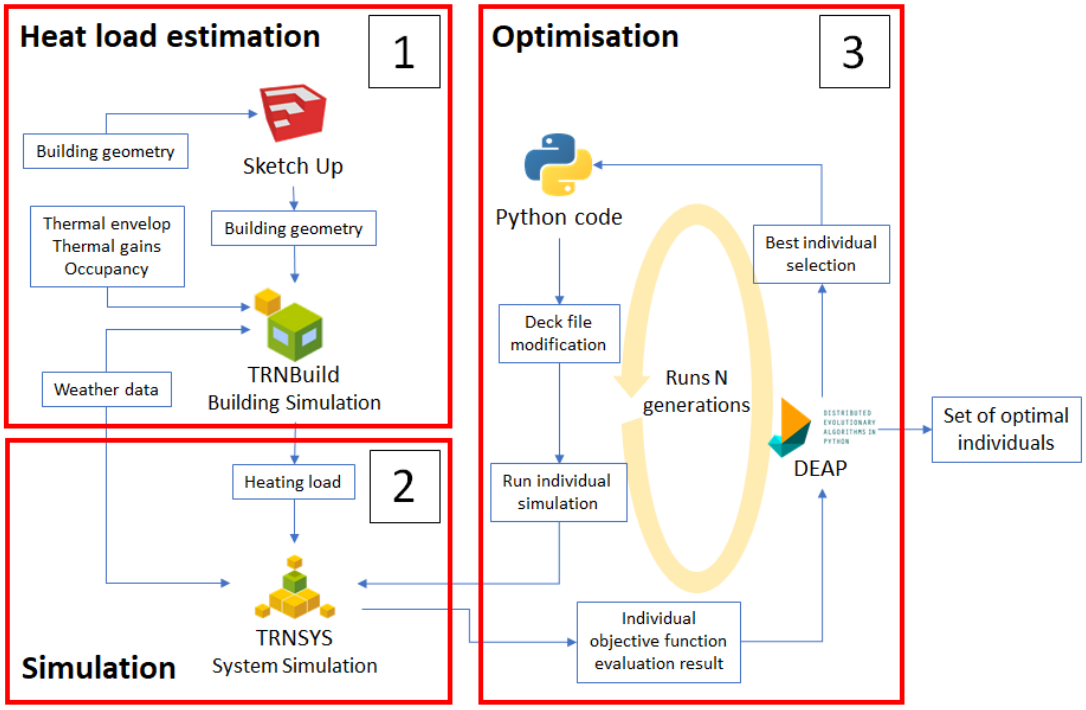

Figure 4.2: Main framework of the analysis showing the three main blocks: heat load estimation, simulation and optimisation

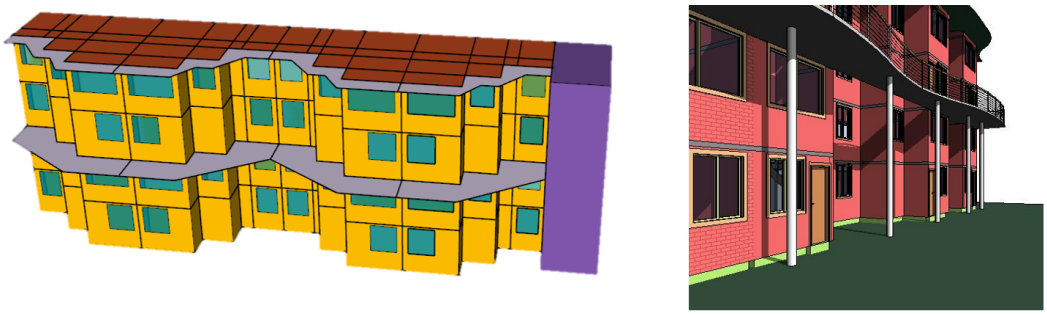

Figure 4.3: SketchUp model of the buildings (left) and original architectonic design (right)

The geometry of the building was imported into TRNbuild. The materials of the thermal envelope were selected according to the minimum requirements in the Chilean thermal standard from 2007 for each climate zone (Gobierno de Chile, 2006). The main parameters for each location are shown in Table 4.2 and the detail of the walls and roof materials considered in the simulation are presented in Appendix A. For the heat gains and heat requirements, an occupancy rate of a typical four people family showed in Figure 4.4 was assumed.

City	Thermal zone number	Maximum U [W/m^{2}K]			Max window wall coverage
		Roof	Wall	Floor	
Temuco	5	0.33	1.6	Not defined	18%
Coyhaique	7	0.25	0.6	Not defined	12%

Table 4.2: Thermal standards used in the model

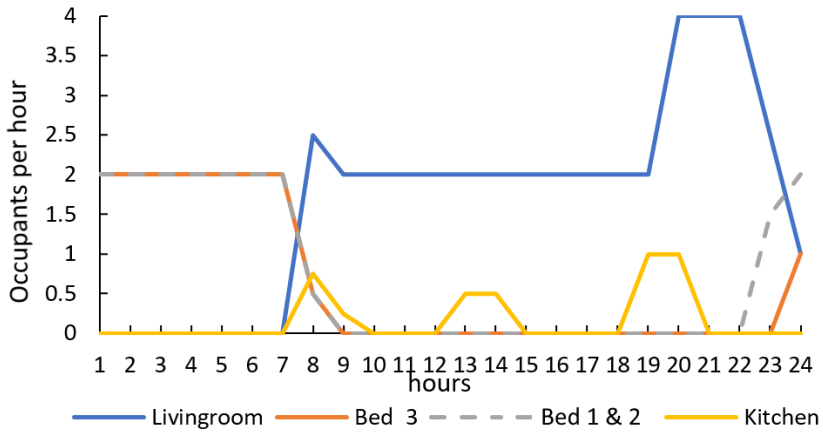

Figure 4.4: Occupancy rates of an average family

The control logic of the heating is on-off and it sets the temperature to 21°C when there are occupants in a zone and 16°C when there are no occupants. This applies to the living room and the bedrooms. The kitchen and toilet are kept at 16°C. There is no heating considered for the staircase. Additionally, heat gains were considered due to the presence of active occupants in the kitchen (170 W), passive occupants in the living room (125 W) and resting occupants in the bedrooms (80 W), according to EN 13799. A heat gain of 600 W was used in the kitchen during the cooking times (assuming an 80% efficiency of a 3,000 W stove/oven) and a constant 8 W/m^2 heat gain was assumed for all the house due to the presence of different electrical equipment (value recommended by TRNSYS for a single family house based on SIA 2024).

Infiltrations were accounted as constant air changes per hour in each zone, depending on the number of windows and exterior doors. It was considered 0.75 air exchanges per hour (ACH/h) for each window and 1 ACH/h for each external door present in each zone. This led to a total average infiltration of 1.57 ACH/h for every flat, which coincides with values found by Navarrete (2016) (1.27-1.52 ACH/h) and with those found by Diaz (2015) (1.7 ACH/h). Besides the uncontrolled air infiltration, it was considered that windows are opened for 5 ACH/h in any zone that exceeded 25 °C if the external temperature was below this value.

The thermal demand of the building was calculated on an hourly basis using TRNSYS v18 according to Figure 4.5, with the building's characteristics modelled by Type 56. As the Chilean thermal regulation used in the simulation does not include any standard for floor insulation, the losses through the floor could be important and had to be modelled accurately. The under-slab ground was modelled using Type 49, which assigns a heat capacity and conductivity to the soil. This reduces the heat loss through the ground floor in winter, as the sub-slab soil absorbs heat and increases its temperature with respect to the surrounding soil exposed to environmental conditions. As may be expected, it can take several years to reach a steady state as at the beginning, the under-slab soil is at the same conditions as the surrounding soil (Kusuda *et al.*, 1982). Therefore, the model was run for four years until the heat transfer and the temperature under the slab reached a steady periodic annual cycle. The weather data used was a typical meteorological year obtained from the solar explorer of the Chilean Ministry of Energy ((CR)2, 2016) which was compiled using data from 2004 to 2016 and was supplied to TRNSYS using a Type 15 weather data reader.

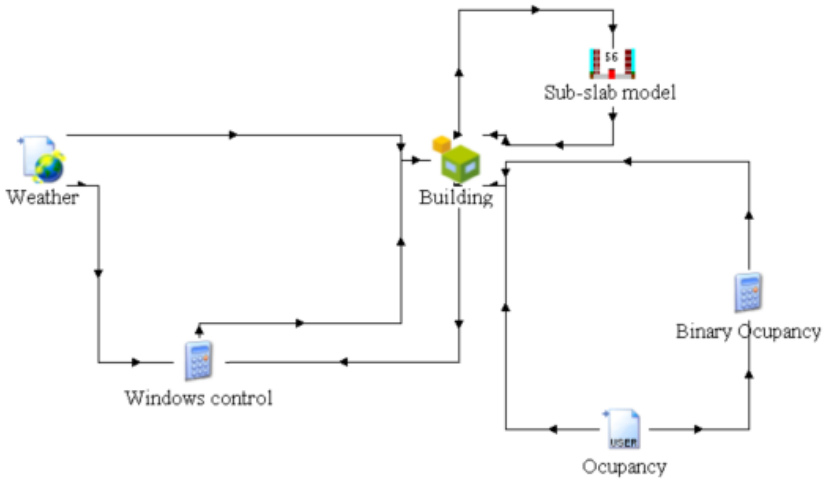

Figure 4.5: Diagram of simulation for calculating building's thermal demand in TRNSYS

The system's performance was modelled for a system supplying heat to a development of 18 buildings such as those in Figure 4.3, totalling 144 flats. This configuration is referred as the Base case and it represents the scale of typical social housing projects in Chile. In order to analyse the effect of heat demand density and scaling up of the system design, an alternative configuration with 1728 flats was also analysed. This configuration consists of a buildings' footprint eight times larger than the Base case and it considers an extra duplex flat on top of those of the Base case. Hence, this second configuration, referred as the Large case, presents a 50% higher demand density and 12 times higher total demand. This information is summarised in Table 4.3.

	Base	Large
Total number of buildings	18	144
Flats per building	8	12
Total number of flats	144	1728
Floors per building	4	6

Table 4.3: Difference in the two cases included in the analysis

4.2.2 TRNSYS Simulation model

The system's operation was modelled using TRNSYS v18 (block 2 in Figure 4.2), extending an existing model developed by Renaldi and Friedrich (2019) that replicates the system implemented in the Drake Landing Solar Community (DLSC) in Canada (Natural Resources Canada, 2020). The main feature of this system is that it includes an underground long term storage system with borehole technology (BTES). This system allows for excess solar energy harvested during the summer to be stored for use in winter and can reach annual efficiencies of up to 60% (Reuss, 2014). The main parts and components of the system are schematically presented in Figure 4.6, while Figure 4.7 presents a to scale 3D view of a system configuration with 3,000 m^2 of flat plate solar collectors and 30,000 m^3 of LTS, along with a district of 144 flats, as the one used in the Base case.

Solar field (SF) loop

The solar loop harvests solar energy in the form of heat. Its main component is the solar field, composed of parallel connected flat plate solar collectors modelled with Type 1b with the efficiency given by equation 4.1, where $T_{SF_{in}}$ corresponds to the inlet temperature to the solar field, T_{ext} is the ambient temperature and G is the global irradiance on the collector's surface.

$$\eta = 0.857 - 3.083\frac{T_{SF_{in}} - T_{ext}}{G} - 0.013\frac{(T_{SFin} - T_{ext})^2}{G} \tag{4.1}$$

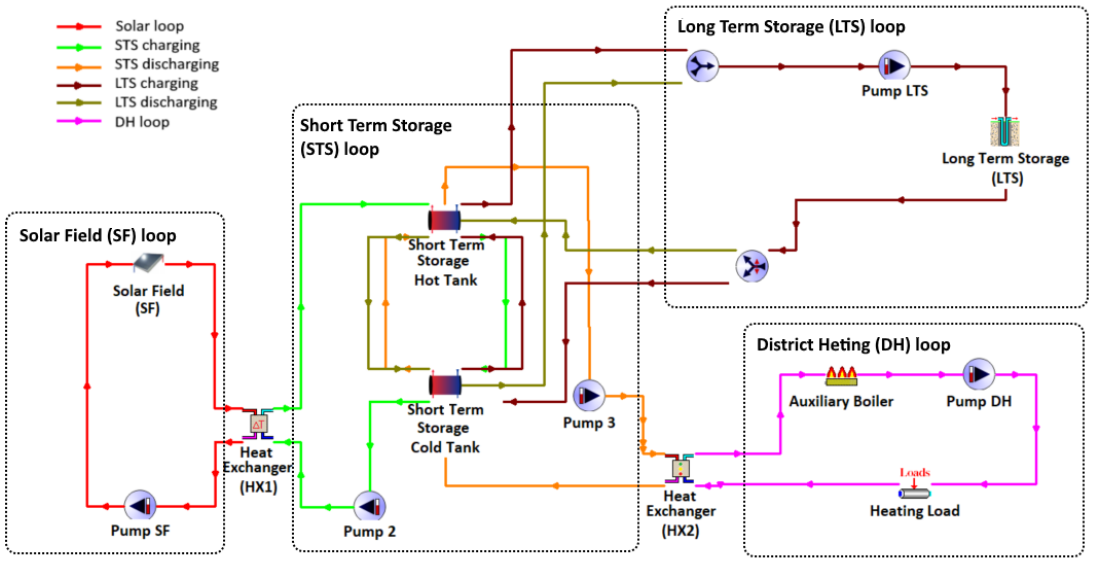

Figure 4.6: Main components of the TRNSYS simulation model

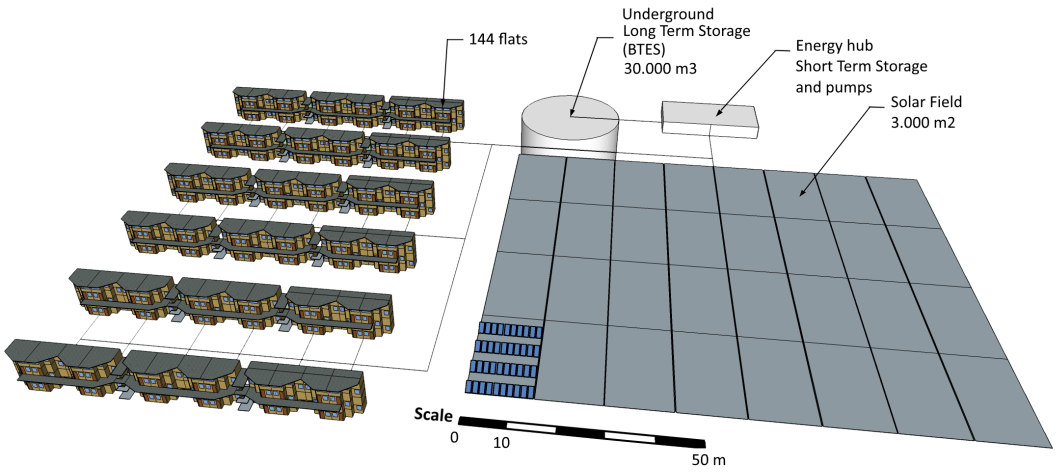

Figure 4.7: Scaled 3D model of a Base scenario system comprised of 144 flats, 3,000 m^2 collectors and 30,000 m^3 LTS

The solar field's working fluid is a glycol-water 30% mixture and is moved by a variable speed pump capable of pumping a maximum of 80 kg/h of fluid per square meter of the solar field, which allows the actual maximum flow rate to change with the solar field's area. A heat exchanger with 80% effectiveness connects the solar loop with the short term storage.

Short term storage (STS)

The short term storage (STS) loop receives the heat from the solar loop and stores it in two stratified hot water tanks modelled with Type 534. One of these tanks stores the hot water coming from the solar loop or the long term storage during discharging at 70-90°C, while the cold water tank stores water coming from the district heating network or the long term storage during charging at 40-60°C. The STS acts as a hub that receives the solar energy collected in the SF and decides whether to store the energy for a short term, deliver it to the district heating loop to fulfil the demand or store or retrieve energy from the borehole long term storage. These decisions are made following the logic explained in Section 4.2.2.

Long term storage (LTS)

The long term storage (LTS) subsystem consists of a borehole thermal energy storage system (BTES) modelled by Type 557, which is based on the model developed by Hellström (1991). The choice of this technology for the LTS follows that it is comparatively one of the cheapest seasonal storage technologies, as shown in Figure 2.9. Furthermore, based on the existing systems presented in the same figure, it is well suited for the expected LTS required volumes (10,000 to 50,000 m^3) of a network such as the one presented in Figure 4.7.

The pump of the LTS subsystem moves water from the centre to the perimeter of the storage during charging and from the perimeter to the centre during discharging at a constant 0.13 kg/s per each parallel string of boreholes (same value used in the DLSC system and by Renaldi and Friedrich (2019)). The geometry of the borehole storage is variable, depending on the total volume of the storage. However, certain rules were set following the model of Renaldi and Friedrich (2019):

- The depth of the boreholes is equal to its diameter to minimise the exposed surface.
- The separation for boreholes in the same string is constant and equal to 2.25 m.
- The total number of boreholes grows proportional to the footprint of the LTS, starting from 144 boreholes for a surface area of 961 m^2 (corresponding to the original DLSC model developed by Renaldi and Friedrich (2019)).

The soil thermal parameters used in the simulation are presented in Table 4.4 and were defined based on the description of the locations' geological conditions by Mella and Quiroz (2010) for Temuco, de la Cruz *et al.* (2003) for Coyhaique, and typical soil characteristics from Reuss (2014).

Location	Description	Thermal conductivity [W/K·m] (Reuss, 2014)	Heat capacity [kJ/m^3] (Reuss, 2014)
Temuco	Unconsolidated glacial gravel and sands deposits (Mella and Quiroz, 2010)	0.9	1,600
Coyhaique	Gravel and sand banks with silts subordinate (de la Cruz *et al.*, 2003)	1	

Table 4.4: Soil characteristics in both locations

LTS initial charge state

The temperature inside a BTES fluctuates with the charging and discharging cycles through the year but, during normal operation, it tends to keep a steady annual average temperature. However, at the beginning of the operation, the BTES's internal temperature is equal to the surrounding ground, and it could require 3 to 6 years of heating to reach a long term average temperature (Sibbitt *et al.*, 2012; Schmidt *et al.*, 2004; Schmidt and Sørensen, 2018), with Welsch *et al.* (2016) even reporting systematic changes in efficiency after 25 years of operation, albeit in a system with comparatively larger 5 m borehole separation, which significantly slows down the dynamics inside the BTES. Figure 4.8 shows the evolution of the temperature of the storage for seven years for two different configurations of LTS size. The plotted temperatures are outputs of Type 557 (module for BTES in TRNSYS) and correspond to the average temperature of all the soil within the boundaries of the BTES, and to the temperature of soil located next to a borehole located at the centre of the BTES.

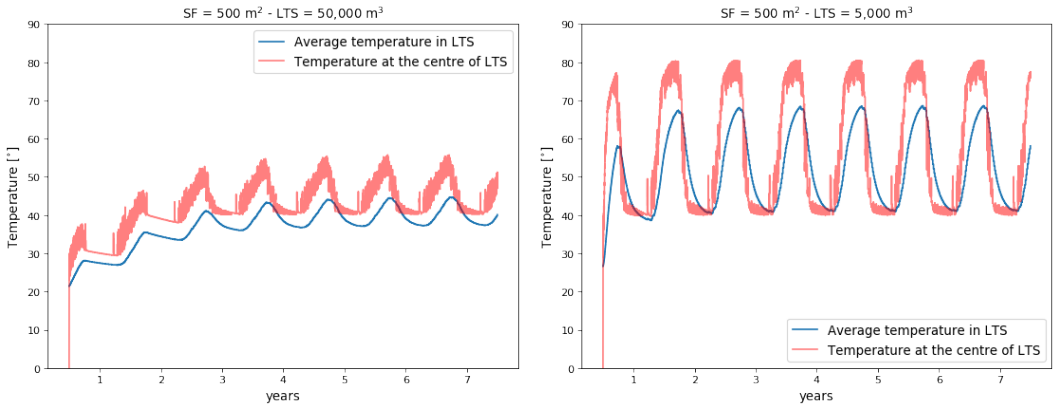

Figure 4.8: Evolution of the temperature of the LTS for the first 7 years of operation for two different system configurations

As it can be noticed, both systems have different times for reaching a stable regime, but in both cases, it is safe to state that it is reached by year 6. Therefore, if the condition of the BTES at the beginning of year 7 could be replicated at the start of the simulation, the optimisation could be run by only simulating 1 year of operation, which would produce an important reduction in running time, considering that one year of simulation takes between 30 to 45 s to run on an Intel Xeon E3-1230 v6 processor.

However, it is clear that the temperatures of stable operation differ depending on the configuration. Therefore, it is not trivial to define the state of the LTS at year 6 for any given configuration. The approach taken to solve this issue was to perform a multiple regression on the variables that present a higher impact on the operational temperature of the LTS. This regression provides a parametrisation of an approximation to the average LTS temperature for the last time step of year 6. This parametrisation was coded in the TRNSYS model, which allowed starting the simulation from a state of charge of the LTS similar to that of year 7. As this methodology provides only an approximation of the average temperature of the LTS, but no internal gradients or heat stratification can be defined in Type 557, the simulations used for the optimisation process were run for two years, with the first year used as a buffer to allow the LTS to reach the real long term operational state. The details of the method for performing the parametrisation and its validation are found in Appendix B.

District heating (DH) loop

The district heating (DH) system delivers hot water to the flats, which are represented in the model by a single node load. The load module (Type 682) fulfils the heating demand profile (calculated previously using Type 56) in each timestep by performing an energy balance on the hot water mass flow circulating in the DH and returning the water at a lower temperature. The water is moved by a variable flow pump and heated to a setpoint by means of a heat exchanger using hot water from the STS. A backup boiler (Type 659) provides the heat that is required to reach the setpoint if there is not enough energy available in the STS. The setpoint for the DH water supply is defined according to equation 4.2, the same used in the original Drake Landing project (Quintana and Kummert, 2015).

$$T_{DH_{sup}} = \begin{cases} 55°C & T_{ext} \leq -40°C \\ 0.48 \cdot T_{ext} + 35.8 & -40° < T_{ext} < -2.5°C \\ 37°C & T_{ext} > -2.5°C \end{cases} \tag{4.2}$$

A minimum heating temperature of 26°C is defined in the load module. This means that if the outlet temperature from the load module falls below 26°C, it is assumed that the load cannot be met by the DH.

Piping and pumps

The pipes were modelled as Type 31 TRNSYS elements. Although, the general piping layout followed the fixed design presented in Figure 4.7 The length of the pipes in the model is adjusted to follow the size of the SF and the number and configuration of the buildings in the district network. The pipe's diameter (D_{pipe}) is also adjusted to keep a maximum flow velocity (v_{max}) of 1 m/s. These values are parameterised in TRNSYS, allowing for automatic adjustment of the dimensions for every configuration being evaluated.

The thermal loss coefficient of the pipes (I_{pipe}) was parameterised as a function of D_{pipe} using an approximation to the high-quality pipes (preinsulated pipes class 2 according to EN 13941) presented by Masatin *et al.* (2016) according to equation 4.3.

$$I_{pipe} = 0.1088 \cdot D_{pipe}^{-0.619} \quad W/m^2K \tag{4.3}$$

The rated power of each pump is calculated using v_{max} and the maximum head loss of each pipe is estimated applying Darcy-Weisbach equation and Haaland's approximation for the Colebrook-White equation. For reference, Zeghadnia *et al.* (2019) presents the definitions of these equations and alternative approximations to calculate head losses in a piping system. Approximated singular head losses, equipment head losses and the head due to buildings height were also included. This approach allows the model to adjust the power rating of the pumps for every configuration being evaluated. The instantaneous power demand of the pumps at each step of the simulation was assumed to change linearly with the flow rate.

Control strategy

The control strategies of the system are mainly the logic behind the operation of the pumps moving the working fluid and the decision whether to charge or discharge the LTS. These are based on the work by Yang *et al.* (2017) with slight modifications.

For the SF loop pump, a differential controller with hysteresis (Type 2b) is used. This controller turns the pump ON if the temperature difference between the fluid coming from the SF and the bottom of the cold STS (the coldest water in the STS) is higher than 10°C. It remains ON until that difference is less than 2°C or if the top of the hot STS (the hottest water in the STS) reaches 90°C. Additionally, during the ON status of the pump, it modulates its flow rate to keep a 10°C difference between the output and the input of the SF using a Type 22 differential controller. The pump connecting the SF loop with the STS modulates its flow to keep a 12°C temperature rise in the heat exchanger (HX1), while the pump connecting the STS with the DH loop modulates its flow to keep the DH water coming out the heat exchanger (HX2) at 37°C (according to equation 4.2). The DH pump is modulated to keep the return temperature in the system according to $T_{DH_{ret}}$ in equation 4.4, which is the approach used by Renaldi and Friedrich (2019).

$$T_{DH_{ret}} = 0.9588 \cdot T_{DH_{sup}} - 4.79°C \tag{4.4}$$

As the approach of fixing the supply temperature of the district heating at the same value that a system designed for different demand and weather conditions may be sub-optimal, it was also explored how the optimal configuration may change by using different supply and return temperatures ($T_{DH_{sup}}$ and $T_{DH_{ret}}$, respectively). For this analysis, these temperatures were defined as optimisation variables (see Section 4.2.5).

The charging of the LTS depends on the season of the year, thus, the controller was adapted from the model of Renaldi and Friedrich (2019) to match the seasons in the southern hemisphere. A diagram of the operation control logic under the different states of the LTS is presented in Figure 4.9. In summer the LTS starts being charged when the temperature difference between the top of the STS storage (hottest water in the STS) and the centre of the LTS (hottest zone of the borehole field) is above 10°C and it stops if that temperature difference falls below 3°C or if the average temperature in the LTS surpasses 90°C. In winter the charging is done only when the difference between the bottom of the STS storage (coldest water in the STS) and the DH water supply setpoint is above 10°C and the top of the STS storage is hotter than the centre of the LTS. The charging stops whenever the temperature difference between the bottom of the STS storage and the DH water supply setpoint falls below 2°C. The discharging process happens when the temperature difference between the centre of the LTS and the bottom of the STS is higher than 10°C and the top of the STS is below 55°C, and it stops when the aforementioned temperature difference falls below 3°C or the top of the STS surpasses 55°C. A hysteresis effect was added to the controller to consider its previous step's state when deciding the next one. This avoids the charging process turning OFF when the temperature stays in between the "dead band". Table 4.5 summarises the logical equations behind the control strategy.

4.2.3 Evaluation of system's operation

The simulation set up in TRNSYS allows for multiple calculations of operation variables in every step and of performance indicators calculated during a year of operation or over the lifetime of the project. To evaluate and compare the performance of different system configurations, a set of indicators are calculated.

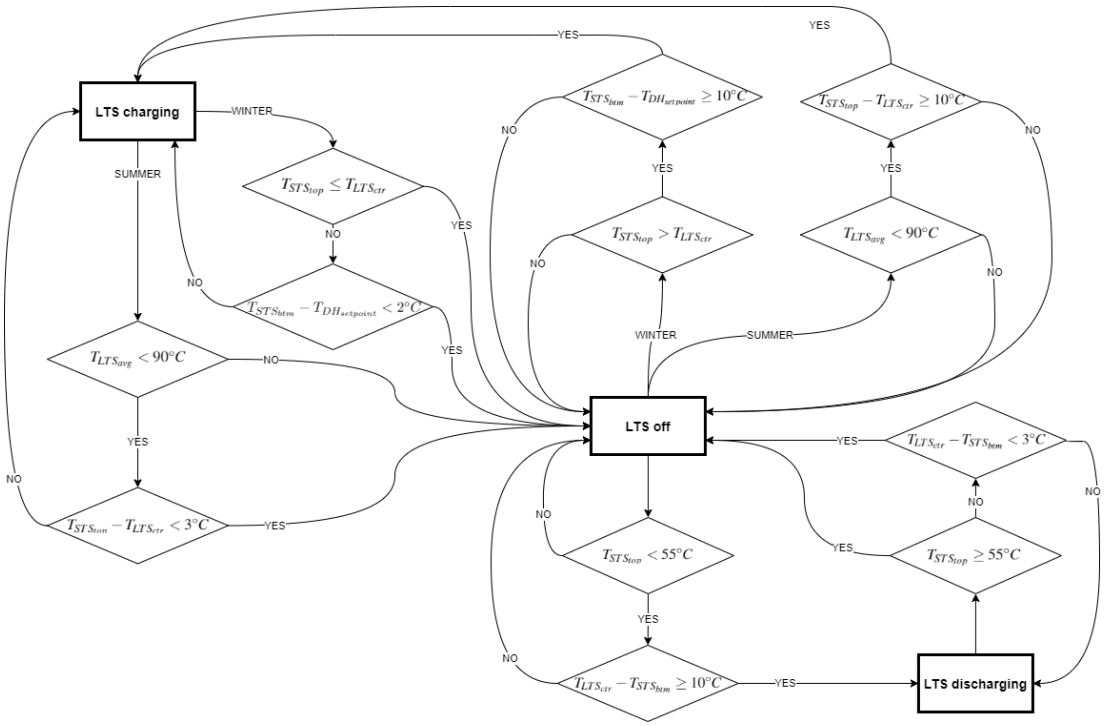

Figure 4.9: Logical operation diagram of the control of the LTS according to Yang *et al.* (2017)

System element	ON status conditions	OFF status conditions
SF loop pump	$T_{SF_{out}} - T_{STS_{btm}} \geq 10°C$	$T_{SF_{Pout}} - T_{STS_{btm}} < 2°C$ $\vee$ $T_{STS_{top}} \geq 90°C$
Pump connecting SF loop and STS	Flow modulated to keep $\Delta T_{HX1_{STS}} = 12°C$	
Pump connecting STS and DH	Flow modulated to keep $\Delta T_{HX2_{DH}} = T_{DH_{sup}}$	
DH pump	Flow modulated to keep condition in equation 4.4	
LTS charge summer	$T_{STS_{top}} - T_{LTS_{ctr}} \geq 10°C$ $\wedge$ $T_{LTS_{avg}} \leq 90°C$	$T_{STS_{top}} - T_{LTS_{ctr}} < 3°C$ $\vee$ $T_{LTS_{avg}} > 90°C$
LTS charge winter	$T_{STS_{btm}} - T_{DH_{sup}} \geq 10°C$ $\wedge$ $T_{STS_{top}} > T_{LTS_{ctr}}$	$T_{STS_{btm}} - T_{DH_{sup}} < 2°C$ $\vee$ $T_{STS_{top}} \leq T_{LTS_{ctr}}$
LTS discharge	$T_{LTS_{ctr}} - T_{STS_{btm}} \geq 10°C$ $\wedge$ $T_{STS_{top}} < 55°C$	$T_{LTS_{ctr}} - T_{STS_{btm}} < 3°C$ $\vee$ $T_{STS_{top}} \geq 55°C$

Table 4.5: Summary of the controller logic

Technical performance indicators

The technical performance indicators of the operation of the system evaluate how well the system manages the different energy fluxes during one year of operation, focusing mostly on the solar energy and the operation of the LTS.

The solar fraction (SFr) is the fraction of the total load that is fulfilled with solar energy, which corresponds to the energy transferred through the heat exchanger connecting the STS and the DH (HX2 in figure 4.6), divided by the total energy used to fulfil the load, which corresponds to the solar energy delivered to the DH plus the energy supplied by the boiler, according to equation 4.5.

$$SFr = \frac{\int \dot{Q}_{HX2}}{\int \dot{Q}_{HX2} + \int \dot{Q}_{boiler}} \tag{4.5}$$

The solar system efficiency (η_{Ssys}) is the performance of the system using the solar energy collected. It is calculated as the ratio between the energy delivered to the DH and the energy collected in the SF, according to equation 4.6.

$$\eta_{Ssys} = \frac{\int \dot{Q}_{HX2}}{\int \dot{Q}_{SF}} \tag{4.6}$$

LTS efficiency (η_{LTS}) is the efficiency of the LTS in storing the energy. It is calculated as the ratio between the energy discharged from the LTS and the energy charged into the LTS, according to equation 4.7.

$$\eta_{LTS} = \frac{\int \dot{Q}_{LTS_{disch}}}{\int \dot{Q}_{LTS_{charge}}} \tag{4.7}$$

Economic indicators

The economic indicator used to evaluate and compare the performance of the system is the levelised cost of energy (LCOE), which takes into consideration the initial investment and the variable and fixed costs of operating the system to calculate an annualised cost of energy production during the lifetime of the project according to equation 4.8.

$$\text{LCOE} = \frac{C_{inv} + \sum_i^n \frac{C_{O\&M} + C_{fuel} + C_{elec}}{(1+r)^i}}{\sum_i^n \frac{Q_{load}}{(1+r)^i}} \tag{4.8}$$

A discount rate r = 0.05 and a lifetime n=25 years are assumed. This discount rate is slightly lower than the 0.06 recommended in Chile for public building projects (Ministerio de Desarrollo Social, 2013) and close to the 5.05% proposed for the long term evaluation of public projects by Edwards (2016).

The different annual costs are calculated in TRNSYS using the values in Table 4.6, while the investment costs are calculated using the unitary costs in Table 4.7. As all these economic parameters are based on various sources and estimations. Appendix C presents a sensitivity analysis of the most relevant economic parameters on the LCOE.

	Cost	Unit	Ref.
O & M [*] ($C_{O\&M}$)	$0.0075 \cdot C_{inv}$	€/a	(Mauthner and Herkel, 2016)
Natural Gas Temuco (C_{fuel})	0.05	€/kWh	(Intergas, 2019)
Diesel Coyhaique (C_{fuel})	0.06	€/kWh	(Comision Nacional de Energia, 2020)
Electricity (C_{elec})	0.1	€/kWh	(CGE, 2020; Saesa, 2020)
Carbon tax	0 [**]	€/kgCO_2	

[*] O & M corresponds to operation and maintenance costs
[**] The 5 US$/t$CO_2$ only applies to boilers above 50 MW

Table 4.6: Unitary costs of energy and the annual cost of operation and maintenance

	Cost	Unit	Ref.
Solar field (C_{SF}) (including pipes)	$3.8 \cdot 10^{-8} \cdot SF_A^2 - 3.9 \cdot 10^{-3} \cdot SF_A + 271$	€/m^2	(Sorensen, 2012)
Short term storage (C_{STS})	$403 \cdot STS_{vol}^{-0.467} + 250$	€/m^3	(Mauthner and Herkel, 2016)
Long term storage (C_{LTS})	$2,600 \cdot LTS_{vol}^{-0.47}$	€/m^3	(Planenergi, 2019)
Buried pipes[*] (C_{pipes})	$4334 \cdot D_{pipe}^2 + 4011.7 \cdot D_{pipe} + 198.7$	€/m	(Nussbaumer and Thalmann, 2016)
Boiler (C_{boiler})	$24.8 \cdot \bar{Q}_{boiler} + 31,850$	€	(Voll, 2013)
Indoor system (C_{HDS})	$12560 \cdot LMTD^{-1} + 522$	€/flat	[**]
Pumps (C_{pumps}) single speed	120	€/kW	[***]
Pumps (C_{pumps}) variable speed	240	€/kW	[***]

[*] Insulated pipes, considers feed and return pipe in the same trench
[**] Considering a linear relation with a standard 75°C supply temperature system at 700 €/flat and a 37°C supply temperature system (DLSC standard) at 1500 €/flat. Internal temperature (T_{int}) assumed 21°C for $LMTD$ calculation. $LMTD = \frac{T_{DH_{sup}} - T_{DH_{ret}}}{\ln \frac{T_{DH_{sup}} - T_{DH_{int}}}{T_{DH_{ret}} - T_{DH_{int}}}}$
[***] Standard values used in Chilean engineering projects according to senior procurement engineer

Table 4.7: Unitary investment costs of equipment

The cost of land was explicitly excluded from the analysis. As the project is supplying energy for a social housing complex, the land where the system is installed is state-owned, therefore it can be assumed that it may be granted at zero cost (which is the assumption in this case). On a deeper economic analysis, it can be argued that, even though the land belongs to

the Government, there is an opportunity cost for its utilisation (for instance, more housing). However, no data on the opportunity cost of land in Chile were found in the literature. For privately developed projects, the cost of land has to be included in the analysis, as it would have to be purchased by the developer.

Emission indicators

As an emission indicator, the specific emission per unit of energy output (SE) is defined according to equation 4.9. This equation considers the emission coming from the fuel burned by the auxiliary boiler as well as the indirect emission from the electricity consumed by the pumps and divides these emissions by the total energy supplied by the system.

$$SE = \frac{EF_{grid} \cdot \int \dot{Q}_{pumps} + EF_{fuel} \cdot \int \dot{Q}_{fuel}}{\int \dot{Q}_{load}} \tag{4.9}$$

The emission factors of the fuels and the electric grid are presented in Table 4.8. The electric grid emission factor for Temuco for 2025 was used, according to scenario "C" and a dry hydrology in the Chilean "long term energy plan" (Ministerio de Energia, 2020g). In the case of Coyhaique, there is no up to date information nor projections of the emission factor of the isolated Aysen system (where Coyhaique is connected). Therefore, the same value as for Temuco was used.

	Emission Factor	Unit	Ref.
Natural Gas	0.204		(Defra, 2020)
Electric grid Temuco	0.25	[kgCO_2/kWh]	(Ministerio de Energia, 2020g)
Electric grid Coyhaique	0.25		*

* In 2016, the emission factor of this system was 0.33 kgCO_2/kWh (Estay and Ovalle, 2017) with a reduction trend expected.

Table 4.8: Emission factors of the fuel and electric systems considered in the model

4.2.4 Simulation parameters

As the optimisation process requires thousands of runs of the simulation model, a balance between simulation run speed and accuracy needed to be reached. Considering this, a 10 minutes time step was chosen, as it allows to run a two year simulation in 1 to 2 minutes and is short enough so Type 31 plug flow pipes model does not have convergence errors, which occur when the residence time inside a pipe element is smaller than the timestep. The simulation of a complete year of operation is important in the context of an LTS economic

operation analysis, as it allows to completely integrate the time domain through a continuous operation. This contrasts with other approaches, that use aggregated time periods to represent typical weeks or days of the year, which allows a faster simulation, but fails to address the time coupling of the LTS state of charge.

As it was explained in Section 4.2.2, due to the slow heating of the soil from its normal temperature, there is a period to get the LTS to a steady state operation. In order to reduce the simulation time, a preliminary analysis was performed and a parametrisation of the average temperature of the LTS as a function of the main variables allowed to define a function that approximates the average temperature conditions in the LTS ($T_{LTS_{avg}}$) at the beginning of a year in a steady state operation. The method applied for this parametrisation is based on a multiple linear regression and is further explained in Appendix B. This method allowed to set the total running time to 17,520 hours (two years).

4.2.5 Optimisation model

The last step of the method used in this chapter, shown in block 3 in Figure 4.2, is a routine that performs the optimisation by running several systems configurations and chooses those that minimise the cost and the emissions. After every generation, a new Pareto front that approximates closer to the true optimal solution is generated. An optimisation routine was implemented in Python using a genetic algorithm provided by DEAP (Fortin *et al.*, 2012) and it was linked to the TRNSYS simulation model, reading TRNSYS's outputs and modifying TRNSYS deck file (inputs). For more information on the operation of a genetic algorithm, refer to Section 2.3 and Figure 2.5.

Objective function

The objective of this optimisation is to determine system configurations that are both cheap and that produce low emissions. Hence, LCOE and SE (equations 4.8 and 4.9) were defined as the objective functions to be minimised, as it is expressed in equation 4.10.

$$Min \begin{cases} \text{LCOE}(x_i) \\ \qquad\qquad i \in \{1,...,n\} \\ SE(x_i) \end{cases} \tag{4.10}$$

$$0 < x_i^{min} < x_i < x_i^{max},$$

with x_i^{min} and x_i^{max} adjusted according to the system being assessed

x^{min} and x^{max} are the lower and upper bounds of the optimisation variables, and have to be adjusted according to the case that is being optimised. These adjustments do not affect the final result, but allow for a quicker convergence of the Pareto front. As LCOE and SE are mutually opposing, a set of optimal configurations that trade between cost and emissions is expected. The next subsection identifies the variables (x_i) used in the optimisation problem.

Optimisation Variables

In a preliminary analysis, the equipment that is more influential in the performance of the system was assessed, and it was found that the most important variables in the system configurations were the area of the solar collectors field (SF_A), volume of long term storage (LTS_{vol}) and volume of short term storage (STS_{vol}). Therefore, these were included as the main optimisation variables in the model. Changing the size of these values has an impact on the investment cost and produces an effect on the performance of the system, as well as on its running cost. A combination of values for these (or any other) optimisation variables defines a system configuration. The run of the simulation with this configuration returns the evaluation of the objective functions, which later could be assessed for the optimality of that configuration. As a fourth variable, the tilt angle of the solar collectors (θ) was included in the optimisation. Although this variable has a comparatively lower influence in the cost and emission assessment, its analysis is interesting as it is a way to produce a slight improvement in the system's performance without any additional cost and, as it will be discussed in Section 4.3.3, the choice of optimal θ is not straightforward. Additionally, as mentioned in Section 4.2.2, the effect of considering different $T_{DH_{sup}}$ and $T_{DH_{ret}}$ in the district heating network was analysed.

As a reference, Table 4.9 presents the bound of the variables used in both scenarios. Ideally, the bounds of the variables should cover most of solution space. However, including values that produce configurations that evidently fall far from optimal objective values increases the optimisation time. Therefore, these bound were later adjusted for each location and case to minimise the convergence time of the optimisation.

	SF_A [m^2]		LTS_{vol} [m^3]		STS_{vol} [m^3]		$T_{DH_{sup}}$ [°C]	$T_{DH_{ret}}$ [°C]	θ [°]
	Base	Large	Base	Large	Base	Large	Both	Both	Both
min	300	500	3,000	3,000	50	100	28	40.01	20
max	6,000	80,000	80,000	650,000	4,000	40,000	40	55	80

Table 4.9: Reference variable bounds used for the optimisation

Optimisation routine

The optimisation is performed by DEAP using the eaSimple algorithm for evolving the population and NSGA II for sorting the best individuals. The mating was performed by two points crossover and the mutation by polynomial bounded mutation (Deap Project, 2020). The main parameters of the optimisation process are presented in Table 4.10.

Parameter	Value	Definition
Number of generations (N)	120	Number of maximum iterations of the algorithm
Population	80	Initial number of individuals and number of individuals that survive after each iteration
Crossover probability	0.7	Probability of an individual exchanging genes with other
Individual mutation probability	Eq. 4.11	Probability of an individual being subjected to a mutating process
Gene mutation probability in a mutating individual	0.3	Probability of an individual gene mutating in each mutating individual

Table 4.10: Main parameters of the genetic algorithm optimisation

As a high mutation probability tends to lead towards a random search of the optimum, while a low probability tends to miss large areas of the solution space and risks missing the global optimum (Hassanat *et al.*, 2019), the mutation probability (P_{mut}) was modified in each iteration i with a Gompertz function according to equation 4.11.

$$P_{mut_i} = P_{mut_0} - (P_{mut_0} - P_{mut_N}) \cdot e^{-b \cdot e^{-c \cdot i}} \tag{4.11}$$

The parameters used for this equation were: P_{mut_0}=0.7, P_{mut_N}=0.03, b=5, c=0.08 and N =10, which produces a curve that allows for some initial exploration of the solution space and a better converging towards the end of the optimisation.

4.3 Results and discussion

This section presents the main results of this chapter, starting with the calculation of the thermal loads in both locations and following with the analysis of the optimisation results for the different locations and configurations.

4.3.1 Heating demand analysis

The results from the thermal load simulation showed that the thermal consumption of the ground level flats is on average 2-4% higher than those in the upper level. This is mostly due to the absence of insulation between the floor and the slab. The results also showed a slightly higher demand during the first year of operation due to the initial ground temperature under the slab. However, this difference was below 1% and the yearly average under-slab temperature stabilised after two years of operation. Table 4.11 shows the annual thermal loads of the flats depending on their location in the block for the two cities. "Exterior" flats correspond to those at the edges of the block with three of their sides exposed to the environment, while "Interior" flats correspond to flats between two neighbours and only two of their sides exposed to the environment.

	GF Ext.	UF Ext.	GF Int.	UF Int.	Average flat	Unit
Temuco	126.2	121.1	112.1	106.4	116.4	[kWh/m^2·a]
Coyhaique	225.2	221.6	202.4	197.1	211.6	

Table 4.11: Results of individual flats' annual thermal load calculations in both locations. (GF: Ground Floor, UF: Upper Floor, Ext.: Exterior, Int.: Interior)

These values agree with those defined as base values for the Chilean thermal rating system that sets a base case for flats at 108 and 220 kWh/m^2·a for Temuco and Coyhaique respectively (Ministerio de Vivienda y Urbanismo, 2018). They also match closely values reported by Bustamante *et al.* (2009) that uses 125 kWh/m^2·a for one floor continuous façade social housing in Temuco and 252 kWh/m^2·a for the same configuration in Punta Arenas, a city with 13% higher annual degree days heating requirements compared to Coyhaique. Figure 4.10 presents the monthly energy load comparison between an average flat in both locations.

Considering these demands and the layout of the system, the main demand parameters of the systems in both locations are presented in Table 4.12. In this table, the annual load factor is calculated as the ratio between the total annual demand and the energy equivalent to the system providing the peak demand non-stop during the entire year. The linear demand

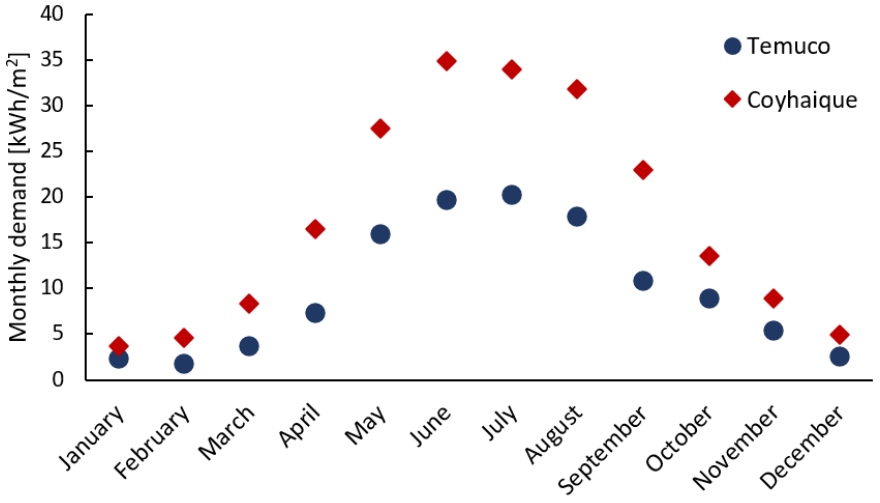

Figure 4.10: Monthly thermal demand for an average flat in both locations

densities are calculated as the ratio between the total annual demand and the length of the main supply pipes (not considering pipes inside the buildings), while the area energy density is calculated by dividing the total annual demand by the area of the smallest rectangle encompassing the group of buildings.

	Temuco		Coyhaique		Unit
	Base	Large	Base	Large	
Total annual demand	854	10,248	1,554	18,648	[MWh]
Peak demand	706	8,472	855	10,260	[kW]
Annual load factor	0.14		0.21		[-]
Linear demand density	1.2	1.9	2.5	3.5	[MWh/m·a]
Area energy density	76	114	139	208	[kWh/m^2·a]

Table 4.12: Main demand metrics of the different locations and systems

In general, the literature mentions a broad band around 1.5 MWh/m·a of linear energy density as a threshold for economic viability for new-constructed district heating networks (Sipilä *et al.*, 2011; Jalil-Vega and Hawkes, 2018) and some works use higher values such as 2.5 MWh/m·a (Dochev *et al.*, 2018) or even 4 MWh/m·a (Heat network partnership for Scotland, 2017). The Chilean guide for district heating project development recommends area densities above 70 kWh/m^2·a for potentially successful projects (Morales *et al.*, 2018). A system with lower linear or area energy density has relatively higher thermal losses and higher cost in piping which makes it economically less competitive. Considering this, it is expected that the Large system would have a better performance due to higher energy densities.

4.3.2 Pareto front analysis

The main outcomes of the optimisation process are the Pareto fronts. These curves present the set of non-dominated solutions that minimise the LCOE and the SE. The TRNSYS simulation presented convergence problems for LTS volumes around 3,000 m^3 and below in Type 557. This meant that two optimisations were run for the same location: one with LTS and volumes of 3,000 m^3 and above, and a second without LTS where the LTS loop, including Type 557, was removed to avoid these convergence problems. As a reference, a cylindrical 3,000 m^3 BTES has an approximate diameter of 15 m and a water equivalent storage volume of close to 2,000 m^3, which is below the smallest systems recorded on Figure 2.9.

The optimisation presented a good convergence of the Pareto front. Within the first 10 generations the Pareto front converged close to its final value and in further generations it populated and diversified the set of solutions, as it was intended by using equation 4.11 for the definition of the optimisation routine parameters. This can be graphically appreciated in Figure 4.11, which presents the evolution of a number of generations for the optimisation of the Base case in Coyhaique.

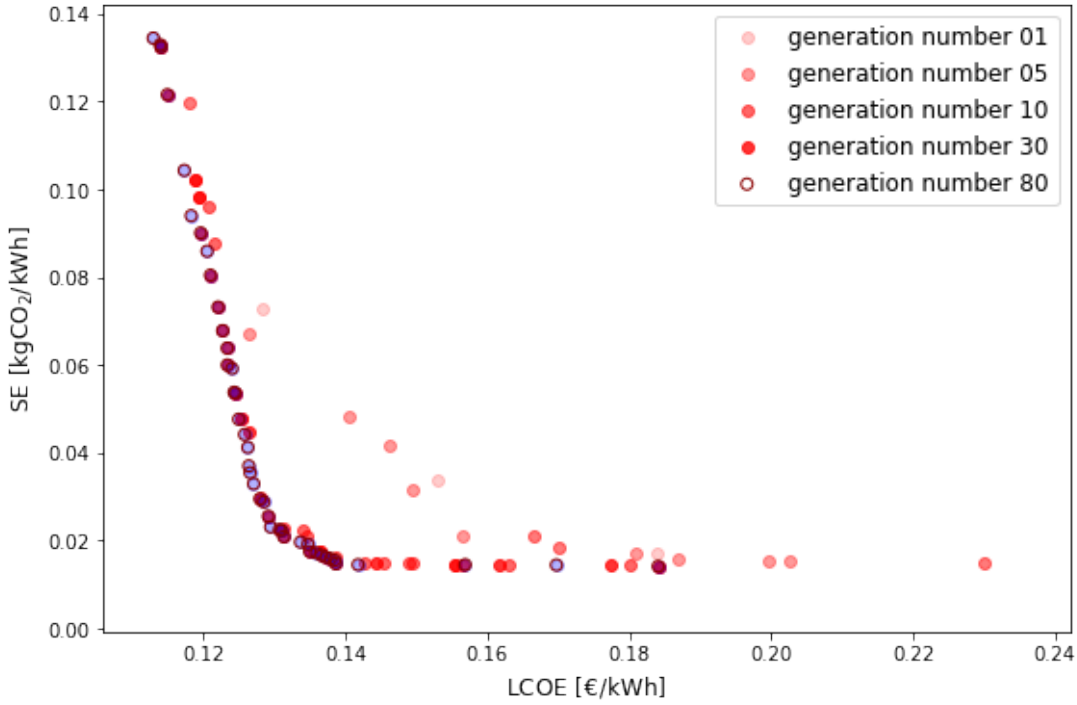

Figure 4.11: Pareto front evolution during an 80 generation run for the Base case in the city of Coyhaique with an initial population of 80 individuals and 4 optimisation variables

Technical variables results

Figure 4.12 presents the Pareto front resulting from these optimisations for the location in the cities of Temuco and Coyhaique for the Base case, while Figure 4.14 presents the results for the Large case. Both cases' configurations are described in Table 4.3 and their demand features in Table 4.12. The final system's Pareto front curve can be approximated by considering the non-dominated points of the addition of both curves. Other than the objective functions, Figures 4.12 and 4.14 provide information of the SFr in the colour scale and η_{LTS} in the size of the point markers.

Figure 4.13 presents the evolution of the optimisation variables and of the performance indicators for the system configurations in the Pareto front in Coyhaique and Temuco for the Base case with LTS, while Figure 4.15 presents the evolution of the optimisation variables and of the performance indicators for the Pareto optimal configurations of the Large case in both cities

Figure 4.16 presents an alternative visualisation of the results, presenting the objective function and design variables values for eight configurations from the Pareto fronts for both cases and cities. In this figure, each configuration is represented by a line that joins the values that both objective functions (LCOE and SE) and the three optimisation variables (SF_A, LTS_{vol} and STS_{vol}) take for each of the chosen configurations. The values above and below the horizontal axes represent the maximum and minimum values that each parameter takes for the configurations presented in the plot, with every other value falling in between these. In contrast to Figures 4.13 and 4.15 which show the changes in individual parameters, Figure 4.16 shows how the whole system configuration changes for some configurations along the Pareto front.

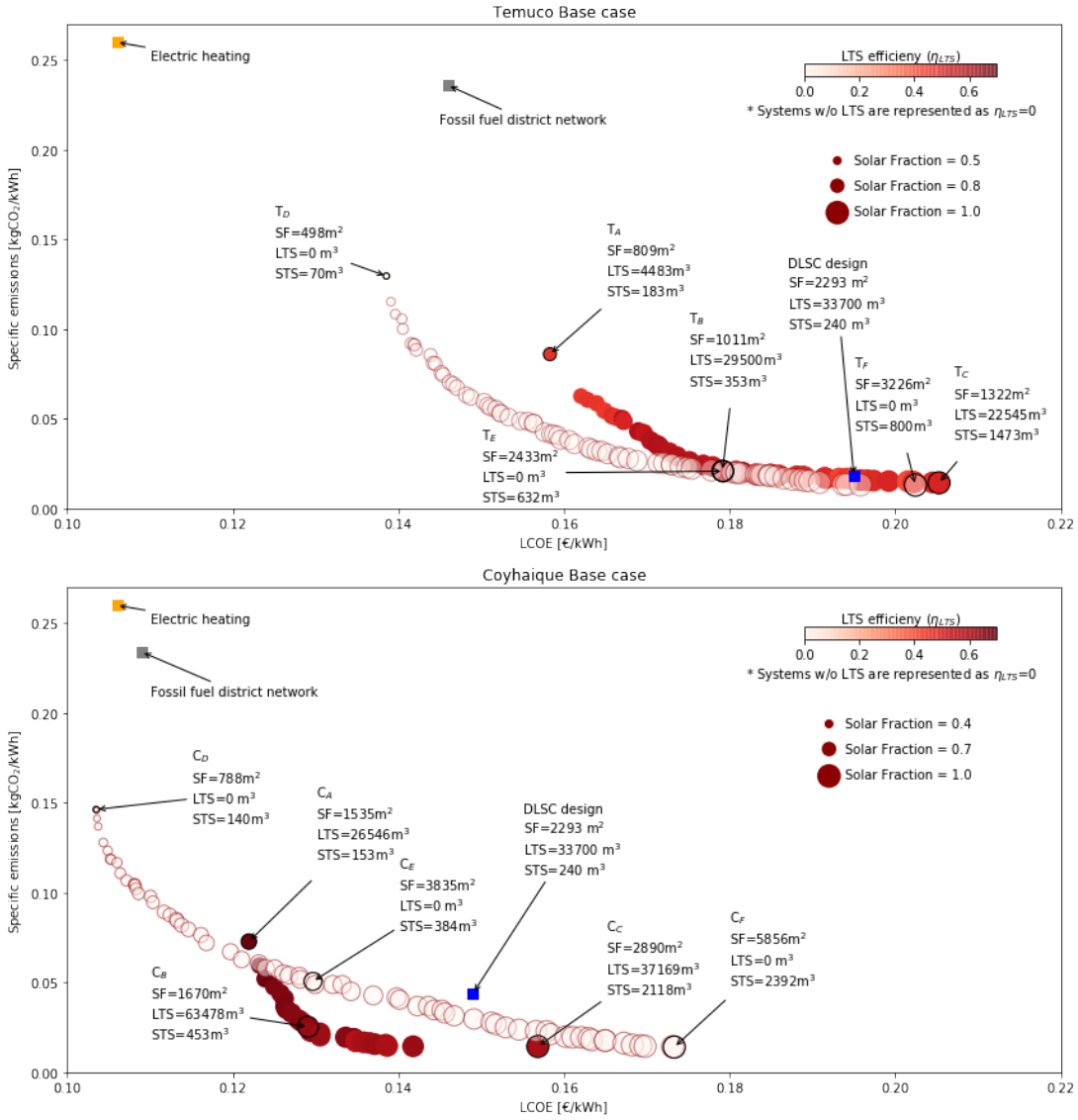

Figure 4.12: Pareto fronts for the Base system with and without LTS (the later represented as white circles with 0% LTS efficiency)

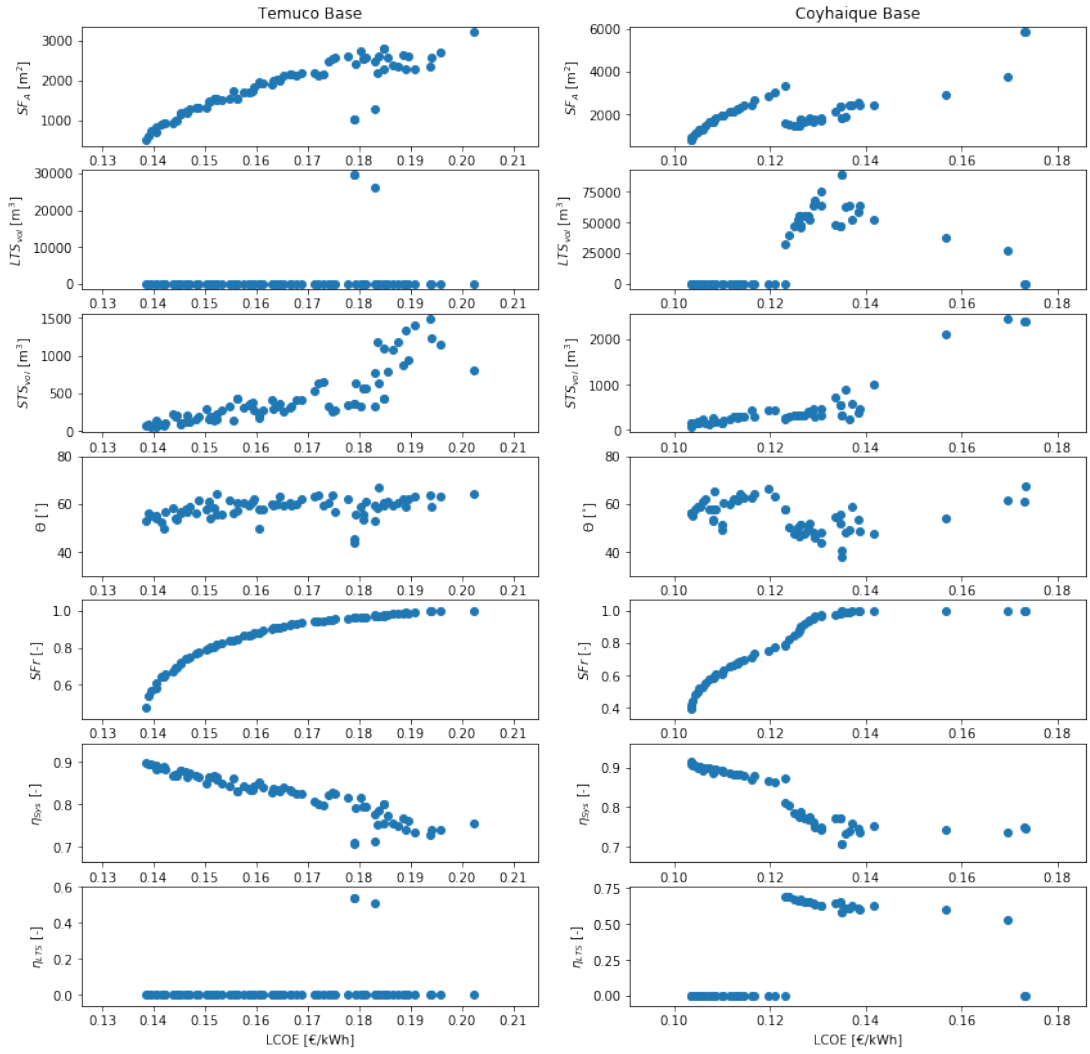

Figure 4.13: Values of optimisation variables and performance indicators for the systems in the Pareto front for the Base case in Temuco (left) and Coyhaique (right)

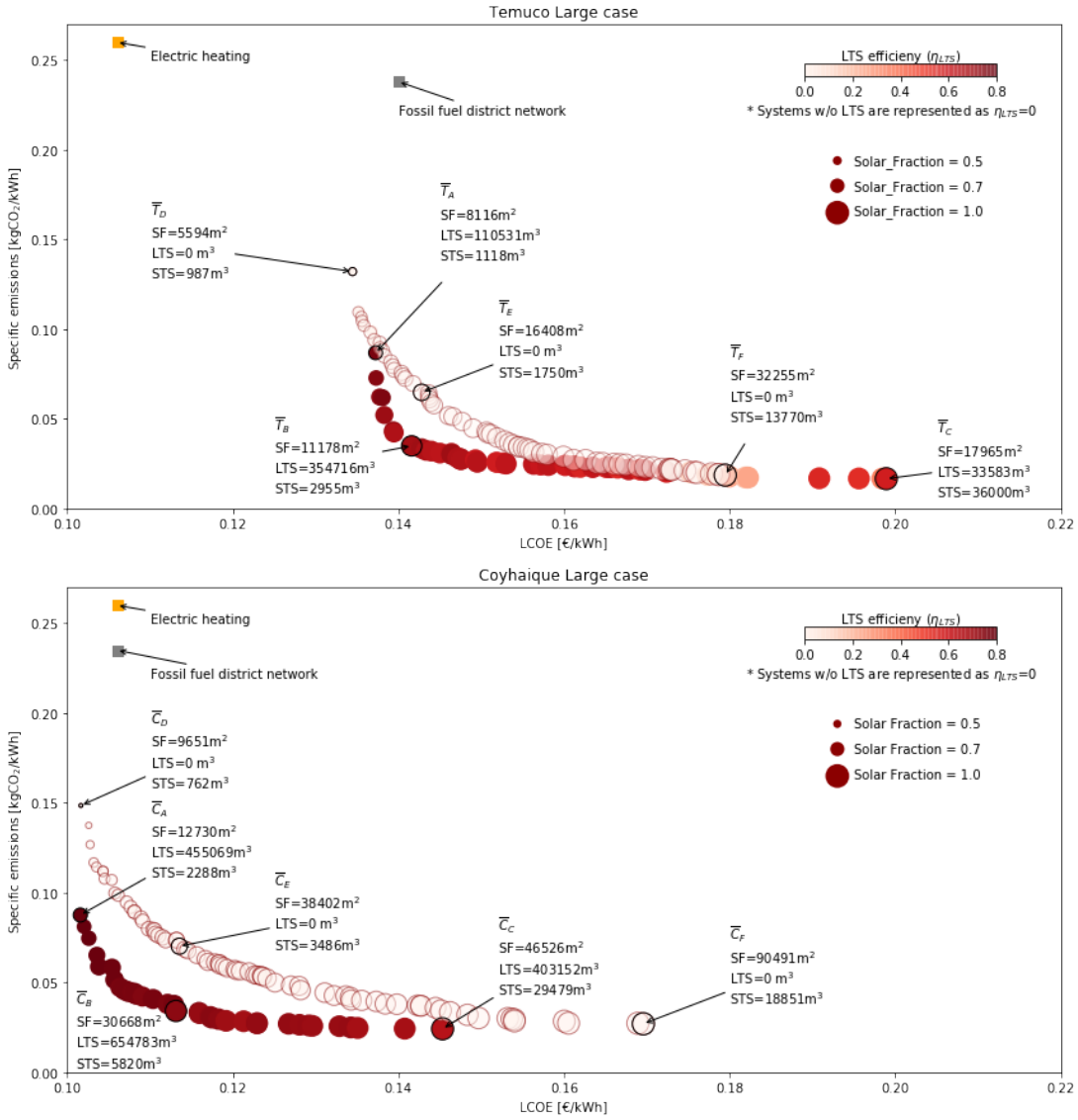

Figure 4.14: Pareto fronts for the Large system with and without LTS (the latter represented as white circles with 0% LTS efficiency)

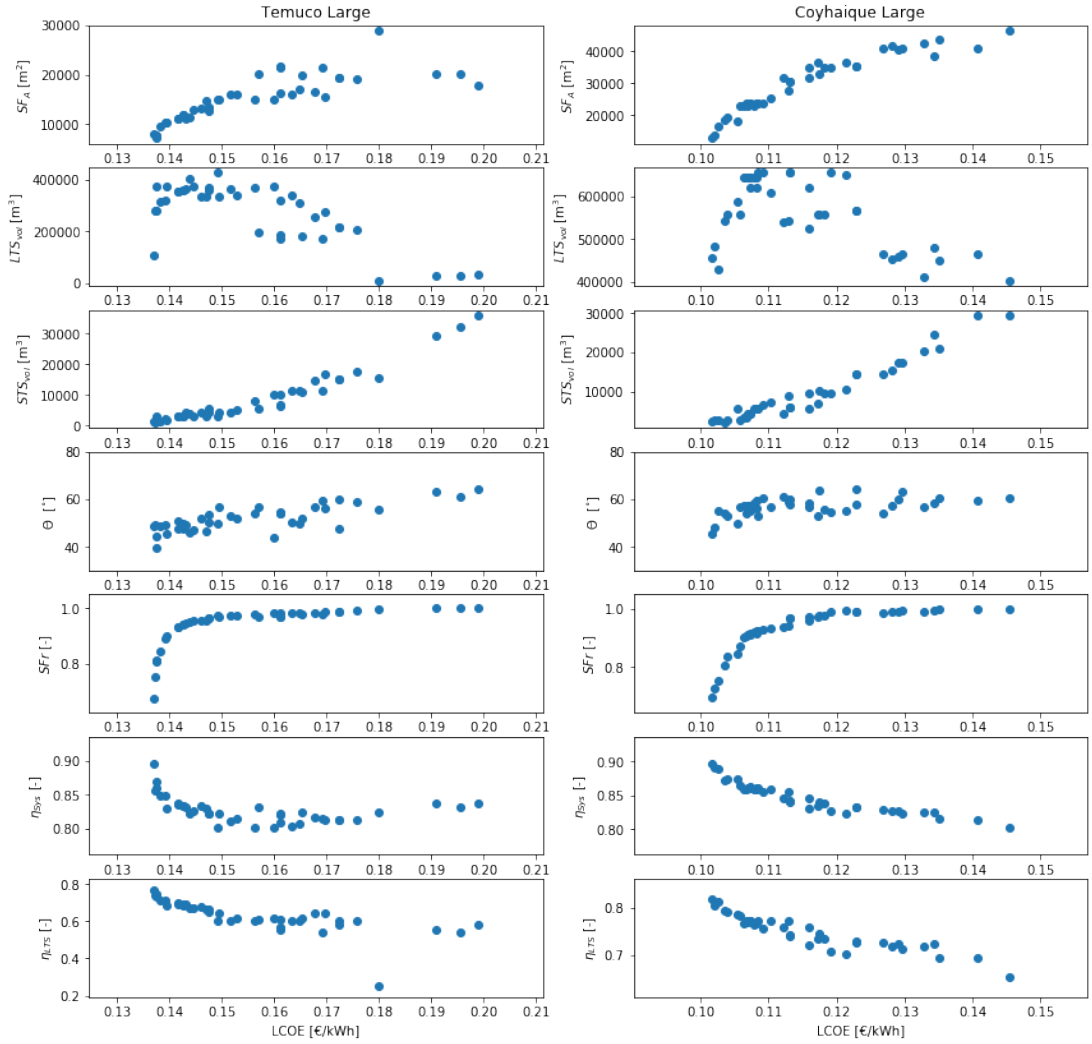

Figure 4.15: Values of optimisation variables and performance indicators for the systems in the Pareto front for the Large case in Temuco (left) and Coyhaique (right)

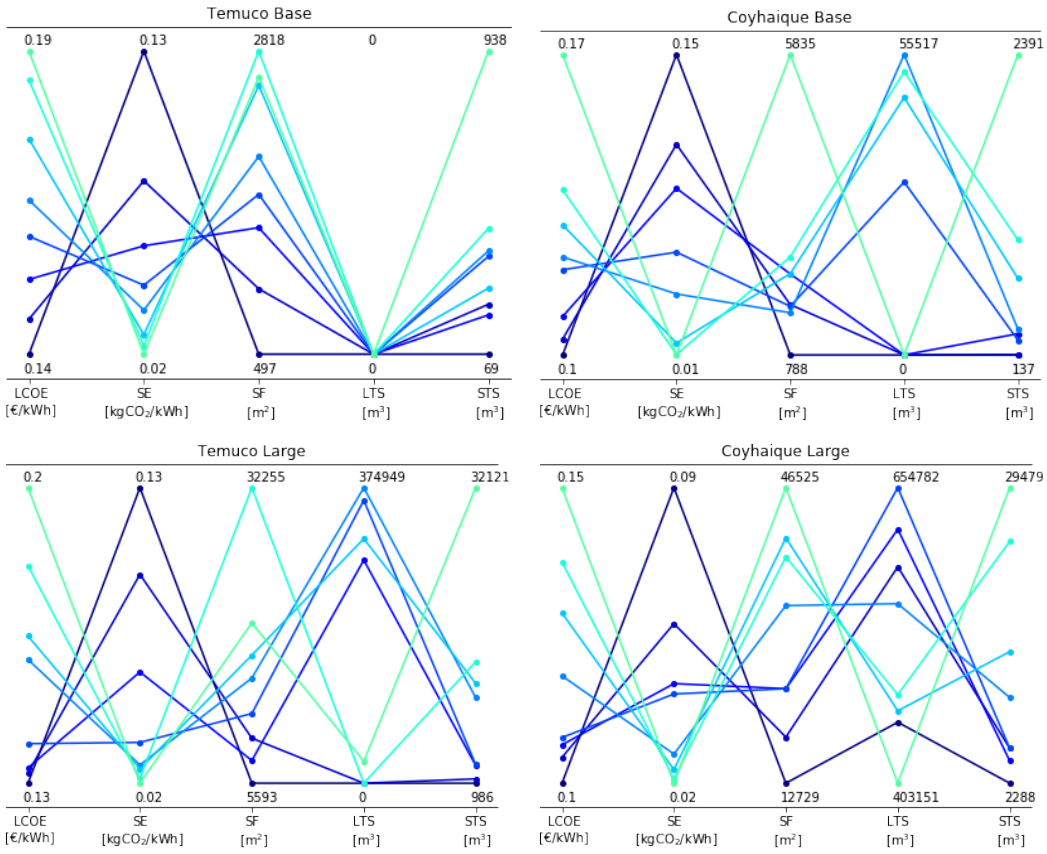

Figure 4.16: Comparison of eight different configurations in the Pareto front for Temuco and Coyhaique and Base and Large systems

Cost structure results

Figures 4.17 and 4.18 present the net cost structure of a subset of configurations in the Pareto front in both locations for the Base and Large case respectively. The investment costs are presented in solid colours and are calculated using the information in Table 4.7, while annual costs are presented in pattern colours and are calculated using the information in Table 4.6, discount rate r = 0.05 and lifetime n=25 years to bring the annual costs to present value. Each configuration's SE is plotted on the right axis as a reference and the configurations highlighted in Figures 4.12 and 4.14 are outlined.

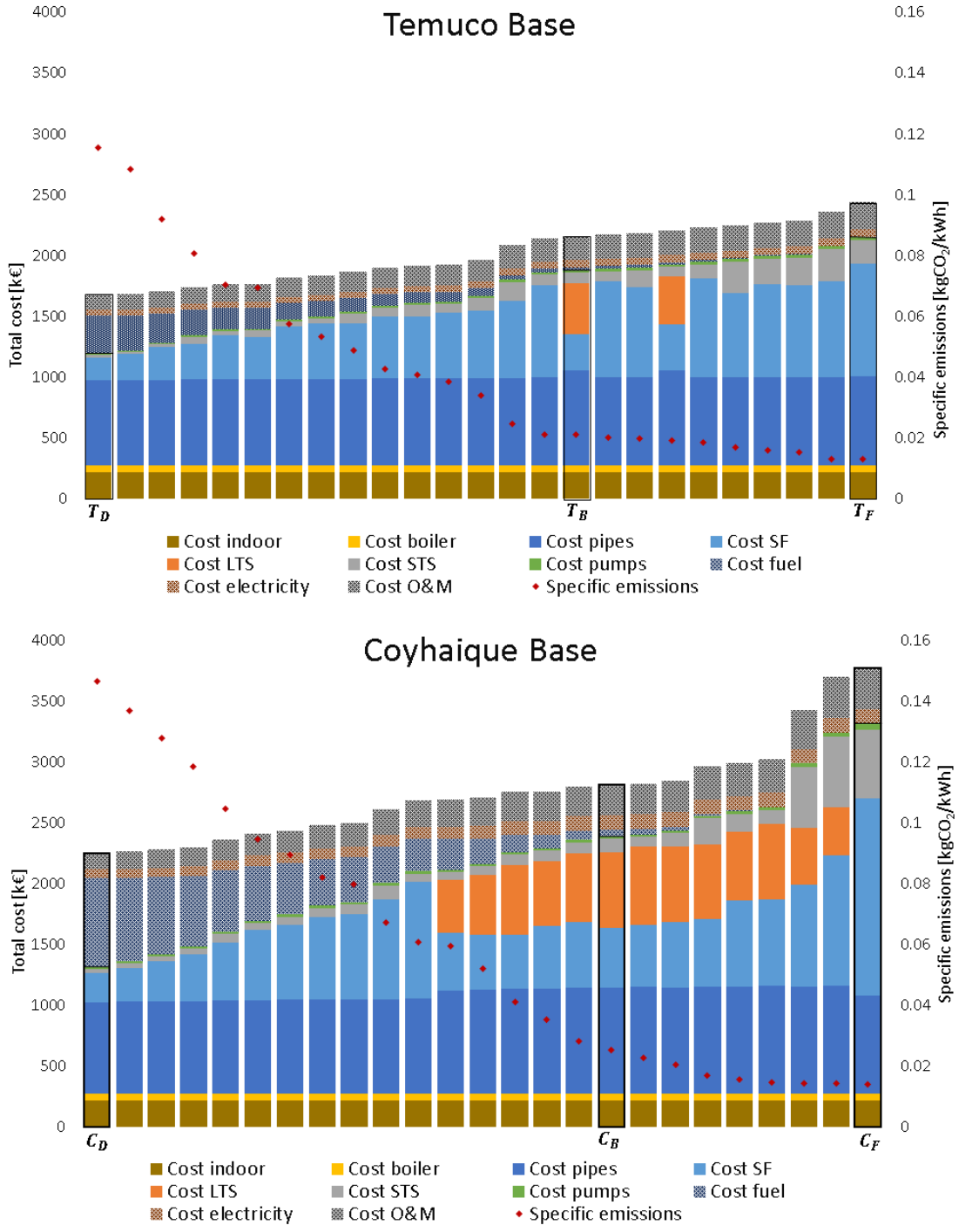

Figure 4.17: Cost structure of different system configurations along the Pareto front for the Base case in both locations

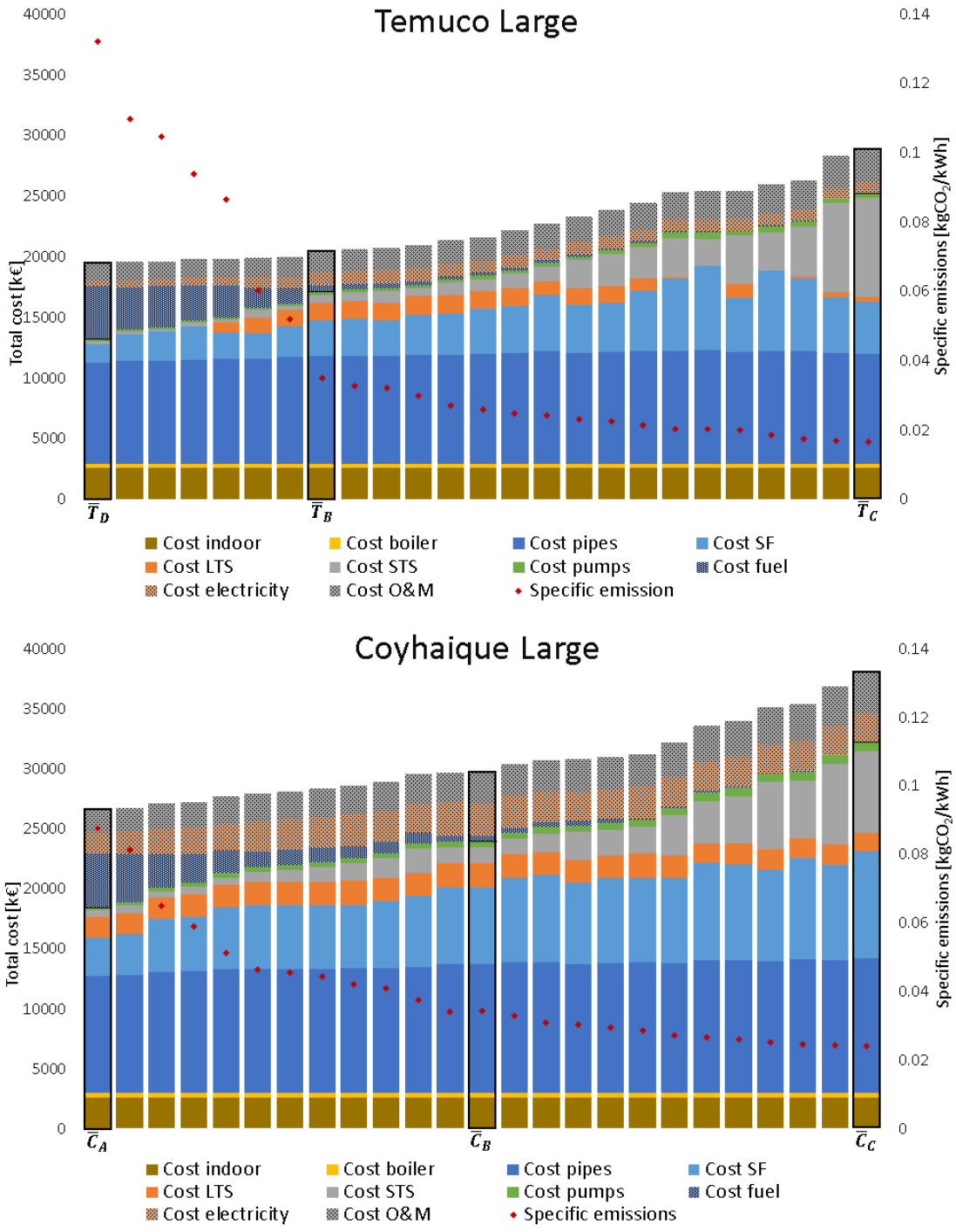

Figure 4.18: Cost structure of different system configurations along the Pareto front for the Large case in both locations

Analysis of Pareto front results

The most evident result from Figure 4.12 is that the system in Coyhaique reaches costs around 0.04 €/kWh lower than Temuco. This is mostly due to the better utilisation of the invested infrastructure in Coyhaique, as it operates longer time closer to its peak capacity, achieving a higher load factor, as shown in Table 4.12. This can be corroborated by Figure 4.17, which shows that the total costs for the system in Coyhaique are between 35% and 60% higher, while the annual energy demand is 82% higher.

As a comparison, two conventional heating options are presented in Figures 4.12 and 4.14. A "fossil district network" represents a district heating system that provides heat from a gas boiler and "electric heaters" represents local electric resistive heaters located in the flats. It can be seen that in both cities a solar DH system can compete in cost with fossil fuel alternatives. However, only in Coyhaique the solar alternatives can compete with electric heaters in the Base case. Most notably, configurations such as that represented by point C_B can decrease the SE by around 90% with respect to conventional alternatives while increasing the costs by less than 20%.

For Temuco, Figure 4.12 shows that the configurations without LTS dominate those with LTS. This means that it is cheaper to have a larger SF and eventually curtail some solar energy than invest in an LTS and store energy, as the operation of the LTS yields efficiencies around 40-45%. For systems with LTS higher than 20,000 m^3 and SF around 1,200 m^2 there is an increase in the efficiency of the LTS to more than 50% and the LCOE of the systems with LTS becomes comparable to those without LTS. This is evident for system configuration T_E and can be seen in Figure 4.13, where some points with LTS $>$ 0 appear in the plots, producing a subsequent drop in SF_A and in η_{Ssys}. This also is evident in Figure 4.17, where for configuration T_B the LTS replaces part of the SF. However, in most of the cases, for the Base case in Temuco it is most cost efficient not to consider an LTS.

It is interesting to note that in Figure 4.12, configurations T_C and T_F have already reached SFr = 1, which implies that the fuel consumption has reached zero and the emissions cannot be reduced more, as increasing the storage or the solar field area would mean higher electricity consumption associated to pumping, thus increasing the SE. This behaviour is common to all the cases analysed, causing the Pareto fronts to not converge to a SE value, as for larger LCOE the emissions start to increase.

In the case of Coyhaique, similarly to Temuco, the Base case without LTS dominates the case with LTS for smaller system configurations. However, the inclusion of LTS in this location leads to further SE reductions. This is probably related to the LTS being used more and reaching η_{LTS} close to 70%. In particular, for a similar LCOE, configuration C_B reduces emissions by more than 50% in comparison with configuration C_E, by reducing SF_A by 50% and adding

an LTS of almost 65,000 m^3. The storage volume range between 30,000 and 70,000 m^3 is relatively common among the existing BTES systems operating with solar energy, with some examples being Drake Landing in Canada (34,000 m^3), Anneberg in Sweden (59,000 m^3) and Neckarsulm in Germany (63,000 m^3) (Nielsen *et al.*, 2019).

From Figure 4.13 in Coyhaique, it can be noticed that the optimal tilt angle (θ) of the solar collectors shows variation along the Pareto front. This finding contrasts to what could be expected, as usually optimal annual yield tilt angles tend to be related to the latitude of the location. The nature of this variation is discussed in depth in Section 4.3.3.

Similarly to the results in Figure 4.12, Figure 4.14 shows that the cost of the Large system in Coyhaique is around 0.04 €/kWh lower than in Temuco. On the other hand, the minimum SE achieved at SFr = 1 is higher in the Large case in comparison to the Base case. This is a direct effect of the systems in the Large case having to use comparatively more energy for pumping, due to longer piping networks in the DH, SF and LTS. This can be seen in Figures 4.17 and 4.18, where the fraction of the total cost represented by the use of electricity increases from around 3-4% in the Base case to around 6-9% in the Large case.

Furthermore, the solar systems are again comparable in cost with conventional alternatives achieving emission reductions of more than 80% in comparison to conventional alternatives by increasing the cost by only 2%, as shown by configuration $\overline{T_B}$ in Figure 4.14. In addition, the LCOE in both cities decreased by 0.015-0.020 €/kWh in comparison with the Base case. This is also an effect of a larger system, but even more, a product of the higher energy density considered for the Large case, highlighting the importance of dense energy demand areas for the competitiveness of DH systems. Another difference with respect to the Base case is that Figure 4.14 shows that the configurations with LTS dominate the curve without LTS in both cities, meaning that it could be cost efficient to implementing LTS for the Large case. In these configurations very large LTS systems of more than 600,000 m^3 reach efficiencies close to 75%. Even though the largest BTES found in the literature are in the range of 350,000 m^3 (Emmaboda in Sweden and Wollerau in Switzerland (Nielsen *et al.*, 2019)), there are no evident technical limitations for constructing larger BTES systems.

Figures 4.17 and 4.18 clearly show that the piping of the district network is one of the dominant costs of the systems. However, its relative importance decreases for systems with larger SFr, as investments in SF and in storage start to dominate. From these figures, it is also interesting to highlight that the increase in the size of LTS has no noticeable effect on the size of STS, but it decreases notably the size of the SF. This is due to the slow thermal inertia of the BTES technology which does not allow it to replace the quick response operating service provided by the STS tanks, but increases the SFr by supplementing the operation of the SF in periods with lower irradiance and higher heating demand.

Discussions on Pareto front results

The LCOE of the systems for both locations and cases ranged between 0.1 and 0.2 €/kWh, depending on the system configuration. This is comparable with other values found in the literature for similar systems. Schmidt *et al.* (2004) calculated values between 0.17 and 0.42 €/kWh for systems with different long term storage technologies in central Germany. Renaldi and Friedrich (2019) estimated values of LCOE of 0.20 and 0.27 €/kWh for locations in Scotland and England for a similar system composition, but without performing an optimisation. Hsieh *et al.* (2017) performed an analysis on a system in Switzerland, achieving close to 0.4 €/kWh for a configuration with centralised long term storage and heat generation, but the system in their case was much smaller, with energy demands around 5 to 10 times lower than those considered in this study. Mauthner and Herkel (2016) analysed systems in central European locations and BTES technology for the long term storage and reached LCOE values between 0.10 and 0.17 €/kWh.

Even though the cost of the solar district heating networks analysed in this study can be competitive with some conventional alternatives, they are not currently competitive with burning firewood (the main source of domestic heating in the cities of southern Chile), which has an LCOE between 0.025 and 0.035 €/kWh (Ambiente Consultores, 2013). In order to compete with this technology, economic incentives that account for the negative externalities caused by the PM2.5 pollution should be put in place. Most of these externalities are related to health issues and subsequently increased load in the health system and increase in sick days. For instance, if considering a social cost of PM2.5 emissions of 15.000 US$/tPM2.5 (Chile Ambiente, 2008) and an emission factor of 0.5 g$PM_{2.5}$/kWh (Ambiente Consultores, 2013) the cost of using firewood increases by around 0.08 €/kWh, leading to a firewood LCOE close to those achieved by the Large system case in the city of Coyhaique.

It is important to note that the thermal load considered for this study does not include domestic hot water (DHW). The inclusion of this additional load is important in further studies, as it represents close to 10% of the total heat demand in the south of Chile and close to 25% in the central area of the country (Tolvett, 2015). The current option for providing DHW in social buildings is through individual liquefied petroleum or natural gas boilers, which work independently from any heating system or appliance. Hence, one alternative to provide DHW with a low emission system is to keep using a system independent from the heating network, such as dedicated rooftop solar collectors. This kind of decentralised system is used in the DLSC project, as a supply temperature of 37°C does not allow to provide DHW from the district heat network without an auxiliary heat source. An alternative could be to use a semi-decentralised system such as the one proposed by Rehman *et al.* (2018), using the district network to preheat the DHW plus auxiliary heaters that increase the temperature of the DHW

close to the demand. Lastly, a centralised system could be assessed, with the district network providing the heat for the DHW. This option would require increasing the district network's supply temperature above 50°C, which would increase the thermal losses but would allow to directly generate domestic hot water. This option is further discussed in Section 4.3.4.

4.3.3 Optimal angle analysis

The optimal annual yield tilt angle has been extensively analysed in the literature and it is mostly defined by the latitude and the local weather conditions (Chinchilla *et al.*, 2021). However, this optimal annual yield angle is calculated based on maximising the radiation available on the collector's surface, but does not include effects such as thermal losses in the collectors (Lv *et al.*, 2018), and more importantly, the existence of a demand that would transform the available radiation into useful energy. Particularly, in the case of heating applications, the mismatch between resource availability and demand (as evident by contrasting Figures 4.1 and 4.10), leads to optimal tilt angles to deviate from the angle that maximises the annual radiation towards angles that maximise radiation in winter (when the demand is higher). Figure 4.19 presents the optimal tilt angles (θ) that minimise LCOE and SE for the cases without LTS in both cities. The SF_A in the horizontal axis has been normalised by the total annual demand, which allows plotting the optimal points of the Base and the Large cases together for each city. As a reference, the angle that maximises the annual solar irradiance on the collector has been marked as AO: 29° for Temuco and 34° for Coyhaique (AO meaning annual optimum, the angle that maximises irradiance for the entire year); and the angle that maximises the winter solar irradiance on the collector has been marked as WO: 55° for Temuco and 61° for Coyhaique (WO meaning the winter optimum, the angle that maximises irradiance for the winter season). From Figure 4.19 it is evident that θ concentrates around WO, with an average of 58.6° for Temuco and 62.4° for Coyhaique. This means that it is worth having a better performance of the solar collectors in winter, because the demand during June, July and August represents close to 50% of the total annual heating requirements.

Figure 4.20 presents θ for the configurations in the Pareto front with LTS. Again, the SF_A has been normalised by the total demand in order to present the configurations for the Base and Large case in the same plot. Plots of θ as a function of LTS_{vol} were added to see the effect of the storage capacity on the optimal angle. LTS_{vol} was also normalised by the total annual demand to present the results of both cities and both cases aggregated in the same plot.

From Figure 4.20, it can be appreciated that the average of θ decreases to 50.1° for Temuco and 54.1° for Coyhaique if compared with the cases without LTS (Figure 4.19). This decrease occurs because the existence of an LTS allows for shifting part of the energy that could be captured in summer to be used in winter, which favours the use of relatively lower θ. Also, it can be noted that there is a decreasing trend of θ with LTS_{vol}, which means that larger LTS allow a higher percentage of the energy captured in summer to be stored and used in

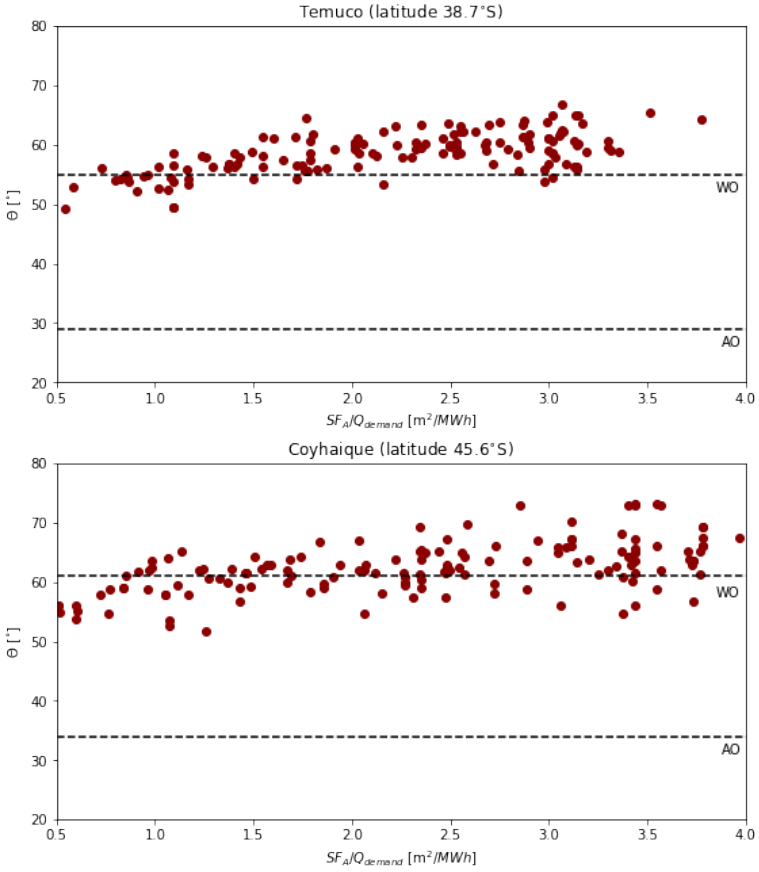

Figure 4.19: Optimal tilt angles (θ) as a function of SF_A for systems without LTS in the Pareto front in both locations

winter, favouring even lower θ. This behaviour explains the big change in θ in Figure 4.13 at LCOE around 0.12 €/kWh, when the Pareto optimal solutions start including relatively large LTS capacities. This analysis shows that including the tilt angle in the optimisation analysis is relevant, as its correct selection is non-trivial and depends on the different characteristics of the solar resource, heat demand and the relative sizes of the solar field and the storage. It was found that designing the Pareto optimal configurations with the angle that maximises the annual energy on the collector surface (AO) leads to results with, on average, 1.1% higher LCOE and 14.6% higher SE than the cases with optimised tilt angles. Also, using the angle that maximises the winter energy on the collector surface (WO) leads to, on average, 0.3% higher LCOE and 1.5% higher SE than optimising the tilt angle for each configuration.

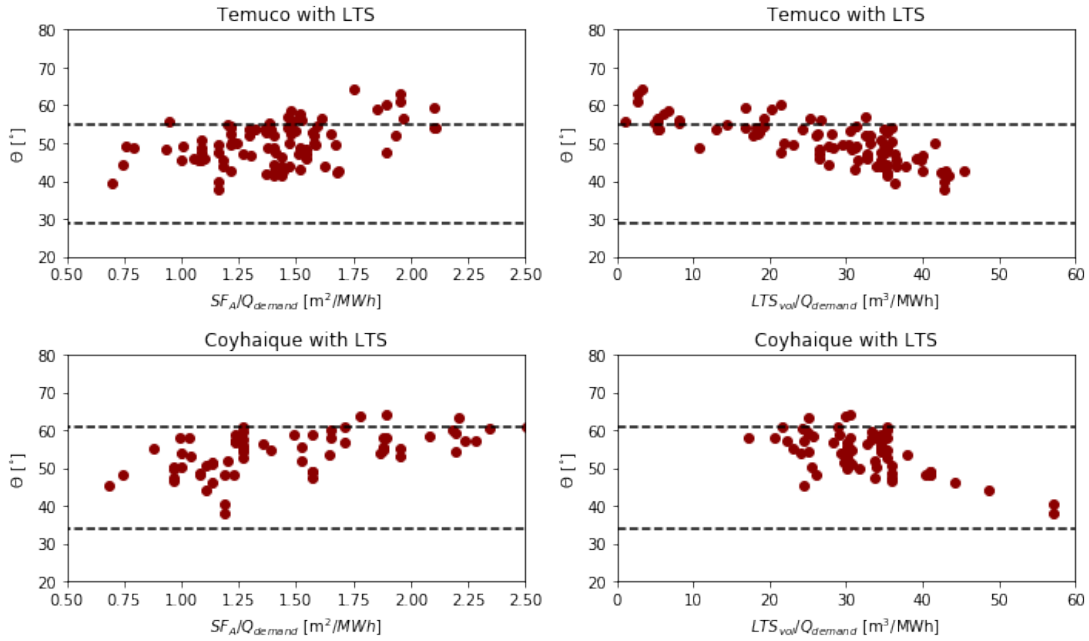

Figure 4.20: Optimal tilt angles (θ) as a function of SF_A (left) and LTS_{vol} (right) for systems with LTS in the Pareto front in both locations

4.3.4 Optimisation of DH temperature operation

A case with six optimisation variables (SF_A, LTS_{vol}, STS_{vol}, θ, $T_{DH_{sup}}$ and $T_{DH_{ret}}$) was run to compare the effect of optimising the supply ($T_{DH_{sup}}$) and return ($T_{DH_{ret}}$) temperatures of the DH water in the Large case.

Figure 4.21 presents in blue the Pareto front resulting from the inclusion of $T_{DH_{sup}}$ and $T_{DH_{ret}}$ as optimisation variables and compares them with the results without optimising the temperature. The colourbar indicates, the ΔT between $T_{DH_{sup}}$ and $T_{DH_{ret}}$, and points with similar SE ($\overline{T}_{BE}$ and $\overline{C}_{BE}$) and similar LCOE ($\overline{T}_{BC}$ and $\overline{C}_{BC}$) to $\overline{T}_B$ and $\overline{C}_B$ have been highlighted for comparison. Figure 4.22 presents the values of $T_{DH_{sup}}$ and $T_{DH_{ret}}$ for the points in the Pareto front in both locations, while Figure 4.23 presents a cost comparison for the points highlighted in Figure 4.21.

From Figure 4.21, it is evident that there is an important decrease in LCOE after optimising the temperatures. This reduction reaches around 0.02 €/kWh in Temuco and 0.01 €/kWh in Coyhaique, between 10 and 20% of LCOE decrease. From the colours it is clear that the optimum ΔT between $T_{DH_{sup}}$ and $T_{DH_{ret}}$ is around 17°C for Temuco and 14°C for Coyhaique instead of the 7°C used from the DLSC case. From Figure 4.22 it can be noted that $T_{DH_{sup}}$ tends to be between 50 and 55°C for Temuco and decreases up to 41°C for Coyhaique. This can be interpreted as higher $T_{DH_{sup}}$ and higher ΔT for the warmer conditions of Temuco, lower $T_{DH_{sup}}$ and ΔT for the cooler conditions in Coyhaique and even lower $T_{DH_{sup}}$ and ΔT (37°C and 7°C, respectively) for the even colder conditions of the original DLSC system in Canada.

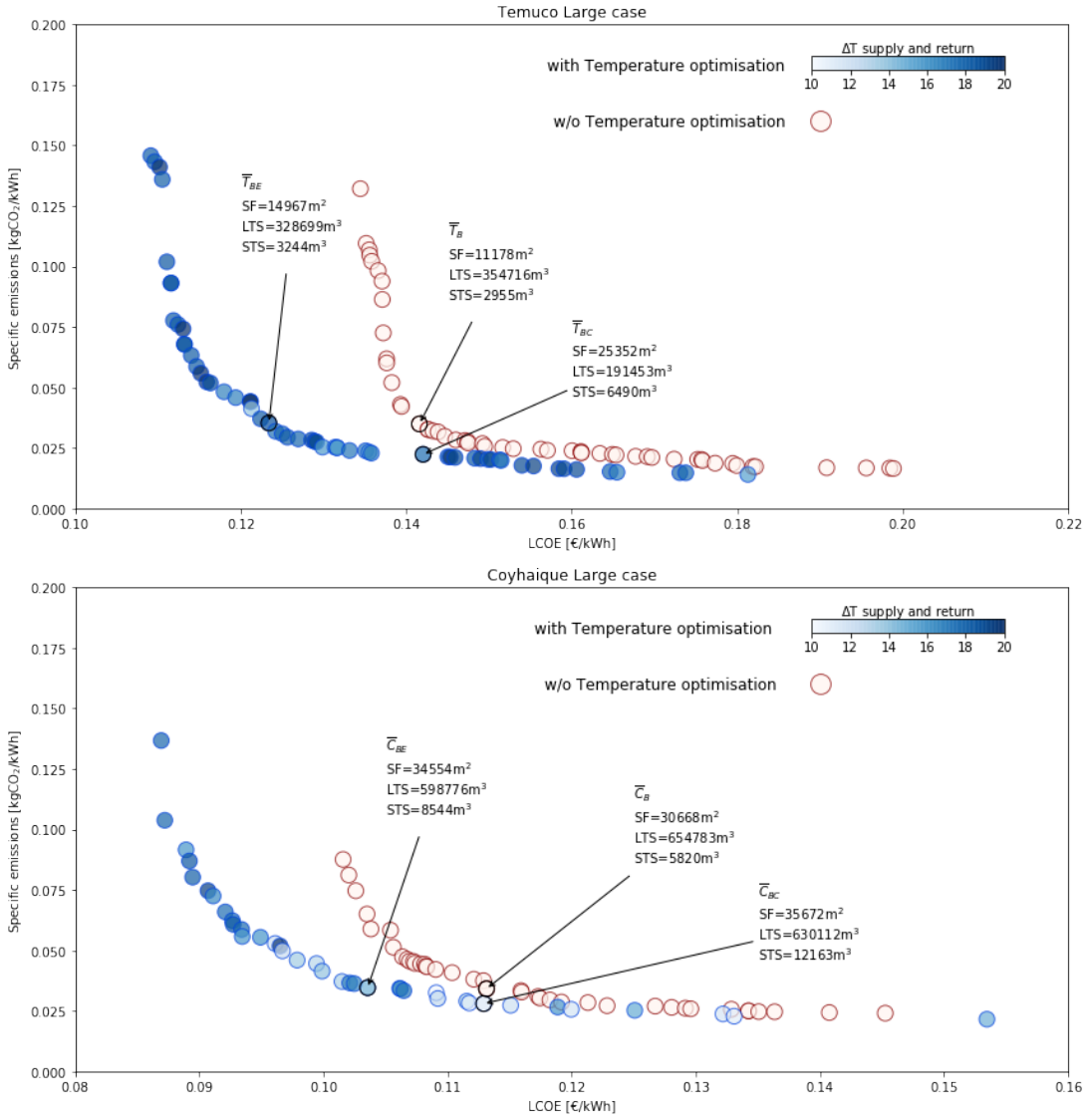

Figure 4.21: Comparison of Pareto fronts with $T_{DH_{sup}}$ and $T_{DH_{ret}}$ optimised and the case without optimisation ($T_{DH_{sup}}$ and $T_{DH_{ret}}$ constant at the DLSC original value as per equations 4.2 and 4.4)

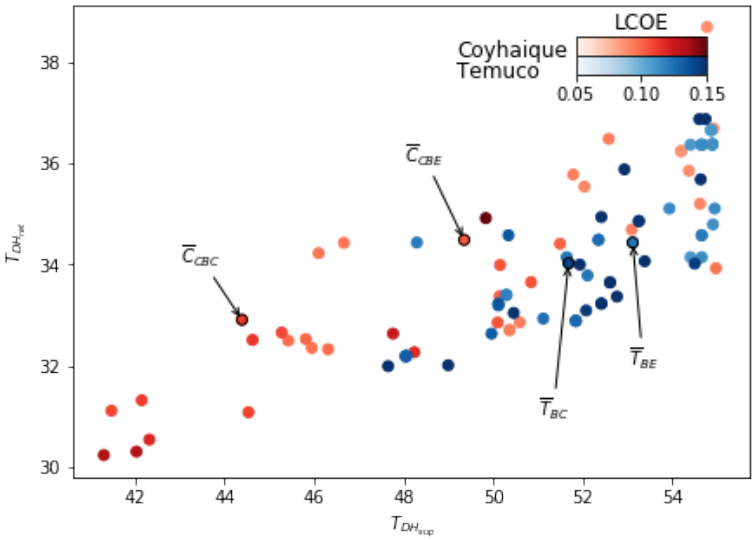

Figure 4.22: Optimal $T_{DH_{sup}}$ and $T_{DH_{ret}}$ for the different configurations in the Pareto front

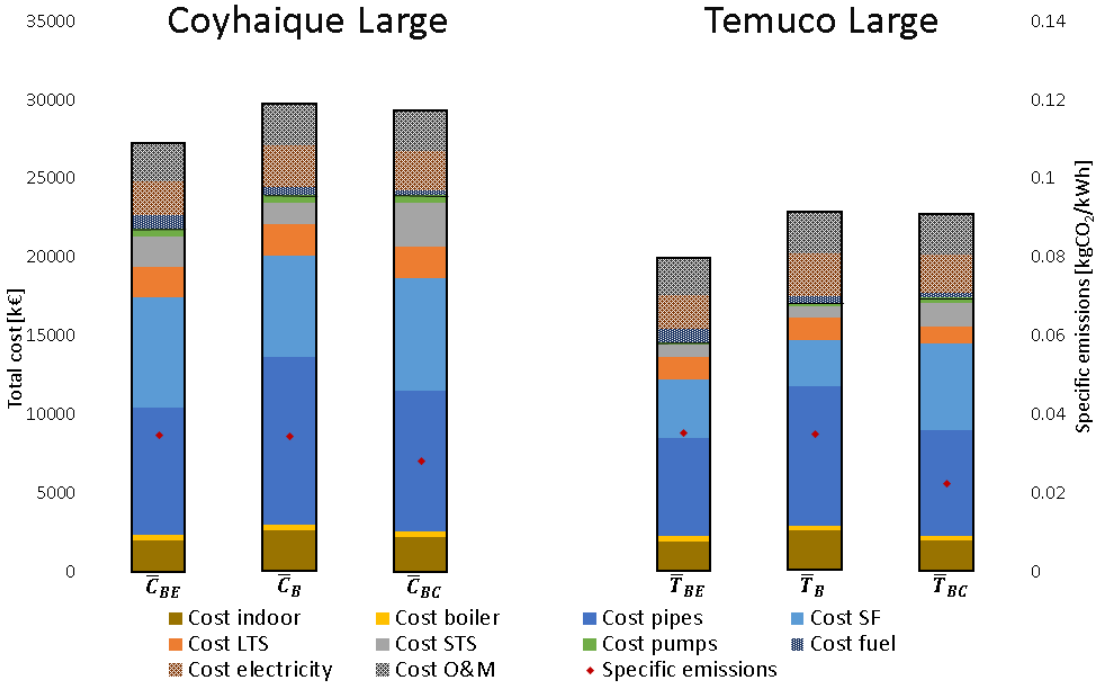

Figure 4.23: Cost comparison for selected configurations from the Pareto front between optimised and not optimised $T_{DH_{sup}}$ and $T_{DH_{ret}}$. The configurations presented are the same highlighted in Figure 4.21

The use of supply temperatures between 45 and 55°C opens the possibility of supplying domestic hot water using the DH network without additional auxiliary heaters. This can be achieved by installing heat exchangers close to the consumption points and using the 45-55°C from the DH network to generate 40-50°C domestic hot water (DHW) by heating cold drinking water from the mains. Although the resulting DHW temperature is within the range of risk for legionella growth, this risk is minimised when the system has no water storage and the heating unit (heat exchanger, in this case) is located close to the final supply point (Lund *et al.*, 2014; Foster *et al.*, 2016). Based on the method presented in Appendix D, it is estimated that the addition of the DHW consumption to the proposed scheme would increase the annual heat demand by close to 40% in Temuco and 25% in Coyhaique and the peak loads by 28% in Temuco and 25% in Coyhaique, which would require upscaling the system's design accordingly. However, as the demand pattern of DHW has a lower seasonal variability than the heating demand (see Appendix D), it would increase the utilisation of solar heat in summer, which tends to increase the annual system's load factor and makes it more cost-efficient.

When comparing $\overline{C}_B$ with $\overline{C}_{BE}$ and $\overline{T}_B$ with $\overline{T}_{BE}$, Figure 4.23 shows that the main decrease in cost comes from the cost of the pipes, which decreases by 25% for $\overline{C}_{BE}$ and 29% for $\overline{T}_{BE}$, followed by a similar decrease in the cost of the indoor heat delivery system (IHDS). The decrease in the cost of the pipes is explained by the lower flow rate of hot water required to fulfil the demand with a higher ΔT in the DH. Meanwhile, the decrease in the cost of the IHDS is due to the decrease of the area required for the heat exchange when the LMTD increases (see footnote on Table 4.7). This investment decrease is partly compensated by an increase in SF_A and STS_{vol}, as supplying water at higher temperatures generated more thermal losses. In aggregate, the change in investment costs represents 84% of the total cost decrease for $\overline{C}_{BE}$ and 95% of the decrease for $\overline{T}_{BE}$. The remaining change in LCOE comes from changes in annual operational costs, such as a decrease of the use of electricity (22% for $\overline{C}_{BE}$ and 12% for $\overline{T}_{BE}$) and an increase in the use of fuel (15% for $\overline{C}_{BE}$ and 8% for $\overline{T}_{BE}$). From these changes, the decrease in electricity consumption follows the reduction in water being pumped in the DH; meanwhile, the increase in fuel use comes from more use of the auxiliary boiler, due to more periods when the STS is not able to supply the higher DH temperature requirements, and from the higher heat losses in the DH pipes network. Figure 4.24 presents the increase in heat losses in the DH pipe network due to the increase in the temperature of the water circulating. It is worth mentioning that the model considers that the insulation level of the pipes changes when the pipe diameter is modified (according to equation 4.3), but it is not adjusted for changes in the fluid's temperature inside the pipe.

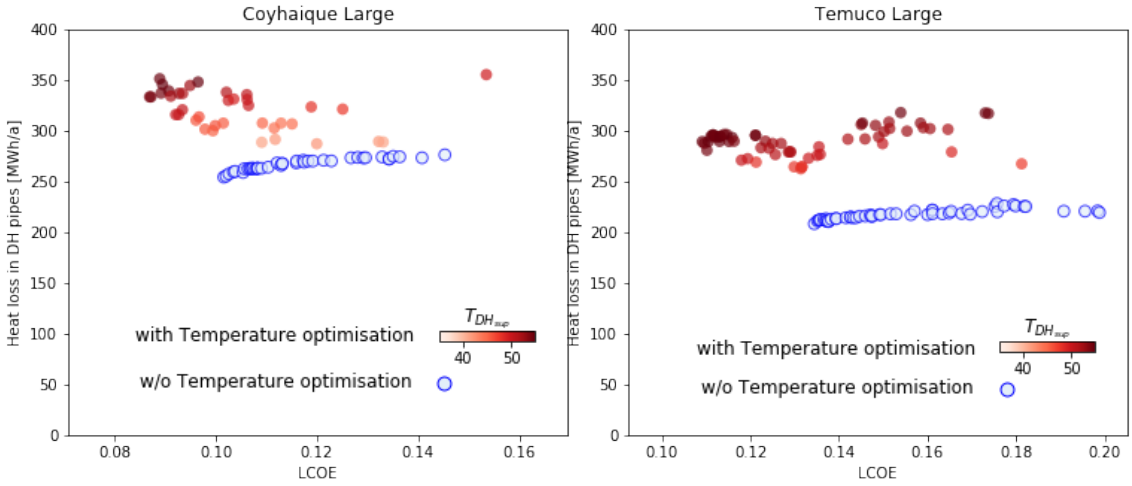

Figure 4.24: Comparison of the annual thermal losses in the pipes of the DH for the case with and without optimisation of the temperature in both locations

4.4 Conclusions

The work presented in this chapter is based on a published article (Maximov *et al.*, 2021) and it develops the first model for multi-objective optimisation of a district heating thermal network with seasonal thermal energy storage in the southern hemisphere and under the special cool and sunny conditions in southern Chile. It is also the first that analyses the optimisation of the collector tilt angle considering the mismatch between solar resource availability and heat demand and the influence of a long term storage system.

The buildings' demands consider the occupancy rates of average families inhabiting social housing buildings, standard energy gains and air infiltration. The framework simulates the operation of several specific system designs that fulfil the demand combining solar thermal energy and fossil fuel back-up and uses a genetic algorithm to select and evolve the system designs towards a set of optimal solutions that minimise the LCOE and the specific emissions of the system.

The proposed optimisation framework allows assessing the cost-effectiveness of solar thermal networks to decarbonise heat supply. It offers flexibility in managing the design and operation of the system with a high level of detail that makes it useful in preliminary project design stages, such as feasibility analysis design evaluation and even in early stages of basic engineering design. The result of the optimisation is a set of Pareto optimal solutions that are equivalent from the optimisation perspective. However, the system designer may have other restrictions, such as budget constraints or emission level caps used to select their optimal design.

The frameworks' application to Temuco and Coyhaique shows the potential to decrease emissions drastically compared to a conventional district heating system or electric heaters. These reductions can be achieved with relatively minor increases in the system's total cost, reaching 90% emissions decrease by increasing by less than 20% the cost for specific optimised system configurations. Furthermore, under certain conditions, this solar district network could be cost-competitive with the use of firewood if externalities such as the social costs of local pollution were considered in the economic analysis.

It was shown that the economic and environmental benefits of these systems can be increased if they are optimised for the local conditions. In particular, it was found that the optimal supply and return temperatures in the district heating network depend on the location of the system, with relatively warmer locations favouring higher supply temperatures and higher differences between supply and return temperature. A correct setting of these operational parameters has an impact on both the investment and the operational costs. In the particular case analysed, it leads to total cost decreases of around 10 to 20% when compared with using values from a different location. Also, for the cases analysed, it was found that using an optimised collector tilt angle that considers the existence of long term storage leads to a decrease in almost 15% in annual emissions and 1% in costs if compared with an angle selected based solely on latitude and 1.5% reduction in annual emissions if compared with an optimal angle that considers the shape of the local thermal demand peaking in winter, but does not consider the effect of long term storage.

The initial investment represents around 70 to 90% of the LCOE of these systems, making them highly sensitive to initial capital finance and the unitary costs of specific elements. In particular, the costs of the piping in the network itself may represent around 40 to 50% of the total investment and may be affected upward in countries such as Chile, where there are no local producers nor experience in these technologies. Hence, there is a risk of real projects' costs being higher than those used for this analysis, but there is also scope for further cost reductions as the market becomes more mature.

The land cost was not considered in this analysis, as social housing projects are built on state owned land. However, it would be interesting to include a cost for land in the decision process of a private project, as it would tilt the results towards smaller solar field areas and perhaps larger storage capacities which in the case of borehole thermal energy storage can be underneath other structures.

The LCOE of these systems is sensitive to the scale of the demand and its spatial density. Moreover, as these systems are highly intensive in capital investment, the LCOE is highly sensitive to the load factor and to the investment cost assumed in the model. For the given costs, demand configuration and locations, the results show clearly that the use of seasonal

storage could provide extra value to the system. This value, as expected, increases for larger thermal demands (larger networks) and higher demand densities (higher population density). This means that, even for small projects, the assessment of possible future growth or interconnection of the system should be considered during the design process.

The minimum emissions of these systems are limited by the indirect emissions of the electricity used by the various pumps. Hence, the minimum achievable emissions tend to increase when the pressure losses in the system increase due to the increased system size, higher buildings or the addition of equipment in the network.

Further research in this field could aim to include domestic hot water demand in the analysis. This would lead to explore other system configurations and potentially increase the value of using higher supply temperature in the district heating network, as this could allow producing domestic hot water using direct heat from the network.

Chapter 5

Integration of electricity in district heating systems with seasonal thermal energy storage

5.1 Introduction

According to IRENA's REMap scenario, to limit the rise in global temperature to 2°C, the global electricity sector would require 85% of its generation from renewable sources by 2050, and 60% of the total would need to come from variable renewable generation, such as solar and wind (IRENA, 2019b). This new electricity system's configuration with high penetration of inflexible generation would require the addition of further flexibility sources downstream of the energy production to overcome the challenges of balancing supply and demand. Some of the possible sources for this additional flexibility may come from improvement in transmission and distribution infrastructure, energy storage and more flexible demand (IRENA, 2018).

The Chilean electricity system is also preparing to face these challenges, as by 2030 it is expected that variable renewable generation will represent more than 50% of the generated electricity (Ministerio de Energia, 2020g), and there is a programmed phase-out of coal power plants, considering the decommissioning of 30% of the current installed capacity by 2024 and aiming to the elimination of coal from the energy mix by 2040 (Ministerio de Energia, 2020a), with some possible scenarios predicting its elimination by 2035 (Ministerio de Energia, 2020g). This has led to the generation of a strategy to increase the flexibility of the electricity system (Ministerio de Energia, 2020b). However, this strategy mostly defines reforms to the electricity market to promote flexibility and reliability of the system, without analysing the possible contribution of specific technological alternatives and focusing mostly on generation and storage. This stresses the importance of providing information on the value of demand flexibility measures.

In the case of increasing flexibilisation of electricity demand, the role of demand-side management in the form of flexible loads has been recognised as an effective measure. However, there is an often overlooked potential in linking the power sector to heating, known as power-to-heat. For instance, Pilpola and Lund (2019) performed a case study for Finland in 2030, and found that power-to-heat is the most efficient grid flexibility alternative for enabling wind integration in terms of costs and carbon reduction when compared to other options, such as power-to-gas, electricity storage, electric vehicles charging and biomass-to-biofuels.

District heating (DH) networks can be specifically designed and operated as energy-balancing tools, maximising their capacity to provide services to the electricity network. By incorporating other technologies, such as heat pumps and thermal storage capacity, heat networks can absorb excess electricity generation when needed by the system. DH networks can also help to mitigate peak demand electricity loads by providing alternative heating (and eventually cooling) supply options (International Energy Agency, 2014a). This concept is already being applied in some commercial plants. For instance, in the Sunstore 4 project, in Marstal, Denmark, where electricity can be converted into heat through the use of a heat pump and stored during periods of high wind power production (Kjaergaard *et al.*, 2014). Additionally, the power-to-heat integration approach allows for coupling electrical and thermal energy production and usage, which optimises the integration of larger amounts of variable renewable electricity compared to an electric-only system view. In a case study in Helsinki, for instance, Niemi *et al.* (2012) concluded that by adding a power-to-heat conversion option, converting excess wind power into heat and using the heat network to deliver the energy to the consumers, the total amount of wind power in the system could typically be increased by 40% to 200%, compared with the case where the heat and electricity networks are disconnected.

Furthermore, this heat-electricity linkage, other than providing flexibility to the electricity grid, could bring benefits to the heat network by taking advantage of low electricity prices and decreasing costs of heat generation (Hers *et al.*, 2015). In addition, in markets with correct incentives towards promoting demand side flexibility, power-to-heat integration could provide an additional revenue stream for heat network operators by getting remunerations for helping to balance supply and demand. All these possible benefits are potentially increased when the heat network has a thermal storage system, which reinforces the flexible coupling of power and heat, allowing for greater flexibility in the heat network's demand for electricity. (IRENA, 2019a)

This chapter explores the effects of the integration of the district network scheme presented in Chapter 4 with the electricity grid through resistance heaters and heat pumps. It assesses how this integration can improve the system's value by decreasing total emissions and reducing the cost of the heat supplied to the end users. For this, the electric heating technologies are implemented in the TRNSYS model (first introduced in Section 4.2.2), and the system is re-

optimised, including additional optimising variables representing the design and operation of the new elements. Furthermore, an analysis of the effect on the electricity grid of a large scale power-to-heat scheme providing flexibility is performed using the model developed in Chapter 3 to evaluate the effects of a flexible demand on the electricity grid.

5.2 Methods

The methods used in this chapter are separated into those used for analysing the effects of coupling an electric heater with solar district heating. The general approach can be divided in two parts. The first, which is detailed in Section 5.2.1, relies on the model developed in Chapter 4 but including an electric heater (heat pump or resistive). The new design is re-optimised using future predicted spot prices. The second part, explained in Section 5.2.2, uses this optimised design to analyse its effect on the electric grid. For this, the model of the Chilean electric system developed in Chapter 3 is used to assess how spot prices adjust if the electric grid operates under an additional demand from the heat network. A general overview of the logical flow of both sub-methods and the different models involved is presented in Figure 5.1

5.2.1 Coupling an electric heater to a solar district network with seasonal storage

The methods used in this analysis are based on the model described in Chapter 4, Section 4.2. The framework showed in Section 4.2 is applied, but the TRNSYS simulation model is modified in order to account for the presence of an electric heater in the form of a resistance heater or an air to the water heat pump (HP), as shown in Figure 5.2. Regardless of the electric heating technology considered, the heaters operate by buying electricity from the grid and transforming it into heat supplied to the STS.

Heater modelling

As shown in Figure 5.2, the relatively cooler water from the bottom of the cold STS is circulated through the heater and pumped into the top of the hot STS. The heater was modelled supplying 90°C, as this is the setpoint temperature of the hot part of the STS.

In order to include this equipment in the TRNSYS model, their costs were parametrised according to Table 5.1. Additionally, a cost for connecting the equipment to the grid was considered, as the installed capacities of the new equipment can largely surpass the connection capacity of the existent electrical equipment, which is composed mostly by the pumps.

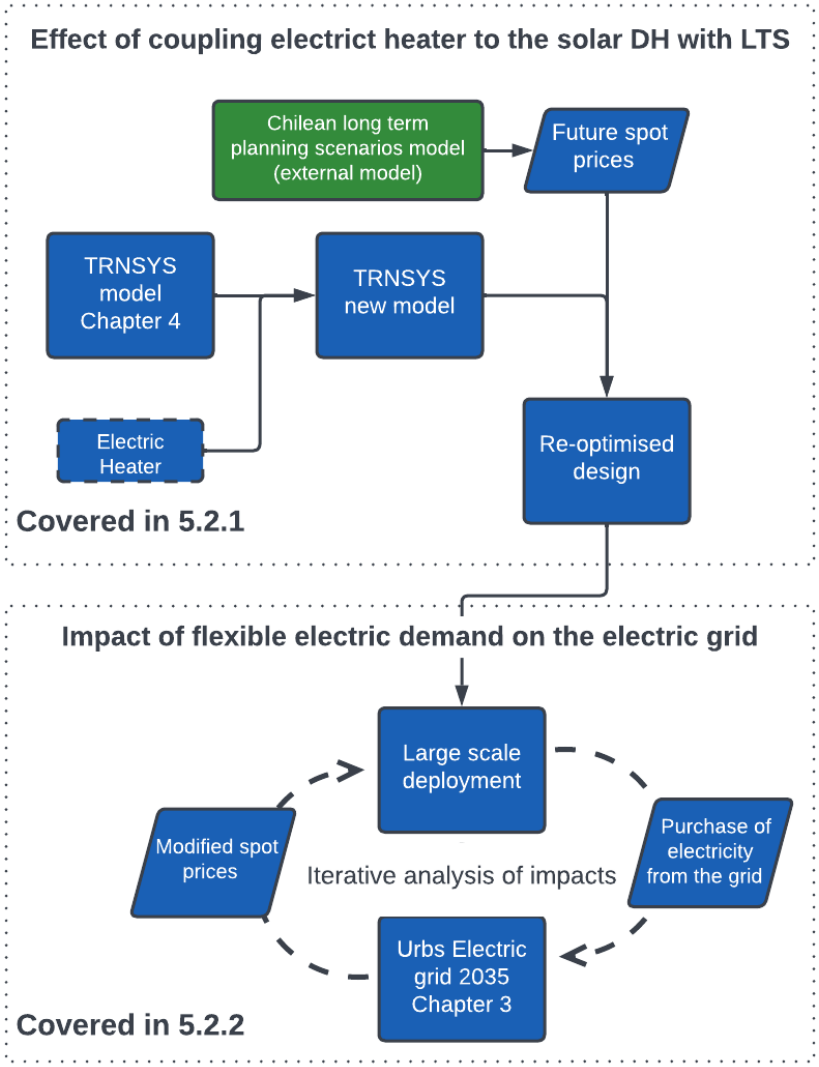

Figure 5.1: Logical flow of the method applied in this chapter

The costs of the resistance heaters were obtained from Hers *et al.* (2015) and was checked against the costs of real industrial immersion heaters published by Advancedwater (2021). The costs of heat pumps were obtained from data published by the Danish Energy Agency (2016) for air source heat pumps with capacities between 1 and 10 MW_e.

For estimating the coefficient of performance (COP) of the heat pumps, information published by the Danish Energy Agency (2016) and Arpagaus *et al.* (2018) were combined in equation 5.1.

$$COP_{HP-2020} = [0.4113 \cdot \ln(HP_{pow}) - 0.2575)] \cdot [23.9 \cdot (T_{STS_{set}} - T_{ambient})^{-0.747}] \quad (5.1)$$

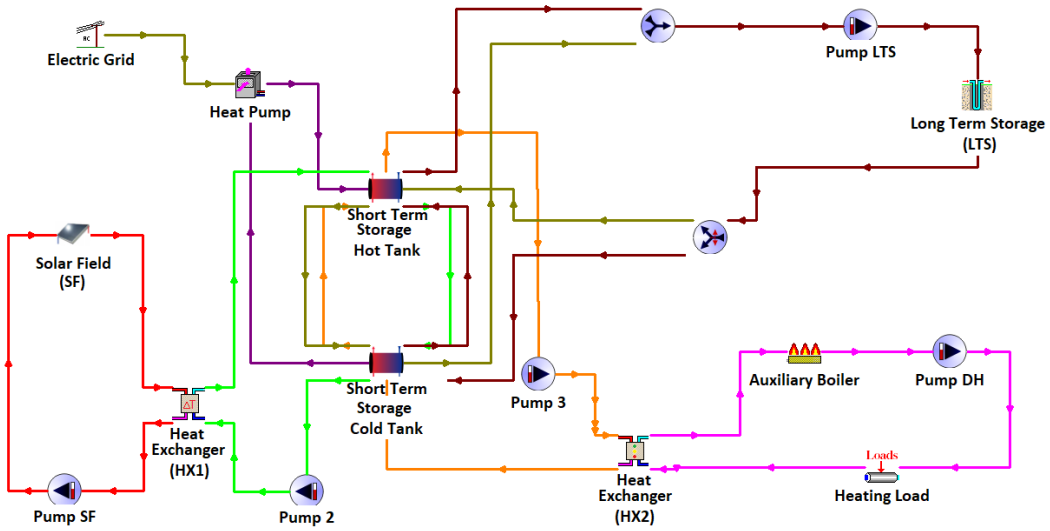

Figure 5.2: Conceptual representation of the TRNSYS simulation model with the addition of a heat pump

	Cost	Unit	Ref.
Resistance heater	60	[€/kW]	(Hers *et al.*, 2015)
Heat pump 2020	$(8518.9 \cdot HP_{pow}^{-0.249}))$	[€/kW]	(Danish Energy Agency, 2016)
Heat pump 2035	$(9169.7 \cdot HP_{pow}^{-0.271}))$	[€/kW]	(Danish Energy Agency, 2016)
Electric connection	100	[€/kW]	(Hers *et al.*, 2015)

Table 5.1: Costs of electric heaters and grid connection

The first factor of equation 5.1 corresponds to the dependency on the size of the heat pump, obtained by fitting a curve to the data published by Danish Energy Agency (2016) for air source heat pumps between 1 and 10 MW. The second factor corrects the COP based on the total temperature that the heat pump needs to lift (ΔT_{lift}), and it is obtained by fitting a curve to the data published by Arpagaus *et al.* (2018) (Figure 5.3). As the COP published by Danish Energy Agency (2016) correspond to pumps with ΔT_{lift} = 71°C (70°C temperature of hot water and -1°C temperature of ambient air), the regression in Figure 5.3 was shifted so ΔT_{lift} = 71°C corresponds to COP = 1, which allows to use it to correct the COP given by the first factor of equation 5.1 depending on the instantaneous ambient temperature ($T_{ambient}$).

According to the Danish Energy Agency (2016), the efficiency of heat pumps is expected to increase by 5% in the 2020-2030 period and by a further 5% in the 2030-2035 period. Thus, the COP of the heat pump in 2035 was defined according to equation 5.2. The efficiency of the resistance heater was assumed to be constant and equal to 100%.

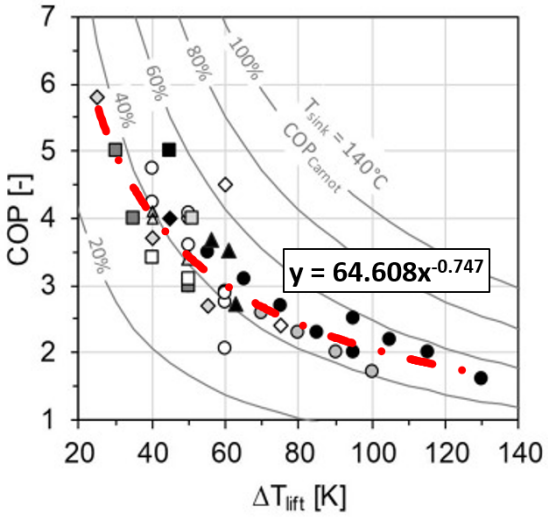

Figure 5.3: Regression of high temperature heat pumps' COP published by Arpagaus *et al.* (2018)

$$COP_{HP-2035} = COP_{HP-2020} \cdot (1+0.05)^2 \tag{5.2}$$

The heater turns on only when the price of electricity is below a certain threshold value ($Price_{purch}$). The heater buys electricity from the grid to increase the temperature of the water from the bottom of the cold STS tank and modulates the heat addition rate to get a constant output temperature of 90°C to the top of the hot STS, which defines the power purchased from the grid. The flow rate through the heater is defined as the one that would increase the temperature of the water from the minimum annual temperature in the bottom of the STS (defined as $T_{DH_{ret}}$+2°C) to 90°C when the heater operates at its rated heat capacity.

New optimisation variables

In order to include the electric heating system in the optimisation, three new optimisation variables were added.

The first of them is the size of the heater in kW (HP_{pow}). This variable defines the capacity of the heater (heat pump or resistance) and is directly linked to the cost and efficiency of the heater.

The second is the threshold electricity price in €/kW ($Price_{purch}$) for the purchase of electricity from the grid by the heater. This variable defines when the heater will operate and thus, how much electricity is purchased and converted into heat through the year. Every time the spot price is below this threshold price, the electric heater will be ready to purchase electricity and convert it to heat. The amount of electricity purchased will depend on the size of the heater (HP_{pow}) and on the capacity of the system to use or store that heat in the system in each timestep.

The third new variable corresponds to the rated flow rate capacity of the pump in the LTS loop in kg/s (LTS_{pump}), which controls the charging and discharging capacity of the LTS. This variable was considered to be relevant, as keeping it fixed could hinder the capacity of the LTS to store the energy bought by the heater. This variable was also added to the base case (without electric heaters) modelled in Chapter 4, thus slightly improving the optimisation results presented in that chapter.

Additionally, to simplify the optimisation, the tilt angle θ was fixed to 50°C, based on the average of the results presented in Figure 4.20 and on that the objective variables do not change drastically with small-angle variations, as discussed in Section 4.3.3.

Spot prices and emission factors for 2035

The Chilean electric market regulation mandates only generators can participate in the market pool by buying electricity at spot price, and that every energy supply to a final consumer has to be backed by a long-term contract. However, the conditions of said contract can be agreed between the client and the generator and can be indexed to the spot prices, which is the assumption for the electric heater's purchase mechanism in the model. In the case of the pumps and other auxiliary equipment of the district network and solar field, it is assumed that the electricity for their operation is still bought through a constant price contract, considering the same values used in Chapter 4 (Table 4.6).

The spot prices for 2020 were obtained from the website of the National Electrical Coordinator (Coordinador eléctrico nacional, 2018), and correspond to real past spot prices at the Temuco 220 kV busbar. The spot prices for 2035 were calculated from the results of the Long Term Energy Planning 2018 exercise, which uses the Ameba model for forecasting several energy scenarios until 2050 (Ministerio de Energia, 2019b). It uses a 27 busbar representation of the Chilean electricity system and approximates a year of operation by using 12 typical days (three per quarter) with each day's demand reduced to nine time periods (Ministerio de Energia, 2020g). Consistent with this approximation, the available spot prices correspond to only 12 representative days. Figure 5.4 shows the spot price for 2035 for the Pichirropulli busbar, located 150 km southwards of Temuco, and assumed to be the one with the most representative spot prices for Temuco, as Temuco busbar is not included among the 27 busbars of the model.

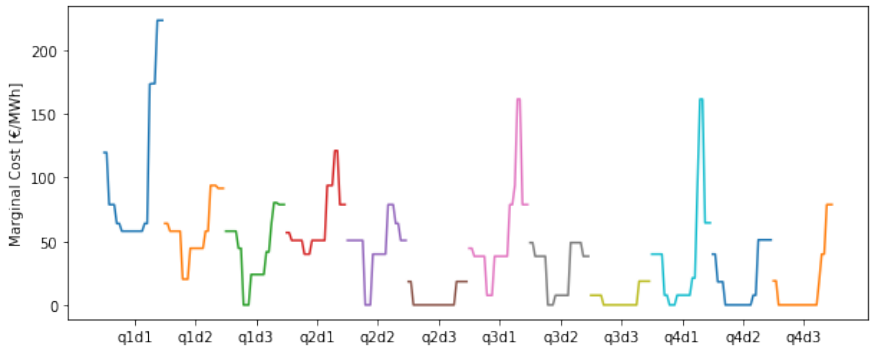

Figure 5.4: Spot prices for typical days in 2035 according to results from Ministerio de Energia (2020g)

In order to provide the simulation with a spot price for each hour of the year, these 12 days were expanded. First, the number of days in each trimester is increased from three to nine by interpolating between the initially available days. This produces a higher variety of days in each quarter, as shown in Figure 5.5.

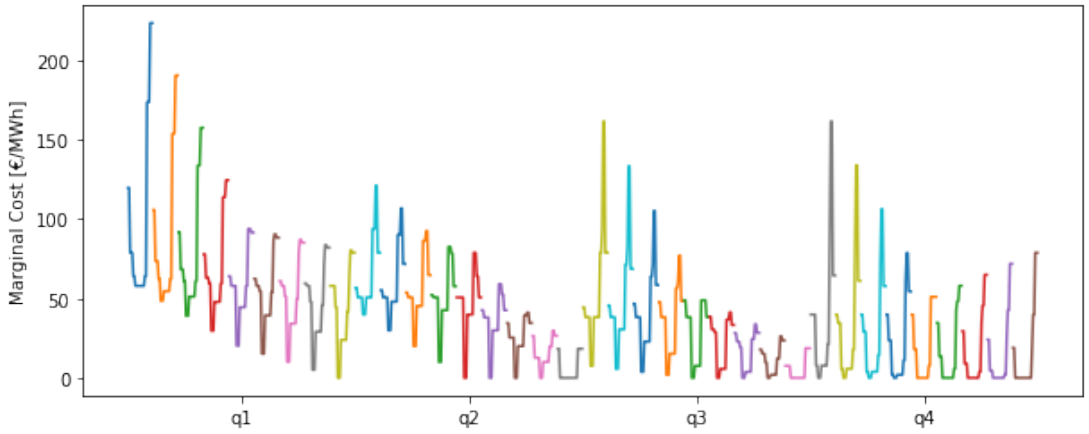

Figure 5.5: Expansion of typical days resulting from interpolating the days in Figure 5.4

Finally, the available days were combined by randomly picking days for each trimester within the available pool of days shown in Figure 5.5. In order to prioritise smoother transitions between contiguous days, a probability rule was imposed. Given the current day, different weights were assigned to each possible next day, based on its similarity to the previous. A random sampling process picked the next day based on these weights.

Figure 5.6 presents an example of weights assigned to the possible days of the first trimester assuming that the previous day was day $q1d4$.This approach generates a smoother annual spot price trend, producing a higher probability of contiguous days being similar, but still allowing large stochastic variations from days with low to days with high spot prices. This feature was implemented based on the assumption of the inter-day spot price variation largely depending on the availability of wind. This method has been proposed as a simple way to obtain a series of 8760 h of future spot prices based on limited available information.

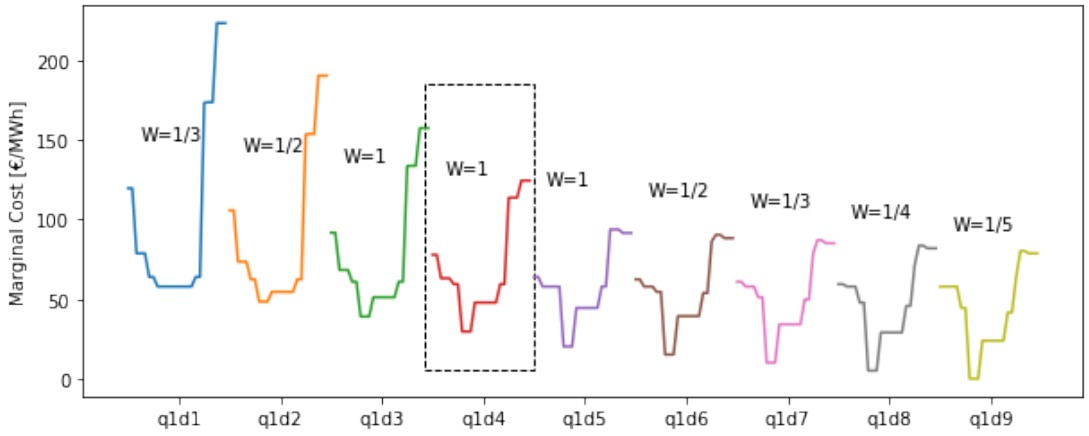

Figure 5.6: Example of probability weights used to expand the spot prices in 2035

This method can predict the average annual and seasonal spot price, as it uses typical days for four different periods of the year. It also can replicate the dependence of the spot price on the wind resource by keeping the average intra-day spot price dependent on the previous period. This follows the same logic of Markov chain methods for generating synthetic wind data (Carapellucci and Giordano, 2013; Mosayebian *et al.*, 2016).

One of the limitations of the modelling approach is that it does not produce any extreme spot price days. Therefore, days with 24 h zero marginal cost, or days without wind and with unusual high marginal costs due to other factors are not produced. This kind of day can realistically occur, although with low frequency. Furthermore, from the model perspective, any period with an extremely high spot price is treated in the same way as any other period with a spot price above the purchase threshold price (introduced in 5.2.1), thus excluding very high spot prices does not affect the model's output.

In the case of the emission factor, it was assumed that in 2035 the grid would emit 0.040 $kgCO_2/kWh$, assuming the value predicted by the mid-case scenario C projected by Ministerio de Energia (2020g).

5.2.2 Effects on the electricity system

For the analysis of the potential effect of the flexible demand provided by the DH systems integrating with electric heaters, it is required to compare its operation against a likely alternative scenario without the added flexibility. It will be assumed that the flexible integrated system is composed of a DH system operating with a HP (DH+HP). For the comparison, two alternative reference scenarios are considered. The first, where 50% of the total heating demand required by the development is supplied with individual heat pumps (which follows the projection of 50 - 70% of heating in Chilean apartments supplied by heat pumps by 2040 (Ministerio de Energia, 2020g)). The second, where the same proportion of the heat that would be supplied by the HP in the DH+HP system is supplied instead by individual heat pumps. As individual heat pumps have to increase the temperature only up to around 35°C, a COP of 3.8 is assumed for both reference scenarios.

The time of electricity purchase by the DH+HP system depends on the local spot price. Usually, it is assumed that the systems purchasing electricity are price takers, which means that the amount of energy bought is small in the context of the entire electricity grid and the equilibrium prices are not affected. However, as in this analysis the intention is to assess the possible impact of these DH+HP systems procuring electricity in a flexible way, the effect of the extra consumption of electricity will alter the electricity grid operation and therefore potentially modify the spot prices, which in turn, will modify the buying pattern of the DH+HP system. In consequence, an iterative process is required to calculate an equilibrium local spot price and electricity buying pattern.

The model used for assessing the impact of the new flexible electricity demand is based on the model developed in Chapter 3. As explained in Section 3.2, this model expands the installed generation capacity, transmission and storage of the system in order to fulfil a given demand while minimising the total cost. It allows the calculation of the spot prices in each node of the system at each hour for one year of operation. The spot prices calculated for the southernmost node (SICS) are then fed into the TRNSYS simulation model of the DH+HP presented in the previous section.[1]

The operation of one specific configuration of the DH+HP is simulated for one year. In the simulation model, the HP purchases electricity for its operation according to the local spot prices and the optimal threshold prices calculated previously (Section 5.2.1). At the end of the simulation, the time series of the energy purchased by the DH+HP system is used as an input in the Urbs electricity grid model as an additional demand. This demand is only fulfilled if the spot price (dynamically calculated by the model) at a given time step is equal to or lower than the price that the DH+HP is willing to pay (obtained from the

1. It is worth no note that these are not the spot prices produced in Section 5.2.1, as those are derived from an external source and can not be dynamically modified to represent the operational change of the electricity grid to fulfil the additional demand.

simulation of the DH+HP operation). The Urbs model is run again with this new additional demand, which eventually modifies the system's operation, bearing a different spot prices time series. Subsequently, this new spot prices series is used to run a new TRNSYS simulation and the whole process is repeated until the difference between the spot prices from two consecutive iterations approaches zero (or decreases below a certain threshold). This process is represented schematically in Figure 5.7.

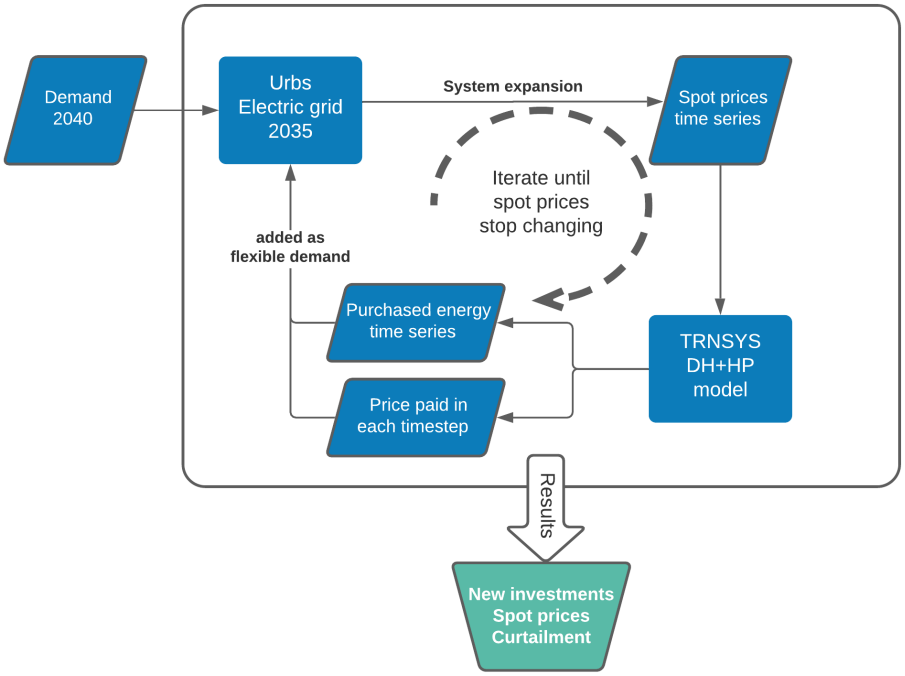

Figure 5.7: Diagram of the process used to evaluate the impact of the new flexible demand on the electricity system

The "purchased energy time series" corresponds to the energy that the simulated DH+HP decides to buy following the logic defined by the $Price_{purch}$ optimisation variable defined in Section 5.2.1. The "price paid in each timestep" refers to the actual price that the DH+HP system pays to the electricity provider, and it is 0 for the periods when no energy is purchased and equal to the spot price when the condition for buying electricity is met.

Figure 5.8 represents the the process described in Figure 5.7 from an economic perspective. It shows that the change in the demand, due to the electrification of part of the heat demand, creates a new equilibrium price P". The iterative method described above approximates to the value of P" by analysing how much (and in which periods) would the thermal system purchase electricity under the original P' spot prices (point P_1). The supply is then reassessed by adding

this additional purchased electricity (demand) to the Urbs electric grid model and assessing the new spot prices under these new conditions (point P_2 in the figure). The process is followed iterative under a point P_6 is reached and the variation in spot prices between one iteration and the next is small enough.

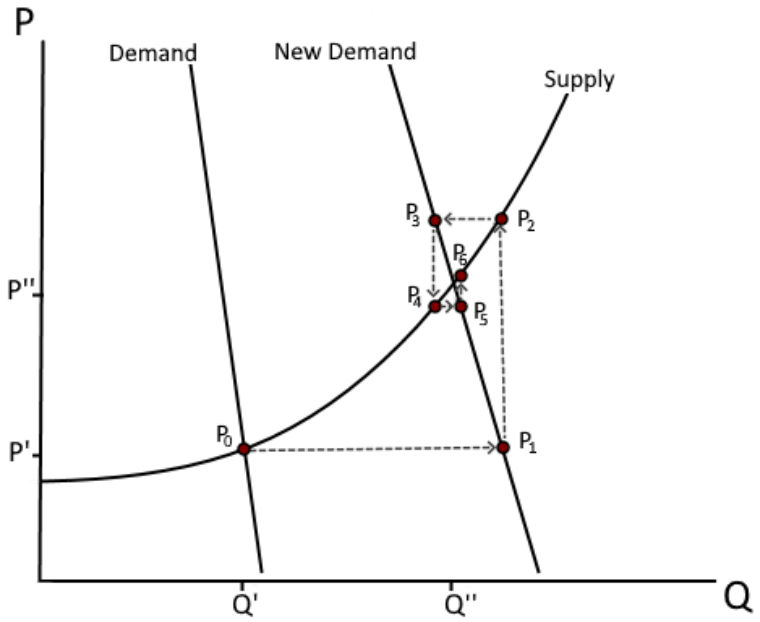

Figure 5.8: Representation of the proposed method from an economic perspective

As seen in Figure 5.7, the demand used in the electricity system's model corresponds to the year 2040, rather than 2035. This is done with the objective to force the system to expand and to see the effects of the added flexibility in this expansion. This might eventually change the supply curve in Figure 5.8, as the technology available for generation can change, but the method for approximating the new equilibrium price remains the same.

For assessing the convergence of the spot prices, the percentage of hours of the year with different spot price values between two iterations (PDSP) and the normalised root-mean square deviation (NRMSD), defined according to equation 5.3, were used.

$$NRMSD = \frac{\sqrt{\frac{\sum_{t=1}^{8760}(SP_{t,i} - SP_{t,i-1})^2}{8760}}}{SP_{i,max} - SP_{i,min}} \tag{5.3}$$

where SP is the spot price, i represents the number of iteration and t each hour (time step) of the year.

After reaching the equilibrium spot price, the effects of the extra flexible demand on the electricity system are compared with a scenario where the demand required to provide heat is not flexible. For this, the two alternative reference scenarios mentioned at the beginning of this section are considered.

Model of the electricity system

As the official model used by the Ministry of Energy (Ameba) is not publicly available, it is not possible to iterate over that model as proposed in Section 5.2.2. Therefore, the spot prices obtained according to Section 5.2.1 are not used in this part of the analysis. Instead, as mentioned in the previous section, an adapted version of the model defined in Section 3.2 and Figure 3.1, was used. This model was modified with the objective to produce spot prices with higher granularity. The main modifications were the disaggregation of the thermal generation technologies by variable cost of generation within each node. The variable operational costs and generation capacity of each technology in each node were defined according to the 2020 actualisation of the Energy Planning Process 2018, considering the scenario C with medium demand growth and average hydrology (Ministerio de Energia, 2020g). The details of the configurations of each node and the variable costs used for each technology are presented in Appendix F.

The demand used for the simulation corresponds to the medium demand projection scenario for the year 2040. The use of this year is to force the system to expand to meet the demand and to simulate how DH+HP systems built in the 2035-2040 period would affect the systems' expansion by the end of the 5-years period.

Other than the generation capacities, the model was modified with the addition of a direct transmission line connection between the node SING and SICC. This DC connection, planned to be in operation by 2030 would allow a 2,000 MW transmission capacity from the solar resource-rich northern node to the zones of highest energy demand. The other transmission lines (SING-SICN, SICN-SICC, SICC-SICS) were kept at 2000 MW of capacity, and a 90% efficiency of transmission was assumed.

5.3 Results and discussions

This section presents the results of applying the methodological changes presented in Section 5.2 to the model introduced in Chapter 4 and discuses their implications on the techno-economic analysis of the DH networks and potential effects on the electricity system development thanks to the provision of additional demand flexibility.

5.3.1 Spot prices for 2035

Figure 5.9 presents the result of applying the method described in Section 5.2.1 for the entire year on the SICS node and compares it with the spot prices used for 2020, while Figure 5.10 and Table 5.2 compare the distribution of the spot price during every hour of both years.

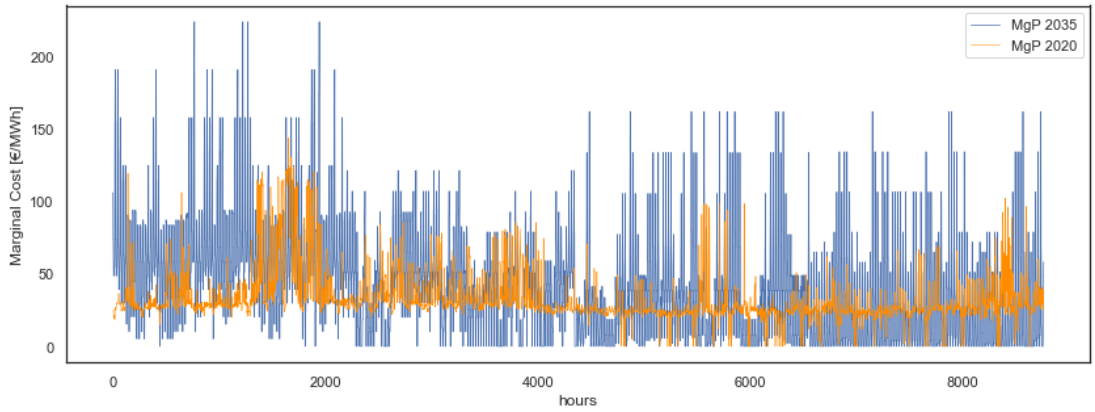

Figure 5.9: Spot prices for 2035 in the SICS node constructed based on Ministerio de Energia (2020g)

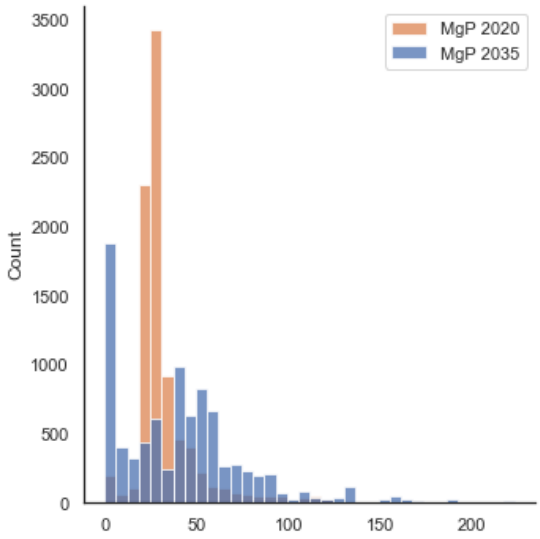

Figure 5.10: Histogram of hourly distribution of spot prices for in 2020 and 2035 in the SICS node

	2020	2035
mean	32.3	41.2
max	143.5	223.5
variance	303.4	1230.1
zeros	133	1187

Table 5.2: Main statistical characteristics of the spot prices in 2020 and 2035 in the SICS node

From these results, it can be summarised that the spot price synthesised for 2035 is on average higher and presents higher variability than in 2020. This is due to the much higher penetration of intermittent generation in 2035, which reaches around 69% of the installed capacity, in comparison to the 36% present by 2020. However, as shown in Figure 5.10, the spot prices in 2035 present a larger proportion of days with zero (or close to zero) prices of electricity, which makes it more suitable for technologies that would take advantage of lower spot electricity prices, such as the DH+HP system proposed in this study.

5.3.2 Electricity integration effects on the DH system

In contrast to Section 4.3.2, the optimisation process with more variables did not converge fast in each case. In some occasions, it was found that the optimisation did not improve the Pareto front after several iterations. This was evidenced even if some clear irregularities or voids (areas of the curve without points) were apparent in the Pareto curve. This suggested possible better configurations might be achieved but the optimisation algorithm was not exploring them. It was found that identifying a pair of "good" points surrounding the area where the solution space was not being explored, and adding configurations resulting from linear interpolations between the values of the variables of those two points, led to an improved Pareto front. Although this process was performed manually, there is potentiality to implement this process into DEAP and to improve the convergence of the optimisation algorithm. This is further discussed in Appendix E.

The results of the optimisation for the system including the electric heaters is presented in Figure 5.11 for the conditions in the year 2020. This figure shows that under the conditions in 2020, there is no economic nor environmental advantage for using resistance heaters and there is limited potential for using heat pumps. The main causes of this are the relatively low number of hours with low spot prices (as shown in Table 5.2), and high emission factor of the electric grid in 2020 (as shown in Table 4.8). This means that, under the system configuration in 2020, the heat supplied presents embedded emissions close to 0.25 $kgCO_2/kWh$ when

supplied by a resistance heater and close to 0.1 $kgCO_2/kWh$ if supplied by a heat pump (for an average annual COP between 2.4 and 2.8). On the other hand, as shown in Figure 5.12, the addition of resistance heaters, and especially heat pumps, contributes substantially to the decrease of emissions and cost of the heat supplied for conditions in 2035.

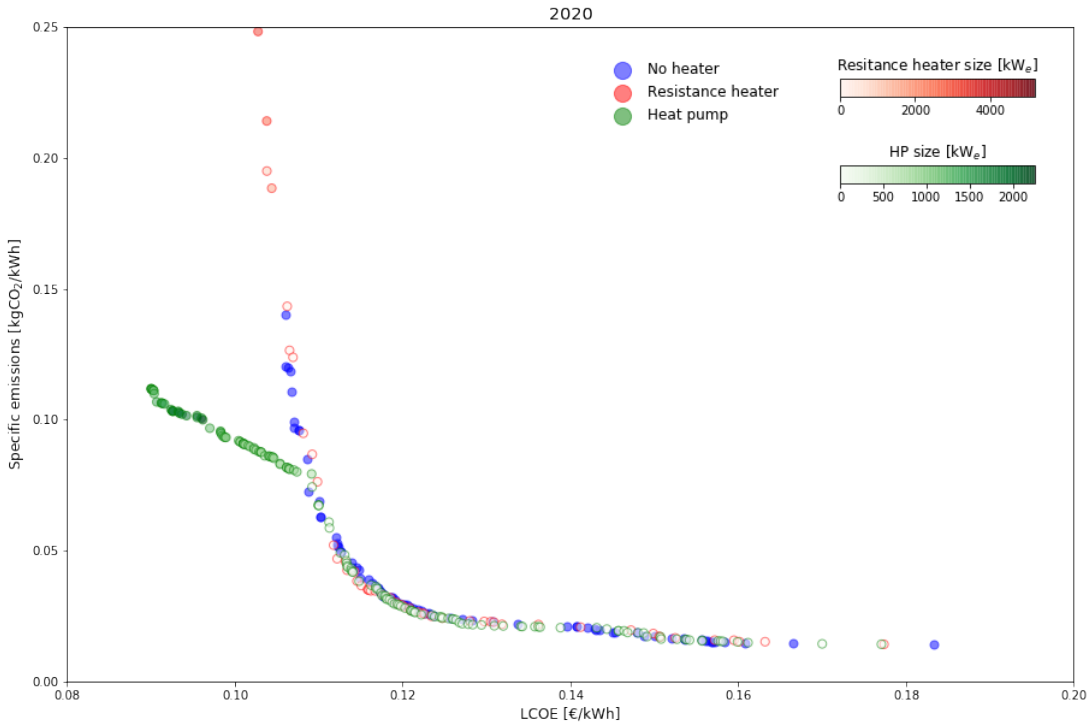

Figure 5.11: Comparison of Pareto fronts resulting for the optimisation of the system with resistance heater, heat pump, and without electric heating for the conditions in the year 2020

From Figure 5.12 it is clear that in 2035 the conditions for using electricity from the grid when prices are low are better than in 2020. For all the configurations there is a decrease in emissions. This is due to the decrease in emission factor of the grid from 0.25 $kgCO_2/kWh$ in 2020 to 0.04 $kgCO_2/kWh$ in 2035, which lowers the emissions associated to water circulation. The figure also shows that under conditions assumed for 2035, using a resistance heater allows for substantial additional decrease in emissions and pushes the minimum LCOE below 0.10 €/kWh. However, this improvement is greatly increased if coupling the system with a heat pump instead of a resistance heater, reaching costs of heat below 0.09 €/kWh with emissions under 0.02 $kgCO_2/kWh$. Therefore, the focus of the further analysis will stay on the case integrating a heat pump (DH+HP).

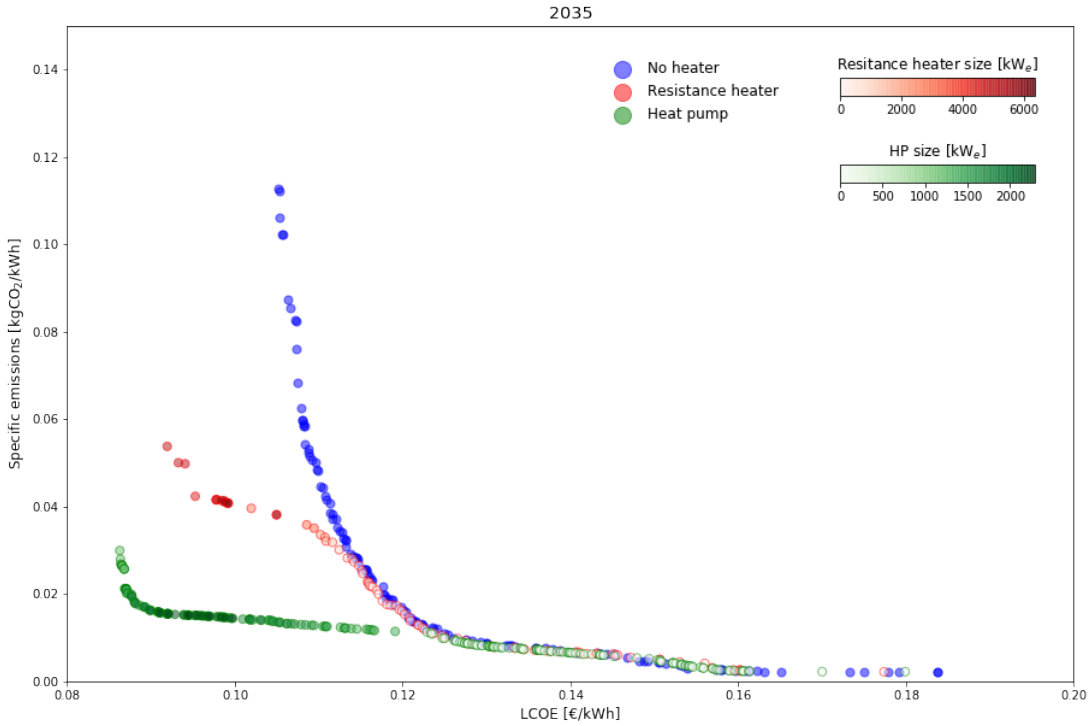

Figure 5.12: Comparison of Pareto fronts resulting for the optimisation of the system with resistance heater, heat pump, and without electric heating for the conditions in the year 2035

Figure 5.13 presents the evolution of the optimisation variables for the different configurations in the Pareto front for the DH+HP system in 2035. It shows that the optimal configurations consist of systems with no LTS (for cheaper systems with higher emissions) or systems with LTS larger than 400,000 m^3. Interestingly, there are no systems that present both LTS and heat pumps. This means that the heat supplied by the heat pump is used for supplying the immediate demand, or at least demand on the same day, as the STS is in the range of 5000 m^3 and has capacities of around 15 hours at peak demand.

Considering a controller based on a single threshold price for purchasing energy around the year might not be cost-efficient, as it forces the system to buy energy at the same rate throughout the year regardless of the demand. This would not be a major problem if the LTS were in use, but as clearly shown in Figure 5.13, there are no cases with heat pump and LTS operating together. Therefore, an alternative considering different purchase prices for the coldest and hottest halves of the year ($Price_{purch_W}$ and $Price_{purch_S}$) were considered. Figure 5.14 compares the optimal configurations considering one and two different threshold prices for purchasing electricity with a heat pump. It shows that considering two different threshold prices decreases the emissions by around 15%.

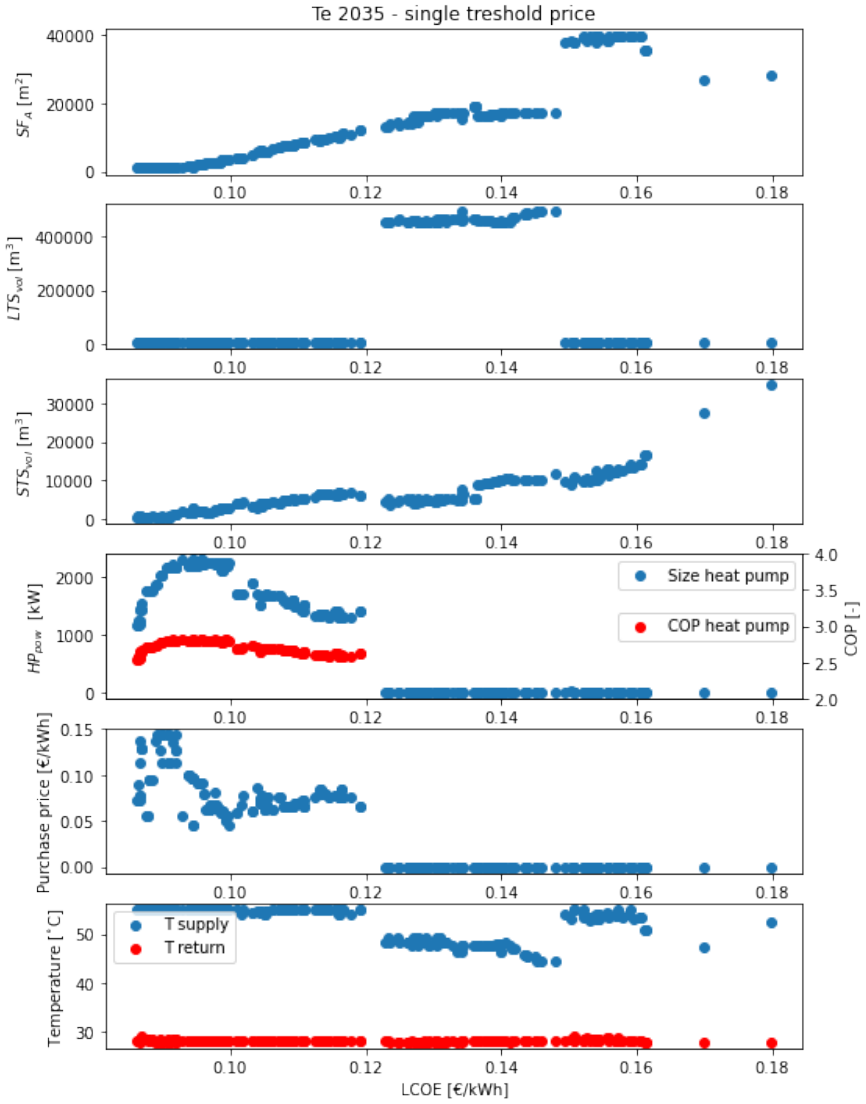

Figure 5.13: Values of optimisation variables and performance indicators for the systems along the Pareto front for the system with heat pump (DH+HP) for the conditions in the year 2035

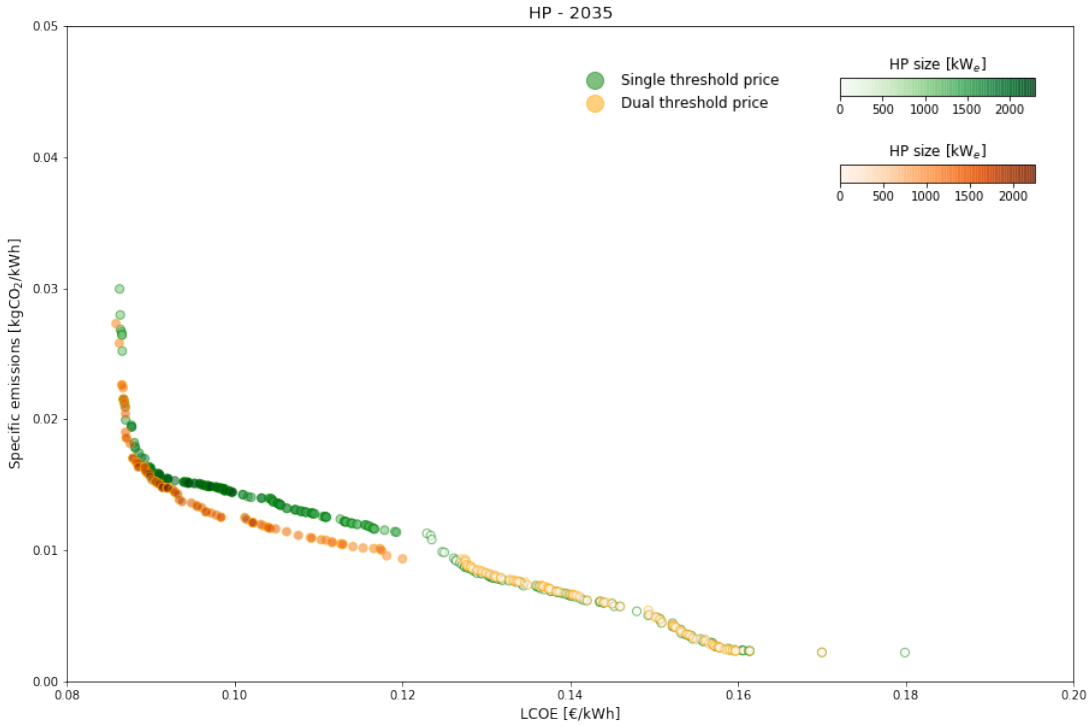

Figure 5.14: Comparison of Pareto fronts resulting for the optimisation of the system using heat pumps, fixing one threshold cost for electricity purchase, and fixing two annual threshold prices, for the conditions in the year 2035

Figure 5.15 presents the evolution of the optimisation variables for the different configurations in the Pareto front for the case with HP in 2035, but considering two different threshold prices in this case. From it, it can be seen that $Price_{purch_W}$ is similar to that in Figure 5.13 (between 0.05 and 0.1 €/kWh). However, $Price_{purch_S}$ decreases almost to zero, as the SF is capable of providing most of the demand in the hottest half of the year. For LCOE < 0.09, $Price_{purch_S}$ increases to around 0.025 €/kWh, because for these configurations it is more effective to rely on the heat pump to supply the summer demand and to have a minimum solar field (or no solar field at all).

5.3.3 Analysis of operation of specific configurations with LTS and HP

In order to understand possible reasons why the optimal configurations never include systems with both HP and LTS, three points have been selected in Figure 5.16.

T_x corresponds to a Pareto optimal configuration with a 1,310 kW heat pump, but almost no LTS. T_y corresponds to a Pareto optimal configuration with a large LTS but with very small HP, while T_z corresponds to a sub-optimal configuration with a performance similar to T_y and with both LTS and HP operating together.

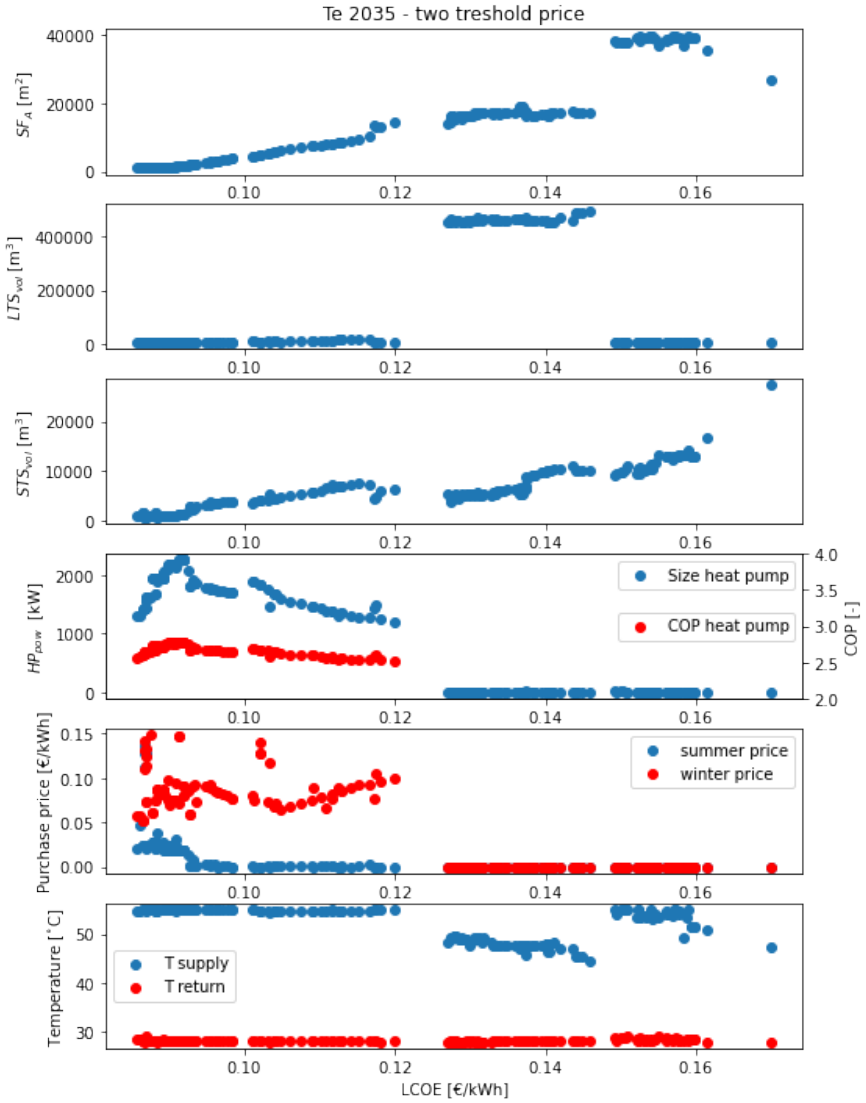

Figure 5.15: Values of optimisation variables and performance indicators for the systems in the Pareto front for the system with heat pump for the conditions in the year 2035

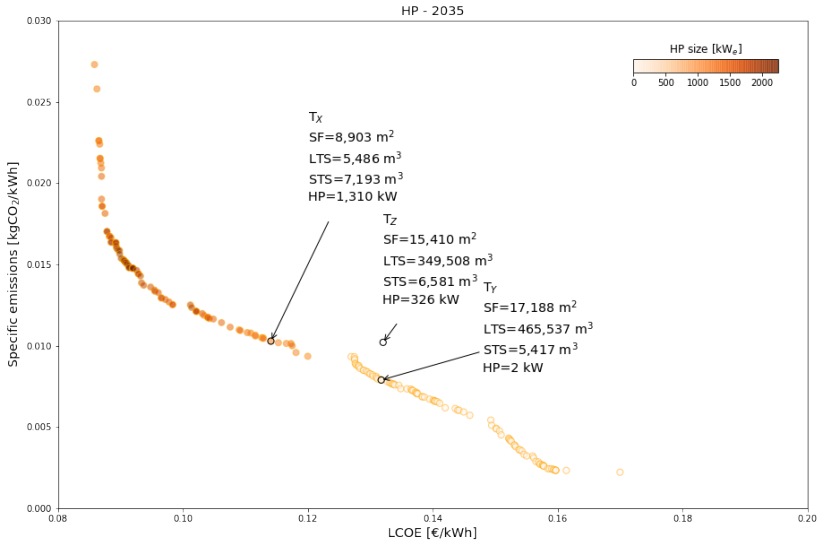

Figure 5.16: Points selected for operation analysis

Figure 5.17 presents Sankey diagrams of the annual energy flows for the three points. It is clear that for T_x, the SF provides most of the heating requirements in the sunniest part of the year, while the HP provides the heating in winter, without the need of relying on an LTS to accumulate energy for the cold season. This is evident from the seasonal threshold prices used by the HP: below 1 €/MWh in summer, and 89 €/MWh in winter, which results in the HP not buying any electricity in the sunniest season, and in it willing to pay relatively high prices for purchasing electricity in the winter season. In the case of T_y almost all the heat is supplied by the solar field, which requires a large LTS to provide heat in winter where the demand is higher and the solar resource less abundant. T_z presents an intermediate case to T_x and T_y, as it has a smaller HP than T_x and a relatively smaller LTS than T_y. The main source of heat is still provided by the SF with support of the LTS, however, around 5% of the heat is supplied by the HP.

Figures 5.18, 5.20 and 5.21 present details of the operation of system configurations T_x, T_y and T_z for a week in winter and in summer. For heat flows, presented in continuous lines on the left axis, negative values mean energy flowing out of the system, such as the heating demand and the charging of the LTS, while positive values mean flows into the system, such as that from the SF, heat produced by the HP and the discharge of the LTS. Temperatures of the STS and LTS are presented as dashed and dotted lines respectively and are read on the right axis. $T_{STS_{top}}$ and $T_{STS_{bot}}$ correspond to the temperatures at the top of the hot STS tank and at the bottom of the cold STS (hottest and coldest temperatures in the STS, respectively). $T_{LTS_{ctr}}$ corresponds to the temperature close to a borehole in the centre of the LTS, while $T_{LTS_{avg}}$ corresponds to the average temperature of all the soil volume of the LTS.

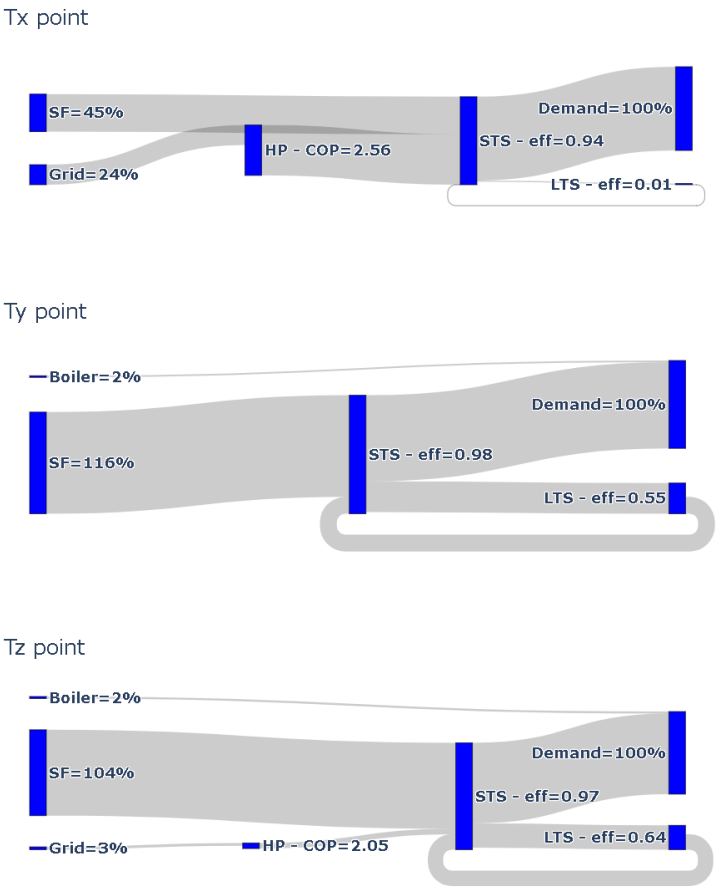

Figure 5.17: Sankey diagrams for selected points selected for operation analysis. All the energy values are presented as percentages in reference to the total annual demand (100%)

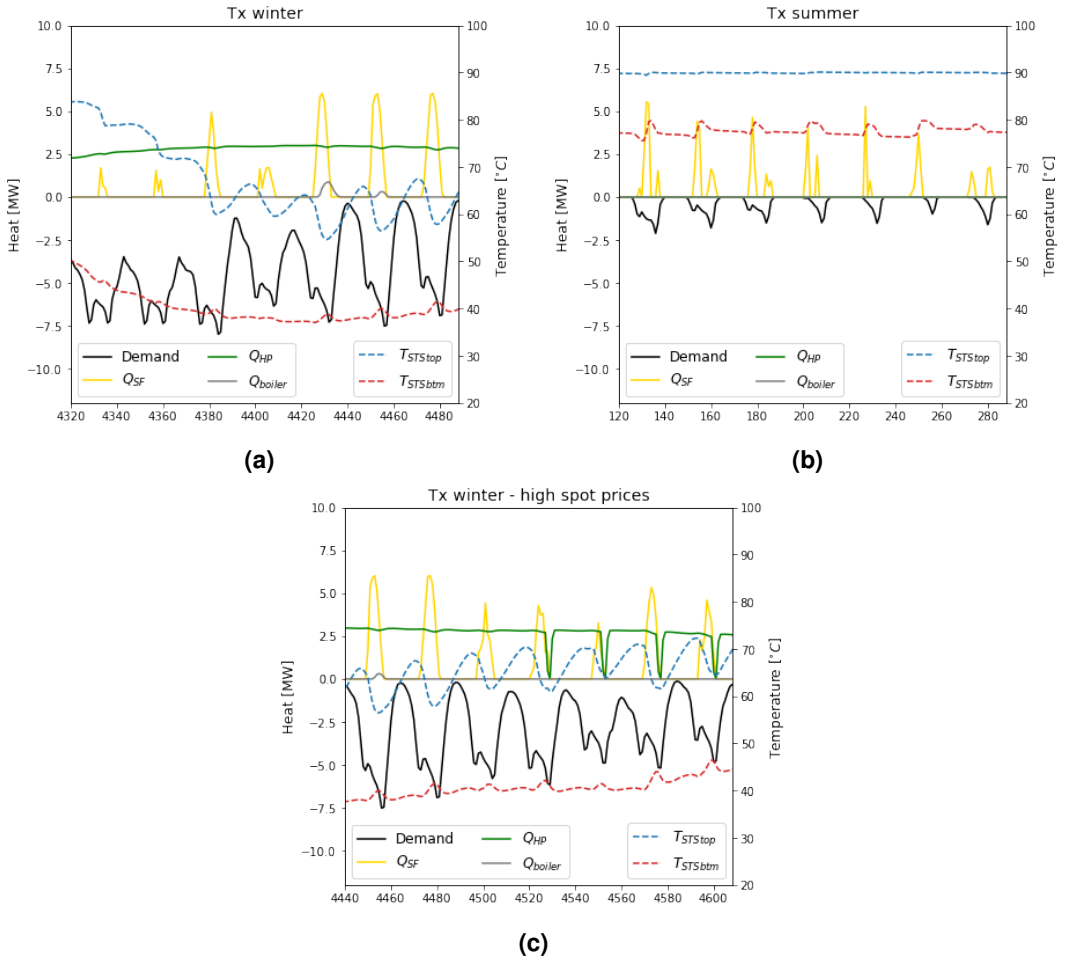

Figure 5.18: Detail of energy flows and storage temperatures of the system configuration T_x for (a) a cold week in winter, (b) a week in summer and (c) a winter week with especially high spot prices

From Figure 5.18a, it can be seen that in general, in winter, the heat is supplied mainly from the HP, which operates constantly and close to its maximum capacity during the selected week, which explains the high threshold purchase price in winter (89 €/MWh). The gas boiler supports the system when $T_{STS_{top}}$ drops approximately below 58°C, at which point there is not enough enthalpy in the stored water to produce water at 55°C in the DH loop. This operation contrasts with the case of a week with high spot prices (Figure 5.18c), when the HP stops its operation for hours when the spot prices are above 100 €/MWh, while the system remains in operation thanks to the flexibility provided by the STS and with no need of using the gas boiler. In summer, on the other hand, the SF provides all the energy required for fulfilling the demand, which explains the low threshold purchase price for the HP in this season (1 €/MWh). Figure 5.19 shows that for this configuration the HP operates for around 60% of the hours of the year, with few of them at close to maximum capacity, which achieves a yearly average capacity factor of 0.24.

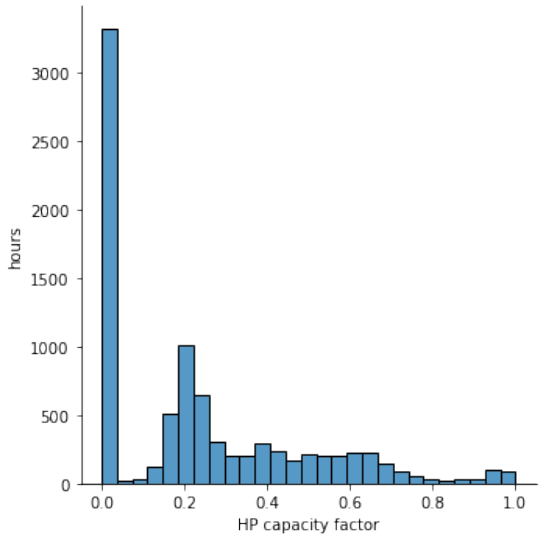

Figure 5.19: Annual distribution of the HP operation capacity factor for configuration T_x

From Figure 5.20a it can be seen that during the winter week with high thermal demand, the heating requirement is fulfilled by a combination of the SF, the LTS and the boiler, with the last turning on when $T_{STS_{top}}$ drops approximately below 51°C, at which point there is not enough enthalpy in the stored water to produce water at 49°C in the DH loop. The LTS discharges energy to the STS for most of the week, only stopping when the $T_{STS_{top}}$ reaches 55°C. In summer, the demand is fulfilled completely by the SF. It is interesting to notice that in the week selected for the case in summer (which represents days in early January), the LTS is not charged, as according to the summer charging rule presented in Table 4.5, the LTS charge starts when $T_{STS_{top}} - T_{LTS_{ctr}} \geq 10$°C, and from the figure it can be seen that the condition is not met. The suitability of this condition and how it may impact the performance of the LTS is further disused in the next section.

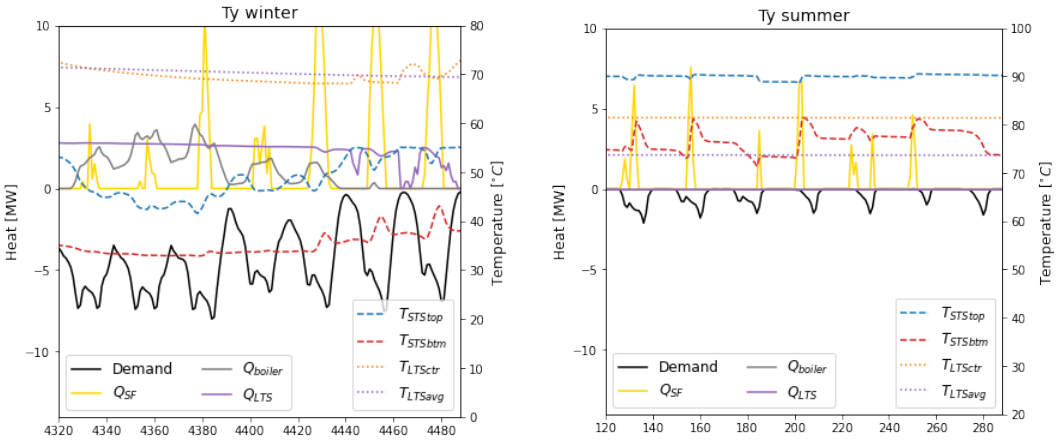

Figure 5.20: Detail of energy flows and storage temperatures of the system configuration T_y (a) in winter and (b) in summer

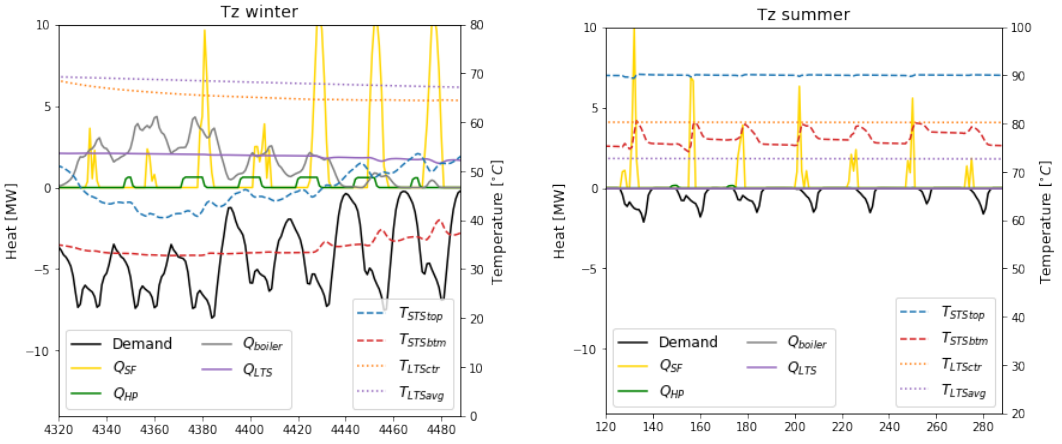

Figure 5.21: Detail of energy flows and storage temperatures of the system configuration T_z (a) in winter and (b) in summer

Figure 5.21a shows that during the high heating demand period, similarly to configuration T_y, most of the energy is supplied by a combination of the SF, the LTS and the boiler. However, in this case, the reduction in LTS decreases its share of heat supply, and it is replaced by a higher participation of the boiler and the occasional provision of heat from the HP, which in this case has a winter threshold price of 9 €/MWh (hence, only operates when spot prices are below 9 €/MWh). In summer (Figure 5.21b), the system behaves almost identically to T_y, with the LTS not being further charged. In this case, the HP purchases electricity a few hours as the purchase threshold price in summer is 23 €/MWh, therefore it should operate more hours in this period of the year, however, the amount of energy purchased in each occasion is small. This is due to the fact that the HP has been modelled as a fixed flow rate system

(as explained in Section 5.2.1), which aims to deliver an output temperature of 90°C, using its rated power when $T_{STS_{btm}}$ is minimum ($\approx$ 32°C), and modulating its power output when $T_{STS_{btm}}$ is higher. This means that in periods of low demand and abundant sunshine, when $T_{STS_{btm}}$ is high ($\approx$ 75°C in this case), the HP only requires around 25% of its rated power.

Figure 5.22 shows that for this configuration the HP only operates less than 35% of the year (explained by the relatively low threshold purchase prices), which leads to an annual average capacity factor of 0.12. This, added to the fact that the decreasing COP and increasing cost/kW for smaller HP, leads to these kinds of configurations not being selected by the optimisation process. Possible options to improve the utilisation of the HP and LTS in summer are discussed in the next section.

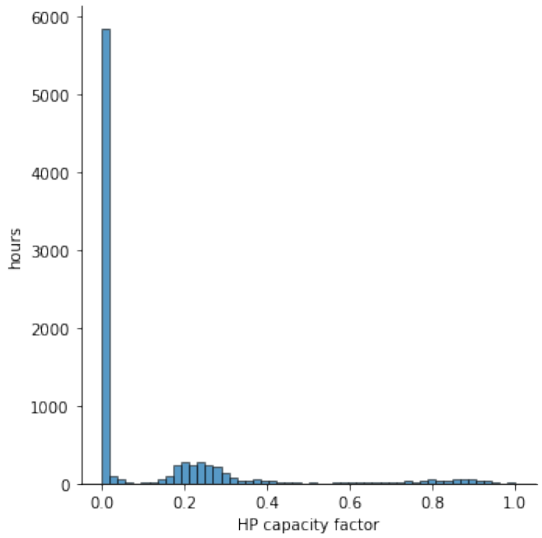

Figure 5.22: Annual distribution of the HP operation capacity factor for configuration T_z

Figure 5.23 presents the cost structure of some of the configurations in the Pareto front in Figure 5.16, with the selected points highlighted (including the addition of point T_z, for comparison). It allows to compare in more detail the cost structure of the different optimal configurations. From it, it can be verified that cheaper systems tend to rely almost exclusively on HP. However, they also require more significant use of fuel in winter times; hence they have higher emissions. To achieve lower emissions, larger SF have to be added, which reduces the size of the HP but ends up increasing the investment cost (as can be seen with T_x). To decrease the emissions even lower, the SF are increased further, but in this case, it is more cost-efficient to include a large LTS instead of using a HP (as can be seen with T_y). Similarly to the results from Chapter 4, Section 4.3.2, the lowest emissions are achieved by oversizing the SF in order to let it cover most of the annual demand, eliminating the need of the LTS and by using a comparatively larger STS with capacities of around 3-4 days for maximum demand and two weeks at average annual demand.

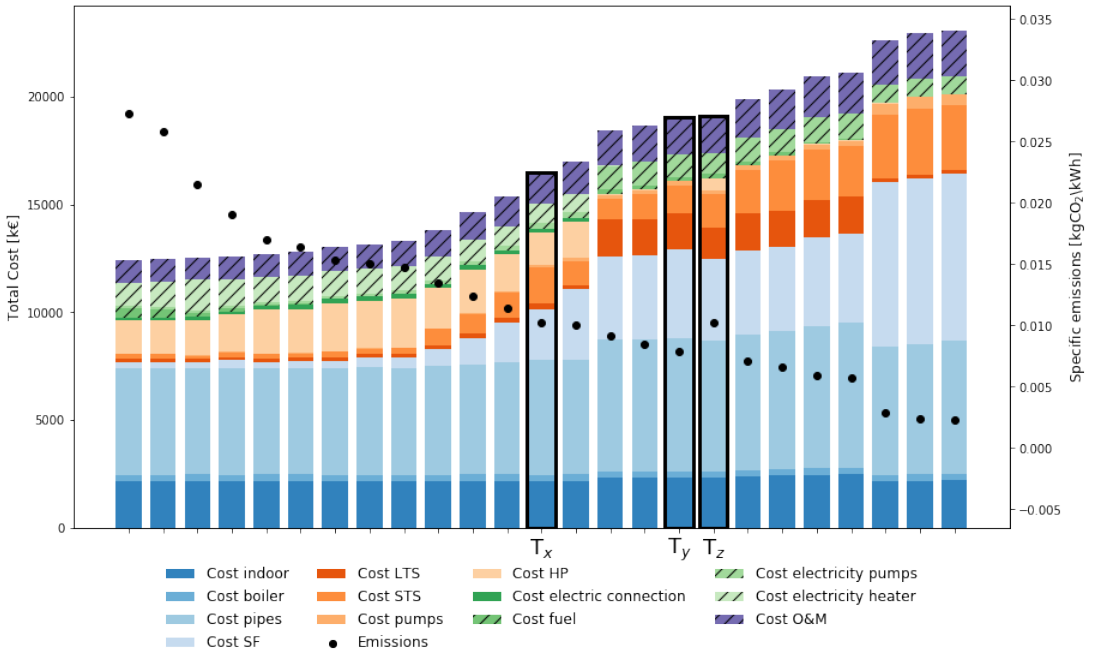

Figure 5.23: Cost structure of all the system configurations in the resulting Pareto front for the case with heat pump and two threshold purchase prices

Analysing the impact of the summer charging rule on the LTS operation

As it was pointed out in the previous analysis, the summer rule for turning on the charging ($T_{STS_{top}} - T_{LTS_{ctr}} \geq 10°C$) may be hindering the charging of the LTS when the sun is most abundant. With the objective of discussing this rule and proposing possible improvements to the control logic, a case that modified the rule to start charging when $T_{STS_{top}} - T_{LTS_{ctr}} \geq 4°C$ and one with charging starting when $T_{STS_{top}} \geq T_{LTS_{ctr}}$ were run for configurations T_y and T_z (those with LTS). In this section these cases will be labelled as T_(10), T_(4) and T_(0), respectively. The results are presented in Figures 5.24 and 5.25. In the case of Figure 5.24, it presents the same week in early January than the analysis in the previous section. For the case of T_z, Figure 5.25 shows the week when the rule from winter charging changes to summer charging (hour 8016 of the year). To illustrate better the thermal dynamics in the charging process, the temperature of the soil close to a borehole on the edge of the LTS ($T_{LTS_{edg}}$) was added to the plots. During the charging process, the location where this temperature is measured represents the last point where some heat exchange happens between the water and the storage.

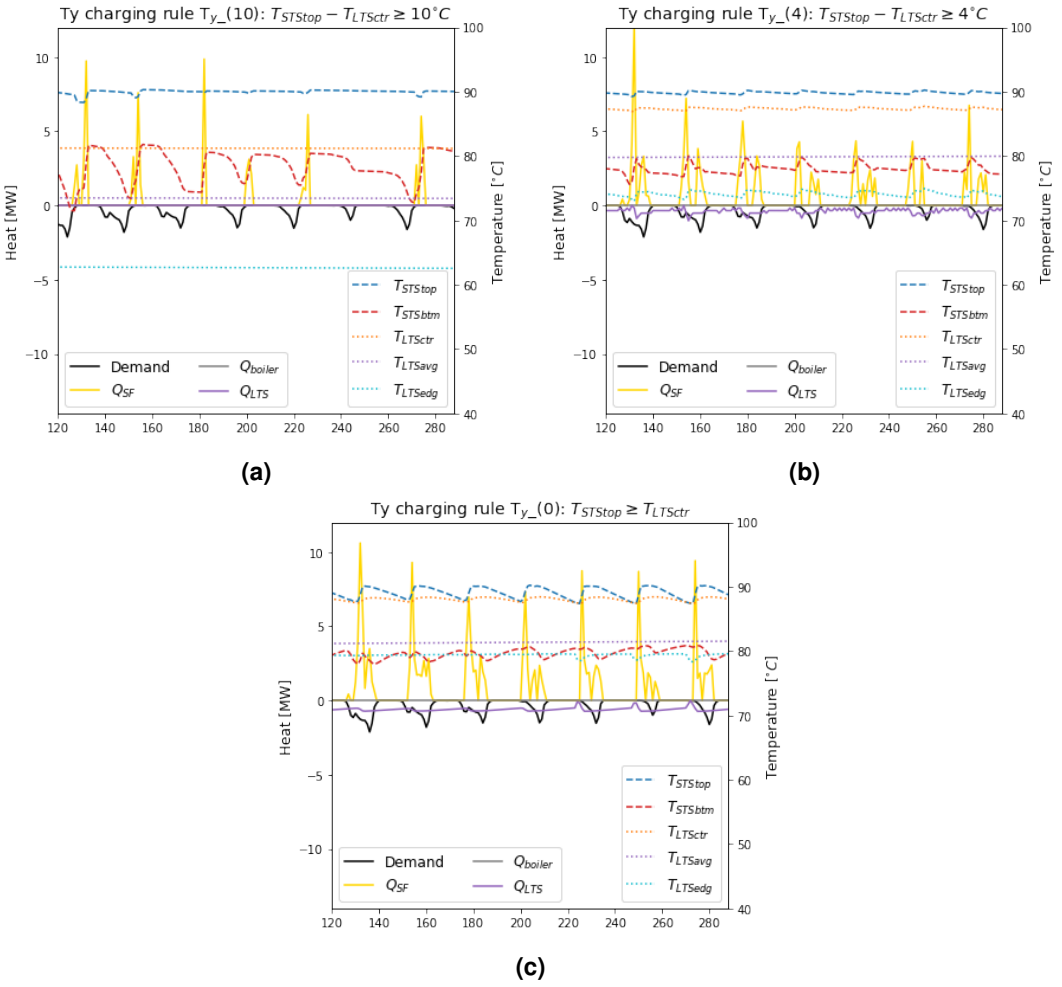

Figure 5.24: Detail of energy flows and storage temperatures of the system configuration T_y for (a) a summer week under the original summer charge rule with $T_{STS_{top}} - T_{LTS_{ctr}} \geq 10°C$, (b) changing the summer rule to $T_{STS_{top}} - T_{LTS_{ctr}} \geq 4°C$, and (c) without the summer charge constrain

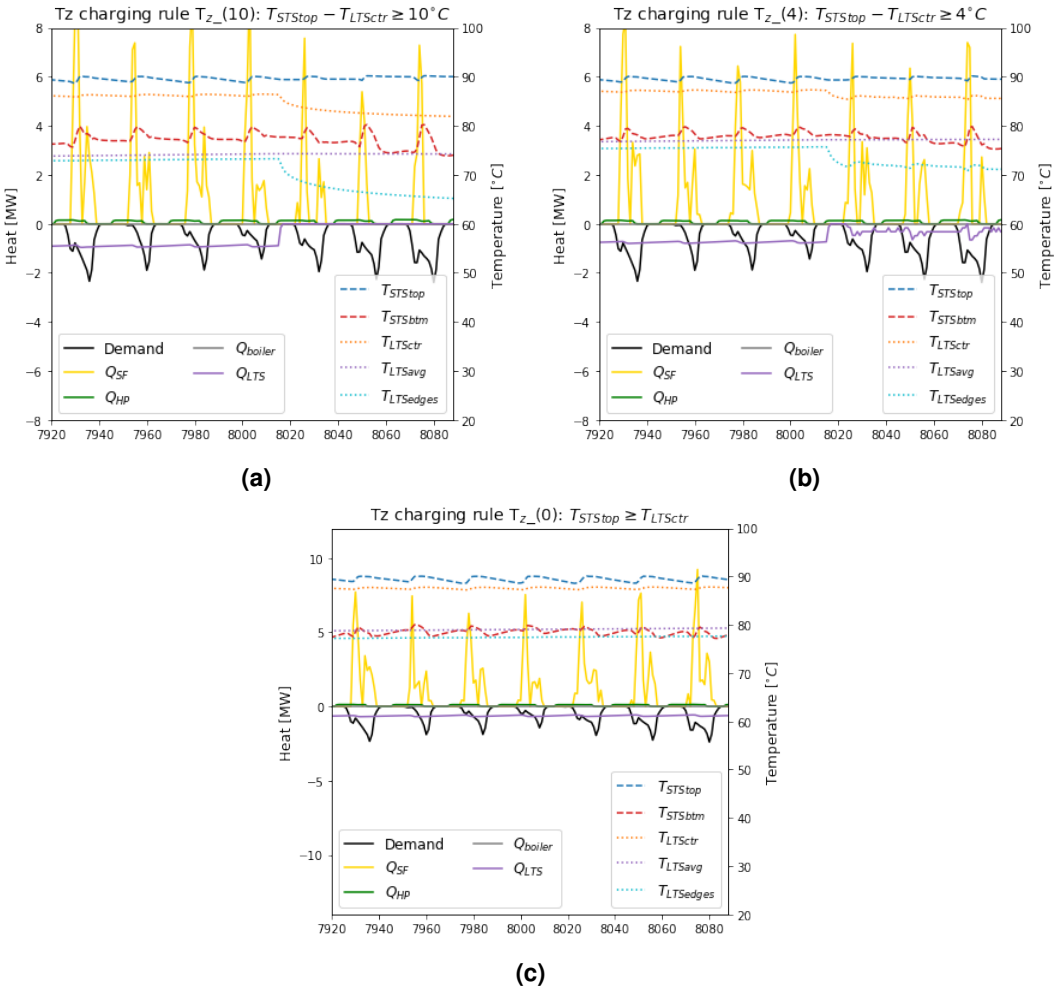

Figure 5.25: Detail of energy flows and storage temperatures of the system configuration T_z for the week when the rule changes from winter so summer, (a) under the original summer charge rule with $T_{STS_{top}} - T_{LTS_{ctr}} \geq 10°C$, (b) changing the summer rule to $T_{STS_{top}} - T_{LTS_{ctr}} \geq 4°C$, and (c) without the summer charge constrain

From both figures, it is evident that changing the rule allows for further charging the LTS. However, the rate of charge is low, as it is still driven by the temperature difference between the hot water at the top of the STS (usually at 90°C) and the temperature in the LTS close to the boreholes $T_{LTS_{edg}}$ and mainly $T_{LTS_{ctr}}$. From this, it follows that the higher is the state of charge of the LTS, the lower is the rate of charge of the system, which agrees with experimental findings by Guo *et al.* (2020), that concluded that there is a linear relationship between the heat-injection rate and the temperature difference between the inlet water and the $T_{LTS_{avg}}$. This behaviour is clearly appreciated in Figure 5.25, where in the case of T$_{z_}$(0) (Figure 5.25c), the charging rate does not change after hour 8016, however, it is lower compared to T$_{z_}$(10) and T$_{z_}$(4) (figures 5.25a and 5.25b). This is because a higher rate of charge means the LTS will be in general at a higher temperature, as can be seen in Figure 5.26. This figure presents the evolution of the temperature inside the LTS during the entire year for the three charging rules

for T_z. In it, $T_{LTS_{avg}}$ represents the average temperature of the entire storage volume, and it is a good representation of the energy stored inside the LTS. The other two parameters represent the temperatures of the soil in points very close to a borehole located in the central area of the LTS ($T_{LTS_{ctr}}$) and to a borehole located on the edge of the storage ($T_{LTS_{edg}}$). The values of these two temperatures are much more variable than $T_{LTS_{avg}}$, as they are highly influenced by the temperature of the water flowing through the LTS during the charging and discharging processes.

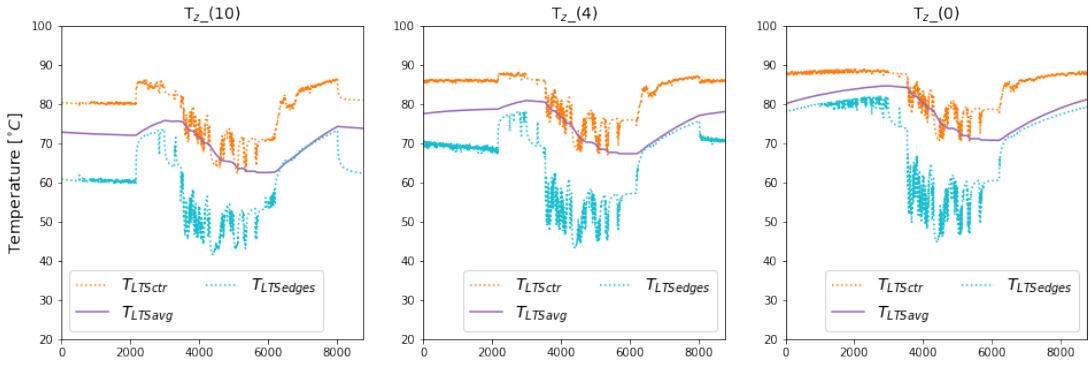

Figure 5.26: Detail of the temperatures of the system configuration T_z for the entire year for the three compared LTS summer charging logics

From the previous analysis, it seems logical that changing the summer charging rule to T_(0) seems to be a sensible approach to improve the performance of the system, as it allows for a higher charge of the LTS with higher internal temperatures and eventually a better utilisation of the stored energy. However, this is not necessarily true, as charging the LTS requires the operation of a water circulation pump, which operates at a constant flow rate and with a lower rate of charge, more units of pumping electricity would be required for every extra unit of heat delivered to the LTS. This can be corroborated in Figure 5.27, that presents the objective functions (LCOE and SE) for the three variations of summer charging logic. From the figure, it can be noticed that for T_y, there is a decrease in emissions when using less restrictive charging logic for summer, which is due to the decrease of winter usage of the boiler due to the higher state of charge of the LTS. However, in doing so, the LCOE increases due to the much higher usage of the pump for charging the storage. In fact, the average annual amount of electricity required to deliver a unit of heat into the storage increases from 0.012 kWh_e/kWh_{th} for T_y_(10) to 0.020 kWh_e/kWh_{th} for T_y_(0). In the case of T_z, it is clear that changing the rule to T_(4) improves both objective functions. Therefore, T_z_(4) is a better option than T_z_(10). As it seems complex to know *a priori* the best summer charging strategy for each configuration, the parameters defining this strategy might be added as optimisation variables. Nonetheless, it will increase the optimisation time and the improvement will not solve the problem of the slow charging of the LTS.

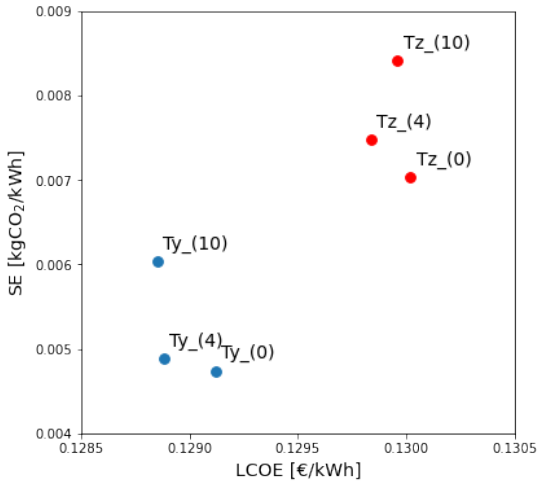

Figure 5.27: Annual techno-economic performance of configuration T_y and T_z under the different variations of the summer charging rule

With regards to the energy purchase logic of the HP, it is clear from Figure 5.14 that considering two different threshold purchase prices is better than using a single one for the entire year. It is expected that further allowing more purchase threshold prices for different periods of the year would improve the economic results, as it would represent more precisely the temporal value of the energy purchased by the HP by considering the availability of solar energy and capacity of using or storing the purchased energy in each short period, rather than using an average over several months. However, implementing this with the current approach would require to use an independent optimisation variable for each period, which would make the optimisation problem impractical to solve. Another limitation of the current approach also assumes a good prediction of the annual (or biannual) average spot prices behaviour, which is affected by many uncertainties and requires information of the grid expansion and operation that may escape the operator of the DH+HP. Considering this analysis, it is hypothesised that a better approach that could be tested in the future would be to use a predictive control logic that would consider the state of charge of the storage systems and day-ahead weather forecast for demand and solar heat estimation, similar to the one proposed by Lizana *et al.* (2018a).

From the analysis of the operation of the system (Figures 5.20 and 5.18), it is clear that the rate of charge is highly limited by the rate at which the heat dissipates from the contact point of the borehole and the hot water stream towards the interior of the storage. This process is restricted by the relatively low conductivity of the soil used in the simulations (0.9 W/m^{2}K). It is possible that considering a higher conductivity would increase the LTS charging rate, as shown by Catolico *et al.* (2016). However, this effect is limited, and it will also increase the heat losses, decreasing the fraction of heat recovered when discharging the system. Also, as suggested by Skarphagen *et al.* (2019), reducing the distance between boreholes

would increase the heat transfer rate allowing for higher charging rates, but it would also decrease the volumetric storage capacity of the system and would increase its cost. Another option proposed by Lim *et al.* (2020) to increase the heat exchange rate is to modify the inlet position of the hot water towards boreholes farther from the centre during charging. This would increase the average temperature difference between inlet water and borehole. However, as shown in Figure 5.26, even the temperature of the borehole at the edge is well above 70°C at the end of the charging season; therefore, the improvement of the charging rate would probably be limited. It seems clear that systems that do not rely on soil conduction for the charging process can reach higher charging rates and be better suited to accommodate higher surges of heat provision, such as in the case of large HP buying power for relatively short periods. In line with this, it is proposed to analyse how the system would integrate with a pit energy storage, where, assuming perfect stratification in the stored water, the cold side of the storage would stay at a near-constant low temperature, allowing for a constant charging rate, regardless of the state of charge of the storage system.

5.3.4 Effects of flexible demand of DH+HP system in the grid

The configuration selected for the analysis was T_x, from Figure 5.16, with an SF of 8,900 m^2, STS of 7,190 m^3, HP of 1,310 kW and negligible LTS of 5,490 m^3. As shown in Figure 5.17, in this configuration, the HP supplies roughly 55% of the annual heating requirements, while 45% was provided from the SF. In this configuration, the system has a very small LTS, therefore the flexibility is supplied by the existence of the STS, which can provide around 20 h of storage capacity at maximum demand (8.5 MW) and around 140 h at average demand (1.2 MW). For simplicity, 100 MW of total HP capacity was assumed for the analysis. This would represent 76 DH+HP systems with the aforementioned configuration, with annual supplied heating of 780 GWh (as a reference, Paardekooper *et al.* (2020) estimated a potential DH capacity of 46,310 GWh/a in Chile by 2050).

When setting the two reference scenarios proposed for comparison in Section 5.2.2, it was found that for the DH+HP system configuration chosen for the analysis, they are equivalent, both supplying roughly 50% of the total heating demand (10,255/2 = 5,127 MWh/a, according to Table 4.12) supplied by 3.8 COP heat pumps. This would require purchasing a total of 1,365 MWh/a of electricity. Expanding this to 76 systems means a total extra electricity demand of 103 GWh/a, following the demand pattern calculated for the Large case in Temuco in Section 4.3.1 in an inflexible way.

As explained in Section 5.2.2, the assessment of the interactions of the electricity grid in the Urbs model and the DH+HP system in TRNSYS were iterated several times. After 6 iterations, it was evident that the NRMSD stopped decreasing and started to alternate between two values. Considering that by this iteration the NRMSD and the PDSP between two iterations were below 0.5%, the iteration process was stopped. The summary of the parameters that were computed at each iteration are presented in Table 5.3

	NRMSE	PDSP	Average spot price
Base - Iter 1	0.86%	10.25%	39.86
Iter 1 - Iter 2	0.60%	9.02%	39.89
Iter 2 - Iter 3	0.42%	0.82%	39.87
Iter 3 - Iter 4	0.39%	0.74%	39.88
Iter 4 - Iter 5	0.39%	0.38%	39.87
Iter 5 - Iter 6	0.39%	0.38%	39.88
Iter 6 - Iter 7	**0.39%**	**0.38%**	**39.87**

Table 5.3: Main parameters computed during the iteration process of spot price convergence

For the Base case (no extra demand due to heating), Flexible case (additional flexible demand due to the operation of the DH+HP system), and Reference case (additional inflexible demand due to the operation of individual heat pumps), the main results are presented in Table 5.4.

	Base Case	Flexible	Reference
Annual demand SICS [GWh]	8,997	9,137	9,100
New Investment [M€]	831.5	835.7	836.4
Overproduction [MWh/a]	4,292	4,299	4,298
Average spot price SICS [€/MWh]	39.85	39.87	39.92
Max spot price SICS [€/MWh]	384.4	384.4	384.4
Max spot price occurrences	2	1	4

Table 5.4: Comparison of results for the base case, the case with flexible additional demand from the DH+HP systems and the inflexible additional demand reference case

The results in Table 5.4 show that the DH+HP systems add 140 GWh of extra demand, while the individual heat pumps add only 103 GWh. This difference is due to the individual heat pumps operating with a COP of 3.8 (Reference scenario), compared with an annual average COP of 2.55 of the high temperature heat pump in the specific configuration chosen for the DH+HP system (Flexible scenario). However, the investment in the Flexible case is lower by 0.7 M€. Both cases install additional wind and off-the-river hydro, which have capacity factors of 0.31 and 0.6, respectively. However, the scenario with flexible demand installs 1040 MW of wind and 432 MW of hydro, while the scenario with inflexible demand requires installing more of the more expensive but less variable generation, installing 1020 MW of wind and 440 MW of hydro.

Interestingly, while these differences in generation capacity are evidenced in the SICS node (where the extra demand is added), there are slight differences in the installed capacity of storage in the SICN node. In this point of the system, in the Reference scenario 106 MW of 8 h capacity storage are installed, while in the case with Flexible demand the installed capacity is reduced to 101 MW. This difference is mostly due to the Flexible scenario having a higher spare capacity in the SICS node to export energy to the SICC node in moments of high demand (such as winter evenings), which decreases the requirements on supplying that energy from the SICN node (which is rich in solar PV), hence requiring less storage to provide the energy after sunset.

Most importantly, the Flexible scenario shows a lower average spot price (39.87 €/MWh) compared to the Reference scenario (39.92 €/MWh). Even though the difference is small, this is interesting, as it suggests that a higher demand, if managed in a flexible way and allocated in periods with greater availability of cheap renewable energy, produces a lower impact on the electricity system than a relatively lower but inflexible demand.

It is important to note that the differences between the scenarios are relatively low, therefore difficult to assess. This is mostly due to the low total installed capacity of HP in relation to the total electricity system and the limited flexibility of the DH+HP configuration (T_x) being analysed due to its (practical) lack of LTS. In this configuration, the flexibility is provided only by the STS, which has capacities in the range of hours or days, rather than weeks or months. This leads to an operation such as the one presented in Figure 5.18, where the heat pump buys electricity most of the winter, only stopping when prices are above 89 €/MW. It can be speculated that in the case of using an LTS technology that could be combined more effectively with a HP, the operation of the DH+HP system would be more flexible and present greater differences with the inflexible scenario. Additionally, the high geographical aggregation of the energy grid model used for the analysis contributes to smaller differences in the effects of the to compared demands. This is because local impacts of the collocation of intermittent generation and flexible demand in areas with constrained transmission may be missed. Consequently, it is expected that by using a more detailed model, it would be possible to detect these local effects and highlight the benefits of more flexible demand.

5.4 Conclusions

The work presented in this chapter builds on the models developed in Chapters 3 and 4 to assess and discuss the value of integrating solar district heating networks with long term storage with electric heaters in the form of resistance heaters or heat pumps (DH+HP). For this, the model developed in Chapter 4 is modified to assess the effects on the cost-effectivity of the integration of HP to the DH system (DH+HP) to provide heat to a large residential

community. Later it integrates the results with the model developed in Chapter 3 to evaluate the possible benefits that the flexible electric demand from a group of DH+HP systems could provide to the electricity grid when compared to providing the same final energy with inflexible options.

The real spot prices for the Temuco area in 2020 were analysed and it was found that the total amount of hours that the electricity price was close to zero was low (less than 2% of the year) due to the relatively low share of interment renewables (25% of the total installed capacity). Therefore, as it can be expected, the conditions for implementing power-to-heat that would take advantage of low electricity price periods are limited. A future marginal cost in a scenario with higher intermittent generation penetration was synthesised for the year 2035 based on representative days from the PELP 2020 process (Ministerio de Energia, 2020g). The spot prices produced for this period had a higher variability and presented a 25% higher average price. However, they also had 14% of hours with prices close to zero, which presents a much more suitable condition for a scheme taking advantage of low spot prices.

The results of the DH+HP system optimisation for conditions in 2020 showed limited improvements on the cost-effectivity of the systems, with the addition of HP to relatively small solar systems reducing the LCOE to around 0.9 €/kWh, but achieving this at high SE of around 0.1 $kgCO_2$/kWh. This is explained by the low amount of hours with low energy prices, but most notably by the high emission factor of the electricity grid (0.26 $kgCO_2$/kWh). In contrast, by 2035, more variable spot prices and a lower grid emission factor (0.04 $kgCO_2$/kWh) enable an important decrease in emission for systems that integrate HP to the DH networks, reaching below 0.02 $kgCO_2$/kWh for systems with LCOE of 0.087 €/kWh and below 0.01 $kgCO_2$/kWh for systems with LCOE of 0.12 €/kWh. To reach the lowest LCOE, the optimal configuration consists in systems relying mostly on a large HP buying energy most of the year and only avoiding periods of very high spot prices (above 100 €/MWh in winter and above 50 €/MWh in summer).

The result of the optimisation shows that it is not Pareto optimal to install HP together with LTS. After an analysis of the operation of specific configurations, it was found that this result was caused by the low charging capacity of the BTES technology which in turn induced a low load factor on the HP, even during hours when the spot prices were low. This behaviour is a product of the limited capacity of the storage to quickly conduct heat inside, which causes low temperature difference between the hot water and the soil close to the borehole. It is proposed to perform the analysis considering a faster charging technology, such as pit thermal storage to check if this technology would promote the collocation of HP and LTS by increasing the utilisation of the HP. In addition, other control strategies for the operation of the HP can be studied, which would benefit the operation of the DH+HP regardless of the LTS technology.

Even though the results of the optimisation showed that under the chosen control strategy and LTS technology, installing LTS and HP in the same system is not Pareto efficient, there are optimal configurations that combine HP with large STS that operate the HP in a flexible way, buying only at periods when it is economically convenient. The effect of a large scale implementation of systems with this configuration on the electricity grid was assessed and compared against an inflexible demand alternative. The results showed that despite the flexible demand being larger than the inflexible alternative, its fulfilment requires lower new investment in generation and on-grid storage and produces a lower increase in the spot price. Although the differences are meagre, this result is interesting as it opens the possibility for the grid operator to create incentives that promote the development of flexible demand. It would be interesting to conduct a similar analysis using a more detailed electric network model to perform a more meticulous evaluation of local effects and an LTS technology that could have better synergies with HP, allowing for a more flexible operation.

Chapter 6

Conclusions and recommendations

The main aim of this thesis has been to address the question of how can thermal energy storage support the transition toward a cleaner energy matrix. It is proposed that various forms of TES are cost-competitive alternatives for enabling higher penetration of intermittent renewable energy generation technologies in the electric and heating systems. This main general question has been addressed by exploring the following specific questions:

1. Can thermal energy storage at grid level increase the penetration of renewable generation in the electricity grid?
2. What are the optimal locations and sizes for on-grid pumped thermal energy storage to minimise the cost of the future energy system?
3. How can thermal energy storage support the use of variable renewable energies in residential heating applications?
4. How can thermal energy storage increase the flexibility of thermal demand and facilitate its integration with the electric grid for the provision of clean heating?

These questions have been addressed by the analysis presented in Chapters 3, 4 and 5 of this thesis. Summaries of the conclusions of each chapter are presented in the following section.

6.1 Conclusions

This section reviews the conclusions drawn from the analyses presented in Chapters 3, 4 and 5 and matches them with the specific research questions.

6.1.1 Thermal storage in the Chilean electric grid

The first specific research question has been addressed in Chapter 3. The potential of pumped thermal energy storage (PTES) was investigated using a linear optimisation model of the annual hourly operation and expansion of the Chilean electricity network. The system configuration of 2016 was modelled and the future cost-optimal development of the system was assessed by increasing the demand in intervals of five years until 2050. Six scenarios for different storage and transmission expansion were evaluated, focusing the analysis on

the deployment of solar photovoltaics (PV) and wind and the carbon intensity decrease of the system. The main findings are that, even though under the modelled scenarios, the increase in the total renewable capacity thanks to the deployment of PTES is moderate, **the deployment of PTES increases the share of intermittent renewables, such as PV, decreasing the need to invest in new natural gas combined-cycle generation (CCGT) and in expensive flexible concentrated solar power (CSP).** This leads to a decrease in the accumulated costs of expanding the system and in the cost of running the system.

It is also found that the main source of CO_2 emissions reduction in the grid is the decommissioning of coal generation and its replacement by a mix of flexible renewable (such as geothermal and CSP), intermittent renewables (wind and PV), and CCGT. As mentioned in the previous paragraph, this mix shifts towards intermittent renewables in scenarios where higher amounts of PTES are deployed.

The second specific research question has also been addressed in Chapter 3. The optimal storage capacities were found to vary along the country. The optimal storage capacity in the northern nodes was approximated 12 h, as in this area the relatively flat demand and high solar penetration require to store energy from the day to fulfil demand during all the night. For the centre and southern nodes, on the other hand, the optimal storage capacities were found to be around 7 h, as in these nodes the residential consumption drives the total demand and the main requirement of storage is to fulfil a relatively short evening peak.

In summary, the installation of storage has the potential to increase the decarbonisation of the Chilean electricity grid. **The role of PTES is potentially important, especially if it can reach the cost and efficiencies assumed in this study, as the required storage capacities match those that this technology can provide.**

6.1.2 The value of seasonal thermal energy storage in solar district heating networks

The third specific research question has been addressed by the techno-economic analysis performed in Chapter 4. For this, the hourly annual thermal demand for social housing dwellings was estimated for two cities in southern Chile (Temuco and Coyhaique). A TRNSYS simulation model of a solar district heating network (DH) with short and long term thermal storage (STS and LTS respectively) based on previous research was adapted and improved. Design characteristics, such as pipe length and diameter or pump size, were parametrised with the objective of automatically follow changes in key design features. An optimisation framework was developed in Python to integrate the simulation with an optimisation based on a genetic algorithm. The system design was optimised focusing on several key design variables with the objective of minimising total systems cost (LCOE) and emissions associated with the system's operation. The set of Pareto optimal configurations was produced and the influence and interplay of the design variables on the optimal configuration were analysed.

The results showed that the system can be economically competitive against conventional alternatives such as electric heating and conventional gas-fired district heating. Moreover, considering the emission factors of the current electricity grid and of natural gas, the proposed system may reach emissions levels several times lower than the aforementioned conventional alternatives. As the proposed system is capital intensive, the economic performance is sensitive to the size and energy density of the supplied demand. Considering this, it is noticed that the economic results are enhanced for larger systems in more densely populated areas. The emissions, however, do not present improvements in larger systems, as they are limited by the emissions associated with the electricity required for pumping the working fluid, and pressure losses tend to increase for larger systems. Following the same logic, the proposed system is economically more competitive in Coyhaique. This better economic performance is due to the higher demand density and better utilisation of the infrastructure, as in this location the higher summer demand allows for a higher overall load factor of the system, therefore yielding lower LCOE.

It was found that optimising the system design and operational conditions for the specific location was important, as it could yield LCOE decreases close to 0.02 €/kWh. For instance, systems located in warmer climates, such as Temuco, are most cost-effective operating with higher supply temperatures than systems in colder areas such as Coyhaique. This is because systems operating in warmer climates present smaller heat losses and they tend to be economically offset by lower investment in pipes due to reduced pipe diameter when operating with a hotter water supply. In addition, it was found that optimising the solar collector tilt angle for the specific location and long term storage size was a cost-free measure that could achieve modest improvements in cost and emissions.

The presence of TES is key in driving down the emissions of the system as in all the Pareto optimal configurations there is an important presence of STS, LTS or a combination of both. For smaller systems, the STS is enough for fulfilling the requirements of the system's operation. For these scales, the use of long term storage is in most cases not optimal, as its investment cost per unit of stored energy increases and the operational efficiency decreases for smaller systems. However, as it was pointed out previously, DH makes more economic sense when the systems are larger and the demand higher. For these larger systems, the use of LTS is desirable, as it drives emissions down, by reducing the need of using gas auxiliary heaters in winter.

6.1.3 Integration of electricity in district heating systems with seasonal thermal energy storage

The third specific research question has been further investigated by modifying the model developed in Chapter 4 and performing a new analysis, which is reported in Chapter 5. Electric resistance heaters and heat pumps are integrated into the TRNSYS simulation of the solar DH with thermal storage. These heaters operate as a power-to-heat scheme, buying electricity from the grid in periods when the spot prices are low due to a surplus of renewable generation and providing heat to the DH system. The optimisation is rerun, and variables associated with the design and operation of the power-to-heat scheme are added to the optimisation. The optimisation was run for conditions in 2020 with real local spot prices and for conditions in 2035 with projected spot prices.

The results showed that heat pumps (HP) perform better than resistance heaters for both studied periods. For the case of 2020, the relatively high emission factor of the grid electricity means that the electricity supplied by the HP has high embedded emissions, thus configurations with HP are only Pareto optimal in cases with a small solar field (SF), which otherwise would mean a heavy reliance on the auxiliary boiler. For these cases, the integration of an HP can drive the LCOE down by around 0.02 €/kWh, but at a relatively high emission of 0.1 $kgCO_2$/kWh. For the case in 2035, the emissions of the DH system go down, as the embedded emissions in the electricity used for operating the pumps are much lower. Notably, integrating an HP into the system helps to keep the emissions low, as the HP replaces a large part of the winter boiler operation. This effect is even more pronounced when the electricity buying logic of the HP is improved by allowing differentiated buying threshold prices for summer and winter. As the HP only operates buying energy at low price periods defined by an abundance of wind generation, it can be concluded that **the presence of TES in the system increases the use of renewable energy for providing domestic heat.**

Contrary to what was assumed, there is no optimal techno-economic case for integrating HP in a system with LTS, as for all the scenarios analysed, the optimal solutions are either systems with HP, small SF and STS (reaching minimum cost but with higher emissions); or configurations with larger SF, STS and big LTS (achieving lower emissions but at higher relative costs). The reason for this is that the chosen technology used for the LTS is borehole energy storage, which is comparatively cheap but has limitations in the charging rate capacity, as at higher states of charge the temperature difference between the hot charging media and the storage interface decreases, which diminishes the heat exchange capacity. Using an alternative LTS technology, such as pit thermal storage, which directly stores the hot heat transfer media and does not rely on water-solid heat exchange, could be a better option to take advantage of the HP's capacity to supply large amounts of heat when electricity prices are low but when there may not be enough thermal demand to use that heat.

The fourth specific research question has been addressed in Chapter 5 by joining the models previously developed and performing a comparative economic assessment of the impact of flexible and inflexible demand on the electricity grid. A specific Pareto optimal configuration of the case of DH with integration of HP (DH+HP) in 2035 was used for the analysis. A total of 76 of these systems were assumed to operate with a joint HP capacity of 100 MW, consuming electricity flexibly at times when the spot prices were lower. The effect of this additional demand was compared with an inflexible demand from individual HP providing heat directly.

The results show that even though the total demand added by the DH+HP systems is higher than that of the individual heat pumps, **due to the flexibility provided by the presence of TES, it posed a smaller burden on the electric grid, requiring less generation and electricity storage investment than the smaller inflexible demand of the individual heat pumps.** This opens the possibility for the grid operator to create market incentives that recognise the value of flexible demand and promote its development.

6.2 Recommendations for future work

The work presented in this thesis can be extended and improved. Several alternatives with interesting potential impacts are discussed in the next paragraphs.

6.2.1 Improvement and actualisation of the Chilean electricity grid model

The model of the electric grid used for the analysis performed in Chapter 3 can undergo several improvements in order to represent more closely the operation of the Chilean electricity system. A first step would be to increase the number of nodes in the southern part of the system, to be able to represent better the specific locations of the main demands and high wind potential areas. This would provide a better understanding of possible local transmission constraints and highlight the value of flexible demand in different locations. Furthermore, the policy-imposed constraints and other projections of future system configurations have to be actualised based on the latest development of the technologies and energy policy goals. The trade-offs of other improvements, like the inclusion of binary variables for simulating minimum operational conditions of conventional power plants, have to be assessed. Including the minimum operational loads of conventional generation adds further limitations to the electricity system which flexible demand could ameliorate but converts the optimisation into a mixed-integer linear problem, which requires more time and computational power.

6.2.2 Addition of domestic hot water demand to the district heating model

In this thesis, the analysis of the design and operation of the DH system has focused only on the supply of the heating demand. However, as it was pointed out in Chapter 4 the provision of domestic hot water (DHW) can represent between 10 and 25% of the total thermal demand of a Chilean dwelling. Therefore, including the provision of this demand in the evaluation of the solar DH system is important. Furthermore, including the DHW demand may improve the economic performance of the system, as it increases the demand density. In addition, as the DHW demand tends to be more constant throughout the year, it can increase the average load rate of the DH equipment. It may also lead to a relative decrease of the LTS, as the ratio between winter and summer demand is likely to decrease.

6.2.3 Modelling of long term storage using pit storage technology

As it was pointed out in the discussion of Chapter 5, it is interesting to repeat the optimisation of the configuration of a DH+HP system with an LTS technology with faster charging capabilities. As mentioned before, one option is to use a pit energy storage, which stores the hot water directly, thus not relying on heat transfer to store and recover the energy. The modelling of this kind of storage can be performed by using TRNSYS type 342, type 1300/1301 or type 1322 (Jensen and Nielse, 2020). The assumption behind this proposed future work is that a system that allows a faster rate of charge would facilitate the operation of the HP at its nominal capacity whenever there are low spot prices, as it will be able to quickly move the hot water to the storage and supply cold water from the bottom of the storage to maintain the operation of the HP at maximum capacity. This would increase the load factor of the HP, raising its economic value for the DH+HP. In addition, it would potentially allow decreasing the prices at which the HP purchases electricity, increasing the flexibility of the system's electricity demand from the point of view of the electricity grid.

6.2.4 Predictive control logic for heat pump operation and long term storage charging

The model developed in Chapter 5 for the integrated district heating and heat pump operation (DH+HP) assumes that the HP uses electricity from the grid based on a threshold purchase price. This approach assumed that there is a relatively good understanding of the spot prices behaviour during the year, which might be questionable. Moreover, it does not consider the availability of heat coming from the SF nor the current or future demand. This may cause that the heat from the HP could displace heat coming from the SF in the absence of demand or spare capacity to charge the LTS. This is not a problem when the electricity spot prices are very close to zero, but is suboptimal when the spot prices increase. The proposal is to use a logic that could consider the state of charge of the STS and LTS and the following days' weather forecast to predict the heat demand and the supply of heat from the SF. This would

allow to maximise the production from the SF. A similar control logic was proposed by Lizana *et al.* (2018a) for a heat pump supplying heating for a single house. A supervised regression model can be implemented to predict future demands based on heating degree days forecast. To predict the SF heat production, a similar regression model can be implemented considering the time of the year and the main weather forecast parameters such as temperature, humidity and precipitation as variables.

6.2.5 Detailed study of flexible power-to-heat demand effect on the electric grid

Assuming that the work proposed in Sections 6.2.3 and 6.2.4 are successful in optimising the integration of the HP and LTS in the DH system and increasing the flexibility of operation of the HP, it would be worth repeating the analysis of the effect of the flexible demand on the grid. This increased flexibility combined with the improved electricity system model proposed in Section 6.2.1 should allow for a much more insightful analysis of the effects of this additional flexible demand against inflexible electrification of heating.

6.2.6 Implementation of Pareto front convergence improvement algorithm

It is worth implementing the proposed improvement for the genetic algorithm included in DEAP. As the number of optimisation variables increases, the random mutation and crossover operators seem not to be enough to promote a quick convergence of the Pareto front. Therefore the algorithm proposed in Appendix E could be implemented by forcing an interpolation between the variables of adjacent Pareto points whose distance exceeds a certain predefined metric.

6.2.7 Surrogate model development for improve optimisation process

In the same line of decreasing the time of the simulation-based optimisation, it is proposed to develop a surrogate model that would approximate the solution of the simulations with a lower order problem. The idea of this surrogate model is to emulate the expensive evaluation of the objective function, which in this case is a simulation running for 1 to 2 minutes, with a much simpler alternative. This surrogate model can be based on a statistical approximation using machine learning techniques and trained on a small set of simulation output data. Therefore, it can be used to predict the objective function results from the simulation almost instantly, reducing the running time of the optimisation, producing a set of approximated optimal results. This set of approximated optimal solutions can be supplied as a starting point for a further optimisation run using the simulation, but the convergence is expected to be much faster as the starting points are already near the optimum. It is important to clarify that this surrogate model would not replace the simulation, as it would only be able to predict approximated values for the objective function, but the simulation will still be needed to obtain any other operational information.

Figure 6.1 presents a diagram of the framework with the surrogate model implemented. N1 represents the first iteration of the optimisation using the simulation model, starting from a random sample. This first iteration is used to generate the training data (used to build the machine learning model) and the testing data (used to check if the model was fit to produce accurate approximations). This first data set could be produced by running simulations with random system configurations. However, training and testing the model with data produced from a short optimisation run would probably lead to a better fit of the surrogate model to the solution space around the optimum. N2 corresponds to the run of the optimisation algorithm using the surrogate model to evaluate the objective functions and generates a large amount of close to optimal solutions with minimal computational requirement. Finally, N3 is the last set of iterations, using the close-to-optimal solutions produced in the previous step as a starting point for the simulation-based optimisation that yields the final set of optimal solutions. Examples of similar approaches to improve accuracy and computational time of optimisation of buildings thermal performance can be found in the works of Ferrara *et al.* (2021) and García Kerdan and Morillón Gálvez (2020). A thorough review of different surrogate models applied for the design of energy systems in buildings, their applications and characteristics is presented by Westermann and Evins (2019).

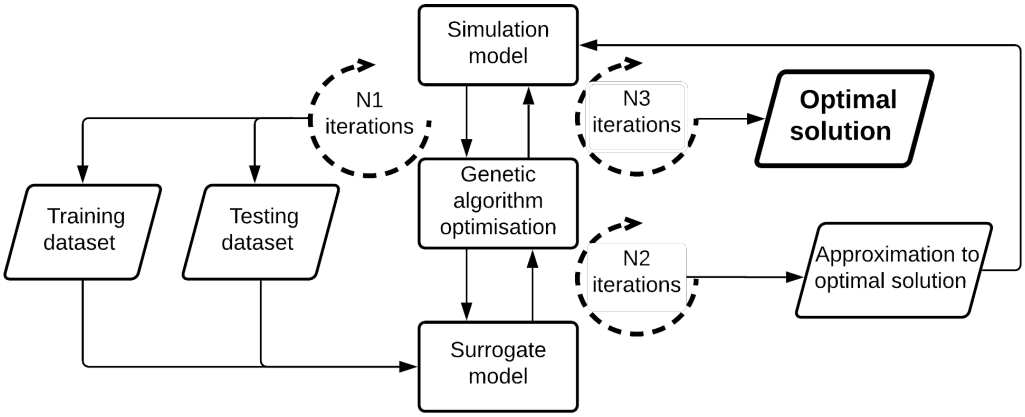

in

Figure 6.1: Diagram of the proposed framework for decrease the optimisation time by using a machine learning surrogate model

Appendix A

Building envelope materials

This appendix presents the details of the materials assumed for the thermal envelope of the buildings composing the development modelled in Chapters 4 and 5.

Surfaces	Material	Temuco		
		Thickness [mm]	Density [kg/m^3]	Thermal conductivity [W/mK]
External wall	Lightweight concrete	20	800	0.26
	Brick	175	1000	0.46
Boundary wall	Cement mortar	10	2000	1.40
	Brick	140	1000	0.46
	Cement mortar	10	2000	1.40
Internal wall	Wall board	50	600	0.29
Internal ceiling/floor	Lightweight concrete	120	800	0.26
	Linoleum	4	1000	1.02
External roof	Ceiling board	10	600	0.29
	Polystyrene	40	20	0.03
	Fiber cement	4	1250	0.23
Ground	Common cement	200	2400	2.10
	Linoleum	4	1000	1.02
Windows	Glass	5	2500	0.9

Table A.1: Building envelope material in the city of Temuco

Surfaces	Material	Temuco		
		Thickness [mm]	Density [kg/m^3]	Thermal conductivity [W/mK]
External wall	Polystyrene	40	20	0.03
	Brick	175	1000	0.46
Boundary wall	Cement mortar	10	2000	1.40
	Brick	140	1000	0.46
	Cement mortar	10	2000	1.40
Internal wall	Wall board	50	600	0.29
Internal ceiling/floor	Lightweight concrete	120	800	0.26
	Linoleum	4	1000	1.02
External roof	Ceiling board	10	600	0.29
	Polystyrene	120	20	0.03
	Fiber cement	4	1250	0.23
Ground	Common cement	200	2400	2.10
	Linoleum	4	1000	1.02
Windows	Glass	5	2500	0.9

Table A.2: Building envelope material in the city of Coyhaique.

Appendix B

Method for estimating the state of the LTS after year 6

The objective of this method is to predict the temperature in an underground Borehole Thermal Energy Storage (BTES) after six years of operation with the objective of shortening the run of the genetic algorithm by decreasing the simulated period from seven to two years. As the resulting approximation of the average BTES's temperature $T_{LTS_{avg}}$ has to be written within the TRNSYS equation environment, it is important for it it be a parametric expression. Hence, a multiple linear regression algorithm provided by Python's Scikit-learn package (Pedregosa *et al.*, 2011) is used.

The first step is generating the training and testing data. For this, 5000 random system configurations are run for seven years. The variables defining the configuration (independent variables) and $T_{LTS_{avg}}$ (dependent variable) are recorded.

As an example, Figure B.1 presents the distribution of $T_{LTS_{avg}}$ for conditions in 2020 are presented for 5000 configurations with nine variables, numbered from 0 to 8: SF_a (0), LTS_{vol} (1), STS_{vol} (2), θ (3), $T_{DH_{sup}}$ (4), $T_{DH_{ret}}$ (5), LTS_{pump} (6), $Price_{purch}$ (7) and HP_{pow} (8).

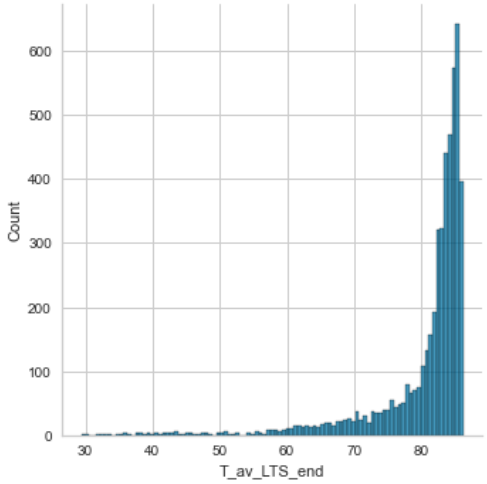

Figure B.1: Distribution of $T_{LTS_{avg}}$ at the end of year 6 for 5000 random configurations

As it is showed in Figure B.1, most of the temperatures tend to fall above 80°C, but some are as low as 30°C. This distribution is very skewed and a transformation is required to get a better fitting of the model. After some try an error, a reflected log transformation (equation B.1) is used to obtain a closer to normal distribution in the independent variable (a requirement for applying a regression model), as shown in Figure B.2.

$$tr(T_{LTS_{avg}}) = ln(0.1 + max(T_{LTS_{avg}}) - T_{LTS_{avg}}) \tag{B.1}$$

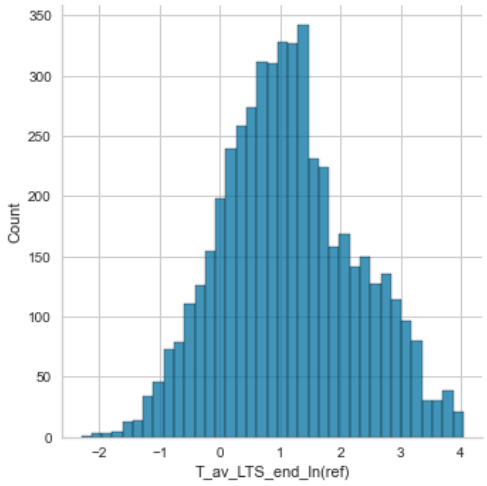

Figure B.2: Distribution of the transformation of $(T_{LTS_{avg}})$

If the regression were performed with all the variables, there is risk of over fitting. Therefore, the next step is to define which variables are going to be included in the regression. This process is known as feature selection, and consists in identifying those features (independent variables) that have higher correlation with the dependent variable or provide more information about it.

After performing the analysis of mutual information and correlation between the independent and the dependent variable, presented in Figure B.3, it is evident that θ (3), $T_{DH_{sup}}$ (4), $T_{DH_{ret}}$ (5) and HP_{pow} (8) present comparatively lower scores (values are non dimensional scores, and the highest the score, the higher the expected relevance of the specific independent variable on the prediction of the dependent variable).

From this analysis it is reasonable to exclude variables 3, 4, 5 and 8 from the regression. In the case of variables 4 and 5 ($T_{DH_{sup}}$, $T_{DH_{ret}}$), this makes sense, as both define processes that occur downstream the LTS, therefore, it is expected they have lower impact in its temperature. In the case of variable 3 (θ), a lower impact on $T_{LTS_{avg}}$ is also expected, as results in presented 4.3.3 show that θ has a relatively low influence on the operation of the system. However,

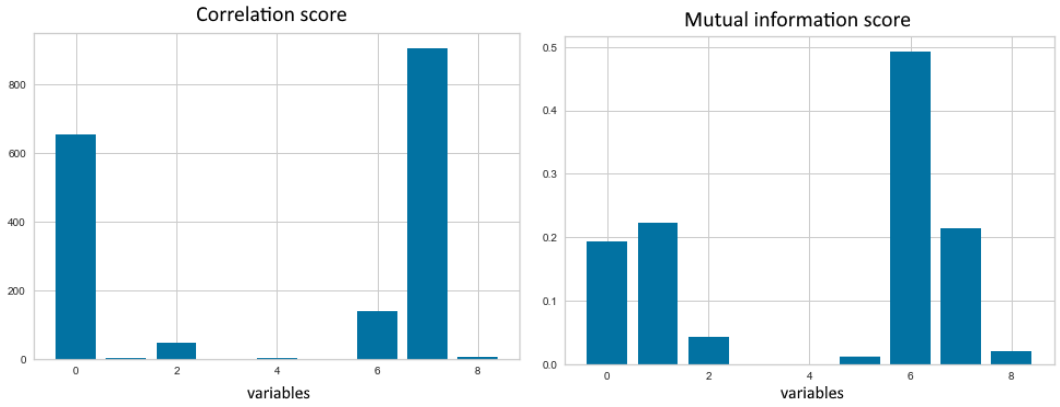

Figure B.3: Scores of the independent variables for predicting the dependent variable for mutual correlation (left) and mutual information (right)

for variable 8 (HP_{pow}), it was expected a higher influence on the dependent variable, as a larger heater should be able to provide more heat to the LTS, therefore achieve higher $T_{LTS_{avg}}$. Considering this analysis, it was decided to exclude $T_{DH_{sup}}$, $T_{DH_{ret}}$ and θ from the analysis, but to keep HP_{pow}.

Several linear regression models with different order variables were tried and the best fit was achieved with a model that included the variables up to a third order, as shown in equation B.2.

$$tr(T_{LTS_{avg}}) = a_0 + a_1 \cdot var_1 + a_2 \cdot var_1^2 + a_3 \cdot var_1^3 + \cdots + a_n \cdot var_n + a_n \cdot var_n^2 + a_n \cdot var_n^3 \quad \text{(B.2)}$$

, where a_i are the coefficients calculated by the regression algorithm and var_i are the different independent variables.

For performing the regression, randomly picked 3000 points where used as training data and the remaining 2000 as testing data. The result of the regression is presented in Figure B.4 and the coefficient of determination of the regression is 0.911.

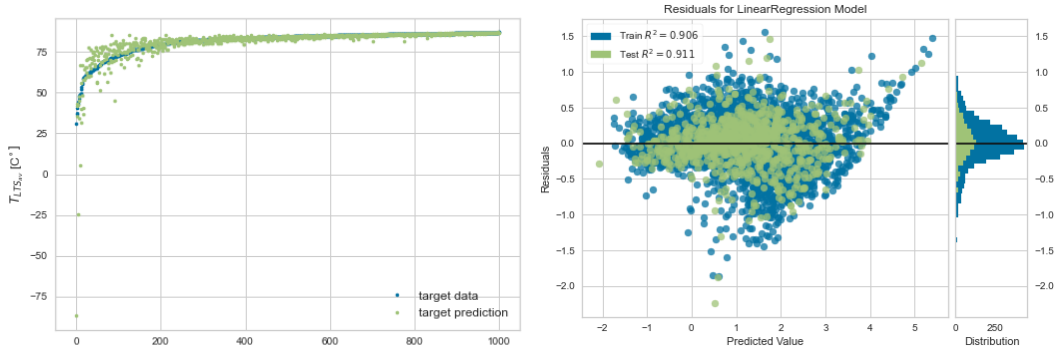

Figure B.4: Comparison of the regression with the objective variable and of their residuals (right)

Although the result shows a reasonable approximation, some heteroscedasticity (changing variability of the residuals along the predicted values) can be noticed in the residuals of the regression (right of Figure B.4). After further analysis it is noticed that it likely comes from the clearly non-convex relation between $Price_{purch}$ and $T_{LTS_{avg}}$ (and $tr(T_{LTS_{avg}})$, in this case), as shown in Figure B.5

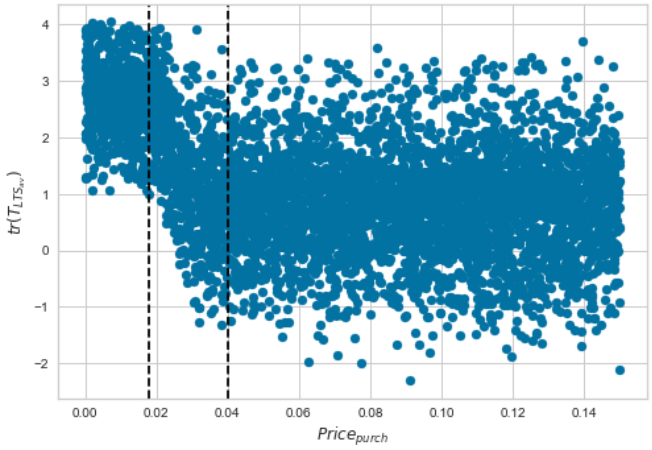

Figure B.5: Relation between the transformed objective variable $tr(T_{LTS_{avg}})$ and the purchase price threshold $Price_{purch}$, with the three different regions identified by dashed lines

Following this, the regression model was repeated, but applied independently for each of the three intervals of $Price_{purch}$ were the relation showed more regularity: $Price_{purch}$<0.018, 0.018<$Price_{purch}$<0.04 and $Price_{purch}$>0.04. The results of this three regression model produced improved coefficient of determination of 0.964, 0.924 and 0.916 for each of the three intervals of $Price_{purch}$, and the heteroscedasticity reduced notably, as it can be noticed in the right plots of Figure B.6.

Finally, the parameters are obtained from the Python script and the three regression models are written within the TRNSYS environment as equations which define the starting average temperature at the beginning of the simulation (equivalent to year 6).

As the simulation is run for two years, the first year smoothens the differences between the prediction and the true value. The difference of LCOE and SE between a 7 years runs and the 2 years runs with prediction of $T_{LTS_{avg}}$ show average discrepancies of 0.56% and 0.98% respectively. Figure B.7 shows comparisons of $T_{LTS_{avg}}$ for a complete 7 years run and a 2 years approximation starting from a preheated LTS according to the regression. This run was performed for a Large case in Temuco with SF_A=10,000 m^2, LTS_{vol}=450,000 m^3, STS_{vol}=6000 m^3, LTS_{pump}=0.297 kg/s, $Price_{purch}$=0.075 €/kWh and HP_{pow}=10 kW.

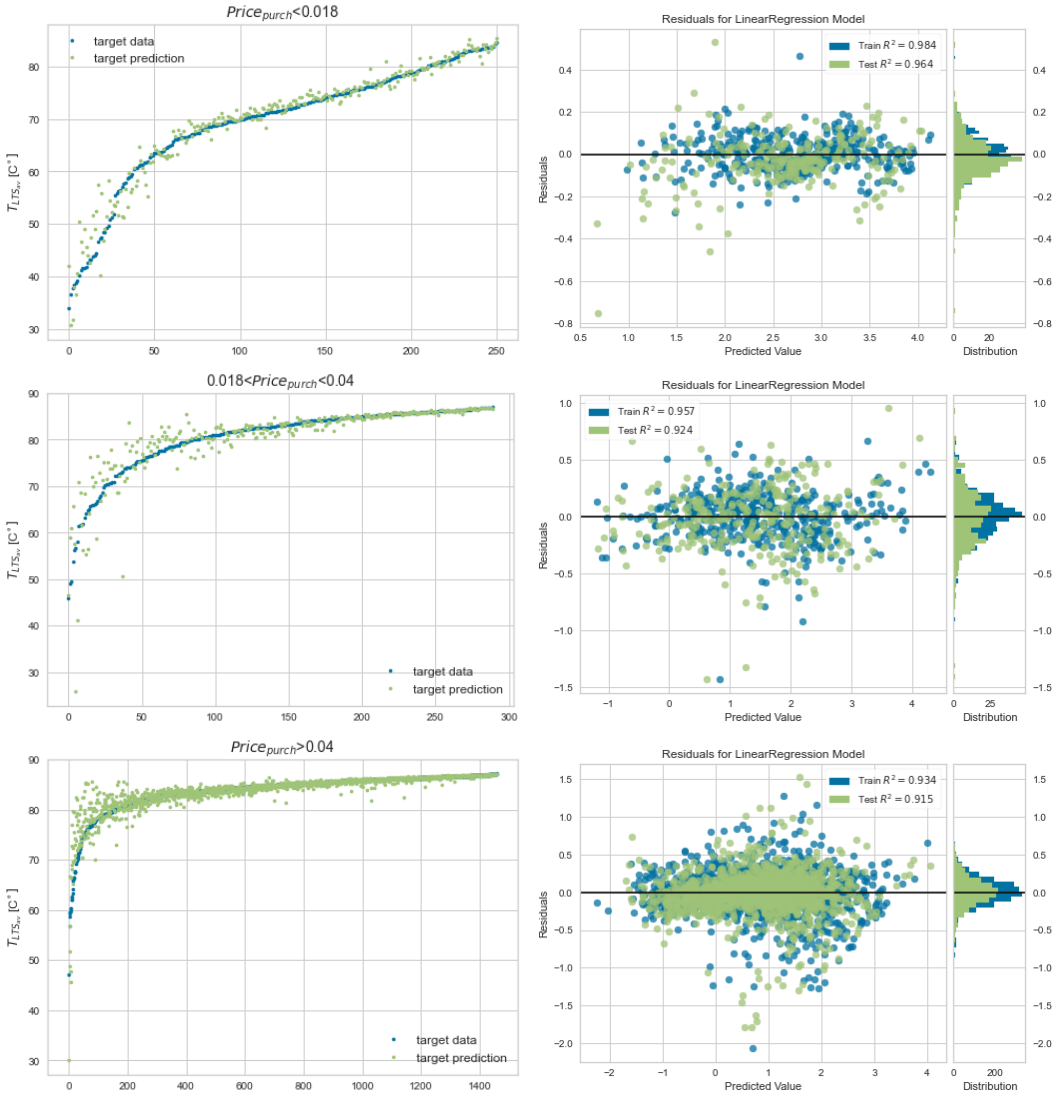

Figure B.6: Comparison of the regression with the objective variable (left) and of their residuals (right)

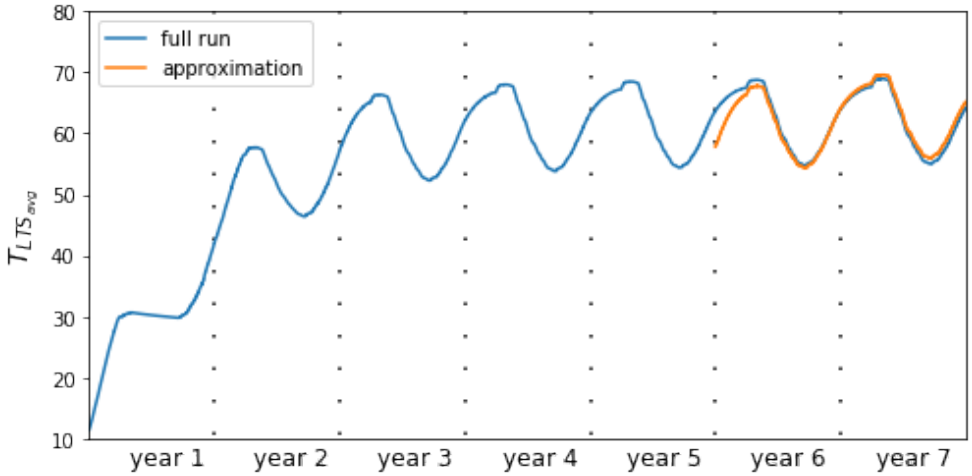

Figure B.7: Comparison of average temperature of a 7 years run and an approximation using the regression method

Appendix C

Sensitivity analysis of the district heating model to the main economic parameters

A sensitivity analysis was performed on the results of the optimisation to evaluate the impact of a variation in the main economic assumptions on the LCOE of the system. To achieve this, the three system configurations highlighted from the Pareto front of the Base and Large case in Figure 4.12 (C_A, C_B and C_C) and Figure 4.14 ($\overline{C}_A$, $\overline{C}_B$, $\overline{C}_C$) respectively were analysed. These system configurations were simulated for different electricity costs (C_{elec}), fuel costs (C_{fuel}), investment costs (C_{inv}) and interest rates (r). Each of these parameters was changed by $\pm$10% and $\pm$50% of its original value. The comparison of the LCOE for these sensitivity simulations are presented in Figure C.1. On the left axis are presented the parameters that were changed and the absolute values that were used in the analysis. The bars represent the variation of the LCOE with respect to the case with the original value (in bold).

From the results it can be seen that the LCOE is very sensitive to variations of the investment cost C_{inv} for all cases. This indicates that the system's LCOE is strongly investment cost dependent and that any decrease in the system's capital investment would lead to an almost corresponding decrease in LCOE. On the other hand, C_{elec} and C_{fuel} produce relatively low variation in the LCOE. A variation of C_{elec} produces a higher impact for the Large case, where more pumping is required for water circulation due to a longer piping network. A variation of C_{fuel} produces a higher impact in those configurations that have relatively small SFr, such as C_A and $\overline{C}_A$, because these systems require more use of the back-up boiler. The effect of a change in r has also a relatively important impact on the LCOE and, similar to the investment cost C_{inv}, its effect is independent of the size and configuration of the system.

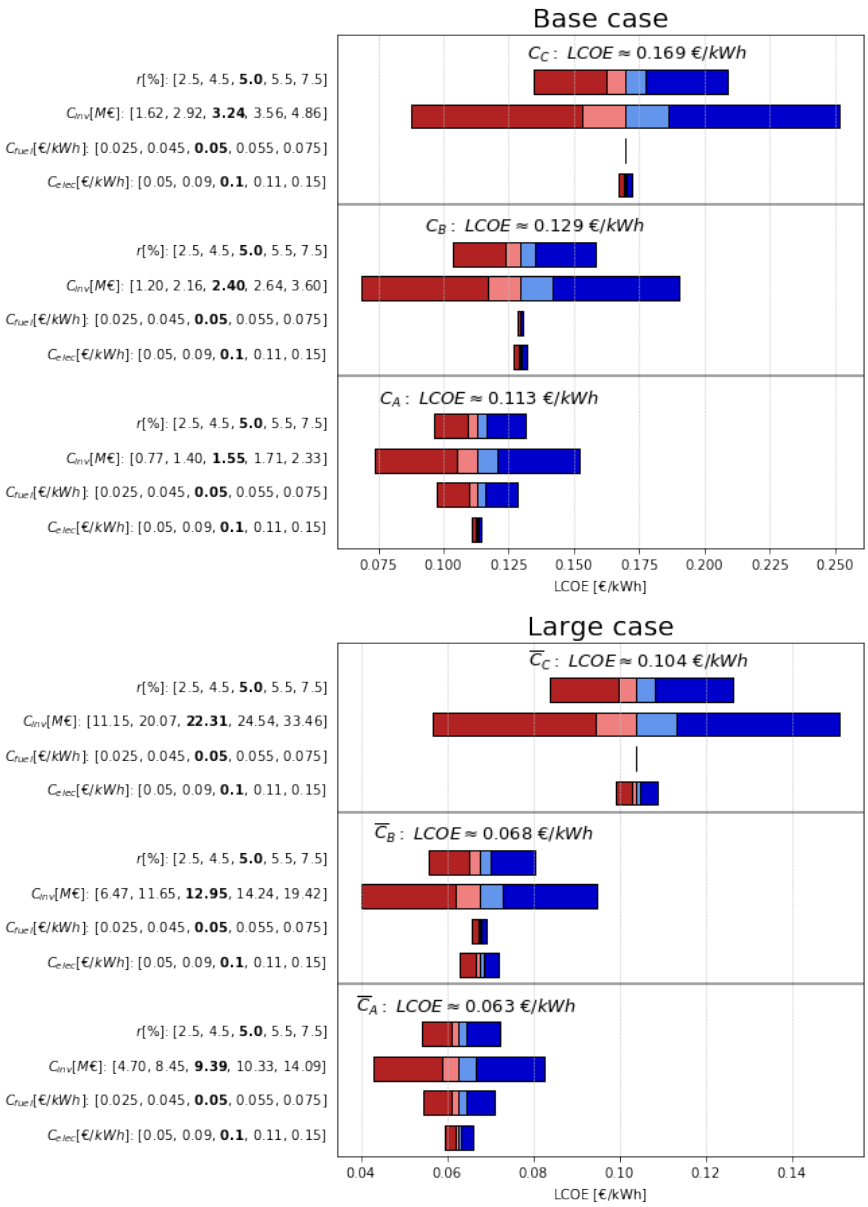

Figure C.1: Results of the sensitivity of LCOE to variation in economical parameters.

Appendix D

Estimation of demand for domestic hot water

For estimating the hourly consumption of DHW, a probabilistic approach was used following the recommendations of Braas *et al.* (2020).

The DHW uses were separated in 3 main categories: shower, dishwasher and other, which add to 160 l of DHW at 45°C consumption each day per flat, according to data used by Carrasco Vidal *et al.* (2016).

For the case of showers, it was assumed that each of the four dwellers of a flat would take a daily shower with a probability of 0.8, and every shower would represent an average water consumption of 40 l with standard deviation of 10 l. For the dishwashing, there would be 2 dishwashes per day per flat, each of them using an average of 3 l with a standard deviation of 1 l. The other DHW uses would add to 40 uses per day in each flat, with an average of 0.7 l per use and a standard deviation of 0.2 l. The previous values are summarised in Table D.1

	shower	dishwash	other	unit
Average DHW consumption per event	40	3	0.7	l
Standard deviation	10	1	0.2	l
Number of events per day per flat	4	2	40	-
Probability of each event happening	0.8	1	1	-

Table D.1: Main assumptions for the calculation of DHW use

Additionally, the average consumption per event, shown in the previous table, are modified depending on the time of the year, as shown in Figure D.1. This assumes that people tend to take longer showers and in general use more hot water in cold months. The actual variation is based on a figure presented by Aiguasol (2019).

The time of the day at which each event would occur is given by the probabilities shown in Figure D.2, based on estimated behaviour of average Chilean families.

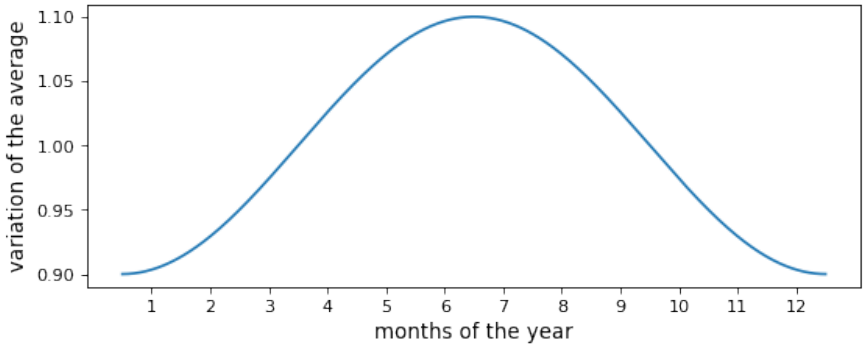

Figure D.1: Variation of water usage per each event (shower, dishwash or other) depending on the time of the year

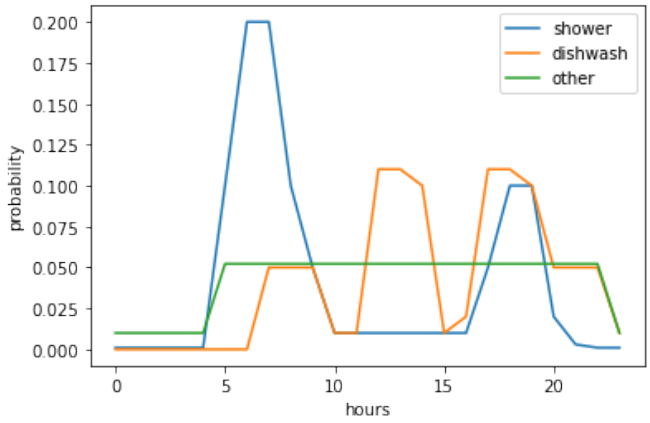

Figure D.2: Probability distribution of different events of DHW's usage occurring at different times of the day

The probabilities presented in Figure D.2 assume that most of people take showers in the morning, but some also do it in the evenings; the dishes are washed mostly after lunch and after dinner, and on a lesser extent after breakfast and that other uses are required throughout the day and much less during the night.

Given all the assumptions presented, the DHW consumption ($DHW(t)$) is calculated for each hour of the year according to equation D.1.

$$DHW(t) = \sum_{i}^{n_{flat}} \left[\sum_{j}^{4} \left(N(\mu_{shw}, \sigma_{shw}) \cdot P_{shw} \cdot Pr_{shw}(t) \right) + \sum_{k}^{2} \left(N(\mu_{dw}, \sigma_{dw}) \cdot Pr_{dw}(t) \right) + \sum_{k}^{40} \left(N(\mu_{other}, \sigma_{other}) \cdot Pr_{other}(t) \right) \right] \cdot SV(day) \tag{D.1}$$

where $N(\mu_x, \sigma_x)$ corresponds to a sample from the distribution with mean and standards deviation according to Table D.1. P_{shw} is a boolean function that returns 1 80% of the time (probability of anyone taking a daily shower). $Pr_x(t)$ is the probability of the event x happening at time t, according to Figure D.2. $SV(day)$ is the seasonal variation correction factor from Figure D.1 depending on the day of the year. i represents the total number of flats, j the dwellers in each flat and k each dishwash or other event in a flat in a day.

After performing the calculation of equation D.1 for each flat and each day of the year, the total consumption is obtained for each hour of the year. The main results of this calculation are presented in Table D.2.

average daily consumption	162	l
average daily consumption summer	148	l
average daily consumption winter	176	l
average daily consumption spring	159	l
average daily consumption autumn	165	l
max hourly demand summer	46	m^3/h
max hourly demand winter	56	m^3/h
max hourly demand spring	52	m^3/h
max hourly demand autumn	54	m^3/h
total annual demand	101,868	m^3/a

Table D.2: Main results of the DHW use for the large development (1,728 flats)

As this method uses random sampling processes of probability distributions, the results might change every time the calculation is performed. However, for a development of 1,728 (the Large case discussed in Chapter 4 and the case included in Chapter 5, this changes are negligible.

The annual extra energy demand required to produce the DHW can be estimated according to equation D.2

$$Q_{DHW} = \frac{V \cdot c_{p_{water}} \cdot (T_{DHW} - T_{cold})}{\eta_{HX}} \tag{D.2}$$

when V is the volumetric annual demand of DHW. T_{DHW} is the required temperature of the DHW. T_{cold} is the annual average mains water temperature. η_{HX} is the efficiency of the heat exchanger. Considering T_{DHW} = 45°C, T_{cold} = 11.5 (Aiguasol, 2019) and a heat exchanger with 90% effectivity, the total annual energy demand for the Large development (1728 flats) in Temuco would be close to 4,400 MWh/a, which would represent close to 30% of the combined heating-DHW annual demand. This is slightly higher than the 25% reported by Yáñez *et al.* (2019) and Tolvett (2015), but it is reasonable considering that those values are for an average household, which include much more thermally inefficient existing buildings with higher relative heating demands.

Appendix E

Proposed algorithm for improving Pareto front convergence

As mentioned in Section 5.3.2, it was found that on some occasions, the optimisation did not improve the Pareto front after several iterations and some clear irregularities or voids (areas of the curve without points) were apparent in the Pareto curve. This is shown in Figure E.1.

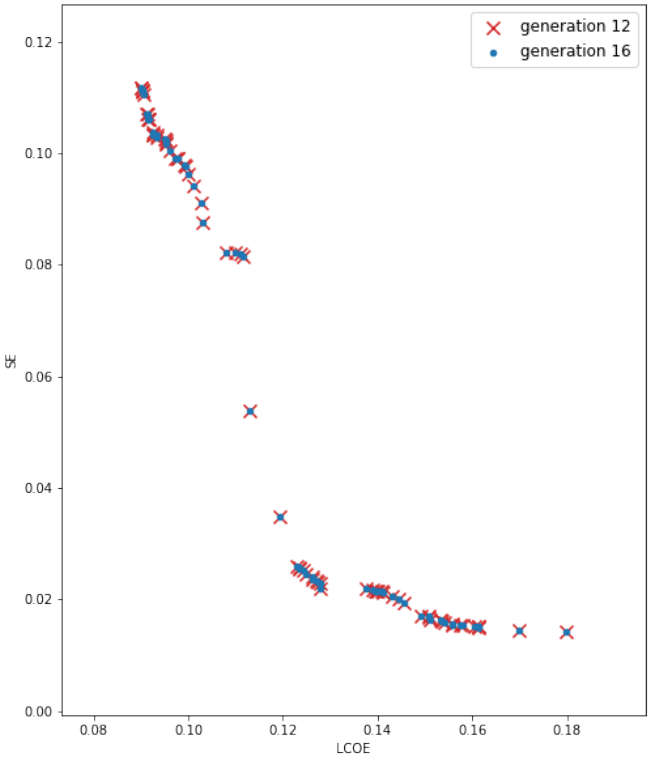

Figure E.1: Pareto front not improving after four generations and with areas with no points

This may be the product of the algorithm getting stuck in some local optimum or just not enough variability of the solutions was set in the initial parameters.

It was found that manually identifying a pair of "good" points surrounding the area with the void and adding configurations resulting from linear interpolations between the values of the variables of those two points led to improving the Pareto front. An example of how this process improved the Pareto population is shown in Figure E.2.

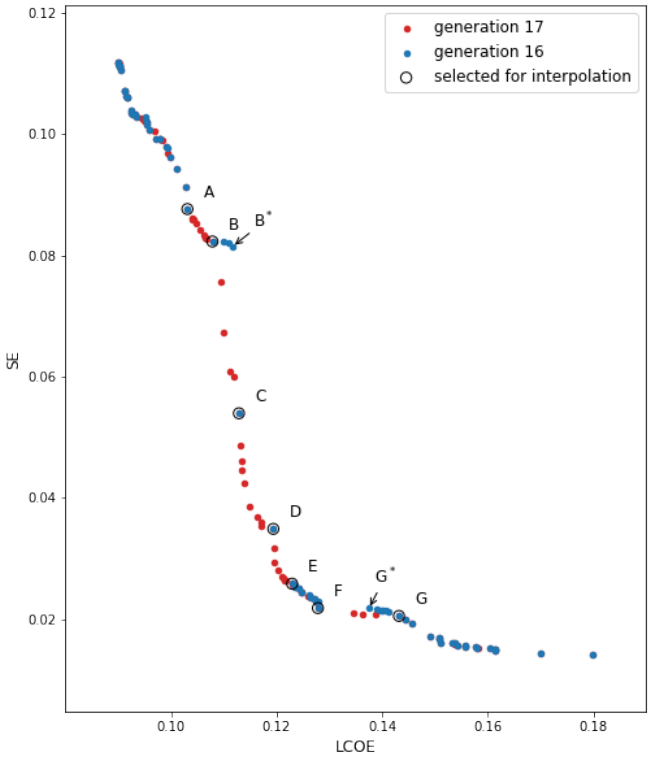

Figure E.2: Pareto front not improved after adding interpolation of good configurations to the population

After just one generation, the spaces with voids populated with Pareto optimal configurations. This shows that there is potential to implement this process into DEAP and improve the convergence of the optimisation algorithm.

The first approach is to calculate the distance along the horizontal and vertical axes between each adjacent point. Then, select a point for interpolation based on some selection criteria such as those whose distance is larger than the average distance plus a standard deviation, therefore points P_i that fulfil condition E.1.

$$\begin{gathered} \frac{\sqrt{(P_i^x - P_{i+1}^x)^2}}{(P_n^x - P_0)^x} > \mu_{\overline{P}^x} + \sigma_{\overline{P}^x} \\ \vee \\ \frac{\sqrt{(P_i^y - P_{i+1}^y)^2}}{(P_n^y - P_0)^y} > \mu_{\overline{P}^y} + \sigma_{\overline{P}^y} \end{gathered} \tag{E.1}$$

were P_i^x is the position on the x axis of point i in the Pareto front. P_n^x and P_0^x the positions in the x axis of the last and first points (max(·) and min(·)), $\mu_{\overline{P}^x}$ and $\sigma_{\overline{P}^x}$ the mean and the standard deviation of the locations on the x axis of all the points in the Pareto front.

For the example presented in the figures, applying the criterion on condition E.1 works well for most of the points in this example. But it fails to recognize that point B is a better candidate for interpolating with point C than point B* (the conditions in E.1 would have chosen B*). Therefore an extra condition should be included to remove potentially sub-optimal points, such as B* and the points between B and B* or those between G and G*. This condition is not trivial, and it might involve some pattern recognition techniques.

However, it is believed that just including the interpolation based on the distance between points would increase the speed of convergence of the genetic algorithm.

Appendix F

Installed capacity in Urbs model for 2035

This appendix presents the detail of the technologies included in each node for the Urbs model in used in Chapter 5. The different thermal technologies were separated according to clusters of their variable costs of generation with the objective of having a more detailed spot price calculation, especially in the low range (bellow 80 €/MWh), where it is expected the HP will buy electricity from the system.

		SING	SICN	SICC	SICS	Total
CSP power block	Capacity [MW]	110	-	-	-	110
	Variable cost [€/MWh]	4	-	-	-	
Wind park	Capacity [MW]	6,343	2,118	2,552	2,191	13,204
	Variable cost [€/MWh]	0	0	0	0	
Photovoltaics	Capacity [MW]	7,120	3,142	1,143	30	11,435
	Variable cost [€/MWh]	0	0	0	0	
Geothermal plant	Capacity [MW]	78	-	-	-	78
	Variable cost [€/MWh]	1	-	-	-	
Hydro reservoir	Capacity [MW]	-	-	3,254	172	3,426
	Variable cost [€/MWh]	-	-	0	0	
Hydro off the river	Capacity [MW]	-	-	3,830	583	4,413
	Variable cost [€/MWh]	-	-	0	0	
Gas OCGT_highEff	Capacity [MW]	238	-	257	-	495
	Variable cost [€/MWh]	108	-	96	-	
Gas OCGT_lowEff	Capacity [MW]	20	-	426	-	446
	Variable cost [€/MWh]	146	-	169	-	
Gas CCGT_highEff	Capacity [MW]	532	-	1,544	-	2,076
	Variable cost [€/MWh]	87	-	60	-	
Gas CCGT_lowEff	Capacity [MW]	608	-	379	-	987
	Variable cost [€/MWh]	50	-	77	-	
Diesel highEff	Capacity [MW]	964	32	176	26	1,198
	Variable cost [€/MWh]	216	207	179	199	
Diesel lowEff	Capacity [MW]	444	1,223	1,361	287	3,315
	Variable cost [€/MWh]	344	350	346	333	
Biomass cheap_highEff	Capacity [MW]	-	-	54	-	54
	Variable cost [€/MWh]	-	-	4	-	
Biomass cheap_midEff	Capacity [MW]	-	-	69	33	102
	Variable cost [€/MWh]	-	-	14	18	
Biomass cheap_lowEff	Capacity [MW]	-	-	257	22	279
	Variable cost [€/MWh]	-	-	25	33	
Biomass med_highEff	Capacity [MW]	-	-	41	26	67
	Variable cost [€/MWh]	-	-	50	60	
Biomass med_lowEff	Capacity [MW]	-	-	69	61	130
	Variable cost [€/MWh]	-	-	106	96	
Biomass exp	Capacity [MW]	-	-	28	-	28
	Variable cost [€/MWh]	-	-	176	-	
Biogas plant	Capacity [MW]	-	-	14	-	14
	Variable cost [€/MWh]	-	-	129	-	
Total capacity [MW]		16,457	6,515	15,454	3,431	41,857
Total annual demand [GWh]		36,634	17,089	71,548	89,978	215,249
Peack demand [MW]		4,852	2,477	10,369	1,304	18,543

Table F.1: Installed capacity and variable generation costs for the system in 2035 used for the Urbs model in Chapter 5.2.2

Bibliography

Aalborg University. EnergyPLAN, 2021. URL https://www.energyplan.eu/.

Advancedwater. Santon Industrial Immersion Heaters, 2021. URL http://www.advancedwater.co.uk/header-540-255-DY.html.

Agostini, C. A., Silva, C., and Nasirov, S. Failure of energy mega-projects in Chile: A critical review from sustainability perspectives. *Sustainability (Switzerland)*, 9(6):1–17, 2017. ISSN 20711050. doi: 10.3390/su9061073.

Aiguasol. Diseño y Evaluación del Sistema de Calefacción Distrital para Conjunto Habitacional Nuevo en las Comunas de Temuco y Padre Las Casas. Technical report, 2019.

AIMMS. Mathematical Optimization and Rapid Optimization Modeling, 2021. URL https://www.aimms.com/platform/aimms-development/.

Alva, G., Lin, Y., and Fang, G. An overview of thermal energy storage systems. *Energy*, 144, 2018. ISSN 03605442. doi: 10.1016/j.energy.2017.12.037.

Ambiente Consultores. Análisis del mercado y estimación del impacto energético, económico, social y ambiental de fijar un estándar mínimo de eficiencia energética en artefactos que consumen leña y otros dendroenergéticos. Technical report, 2013.

Arpagaus, C., Bless, F., Uhlmann, M., Schiffmann, J., and Bertsch, S. S. High temperature heat pumps: Market overview, state of the art, research status, refrigerants, and application potentials. *Energy*, 152:985–1010, 6 2018. ISSN 03605442. doi: 10.1016/j.energy.2018.03.166.

Avghad, S. N., Keche, A. J., and Kousal, A. Thermal Energy Storage: A Review. *IOSR Journal of Mechanical and Civil Engineering (IOSR-JMCE*, 13(3):72–77, 2016. doi: 10.9790/1684-1303027277.

Babonneau, F. and Haurie, A. Modeling Energy and Technology Choices in Smart Regional Energy Systems. 2015.

Babonneau, F., Barrera, J., and Toledo, J. Decarbonizing the Chilean Electric Power System: A Prospective Analysis of Alternative Carbon Emissions Policies. *Energies*, 14(16):4768, 8 2021. ISSN 19961073. doi: 10.3390/EN14164768.

Banister, C. J. and Collins, M. R. Development and performance of a dual tank solar-assisted heat pump system. *Applied Energy*, 149:125–132, 7 2015. ISSN 0306-2619. doi: 10.1016/j.apenergy.2015.03.130.

Barbour, E. and Pottie, D. L. Adiabatic compressed air energy storage technology. *Joule*, 5 (8):1914–1920, 8 2021. ISSN 2542-4351. doi: 10.1016/j.joule.2021.07.009.

Barbour, E., Mignard, D., Ding, Y., and Li, Y. Adiabatic Compressed Air Energy Storage with packed bed thermal energy storage. *Applied Energy*, 155:804–815, 10 2015. ISSN 0306-2619. doi: 10.1016/j.apenergy.2015.06.019.

Barbour, E. R., Pottie, D. L., and Eames, P. Why is adiabatic compressed air energy storage yet to become a viable energy storage option? *iScience*, 24(5):102440, 5 2021. ISSN 2589-0042. doi: 10.1016/j.isci.2021.102440.

Bardeen, S. International Rivers, 2018. URL `https://www.internationalrivers.org/blogs/433/victory-in-chile-dams-scrapped-on-five-rivers`.

Bauer, T., Odenthal, C., and Bonk, A. Molten Salt Storage for Power Generation. *Chemie Ingenieur Technik*, 93(4):534–546, 4 2021. ISSN 1522-2640. doi: 10.1002/CITE.202000137.

BEIS. Electricity generation cost. Technical report, Department for Business, Energy and Industrial Strategy, 2016a.

BEIS. Evidence Gathering: Thermal Energy Storage (TES) Technologies. Technical report, Department for Business, Energy andIndustrial Strategy, 2016b.

Benato, A. and Stoppato, A. Pumped Thermal Electricity Storage: A technology overview, 2018. ISSN 24519049.

Benes, K. J. and Augustin, C. Beyond LCOE: A simplified framework for assessing the full cost of electricity. *Electricity Journal*, 29(8):48–54, 10 2016. ISSN 10406190. doi: 10.1016/J.TEJ.2016.09.013. URL `http://dx.doi.org/10.1016/j.tej.2016.09.013`.

Blackburn, L., Young, A., Rogers, P., Hedengren, J., and Powell, K. Dynamic optimization of a district energy system with storage using a novel mixed-integer quadratic programming algorithm. *Optimization and Engineering*, 20(2):575–603, 2019. ISSN 15732924. doi: 10.1007/s11081-018-09419-w.

Bohórquez-Órdenes, J., Tapia-Calderón, A., Vasco, D. A., Estuardo-Flores, O., and Haddad, A. N. Methodology to reduce cooling energy consumption by incorporating PCM envelopes: A case study of a dwelling in Chile. *Building and Environment*, 206:108373, 12 2021. ISSN 0360-1323. doi: 10.1016/j.buildenv.2021.108373.

Borquez, R. *Energy policies in Chile the deliberative turn in a post-dictatorship democracy*. PhD thesis, King's College London, 2020.

Braas, H., Jordan, U., Best, I., Orozaliev, J., and Vajen, K. District heating load profiles for domestic hot water preparation with realistic simultaneity using DHWcalc and TRNSYS. *Energy*, 201:117552, 2020. ISSN 03605442. doi: 10.1016/j.energy.2020.117552.

Bravo, R. and Friedrich, D. Two-stage optimisation of hybrid solar power plants. *Solar Energy*, 164:187–199, 2018. doi: 10.1016/j.solener.2018.01.078.

Bravo, R., Ortiz, C., Chacartegui, R., and Friedrich, D. Hybrid solar power plant with thermochemical energy storage: A multi-objective operational optimisation. *Energy Conversion and Management*, 205:112421, 2 2020. ISSN 0196-8904. doi: 10.1016/J.ENCONMAN.2019.112421.

Bustamante, W., Cepeda, R., Matrinez, P., and Santa Maria, H. Eficiencia energética en vivienda social: un desafío posible. Technical report, Gobierno de Chile, 2009.

Carapellucci, R. and Giordano, L. A methodology for the synthetic generation of hourly wind speed time series based on some known aggregate input data. *Applied Energy*, 101:541–550, 1 2013. ISSN 0306-2619. doi: 10.1016/J.APENERGY.2012.06.044.

Carrasco Vidal, R., Jiménez Del Río, J., and Mardones Poblete, C. Análisis costo-beneficio de la calefacción distrital en la zona central de Chile. *Revista Internacional de Contaminacion Ambiental*, 32(1):35–45, 2016. ISSN 01884999.

Castillejo-Cuberos, A. and Escobar, R. Understanding solar resource variability: An in-depth analysis, using Chile as a case of study. *Renewable and Sustainable Energy Reviews*, 120: 109664, 2020. ISSN 18790690. doi: 10.1016/j.rser.2019.109664.

Catolico, N., Ge, S., and McCartney, J. S. Numerical Modeling of a Soil-Borehole Thermal Energy Storage System. *Vadose Zone Journal*, 15(1):1–17, 1 2016. ISSN 1539-1663. doi: 10.2136/vzj2015.05.0078.

CDEC-SING. Efectos Técnico-Económicos De La Integracion de Energía Eólica y Solar en el SING. Technical report, CDEC-SING, 2012. URL `http://cdec2.cdec-sing.cl/pls/portal/cdec.pck_pag_web_pub.get_file?p_file=INFORME_ERNC_2012_V1.pdf`.

Cerro Dominador. Cerro Dominador Concentrated Solar Power, 2020. URL `https://cerrodominador.com/en/projects/`.

CGE. Tarifas de suministro, 2020. URL `https://www.cge.cl/wp-content/uploads/2020/01/Tarifas-de-Suministro-CGE-Enero-2020.pdf`.

Chen, L. X., Xie, M. N., Zhao, P. P., Wang, F. X., Hu, P., and Wang, D. X. A novel isobaric adiabatic compressed air energy storage (IA-CAES) system on the base of volatile fluid. *Applied Energy*, 210:198–210, 1 2018. ISSN 0306-2619. doi: 10.1016/j.apenergy.2017.11.009.

Chile Ambiente. Estudio de Análisis del Potencial Estratégico de la Leña en la Matriz Energética Chilena. Technical report, Comision Nacional de Energia, 2008.

Chinchilla, M., Santos-Martín, D., Carpintero-Rentería, M., and Lemon, S. Worldwide annual optimum tilt angle model for solar collectors and photovoltaic systems in the absence of site meteorological data. *Applied Energy*, 281:116056, 2021. ISSN 03062619. doi: 10.1016/j.apenergy.2020.116056.

CNE. Política Energética: Nuevos Lineamientos. Technical report, Comision Nacional de Energia, 2008.

Comision Nacional de Energia. Estudio de transmision troncal 2015-2018. Technical report, 2015.

Comision Nacional de Energia. Energia Abierta - Capacidad total instalada, 2018. URL http://energiaabierta.cl/visualizaciones/capacidad-instalada/.

Comision Nacional de Energia. Mapa Precio de Combustibles – Energía Abierta, 2020. URL http://energiaabierta.cl/visualizaciones/mapa-precio-de-combustibles/.

Comité Consultivo de Energía 2050. Hoja de Ruta 2050. Technical report, 2015.

Coordinador eléctrico nacional. Coordinador eléctrico nacional, 2018. URL https://www.coordinador.cl.

Coordinador Eléctrico Nacional. Map - Sistemas eléctricos de Chile 2017, 2017. URL https://sic.coordinador.cl/wp-content/uploads/2016/11/Mapa-Coordinador-Eléctrico-Nacional_enero_20171.pdf.

Cortés, A. and Ridley, I. Efectos de la combustión a leña en la calidad del aire intradomiciliario. La ciudad de Temuco como caso de studio. *Revista INVI*, 28(78):257–271, 2014. ISSN 07181299. doi: 10.4067/s0718-83582013000200008.

(CR)2. Explorador climático, 2016. URL http://explorador.cr2.cl/.

Danish Energy Agency. Technology Data-Energy Plants for Electricity and District heating generation. Technical report, 2016.

Davenne, T. R. and Peters, B. M. An Analysis of Pumped Thermal Energy Storage With Decoupled Thermal Stores. *Frontiers in Energy Research*, 8:160, 8 2020. ISSN 2296598X. doi: 10.3389/fenerg.2020.00160.

de la Cruz, R., Suarez, M., Belmar, M., Quiroz, D., and Bell, M. Geologia del area Coihaique - Balmaceda. *Serie de geología basica*, 80, 2003.

Deap Project. DEAP documentation — DEAP 1.3.1 documentation, 2020. URL https://deap.readthedocs.io/en/master/index.html.

Defra. Greenhouse gas reporting: conversion factors 2020 - GOV.UK, 2020. URL https://www.gov.uk/government/publications/greenhouse-gas-reporting-conversion-factors-2020.

Diaz, G., Munoz, F. D., and Moreno, R. Equilibrium Analysis of a Tax on Carbon Emissions with Pass-through Restrictions and Side-payment Rules. *The Energy Journal*, 41(2), 2020. ISSN 1944-9089. doi: 10.5547/01956574.41.2.GDIA.

Diaz, M. *Evaluación de impacto de mejoras aplicadas a la hermeticidad al aire y aislación térmica para la verificación de la eficiencia energética mediante simulación térmica dinámica de dos viviendas tipo en Concepción*. PhD thesis, Universidad del Bio-Bio, 2015.

Ding, Y., Tong, L., Zhang, P., Li, Y., Radcliffe, J., and Wang, L. Liquid Air Energy Storage. In Letcher, T. M., editor, *Storing Energy: With Special Reference to Renewable Energy Sources*, pages 167–181. Elsevier, 1 2016. ISBN 9780128034408. doi: 10.1016/B978-0-12-803440-8.00009-9.

DLSC. Drake Landing Solar Community, 2019. URL https://www.dlsc.ca/.

Dochev, I., Peters, I., Seller, H., and Schuchardt, G. K. Analysing district heating potential with linear heat density. A case study from Hamburg. In *Energy Procedia*, volume 149, pages 410–419. Elsevier Ltd, 2018. doi: 10.1016/j.egypro.2018.08.205.

Dorfner, J. Urbs Documentation Release 0.7.1. Technical report, 2018.

Dumont, O., Frate, G. F., Pillai, A., Lecompte, S., De paepe, M., and Lemort, V. Carnot battery technology: A state-of-the-art review. *Journal of Energy Storage*, 32:101756, 12 2020. ISSN 2352152X. doi: 10.1016/j.est.2020.101756.

EASE. Adiabatic Compressed Air Energy Storage. Technical report, European Association for Storage of Energy, 2016a.

EASE. Liquid Air Energy Storage. Technical report, European Association for Storage of Energy, 2016b.

EBP Chile. Metodología para la elaboración de mapas de calor en Chile. Technical report, 2019.

Edwards, G. Estimacion de la tasa docial de descuento a largo plazo en el marco de los sistemas nacionales de inversion - Aplicacion al caso chileno. *El trimestre economico*, LXXXIII(1):99–125, 2016.

Energy Live. Chile agrees to phase out coal power plants, 2018. URL https://www.energylivenews.com/2018/02/01/chile-agrees-to-phase-out-coal-power-plants/.

Ernst Basler + Partner. Hoja de ruta calefacción distrital en chile – Ejes estratégicos de acción 2016-2025. Technical report, Santiago, Chile, 2016. URL http://achbiom.cl/wp-content/uploads/2017/08/documento-hoja-de-ruta.pdf.

Estay, T. and Ovalle, X. Desarrollo de factores de emisión específicos para el programa HuellaChile. Technical report, Universidad Andres bello, 2017.

Fernández, A. G., Gomez-Vidal, J., Oró, E., Kruizenga, A., Solé, A., and Cabeza, L. F. Mainstreaming commercial CSP systems: A technology review. *Renewable Energy*, 140: 152–176, 9 2019. ISSN 0960-1481. doi: 10.1016/j.renene.2019.03.049.

Ferrara, M., Della Santa, F., Bilardo, M., De Gregorio, A., Mastropietro, A., Fugacci, U., Vaccarino, F., and Fabrizio, E. Design optimization of renewable energy systems for NZEBs based on deep residual learning. *Renewable Energy*, 176:590–605, 10 2021. ISSN 0960-1481. doi: 10.1016/j.renene.2021.05.044.

Fleuchaus, P., Godschalk, B., Stober, I., and Blum, P. Worldwide application of aquifer thermal energy storage – A review. *Renewable and Sustainable Energy Reviews*, 94:861–876, 10 2018. ISSN 1364-0321. doi: 10.1016/J.RSER.2018.06.057.

Forrester, S. P., Zaman, A., Mathieu, J. L., and Johnson, J. X. Policy and market barriers to energy storage providing multiple services. *The Electricity Journal*, 30(9):50–56, 2017. ISSN 1040-6190. doi: 10.1016/J.TEJ.2017.10.001.

Fortin, F.-A., Marc-André Gardner, U., Parizeau, M., and Gagné, C. DEAP: Evolutionary Algorithms Made Easy François-Michel De Rainville. *Journal of Machine Learning Research*, 13:2171–2175, 2012.

Foster, S., Love, J., Walker, I., and Crane, M. Heat Pumps in District Heating. Technical report, Element Energy, 2016.

Foy, K., Garcia, I., Lunn, D., and Roberts, D. Coal and Gas Assumptions. Technical report, DECC, 2014.

Frate, G. F., Ferrari, L., and Desideri, U. Multi-criteria investigation of a pumped thermal electricity storage (PTES) system with thermal integration and sensible heat storage. *Energy Conversion and Management*, 208, 3 2020. ISSN 01968904. doi: 10.1016/j.enconman.2020.112530.

Freund, S. Webinar on Carnot Batteries - Malta, 2019. URL https://atainsights.com/wp-content/uploads/2019/04/190404-_Michael-Geyer-Sebastian-Freund-Webinar-Carnot-Batteries-distr.pdf.

Fripp, M. Switch: A planning tool for power systems with large shares of intermittent renewable energy. *Environmental Science and Technology*, 46(11):6371–6378, 6 2012. ISSN 0013936X. doi: 10.1021/ES204645C/SUPPLFILE/ES204645CSI001.PDF.

Furbo, S. Using water for heat storage in thermal energy storage (TES) systems. In Cabeza, L., editor, *Advances in Thermal Energy Storage Systems*. Woodhead Publishing, 2015.

Gaete-Morales, C., Gallego-Schmid, A., Stamford, L., and Azapagic, A. A novel framework for development and optimisation of future electricity scenarios with high penetration of renewables and storage. *Applied Energy*, 250:1657–1672, 9 2019. ISSN 0306-2619. doi: 10.1016/j.apenergy.2019.05.006.

Gallo, A. B., Simões-Moreira, J. R., Costa, H. K., Santos, M. M., and Moutinho dos Santos, E. Energy storage in the energy transition context: A technology review. *Renewable and Sustainable Energy Reviews*, 65:800–822, 11 2016. ISSN 1364-0321. doi: 10.1016/J.RSER.2016.07.028.

García Kerdan, I. and Morillón Gálvez, D. Artificial neural network structure optimisation for accurately prediction of exergy, comfort and life cycle cost performance of a low energy building. *Applied Energy*, 280:115862, 12 2020. ISSN 0306-2619. doi: 10.1016/J.APENERGY.2020.115862.

Garvey, S. D. The dynamics of integrated compressed air renewable energy systems. *Renewable Energy*, 39(1):271–292, 3 2012. ISSN 0960-1481. doi: 10.1016/j.renene.2011.08.019.

Gobierno de Chile. Reglamentacion Termica - Manual de aplicacion. Technical report, Ministerio de Vivienda y Urbanismo, Santiago, Chile, 2006.

Gobierno de Chile. Intended nationally determined contribution of Chile towards the climate agreement of Paris 2015. Technical report, 2015.

Gobierno de Chile. Chile's national determined contributions. Technical report, 2020.

Guo, F., Zhu, X., Zhang, J., and Yang, X. Large-scale living laboratory of seasonal borehole thermal energy storage system for urban district heating. *Applied Energy*, 264(November 2019):114763, 2020. ISSN 03062619. doi: 10.1016/j.apenergy.2020.114763.

Gurobi Optimization Inc. Gurobi Optimizer, 2010. URL `http://www.gurobi.com`.

Haas, J., Nowak, W., and Palma-Behnke, R. Multi-objective planning of energy storage technologies for a fully renewable system: Implications for the main stakeholders in Chile. *Energy Policy*, 126:494–506, 3 2019. ISSN 0301-4215. doi: 10.1016/j.enpol.2018.11.034.

Haas, J. Inputs for LEELO (Long-term Energy Expansion Linear Optimization), 8 2018. URL `https://zenodo.org/record/1344412`.

Haas, J., Palma-Behnke, R., Valencia, F., Araya, P., Díaz-Ferrán, G., Telsnig, T., Eltrop, L., Díaz, M., Püschel, S., Grandel, M., Román, R., and Jiménez-Estévez, G. Sunset or sunrise? Understanding the barriers and options for the massive deployment of solar technologies in Chile. *Energy Policycy*, 112:399–414, 2018. doi: 10.1016/j.enpol.2017.10.001.

Hamdy, S., Moser, F., Morosuk, T., and Tsatsaronis, G. Exergy-Based and Economic Evaluation of Liquefaction Processes for Cryogenics Energy Storage. *Energies 2019, Vol. 12, Page 493*, 12(3):493, 2 2019. ISSN 19961073. doi: 10.3390/EN12030493.

Hart, W. E., Laird, C. D., Watson, J.-P., Woodruff, D. L., Hackebeil, G. A., Nicholson, B. L., and Siirola, J. D. *Optimization Modeling in Python - Springer Optimization and Its Applications*, volume 67. 2017. ISBN 9783319588193. doi: 10.1007/978-3-319-58821-6.

Hassanat, A., Almohammadi, K., Alkafaween, E., Abunawas, E., Hammouri, A., and Prasath, V. B. S. Choosing Mutation and Crossover Ratios for Genetic Algorithms—A Review with a New Dynamic Approach. *Information*, 10(12):390, 2019. ISSN 2078-2489. doi: 10.3390/info10120390.

Hast, A., Syri, S., Lekavičius, V., and Galinis, A. District heating in cities as a part of low-carbon energy system. *Energy*, 152:627–639, 2018. ISSN 03605442. doi: 10.1016/j.energy.2018.03.156.

Hayward, J. and Graham, P. Electricity generation technology cost projections 2017-2050. Technical report, CSIRO, 2017.

Heat network partnership for Scotland. District Heating Strategy Factsheet. Technical report, 2017.

Heat Roadmap Europe. Models and Methodology – Heat Roadmap Europe, 2020. URL `https://heatroadmap.eu/models-and-methodology/`.

Hellström, G. *Ground heat storage : thermal analyses of duct storage systems*. PhD thesis, Lund University, Lund, 1991.

Hers, S., Afman, M., Cherif, S., and Rooijers, F. Potential for Power-to-Heat in the Netherlands. Technical report, CE Delft, 2015.

Hsieh, S., Omu, A., and Orehounig, K. Comparison of solar thermal systems with storage: From building to neighbourhood scale. *Energy and Buildings*, 152:359–372, 2017. ISSN 03787788. doi: 10.1016/j.enbuild.2017.07.036.

Hu, J., Harmsen, R., Crijns-Graus, W., Worrell, E., and van den Broek, M. Identifying barriers to large-scale integration of variable renewable electricity into the electricity market: A literature review of market design. *Renewable and Sustainable Energy Reviews*, 81:2181–2195, 2018. ISSN 1364-0321. doi: 10.1016/J.RSER.2017.06.028.

IEA. Status of Power System Transformation Advanced Power Plant Flexibility. Technical report, International Energy Agency, 2018a.

IEA. Energy Policies Beyond IEA Countries - Chile Review 2018. Technical report, 2018b.

Intergas. Informativo tarifas Temuco, 2019. URL `https://www.intergas.cl/docs/InformativoTarifasTemuco.pdf`.

International Energy Agency. Perspective for the Clean Energy Transition - the Critical Role of Buildings. Technical report, IEA, 2019a.

International Energy Agency. Renewables 2019: Analysis and forecast to 2024. Technical report, IEA, 2019b.

International Energy Agency. Linking Heat and Electricity Systems - Co-generation and District Heating and Cooling Solutions for a Clean Energy Future. Technical report, 2014a.

International Energy Agency. Technology Roadmap: Energy Storage. Technical report, 2014b. URL `http://www.iea.org/termsandconditionsuseandcopyright/`.

IRENA. Electricity storage and renewables: cost and markets to 2030. Technical report, International Renewable Energy Agency, Abu Dhabi, 2017.

IRENA. Power system flexibility for the energy transition, Part 1: Overview for policy makers. Technical report, International Renewable Energy Agency, Abu Dhabi, 2018.

IRENA. Innovation landscape brief: Renewable power-to-heat. Technical report, International Renewable Energy Agency, Abu Dhabi, 2019a.

IRENA. Global Energy Transformation: The REmap transition pathway (Background report to 2019 Edition). Technical report, International Renewable Energy Agency, Abu Dhabi, 2019b.

IRENA. Innovation outlook: Thermal energy storage. Technical report, 2020.

Jalil-Vega, F. and Hawkes, A. D. Spatially resolved model for studying decarbonisation pathways for heat supply and infrastructure trade-offs. *Applied Energy*, 210:1051–1072, 2018. ISSN 03062619. doi: 10.1016/j.apenergy.2017.05.091.

Jensen, M. V. and Nielse, J. E. Task 55 Large Solar Heating & Cooling Systems - Seasonal pit heat storages - Guidelines for materials & construction. Technical report, 2020.

Jouhara, H., Żabnieńska-Góra, A., Khordehgah, N., Ahmad, D., and Lipinski, T. Latent thermal energy storage technologies and applications: A review. *International Journal of Thermofluids*, 5-6:100039, 8 2020. ISSN 2666-2027. doi: 10.1016/J.IJFT.2020.100039.

Kjaergaard, L., Jensen, N. A., and Fjernvarme, M. Innovative, multi-applicable and cost efficient hybrid solar (55 %) and biomass energy (45 %) large scale (district) heating system with long term heat storage – and Organic Rankine Cycle electricity production. Technical report, European Union's Seventh Framework Programme, 2014.

Krug, R., Mehrmann, V., and Schmidt, M. Nonlinear optimization of district heating networks. *Optimization and Engineering*, pages 1–37, 2020. ISSN 15732924. doi: 10.1007/s11081-020-09549-0.

Kumar, P. H. and Mageshvaran, R. Methods And Solvers Used For Solving Mixed Integer Linear Programming And Mixed Nonlinear Programming Problems: A Review. *International journal of scientific and technology research*, 9:1, 2020. ISSN 2277-8616.

Kusuda, T., Mizuno, M., and Bean, J. Seasonal Heat Loss Calculation for Slab-On-Grade Floors. Technical report, U.S. Department of Commerce, 1982.

Lim, H. S., Ok, J. S., Park, J. S., Lee, S. J., Karng, S. W., and Kang, Y. T. Efficiency improvement of energy storage and release by the inlet position control for seasonal thermal energy storage. *International Journal of Heat and Mass Transfer*, 151:119435, 4 2020. ISSN 0017-9310. doi: 10.1016/j.ijheatmasstransfer.2020.119435.

Lima, J. L., R., Rivera, J., Palma, R., Jimenez, G., Benavente, J. M., and Castillo, E. Informe Costo de Falla. Technical report, Intelis, Santiago, Chile, 2012.

Lizana, J., Friedrich, D., Renaldi, R., and Chacartegui, R. Energy flexible building through smart demand-side management and latent heat storage. *Applied Energy*, 230:471–485, 11 2018a. ISSN 0306-2619. doi: 10.1016/j.apenergy.2018.08.065.

Lizana, J., Chacartegui, R., Barrios-Padura, A., and Valverde, J. M. Advances in thermal energy storage materials and their applications towards zero energy buildings: A critical review. *Applied Energy*, 203:219–239, 2017. ISSN 03062619. doi: 10.1016/j.apenergy.2017.06.008.

Lizana, J., Chacartegui, R., Barrios-Padura, A., and Ortiz, C. Advanced low-carbon energy measures based on thermal energy storage in buildings: A review. *Renewable and Sustainable Energy Reviews*, 82:3705–3749, 2 2018b. ISSN 1364-0321. doi: 10.1016/J.RSER.2017.10.093.

Lund, H., Werner, S., Wiltshire, R., Svendsen, S., Thorsen, J. E., Hvelplund, F., and Mathiesen, B. V. 4th Generation District Heating (4GDH): Integrating smart thermal grids into future sustainable energy systems. *Energy*, 68:1–11, 2014. ISSN 0360-5442. doi: 10.1016/j.energy.2014.02.089.

Lund, H., Østergaard, P. A., Connolly, D., Ridjan, I., Mathiesen, B. V., Hvelplund, F., Thellufsen, J. Z., and Sorknses, P. Energy Storage and Smart Energy Systems. *International Journal of Sustainable Energy Planning and Management*, 11:3–14, 10 2016. ISSN 2246-2929. doi: 10.5278/IJSEPM.2016.11.2.

Lund, H., Arler, F., Østergaard, P. A., Hvelplund, F., Connolly, D., Mathiesen, B. V., and Karnøe, P. Simulation versus optimisation: Theoretical positions in energy system modelling. *Energies*, 10(7), 6 2017. ISSN 19961073. doi: 10.3390/en10070840.

Lund, P., Lindgren, J., Mikkola, J., and Salpakari, J. Review of energy system flexibility measures to enable high levels of variable renewable electricity. *Renewable and Sustainable Energy Reviews*, 45:785–807, 2015. ISSN 13640321. doi: 10.1016/j.rser.2015.01.057. URL `http://dx.doi.org/10.1016/j.rser.2015.01.057`.

Lv, Y., Si, P., Rong, X., Yan, J., Feng, Y., and Zhu, X. Determination of optimum tilt angle and orientation for solar collectors based on effective solar heat collection. *Applied Energy*, 219: 11–19, 2018. ISSN 03062619. doi: 10.1016/j.apenergy.2018.03.014.

Madariaga, A. and Gladina, E. La transformación de la política energética como cambio de paradigma. In González, F. and Madariaga, A., editors, *La constitución social, política y moral de la economía chilena*. RIL Editores, 2018. URL `https://www.researchgate.net/publication/320045756`.

Mahon, H., O'Connor, D., Friedrich, D., and Hughes, B. A review of thermal energy storage technologies for seasonal loops. *Energy*, 239:122207, 1 2022. ISSN 0360-5442. doi: 10.1016/j.energy.2021.122207.

Mangold, D. and Deschaintre, L. Task 45 Large Systems Seasonal thermal energy storage - Report on state of the art and necessary further R+D. Technical report, Solites, 2015.

Masatin, V., Latõšev, E., and Volkova, A. Evaluation Factor for District Heating Network Heat Loss with Respect to Network Geometry. *Energy Procedia*, 95:279–285, 2016. doi: 10.1016/j.egypro.2016.09.069.

Mauthner, F. and Herkel, S. Technology and demonstrators - Technical Report Subtask C – Part C1. Technical Report January, IEA, 2016.

Maximov, S. A., Harrison, G. P., and Friedrich, D. Long term impact of grid level energy storage on renewable energy penetration and emissions in the chilean electric system. *Energies*, 12(6), 2019. ISSN 19961073. doi: 10.3390/en12061070.

Maximov, S. A., Mehmood, S., and Friedrich, D. Multi-objective optimisation of a solar district heating network with seasonal storage for conditions in cities of southern Chile. *Sustainable Cities and Society*, 73:103087, 2021. ISSN 2210-6707. doi: 10.1016/J.SCS.2021.103087.

Mazloum, Y., Sayah, H., and Nemer, M. Dynamic modeling and simulation of an Isobaric Adiabatic Compressed Air Energy Storage (IA-CAES) system. *Journal of Energy Storage*, 11:178–190, 6 2017. ISSN 2352-152X. doi: 10.1016/J.EST.2017.03.006.

McTigue, J. D., White, A. J., and Markides, C. N. Parametric studies and optimisation of pumped thermal electricity storage. *Applied Energy*, 137:800–811, 2015. ISSN 03062619. doi: 10.1016/j.apenergy.2014.08.039.

Mella, M. and Quiroz, D. Geología del área de Temuco-Nueva Imperial. *Serie de geología basica*, 122, 2010.

Mena, R., Escobar, R., Lorca, Negrete-Pincetic, M., and Olivares, D. The impact of concentrated solar power in electric power systems: A Chilean case study. *Applied Energy*, 235:258–283, 2 2019. ISSN 0306-2619. doi: 10.1016/j.apenergy.2018.10.088.

Ministerio de Desarrollo Social. Metodologogia de preparacion y evaluacion proyectos de edificacion publica. Technical report, Ministerio de Planificación y Desarrollo Social, 2013.

Ministerio de Energia. Planificación Energética de Largo Plazo 2018. Technical report, 2018.

Ministerio de Energia. Proyectos en Construcción e Inversión en sector Energía a septiembre 2017. Technical report, Santiago, Chile, 2017a.

Ministerio de Energia. Plan de retiro y/o conversion de unidades a carbon. Technical report, 2020a.

Ministerio de Energia. Explorador Solar, 2017b. URL `https://solar.minenergia.cl/exploracion`.

Ministerio de Energia. Balance Nacional de Energia Regional. Technical report, 2017c.

Ministerio de Energia. Energia 2050 - Politica energetica de Chile. Technical report, 2015.

Ministerio de Energia. Estrategia de flexibilidad para el sistema eléctrico nacional. Technical report, Santiago, 2020b.

Ministerio de Energia. Reconversión de centrales a carbón en plantas de almacenamiento térmico con energía renovable en Chile. Technical report, 2020c.

Ministerio de Energia. Estrategia de transicion energetica residencial. Technical report, 2020d.

Ministerio de Energia. Plan de Retiro y/o Reconversion de Unidades a Carbon. Technical report, 2020e.

Ministerio de Energia. Actualización 2021 Política Energética Nacional. Technical report, 2021a.

Ministerio de Energia. Estudio de análisis de dos opciones tecnológicas de reconversión de las termoeléctricas y su integración al Sistema Eléctrico Nacional. Technical report, 2021b.

Ministerio de Energia. Informe Balance Nacional de Energía 2019. Technical report, 2019a. URL https://energia.gob.cl/sites/default/files/documentos/2020_informe_anual_bne_2019.pdf.

Ministerio de Energia. Plan of Phase-out and/or Reconversion of Coal Units. Technical report, 2020f.

Ministerio de Energia. Estrategia Nacional de Calor y Frío. Technical report, 2021c.

Ministerio de Energia. Planificacion energetica de largo plazo. Technical report, 2019b.

Ministerio de Energia. Planificacion energetica de largo plazo 2018 - IAA2020. Technical report, 2020g.

Ministerio de Energia. Planificacion energetica de largo plazo - Informe preliminar. Technical report, 2021d.

Ministerio de Vivienda y Urbanismo. Calificación energética de viviendas. Technical report, Ministerio de Vivienda y Urbanismo, 2018.

Ministerio del Medio Ambiente. Cuarto Reporte del Estado del Medio Ambiente. Technical report, Ministerio del Medio Ambiente, Santiago, Chile, 2018.

Ministerio del Medio Ambiente. Gobierno anuncia el retiro del 50% de las centrales a carbón al 2025, 2021. URL https://mma.gob.cl/gobierno-anuncia-el-retiro-del-50-de-las-centrales-a-carbon-al-2025/.

Molina, A., Falvey, M., and Rondanelli, R. A solar radiation database for Chile. *Scientific Reports*, 7(1):1–11, 12 2017. ISSN 20452322. doi: 10.1038/s41598-017-13761-x.

Molod, A., Takacs, L., Suarez, M., and Bacmeister, J. Development of the GEOS-5 atmospheric general circulation model: Evolution from MERRA to MERRA2. *Geoscientific Model Development*, 8(5):1339–1356, 5 2015. ISSN 19919603. doi: 10.5194/GMD-8-1339-2015.

Morales, F., De, C., Roger, C., Eggen, W. B., and Henríquez, M. Manual de desarrollo de proyectos de energia distrital. Technical report, EBP, Santiago, 2018.

Morandin, M., Maréchal, F., Mercangöz, M., and Buchter, F. Conceptual design of a thermo-electrical energy storage system based on heat integration of thermodynamic cycles - Part B: Alternative system configurations. *Energy*, 45(1):386–396, 2012. ISSN 03605442. doi: 10.1016/j.energy.2012.03.033.

Moreno, B. R., Ferreira, R., Barroso, L., Rudnick, H., and Pereira, E. Facilitating the integration of renewables in Latin America. *IEEE Power and Energy Magazine*, (october), 2017. doi: 10.1109/MPE.2017.2708862.

Mosayebian, M. E., Soleymani, S., and Mozafari, S. B. Synthetic generation of wind power time series for wind/storage systems integration studies. *Journal of Renewable Sustainable Energy*, 8, 2016.

Mousavi, S., Rismanchi, B., Brey, S., and Aye, L. PCM embedded radiant chilled ceiling: A state-of-the-art review. *Renewable and Sustainable Energy Reviews*, 151(February): 111601, 2021. ISSN 18790690. doi: 10.1016/j.rser.2021.111601.

Munoz, F. D., Pumarino, B. J., and Salas, I. A. Aiming low and achieving it: A long-term analysis of a renewable policy in Chile. *Energy Economics*, 65:304–314, 2017. ISSN 01409883. doi: 10.1016/j.eneco.2017.05.013.

Nasirov, S., Silva, C., and Agostini, C. A. Investors' Perspectives on Barriers to the Deployment of Renewable Energy Sources in Chile. *Energies*, 8:3794–3814, 2015. ISSN 1996-1073. doi: 10.3390/en8053794.

Natural Resources Canada. Drake landing solar community, 2020. URL `https://www.dlsc.ca/`.

Navarrete, S. *Infiltraciones de Aire en la Vivienda.* PhD thesis, Universidad de Concepción, 2016.

Nielsen, J., Sørensen, P. A., Bakema, G., Drijver, B., Pittens, B., Buik, N., Egermann, P., Rey, C., Maragna, C., Hamm, V., Hahn, F., Nardini, I., Koornneef, J., and Dideriksen, K. HEATSTORE Underground Thermal Energy Storage (UTES)-state-of-the-art, example cases and lessons learned. Technical report, 2019. URL `www.heatstore.eu`.

Nielsen, L. and Leithner, R. Dynamic Simulation of an Innovative Compressed Air Energy Storage Plant-Detailed Modelling of the Storage Cavern. *WSEAS Transactions on Power Systems*, 4(8), 2009.

Niemi, R., Mikkola, J., and Lund, P. D. Urban energy systems with smart multi-carrier energy networks and renewable energy generation. *Renewable Energy*, 48:524–536, 2012. ISSN 0960-1481. doi: 10.1016/j.renene.2012.05.017.

NREL. EnergyPlus, 2021. URL `https://energyplus.net/`.

Nussbaumer, T. and Thalmann, S. Influence of system design on heat distribution costs in district heating. *Energy*, 101:496–505, 2016. ISSN 03605442. doi: 10.1016/j.energy.2016.02.062.

Osorio-Aravena, J. C., Aghahosseini, A., Bogdanov, D., Caldera, U., Ghorbani, N., Mensah, T. N. O., Khalili, S., Muñoz-Cerón, E., and Breyer, C. The impact of renewable energy and sector coupling on the pathway towards a sustainable energy system in Chile. *Renewable and Sustainable Energy Reviews*, 151:111557, 11 2021. ISSN 1364-0321. doi: 10.1016/j.rser.2021.111557.

Paardekooper, S., Chang, M., Nielsen, S. ., Moreno, D., Lund, H., Grundahl, L. ., Dahlbaek, J. ., and Mathiesen, B. Heat Roadmap Chile: Quantifying the potential of clean district heating and energy efficiency for a long-term energy vision for Chile. Technical report, Aalborg University, 2019.

Paardekooper, S., Lund, H., Chang, M., Nielsen, S., Moreno, D., and Thellufsen, J. Z. Heat Roadmap Chile: A national district heating plan for air pollution decontamination and decarbonisation. *Journal of Cleaner Production*, 272:122744, 11 2020. ISSN 0959-6526. doi: 10.1016/J.JCLEPRO.2020.122744.

Pedregosa, F., Varoquaux, G., Gramfort, A., Michel, V., Thirion, B., Grisel, O., Blondel, M., Prettenhofer, P., Weiss, R., Dubourg, V., Vanderplas, J., Passos, A., Cournapeau, D., Brucher, M., Perrot, M., and Duchesnay, E. Scikit-learn: Machine Learning in Python. *Journal of Machine Learning Research*, 12(85):2825–2830, 2011. ISSN 1533-7928.

Peña, K. Valhalla ajusta fechas de sus proyectos eléctricos y continúa en búsqueda de financiamiento - Diario Financiero, 2021. URL `https://www.df.cl/noticias/empresas/energia/valhalla-ajusta-fechas-de-sus-proyectos-electricos-y-continua-en/2021-04-01/191634.html`.

Pfenninger, S. and Staffell, I. Renewables.Ninja, 2017. URL `www.renewables.ninja`.

Pilpola, S. and Lund, P. D. Different flexibility options for better system integration of wind power. *Energy Strategy Reviews*, 26:100368, 2019. ISSN 2211-467X. doi: 10.1016/J.ESR.2019.100368.

Pimm, A. J., Garvey, S. D., and de Jong, M. Design and testing of Energy Bags for underwater compressed air energy storage. *Energy*, 66:496–508, 3 2014. ISSN 0360-5442. doi: 10.1016/j.energy.2013.12.010.

Pizarro, R., Pinto, F., and Ainzua, S. Chiles Green Tax Strategy. Technical report, GIZ, Santiago, 2019.

Planenergi. Best practice for implementation and operation of large sale borehole and pit heat thermal storage. Technical report, PlanEnergi, 2019.

Porras-Salazar, J. A., Contreras-Espinoza, S., Cartes, I., Piggot-Navarrete, J., and Pérez-Fargallo, A. Energy poverty analyzed considering the adaptive comfort of people living in social housing in the central-south of Chile. *Energy and Buildings*, 223:110081, 9 2020. ISSN 0378-7788. doi: 10.1016/j.enbuild.2020.110081.

Prina, M. G., Manzolini, G., Moser, D., Nastasi, B., and Sparber, W. Classification and challenges of bottom-up energy system models - A review. *Renewable and Sustainable Energy Reviews*, 129:109917, 9 2020. ISSN 1364-0321. doi: 10.1016/J.RSER.2020.109917.

Quintana, H. J. and Kummert, M. Optimized control strategies for solar district heating systems. *Journal of Building Performance Simulation*, 8(2):79–96, 2015. ISSN 1940-1493. doi: 10.1080/19401493.2013.876448.

Ramstein, C., Goyal, R., Gray, S., Kallhauge, A. C., Lam, L., Klein, N., Wong, L., Quant, M., Nierop, S., Berg, T., and Leuschner, P. State and Trends of Carbon Pricing 2018. Technical report, World Bank, Washington, 2018.

Reddy Prasad, D., Senthilkumar, R., Lakshmanarao, G., Krishnan, S., and Naveen Prasad, B. A critical review on thermal energy storage materials and systems for solar applications. *AIMS Energy*, 7(4):507–526, 2019. ISSN 2333-8334. doi: 10.3934/energy.2019.4.507.

Rehman, H. u., Hirvonen, J., and Sirén, K. Performance comparison between optimized design of a centralized and semi-decentralized community size solar district heating system. *Applied Energy*, 229(March):1072–1094, 2018. ISSN 03062619. doi: 10.1016/j.apenergy.2018.08.064.

Renaldi, R., Kiprakis, A., and Friedrich, D. An optimisation framework for thermal energy storage integration in a residential heat pump heating system. *Applied Energy*, 186:520–529, 1 2017. ISSN 0306-2619. doi: 10.1016/j.apenergy.2016.02.067.

Renaldi, R. *Modelling and Optimisation of Energy Systems with Thermal Energy Storage*. PhD thesis, University of Edinburgh, 2018.

Renaldi, R. and Friedrich, D. Techno-economic analysis of a solar district heating system with seasonal thermal storage in the UK. *Applied Energy*, 236:388–400, 2019. ISSN 03062619. doi: 10.1016/j.apenergy.2018.11.030.

Reuss, M. The use of borehole thermal energy storage (BTES) systems. In *Advances in Thermal Energy Storage Systems: Methods and Applications*, pages 117–147. Elsevier Inc., 2014. ISBN 9781782420965. doi: 10.1533/9781782420965.1.117.

Revista de Electricidad. Baterías en Chile buscan dar un paso más en Servicios Complementarios, 2018. URL `http://www.revistaei.cl/informes-tecnicos/baterias-chile-buscan-dar-paso-mas-servicios-complementarios/`.

Reyes, R., Schueftan, A., Ruiz, C., and González, A. D. Controlling air pollution in a context of high energy poverty levels in southern Chile: Clean air but colder houses? *Energy Policy*, 124:301–311, 1 2019. ISSN 0301-4215. doi: 10.1016/j.enpol.2018.10.022.

Romanchenko, D., Nyholm, E., Odenberger, M., and Johnsson, F. Impacts of demand response from buildings and centralized thermal energy storage on district heating systems. *Sustainable Cities and Society*, 64, 2021. ISSN 22106707. doi: 10.1016/j.scs.2020.102510.

Roth, P., Georgiev, A., Busso, A., and Barraza, E. First in situ determination of ground and borehole thermal properties in Latin America. *Renewable Energy*, 29(12):1947–1963, 10 2004. ISSN 0960-1481. doi: 10.1016/j.renene.2004.02.014.

Saesa. Tarifas Vigentes, 2020. URL `https://www.gruposaesa.cl/edelaysen/tarifas-vigentes/`.

Santana, C., Falvey, M., Ibarra, M., and García, M. Energías Renovables en Chile. Technical report, Santiago, Chile, 2014.

Sarbu, I. and Sebarchievici, C. A Comprehensive Review of Thermal Energy Storage. *Sustainability*, 10(2):191, 1 2018. ISSN 2071-1050. doi: 10.3390/su10010191.

Schmidt, O., Hawkes, A., Gambhir, A., and Staffell, I. The future cost of electrical energy storage based on experience rates. *Nature Energy*, 2(8):1–8, 2017. ISSN 2058-7546. doi: 10.1038/nenergy.2017.110.

Schmidt, T., Mangold, D., and Müller-Steinhagen, H. Central solar heating plants with seasonal storage in Germany. *Solar Energy*, 76(1-3):165–174, 2004. ISSN 0038092X. doi: 10.1016/j.solener.2003.07.025.

Schmidt, T. and Sørensen, A. Monitoring Results from Large Scale Heat storages for District Heating in Denmark. Technical report, 2018.

Shah, S. K., Aye, L., and Rismanchi, B. Multi-objective optimisation of a seasonal solar thermal energy storage system for space heating in cold climate. *Applied Energy*, 268: 115047, 2020. ISSN 03062619. doi: 10.1016/j.apenergy.2020.115047.

Short, W., Packey, D., and Holt, T. A manual for the economic evaluation of energy efficiency and renewable energy technologies. *Renewable Energy*, 95(March):73–81, 1995. doi: NREL/TP-462-5173. URL `http://large.stanford.edu/publications/coal/references/troughnet/market/docs/5173.pdf`.

Sibbitt, B., McClenahan, D., Djebbar, R., Thornton, J., Wong, B., Carriere, J., and Kokko, J. The performance of a high solar fraction seasonal storage district heating system - Five years of operation. In *Energy Procedia*, volume 30, pages 856–865. Elsevier Ltd, 2012. doi: 10.1016/j.egypro.2012.11.097.

Simsek, Y., Lorca, A., Urmee, T., Bahri, P. A., and Escobar, R. Review and assessment of energy policy developments in Chile. *Energy Policy*, 127:87–101, 4 2019. ISSN 0301-4215. doi: 10.1016/j.enpol.2018.11.058.

Sipilä, K., Rämä, M., Zinko, H., Ottosson, U., Williams, J., Aguiló-Rullán, A., and Bøhm, B. District heating for energy efficient building areas. Technical report, IEA, 2011.

Skarphagen, H., Banks, D., Frengstad, B. S., and Gether, H. Design Considerations for Borehole Thermal Energy Storage (BTES): A Review with Emphasis on Convective Heat Transfer. *Geofluid*, 2019, 2019. doi: 10.1155/2019/4961781.

Smallbone, A., Jülch, V., Wardle, R., and Roskilly, A. P. Levelised Cost of Storage for Pumped Heat Energy Storage in comparison with other energy storage technologies. *Energy Conversion and Management*, 152:221–228, 2017. doi: 10.1016/j.enconman.2017.09.047.

Soltero, V. M., Chacartegui, R., Ortiz, C., and Velázquez, R. Evaluation of the potential of natural gas district heating cogeneration in Spain as a tool for decarbonisation of the economy. *Energy*, 115:1513–1532, 2016. ISSN 03605442. doi: 10.1016/j.energy.2016.06.038.

Sorensen, A. Solar district heating guidelines. Technical report, Planenergi, 2012.

Steinmann, W. The CHEST (Compressed Heat Energy STorage) concept for facility scale thermo mechanical energy storage. *Energy*, 69:543–552, 5 2014. ISSN 03605442. doi: 10.1016/j.energy.2014.03.049.

Steinmann, W.-D. Thermo-mechanical concepts for bulk energy storage. *Renewable and Sustainable Energy Reviews*, 75:205–219, 2017. doi: 10.1016/j.rser.2016.10.065.

Steinmann, W. D., Bauer, D., Jockenhöfer, H., and Johnson, M. Pumped thermal energy storage (PTES) as smart sector-coupling technology for heat and electricity. *Energy*, 183: 185–190, 2019. ISSN 03605442. doi: 10.1016/j.energy.2019.06.058.

Strbac, G., Aunedi, M., Pudjianto, D., Sanders, D., Hart, A., and Brunert, J. An analysis of electricity system flexibility for Great Britain. Technical report, Imperial College London and The Carbon Trust, 2016.

Suazo-Martinez, C., Pereira-Bonvallet, E., and Palma-Behnke, R. A simulation framework for optimal energy storage sizing. *Energies*, 7(5):3033–3055, 2014. ISSN 19961073. doi: 10.3390/en7053033.

Svendsen, H. powergama · PyPI, 2021. URL `https://pypi.org/project/powergama/`.

Tolvett, S. Futuro de la calefacción en Chile: Opciones y Consecuencias. Technical report, Ministerio del Medio Ambiente, 2015.

Urquiza, A., Amigo, C., Billi, M., Leal, T., Araya, P., Cortés, A., Rivas, I., Valdés, M., and Valencia, F. Analisis de fuentes secundarias disponibles de alcance nacional. Technical report, Red de Pobreza Energética, 2017.

Valhalla Energy. Espejo de Tarapaca, 2017. URL http://valhalla.cl/espejo-de-tarapaca/.

Van-Rossum, G. Python Software Foundation. Python Language Reference, version 3.2.7, 1995. URL http://www.python.org.

Vargas, X., Ayala, A., Meza, R., and Rubio, E. Disponibilidad futura de los recursos hídricos frente a escenarios de cambio climático en Chile. Technical report, United Nations Economic Commission for Latin America and the Caribbean, Santiago, Chile, 2012.

Vecchi, A., Li, Y., Ding, Y., Mancarella, P., and Sciacovelli, A. Liquid air energy storage (LAES): A review on technology state-of-the-art, integration pathways and future perspectives. *Advances in Applied Energy*, 3:100047, 8 2021. ISSN 2666-7924. doi: 10.1016/j.adapen.2021.100047.

Venegas-Troncoso, T., Ugarte-Larraguibel, G., Vasco, D. A., Rouault, F., and Pérez, R. Feasibility study of the application of a cooling energy storage system in a chiller plant of an office building located in Santiago, Chile. *International Journal of Refrigeration*, 102:142–150, 6 2019. ISSN 0140-7007. doi: 10.1016/j.ijrefrig.2019.01.028.

Verastegui, F., Lorca, A., Negrete-Pincetic, M., and Olivares, D. Firewood heat electrification impacts in the Chilean power system. *Energy Policy*, 144:111702, 9 2020. ISSN 0301-4215. doi: 10.1016/j.enpol.2020.111702.

Verastegui, F., Lorca, A., Olivares, D., and Negrete-Pincetic, M. Optimization-based analysis of decarbonization pathways and flexibility requirements in highly renewable power systems. *Energy*, 234:121242, 11 2021. ISSN 0360-5442. doi: 10.1016/j.energy.2021.121242.

Voll, P. *Automated optimization-based synthesis of distributed energy supply systems*. PhD thesis, Aachen University, 2013.

Wang, S. and Baldea, M. Temperature Control and Optimal Energy Management using Latent Energy Storage. *Industrial and Engineering Chemistry Research*, 52(9):3247–3257, 3 2013. doi: 10.1021/IE303073N.

Welsch, B., Rühaak, W., Schulte, D. O., Bär, K., and Sass, I. Characteristics of medium deep borehole thermal energy storage. *International Journal of Energy Research*, 40(13):1855–1868, 2016. ISSN 1099-114X. doi: 10.1002/ER.3570.

Westermann, P. and Evins, R. Surrogate modelling for sustainable building design – A review. *Energy and Buildings*, 198:170–186, 9 2019. ISSN 0378-7788. doi: 10.1016/j.enbuild.2019.05.057.

White, A., Parks, G., and Markides, C. N. Thermodynamic analysis of pumped thermal electricity storage. *Applied Thermal Engineering*, 53(2):291–298, 2013. ISSN 13594311. doi: 10.1016/j.applthermaleng.2012.03.030.

World Bank. Offshore Wind Technical Potential in Chile. Technical report, 2020. URL http://documents.worldbank.org/curated/en/716891572457609829/pdf/Going-http://documents.worldbank.org/curated/en/716891572457609829/.

Yáñez, C., Fissore, A., and Leiva, A. Informe final de usos de la energía de los hogares Chile 2018. Technical report, CDT, 2019.

Yang, L., Entchev, E., Rosato, A., and Sibilio, S. Smart thermal grid with integration of distributed and centralized solar energy systems. *Energy*, 122:471–481, 2017. ISSN 03605442. doi: 10.1016/j.energy.2017.01.114.

Yang, T., Liu, W., Kramer, G. J., and Sun, Q. Seasonal thermal energy storage: A techno-economic literature review. *Renewable and Sustainable Energy Reviews*, 139:110732, 4 2021. ISSN 1364-0321. doi: 10.1016/J.RSER.2021.110732.

Zeghadnia, L., Robert, J. L., and Achour, B. Explicit solutions for turbulent flow friction factor: A review, assessment and approaches classification, 2019. ISSN 20904479.